School of Chemistry

University of Nottingham

Analysis of molecular links between epigenetic regulations and energy metabolism

Agata Miezaniec BSc, MSc

Thesis submitted to the University of Nottingham

for the degree of Doctor of Philosophy

June 2019

Acknowledgements

This Ph. D. thesis would have never happened without the help and support of many important people.

First, I would like to thank Christoph's Loenarz research group: to my supervisor Professor Christoph Loenarz for the lesson of patience and resistance I have received from him; to master students Zoe Jane Lee and Alen Krajnc, who not only supported my research by giving a hand in the laboratory, but also provided a fantastic atmosphere during this time. Mentoring these two young scientists was the greatest experience during my Ph. D. Additionally, I would like to thank James Jarratt and Peter Jessop for common fights with *S. Cerevisiae* during my first months of Ph. D. In addition, I would like to acknowledge Johanna Mattay, whose visit from the University of Freiburg significantly improved my HPLC skills.

Secondly, I would like to express my gratefulness to Professor Neil Oldham and his research group for support and help during the toughest time of my Ph. D. Special thanks to Jedd, Van, Nkazi and Lucio for endless consultations regarding HPLC columns and mass spectrometry.

Also, I would like to thank Ben Pointer–Gleadhill who was always my primary contact regarding issues with mass spectrometry. He was always patient and smiley in the times when I thought there was no hope.

I would like to thank Tissue Engineering group where I was able to perform tissue culture.

Additionally, I would like to acknowledge all friends from the Center for Biomolecular Sciences, School of Chemistry and other friends from the University of Nottingham who replaced my family during my Ph. D. time abroad.

Last, but not least, I would like to thank my family and Diego who were constantly supporting me during the entire Ph. D. Without their help, this thesis would not exist.

Additionally, I would like to thank Miriam Colombo and Net4FS programme for a valuable internship in biopharmaceutical company in Shanghai, China. This experience has helped me to see the broader aspects of science and to shape my future carrier choices.

Abstract

Oxidation of fatty acids is an important energy source for skeletal muscle and heart, particularly during aerobic exercise and long-term fasting, and requires L-carnitine. L-carnitine has important roles in metabolism including cellular acetyl- and acyl-transport; its disorders lead to cardiomyopathy and skeletal muscle weakness. Carnitine is biosynthesized from trimethyllysine, whose only cellular sources are histones and other proteins containing trimethylated lysines. Surprisingly to date, this link between epigenetics and energy metabolism has received little attention.

This work investigated the fundamental question of whether protein methylation modulates fatty acid metabolism via carnitine biosynthesis. Specific objectives included the role of individual methyltransferase substrates for carnitine metabolism, the role of protein degradation in this pathway and its manipulation by small molecules (Figure 0-1).

An optimised high-pressure liquid chromatography-tandem mass spectrometry (HPLC-MS/MS) method allowed for detection and quantification of carnitine and fatty acid metabolites from whole lysates of yeast and human cells exposed to genetic or pharmaceutical modulators.

The key result was that genetic deletion of individual protein methyltransferases affected cellular carnitine levels. That effect was also observed by treatment with hypomethylating agents, with clinically used iron chelators and anti-obesity drugs. Together with time-scale studies, these results suggested that it may be possible to modulate carnitine levels via changes in protein methylation status.

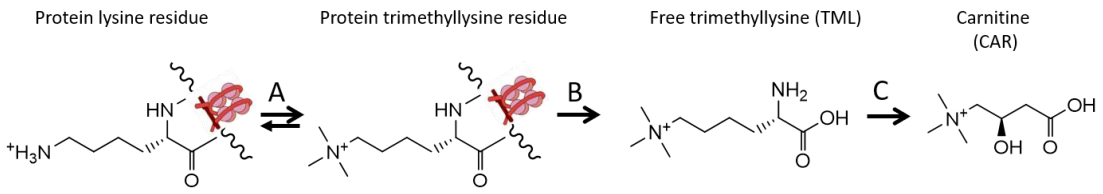


Figure 0-1: Carnitine (CAR) biosynthesis in mammalian cells; A: Protein lysyl cellular methylation; B: Degradation of proteins containing trimethylated lysine residues; C: Carnitine biosynthesis from free trimethyllysine (TML).

Abbreviations

2-HG – 2-hydroxyglutarate

2OG – 2-oxoglutarate

2OGX – 2OG, Fe^{2+}, O_2 dependent oxygenase

5-FAA – 5-fluoroanthranilic acid

A-CAR – acetyl-carnitine, acetyl-CAR

A-CAR-d_9 – acetyl-carnitine-(trimethyl-d_9)

Acr1p – succinate transporter

AdoHcy – *S*-adenosylhomocysteine

AdoMet – *S*-adenosylmethionine

AdOx – adenosine-2',3'-dialdehyde

ALA – L-alanine

APS – ammonium persulfate

AUC – peak area under the curve

BCA – bicinchoninic acid assay

BSA – bovine serum albumin

CACT – mitochondrial carnitine-acylcarnitine translocase

CAR – L-carnitine, carnitine

CAR-d_9 – DL-carnitine-(trimethyl-d_9)

CAT, Cat2p – carnitine *O*-acetyltransferase

CCT5-166 – dimethyl *R*-hydroxyglutarate

CCT5-168 – dimethyl *S*-hydroxyglutarate

CID – collision-induced dissociation

Cit2p – peroxisomal citrate synthase

CoA – coenzyme A

CPT1A – carnitine palmitoyltransferase 1A gene

CPT-1 – palmitoyltransferase-1

Crc1p – mitochondrial carnitine transporter

CTM1 – cytochrome c methyltransferase gene

DDA – data-dependent acquisition

DFO – deferoxamine mesylate salt

DMOG – dimethyl *N*-oxalylglycine

DOT1 – disruptor of telomeric silencing gene

DTT – dithiothreitol

eEF1A, EF1α – eukaryotic translation elongation factor 1 alpha

eEF2, EF2 – eukaryotic translation elongation factor 2

EF3 – elongation factor 3

EFM2 – elongation factor methyltransferase gene

EFM3 – elongation factor methyltransferase gene

EFM5 – elongation factor methyltransferase gene

EFM6 – elongation factor methyltransferase gene

ESI – electrospray ionization

EZH2 – enhancer of zeste homolog 2 gene

FAD – flavin adenine dinucleotide

FH – fumarate hydratase

FIH – factor inhibiting HIF

FTO – fat mass and obesity-associated gene

GBBH – γBB dioxygenase

GC – gas chromatography

GIS1 – Gig1-2 suppressor

GLU – L-glutamine

HAT – histone acetyltransferase

HDAC – histone deacetylase

HEK – human embryonic kidney 293T cell line

HeLa – human cervical epithelial adenocarcinoma cell line

HepG2 – human hepatocellular carcinoma cell line

HIF – hypoxia-inducible factor

HILIC – hydrophilic interaction liquid chromatography

hphMX – hygromycin gene

HPLC-MS/MS – high-pressure liquid chromatography-tandem mass spectrometry

HRP – horseradish peroxidase

HTML – 3-hydroxy TML

HTMLA – HTML aldolase

IDH1 – isocitrate dehydrogenase

IOX1 – 5-carboxy-8-hydroxyquinoline

ISO – L-isoleucine

JHD1 – JmjC domain-containing histone demethylase gene

JHD2 – JmjC domain-containing histone demethylase gene

JmjC – jumonji C domain

KDM – lysine demethylase

KMT – lysine methyltransferase

LC – liquid chromatography

LEU – L-leucine

LSD – lysine-specific demethylase

m/z – mass-to-charge ratio

MG132 – carbobenzoxy-Leu-Leu-leucinal, Z-Leu-Leu-Leu-al.

MRM – multiple reaction monitoring

MS – mass spectrometry

MS/MS – tandem mass spectrometry

NAD^+ – nicotinamide adenine dinucleotide

NOG – *N*-oxalylglycine

OCT – organic cation transporter

OCTN1 – organic cation/carnitine transporter 1

OCTN2 – organic cation/carnitine transporter 2

OD – optical density

PBS – phosphate buffered saline

PHD – plant homeodomain

PLP – pyridoxal 5'-phosphate

PMSF – phenylmethylsulfonyl fluoride

PTM – posttranslational modification

RKM2 – ribosomal protein lysine methyltransferase

RPH1 – regulator of PHR1 (photoreactivation repair deficient)

SAHA – suberoylanilide hydroxamic acid, vorinostat

SD medium – synthetic defined medium

SDEG medium – synthetic defined medium supplemented with ethanol and glycerol

SDH – succinate dehydrogenase

SDS – sodium dodecyl sulfate

SET – Su(var)3-9, Enhancer-of-zeste and Trithorax

SET1 – SET domain-containing histone methyltransferase 1

SET2 – SET domain-containing histone methyltransferase 2

Shm1p – serine hydroxymethyltransferase 1

Shm2p – serine hydroxymethyltransferase 2

SHMT – serine hydroxymethyltransferase

SILAC – stable isotope labelling with amino acid

SLC – solute carriers

T1D – type 1 diabetes

T2D – type 2 diabetes

TBST – tris-buffered saline

TCA – tricarboxylic acid cycle, Krebs cycle

TEMED – tetramethylethylenediamine

TMABA – 4-*N*-trimethylaminobutyraldehyde

TMABA-DH – TMABA-dehydrogenase

TMG – trimethylglycine, betaine

TML – 6-*N*-trimethyllysine, free trimethyllysine

TMLH – TML dioxygenase

ToF – time-of-flight

WT – wild-type

Yat1p – outer mitochondrial carnitine acetyltransferase

YPD medium – yeast peptone dextrose medium

γBB – 4-*N,N,N*-trimethylaminobutyrate, γ-butyrobetaine

γBB-d_9 – 4-*N,N,N*-trimethylaminobutyrate-(trimethyl-d_9)

Contents

1. Introduction 1

1.1 Epigenetics and its importance 1

1.1.1 Posttranslational modifications 1

1.1.2 Epigenetics enzymes 2

1.1.3 Therapeutic aspects of epigenetics 5

1.2 Energy metabolism 6

1.2.1 Carnitine importance in fatty acids metabolism in yeast and human 7

1.2.2 Carnitine shuttle in mammalian cells 7

1.2.3 Carnitine shuttle in yeast *S. cerevisiae* 8

1.2.4 Eukaryotic carnitine biosynthesis 9

1.2.5 Diseases associated with carnitine deficiency 11

2. Aims and objectives 13

3. Materials and methods 14

3.1 Yeast Saccharomyces cerevisiae 14

3.1.1 Strains 14

3.1.2 Plasmids 16

3.1.3 Primers 17

3.1.4 Stock solutions 19

3.1.5 Yeast medium 19

3.1.6 Yeast liquid cultures 20

3.1.7 Glycerol stocks 21

3.1.8 Plasmid MiniPrep purification 21

3.1.9 PCR reactions 21

3.1.10 Agarose gel electrophoresis 22

3.1.11 Transformation of yeast cells with LiOAc 22

3.1.12 Genotype analysis of yeast deletion strains 23

3.1.13 Selection of plasmid with 5-fluoroanthranilic acid 23

3.1.14 Carnitine dependency of *cit2Δ* strain 23
3.1.15 Carnitine requirement for *cit2Δ* strain 23
3.1.16 Yeast carnitine complementation assay ("halo formation assay") 24
3.1.17 Fluorometric detection of carnitine 24
3.1.18 Yeast harvesting and sample preparation for HPLC-ESI-MS/MS analysis 25
3.2 Human cell lines 25
3.2.1 Cell culture 25
3.2.2 Sample preparation for HPLC-MS/MS analysis 26
3.2.3 Sample preparation for histone analysis 26
3.2.4 Sample preparation for mitochondria analysis 27
3.2.5 Cytotoxicity assay 27
3.2.6 L-methionine and L-methionine-d_3 supplementation 28
3.3 Small molecules 28
3.3.1 Materials 28
3.3.2 Iron chelation with metformin and DFO 29
3.4 Proteins 30
3.4.1 Protein concentration measurement 30
3.4.2 SDS-PAGE gel electrophoresis 30
3.4.3 Western blotting 30
3.4.4 Protein in-gel digestion 31
3.5 Peptide mass spectrometry 32
3.5.1 HPLC-MS/MS peptide analysis 32
3.6 Metabolite mass spectrometry 32
3.6.1 HPLC-ESI-MS/MS instrument and software 32
3.6.2 ESI-MS/MS parameters 33
3.6.3 HPLC columns 33
3.6.4 Zorbax mobile phase 33
3.6.5 HILIC mobile phase 34

3.6.6 Standard samples preparation 34
3.6.7 HPLC method optimisation for Zorbax column 34
3.6.8 HPLC method optimisation for HILIC 50 mm and HILIC 150 mm columns 35
4. Establishing methods for metabolic studies 36
4.1 *S. cerevisiae* as a model organism 37
4.1.1 Carnitine dependency of the *S. cerevisiae cit2Δ* strain 37
4.1.2 Carnitine requirement for *S. cerevisiae cit2Δ* strain 39
4.1.3 Carnitine biosynthesis reconstruction in *S. cerevisiae* 40
4.1.4 Validation of *S. cerevisiae* FY23 1,2,3,4 strain capability of carnitine synthesis 41
4.2 Fluorometric method for carnitine quantification 42
4.3 HPLC-ESI-MS/MS method 44
4.3.1 Method optimisation workflow 45
4.3.2 Mass spectrometry optimisation 45
4.3.3 Liquid chromatography optimisation 46
4.3.4 Method validation for TML, γBB, CAR and A-CAR 48
4.3.5 MS/MS analysis of TML, γBB, CAR, A-CAR and CAR-d_9 50
4.3.6 HPLC-MS/MS method evaluation in yeast and human cell samples 52
4.3.7 Analysis automation 55
4.3.8 Method normalization 55
4.4 Discussion 62
5. Establishing a method for protein studies 64
5.1 Histone extraction method 64
5.2 Histones identification with HPLC-MS/MS 65
5.2.1 In-gel histone digestion 66
5.3 Discussion 71
6. Epigenetic links to carnitine metabolism in *S. cerevisiae* 72
6.1 Validation of the enzymes required for carnitine production 73

6.1.1 Obtaining FY23 1,3,4 and FY23 1,4 strains 73
6.1.2 Validation of the requirement of the second enzyme in CAR biosynthesis in FY23 strains 74
6.2 Optimisation of CAR biosynthesis in *S. cerevisiae* 75
6.2.1 Deletion of SHM1 gene in FY23 1,3,4 strain 76
6.2.2 HPLC-MS/MS analysis of *shm1*Δ strain 77
6.3 Role of *S. cerevisiae* genes linked to the cellular methylation in CAR biosynthesis 79
6.3.1 Selection of *S. cerevisiae* genes linked to the cellular methylation 79
6.3.2 Deletion of selected genes in *S. cerevisiae* strain capable of producing CAR 81
6.3.3 HPLC-MS/MS analysis of depleted strains 83
6.3.4 Summary of deletion work and conclusions 92
6.4 Effect of small molecules accessibility on lysine methylation and carnitine biosynthesis 94
6.4.1 Cellular methylation pathway inhibition 95
6.4.2 JmjC-domain mechanism inhibition 96
6.5 Discussion 97
7. Study of the role of protein methylation on carnitine biosynthesis in a human cell line model 100
7.1 Analysis of CAR biosynthesis in various cell lines 101
7.2 Role of methylation pathway on CAR biosynthesis 101
7.2.1 Treatment with methylation inhibitor 101
7.2.2 Treatment with methyl donors 106
7.3 Role of protein degradation on CAR biosynthesis 111
7.3.1 Inhibition of serine proteases using PMSF 112
7.3.2 Inhibition of the proteasomes using MG132 113
7.4 Role of PTMs cross-talk on CAR biosynthesis 117
7.5 Discussion 118

8. Study of the role of oxygenases in carnitine biosynthesis in human cell line model 121
8.1 Investigation the iron-dependent oxygenases mechanism of action 124
8.1.1 Supplementation of Fe^{2+} and vitamin C 124
8.1.2 Inhibition studies with iron chelators 125
8.2 Investigating the mechanism of action of 2-oxoglutarate-dependent oxygenases 129
8.2.1 Supplementation with 2-oxoglutarate 129
8.2.2 Competitive inhibition with dimethyloxalylglycine 129
8.2.3 Investigation the role of the Krebs cycle 132
8.2.4 Treatment with 2-hydroxyglutarate 133
8.2.5 Treatment with dimethyl-succinate and dimethyl-fumarate 135
8.3 Investigating the role of specific inhibitors 137
8.4 Discussion 139
9. Investigating the impact of metabolic modulators on CAR biosynthesis and function 142
9.1 Impact of selected metabolic modulators on CAR levels 143
9.1.1 Mildronate 143
9.1.2 Metformin 144
9.1.3 Phenformin 146
9.1.4 Combined treatments 148
9.2 Examination of metformin mode of action 150
9.2.1 Investigation of iron chelation ability of metformin 150
9.2.2 Impact of metformin on carnitine acetyltransferases 151
9.2.3 Study of competitive blockade of carnitine transporter receptors 153
9.2.4 Examination of cell viability after metformin treatment 163
9.2.5 Impact of chosen modulators on epigenetic modifications 164
9.3 Discussion 168
10. Summary 172

11. Appendix 175
11.1 Figures 175
11.2 Tables 185
12. References 186

1. Introduction

1.1 Epigenetics and its importance

In eukaryotic cells, long DNA chains are very efficiently packaged in the nucleus by being wound around nuclear proteins called histones. Four core histones (H2A, H2B, H3 and H4) create a nucleosome; an octamer unit that can host ~147 wrapped base pairs. Nucleosomes are fundamental in creating dynamic chromatin structure that play a crucial role in regulating DNA transcription [1].

Histones are globular shaped proteins possessing N-terminal tails that protrude from their own nucleosome and interact with neighbouring nucleosomes. The histone tail as an unstructured amino acid sequence is highly liable for posttranslational modifications (PTMs). By altering properties of amino acid residue, PTMs affect the histone tails structure and, thereby, modulate chromatin dynamics [2]–[4].

Histone PTMs together with DNA methylation and non-coding RNA introduce changes to the DNA transcription that may influence the outcome of the cellular phenotype [5]. In general, the study of such modifications that inheritably alter phenotype but do not change the DNA sequence is defined as epigenetics [6], [7]. Epigenetics plays a crucial role in the process of cell division as epigenetics marks guide cell differentiation pathway. It is especially important during embryonic stem differentiation or in carcinogenesis [8], [9].

1.1.1 Posttranslational modifications

To date, approximately 20 types of histones PTMs have been found including methylation (mono-, di- and tri-) [10], [11], acetylation [11], [12], phosphorylation [13], [14], propionylation[11], [15], [16] or ubiquitination [17]. It is highly probable that more PTMs will be discovered as more efficient methods of PTMs studies are being developed, e.g. sequence-specific antibodies or mass spectrometry (MS) [10]. The improvement of these methods may also contribute to a better understanding of PTMs functionality in chromatin dynamics and DNA expression.

It is known that histone PTMs regulate chromatin structure by interactions within nucleosome or through changing of histones charge states. These mechanisms affect the DNA accessibility for proteins such as transcription factors. As a result, depending on the location and the type, some PTMs are associated with gene activation or repression. For example, methylation of the histone H3 lysine 4 (H3K4) is correlated with gene activation, while methylation of lysine 9 of the same histone H3 (H3K9) is associated with

gene repression [18]. Additionally, a different type of modification at the same exact site may also result in opposite change. For example, monomethylation of H3K27 is correlated to gene activation, whereas H3K27 trimethylation is linked to transcriptional repression [19]. Therefore, the combination of different PTMs enables for complex context-dependent transcription regulation, in-depth studies of each histone site mark are crucial for understanding the epigenetic regulations in "histone code" [4].

1.1.2 Epigenetics enzymes

1.1.2.1 Lysine methylation

PTMs occur on histone tails due to the action of PTM-specific enzymes that catalyse addition or removal of these modifications. These enzymes are also called "writers" and "erasers", respectively [20].

Lysine modifications are one of the most diverse and extensively utilised modifications among PTMs [21]. Only lysine methylation provides three regulatory stages: mono-, di- and tri- methylation, each having a different impact on gene expression, however, all share a similar mechanism of methyl group adding to a lysine residue.

"Writers" that catalyse each methylation step are called lysine methyltransferases (KMTs). They require *S*-adenosylmethionine (AdoMet) as a methyl donor. The lysine residue of the substrate together with AdoMet bind to the catalytic pocket of KMT. This catalytic pocket is usually located in the SET (Su(var)3-9, Enhancer-of-zeste and Trithorax) domain, which is conserved in almost all KMTs (except for DOT1 methyltransferases), and in which the ε-amino group of the lysine residue becomes deprotonated. Once lysine is deprotonated, a methyl group of AdoMet can be transferred onto the lysine chain, which results in the liberation of methylated product and demethylated *S*-adenosylhomocysteine (AdoHcy) (Figure 1-1).

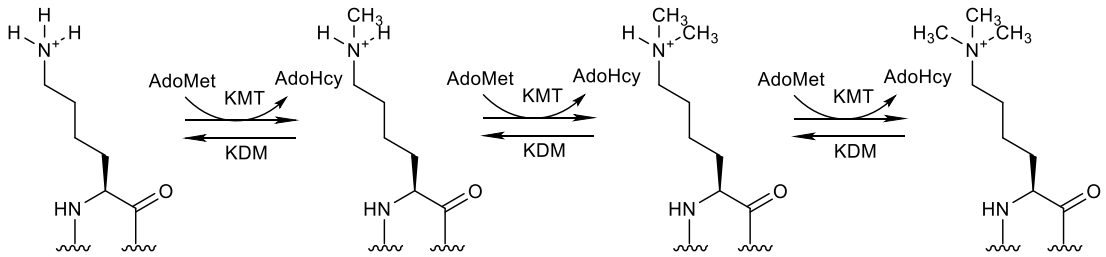


Figure 1-1: Lysine methylation states. Lysine residue can incorporate up to three methyl groups. Each of the methylation steps is regulated by specific lysine methyltransferase (KMT) ("writer") and each of the demethylation step is regulated by specific lysine demethylase (KDM) ("eraser").

AdoMet and AdoHcy are molecules involved in the cellular methylation cycle that is a highly regulated process. L-methionine is a precursor and methyl group donor for AdoMet and, therefore, directly influences cellular AdoMet abundance. In turn, methionine level is dependent on homocysteine, betaine, choline and molecules involved in the folate cycle, transsulfuration, and several other reactions (Figure 1-2).

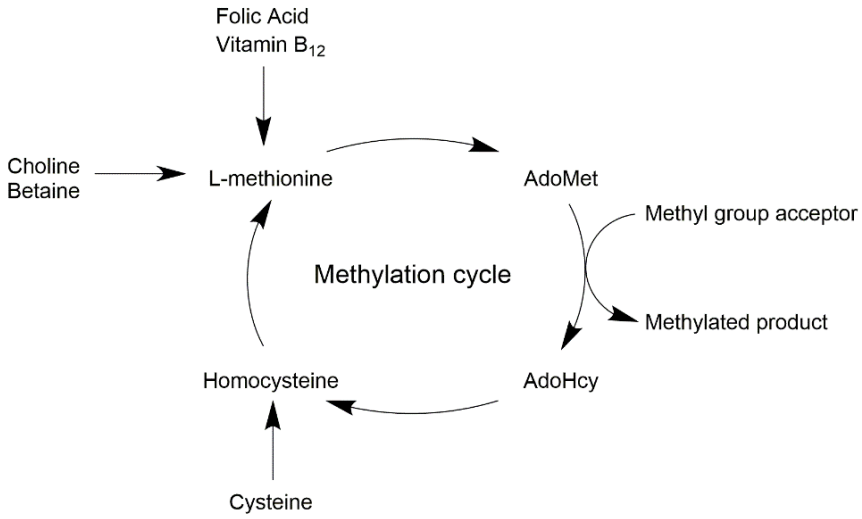


Figure 1-2: Cellular methylation cycle. AdoMet is a direct methyl group donor for acceptor. Methylation cycle involves also AdoHcy, homocysteine, L-methionine as well as transsulfuration reaction and folate cycle.

1.1.2.2 Lysine demethylation

For a long time it was believed that methylation process is stable and irreversible until the discovery of the "erasers", a large family of lysine demethylases (KDMs) capable of antagonizing lysyl methylation [22], [23].

KDMs are divided into two classes of enzymes that catalyse demethylation reaction through different mechanisms of action. The first class of KDMs, KDM1 subfamily, contains lysine-specific demethylases (LSDs) which are oxygen and flavin adenine dinucleotide (FAD)-dependent amine oxidases [22]. Only di- and mono-methylated lysine can act as a substrate for LSDs because it requires a lone pair on the methyl lysyl amine to create the imine intermediate.

The second and the largest class of KDMs (from KDM2 to KDM7 subfamilies) are 2-oxoglutarate dependent oxygenases (2OGXs) containing the Jumonji C (JmjC) domain that is conserved across all eukaryotes [23]–[25]. In contrast to the LSD class of KDMs, the 2-oxoglutarate (2OG) dependent KDMs are able to demethylate tri-, di- and monomethyl lysine residues.

2OGXs mechanism of action relies on coupling the two-electron substrate (proteins, lipids, nucleic acids, small molecules) oxidation with the oxidative decarboxylation of 2OG. This catalysis requires Fe^{2+} as a cofactor that binds to facial oxygenases amino acid triad (His-Asp/Glu-His) of a common double-stranded β-helix core ("jelly-roll"). During the reaction, the molecular oxygen is split, and one atom is transported into substrate residue, while the second oxygen atom is incorporated into succinate. The reaction also releases carbon dioxide as a by-product (Figure 1-3) [24], [26]–[31].

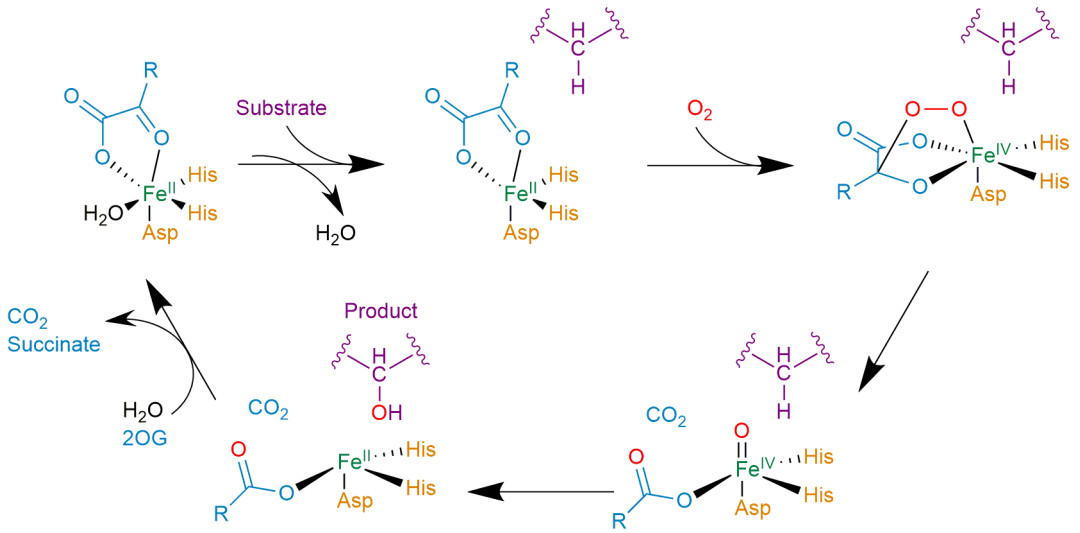


Figure 1-3: Mechanism of action of 2OG, Fe^{2+}, O_2 dependent JmjC KDMs. Colours on red indicate incorporated oxygen; green: Fe^{2+}; blue: 2OG/its products; orange: oxygenase amino acid triad; purple: substrate undergoing hydroxylation/product.

1.1.2.3 Lysine acetylation

Another well-studied lysine modification is acetylation that, occurring in histones, has been mainly linked with the open structure of chromatin enabling access for gene expression. Currently, in nomenclature, lysine acetylases are still frequently called HATs (histone acetyltransferases), while deacetylases are named HDACs (histone deacetylases) regardless of whether they act on histone or non-histone proteins [32].

HATs neutralize histone positive charge by bringing acetyl group to the lysine what in turn allows appropriate conformation for negatively charged DNA [33]. These enzymes are divided into two types depending on their localization. Type A is mainly localized in the nucleus while type B can be found in the cytoplasm [34].

HDACs remove acetyl groups from histones which brings them back the positive charge that attracts negatively charged DNA causing transcriptional silencing [33]. HDAC proteins are divided into four classes based on their homology to yeast HDACs.

Mechanism of class I and class II HDACs requires zinc for their enzymatic activity, however, their localization in cell differs. Class I HDAC is mainly nuclear, while class II can probably migrate between cytoplasm and nucleus. Class III are sirtuins that are nicotinamide adenine dinucleotide (NAD^+)-dependent enzymes [35].

1.1.2.4 Non-histone targets

In the past, researchers have believed that epigenetic enzymes only target histones, however recently many homologues have been found to be active on non-histone proteins [36]–[38]. Lysyl methylations regulate the enzymatic activity of proteins, as well as protein-protein interactions [39]. Moreover, the specificity of epigenetic enzymes is very complex as each may target more than one substrate [40]. An excellent example is a G9a methyltransferase, which is capable of dimethylating lysine K9 and K27 on histone H3, but also targets non-histone proteins including p53, G9a, reptin and others [41]–[45]. Due to that fact, appropriate nomenclature of some "writers" and "erasers" had to be modified. For instance, previously called histone methyltransferases (HMTs) ("writers") are now named as lysine methyltransferases (KMTs) to expand this classification beyond histones.

1.1.3 Therapeutic aspects of epigenetics

Epigenetics may be strictly linked to human diseases such as mental disorders or cancers [46]. Typically, human cancers are associated with DNA hypomethylation of the tumour suppressor gene promotors causing their transcriptional repression [47], [48]. The reported relationships of epigenetics with human diseases are sometimes based on finding mutations of genes coding "erasers" and "writers" leading to their impaired activities in methyl group transfer. For example, some lymphomas are correlated with mutations in *EZH2* (enhancer of zeste homolog 2) or *MLL2* (mixed-lineage leukemia 2) histone methyltransferases genes or in *UTX* (ubiquitously-transcribed X chromosome tetratricopeptide repeat protein) demethylase gene [49]–[51]. Additionally, mutations in DNA methyltransferases have been also correlated with impaired development and cancer [52]–[55]. Also, some JmjC KDMs are linked with mental retardation [46].

Currently, there is extensive work on the development of molecules targeting the altered epigenetic changes and search for their potential use for therapies against cancer. However, designing inhibitors against some classes of histone enzymes are extremely challenging due to their structural similarity and complex role of the histone marks they bring. Many discovered inhibitors are highly unselective, disturbing simultaneously multiple catalytic reactions. Lack of selectivity is also associated with the fact that most of

inhibitors target enzymes general mechanism of action. For instance, a large number of KDMs inhibitors compete with 2OG or FAD cofactors and, therefore, influence several KDMs and lysine residues. Another problem is that some of the inhibitors bind covalently to targeted enzymes causing an irreversible blockage. Nevertheless, several developed molecules were found to be promising drugs and currently undergoing clinical trials, e.g. LSD inhibitor (GSK2879552) with reversible binding characteristics or decitabine that is a DNA methyltransferase inhibitor [56]. Zinc-dependent HDAC inhibition, for instance using vorinostat (SAHA, suberoylanilide hydroxamic acid), has been recently a focus of anti-cancer therapies for T-cell lymphoma, cervical cancer or acute myeloid leukaemia [57]–[62].

Intensive research on the exact mode of action of specific "writers" and "erasers" subfamilies may allow for improving selective drug development and implying new small-molecules therapies based on epigenetic regulations. Taking into account the complexity of "histone code" interactions it may be possible that such epigenetic therapies may require multiple highly selective drugs usage to achieve an optimal clinical result [63].

1.2 Energy metabolism

While the association of epigenetics with cancer is found to be clear and has been extensively studied, the epigenetic link to energy and fatty acid metabolism is still not well explored. Such investigation is important as it may uncover key epigenetic functions for better understanding the origins of diseases such as diabetes, obesity or cardiovascular disorders. For now, preclinical studies of heart failure indicated the therapeutic potential of HDAC inhibition [64]. Also, some indirect links between diabetes and epigenetic proteins such as SET7 methyltransferase have been described [65]. Additionally, there is evidence that the maternal malnutrition during pregnancy may epigenetically influence on the risk of developing type 2 diabetes (T2D) in mature offspring [66], [67]. Currently, one of the most important findings in the area of diabetes is from GWAS studies which demonstrated that the hypermethylation of fat mass and obesity-associated (*FTO*) gene is being associated with obesity and T2D development, and same *FTO* gene encodes a 2OG-dependent demethylase [68], [69].

Moreover, since many epigenetic enzymes require metabolites or micronutrients as cofactors, e.g. KDMs uses 2OG that is intermediate in the Krebs cycle, more attention has to be placed on the epigenetic control over the energy and fatty acids metabolism.

1.2.1 Carnitine importance in fatty acids metabolism in yeast and human

One of the crucial metabolites that play an important role in fatty acid metabolism is L-carnitine (carnitine, CAR) (Figure 1-4). Carnitine shuttles the products of fatty acid β-oxidation to mitochondria. Although carnitine can be found in all types of human cells, it mainly occurs in skeletal and cardiac muscles [70]. Carnitine is popular in the fitness supplements industry as a booster of fat oxidation. Compounds interfering with carnitine biosynthesis are known human doping agents [71], thus carnitine is a subject of research on energy metabolism.

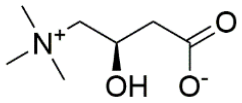


Figure 1-4: L-carnitine structure.

Carnitine was discovered during research on the insect *Tenebrio molior* as a nutrient supporting growth of its larvae and named as vitamin B_T [72]. Nowadays, carnitine is classified as a quasi-vitamin or as being conditionally-essential, similar to choline, taurine and lipoic acid [73].

1.2.2 Carnitine shuttle in mammalian cells

In mammalian cells, carnitine allows transportation of activated fatty acids to peroxisomes or to mitochondria depending on the length of the carbon chain.

In the case of long-chain fatty acids, free fatty acids are activated in the cytosol then transported across the membrane to peroxisomes, where they are shortened in the β-oxidation process. Subsequent to shortening, acetyl-coenzyme A (acetyl-CoA) molecules undergo reactions with carnitine catalysed in humans by carnitine acetyltransferase (CAT) yielding acetyl-carnitine (acetyl-CAR, A-CAR). Longer acyl groups in peroxisomes are bound to carnitine by palmitoyltransferase-1 (CPT-1). These acetyl and acyl groups in the form of carnitine esters are transported to mitochondria by carnitine-acylcarnitine translocase (CACT).

Carnitine also transports free medium-chain fatty acids directly to the mitochondria, without shortening them in peroxisomes also by actions of CPT-1 and CACT. Then, medium chain acyl-residues need to be shortened in the mitochondria to acetyl-CoA in β-oxidation process. Finally, in mitochondria, all acetyl groups are removed from carnitine

by palmitoyltransferase-2 (CPT-2) and may be utilised in the Krebs cycle (TCA) to generate energy (Figure 1-5) [74], [75].

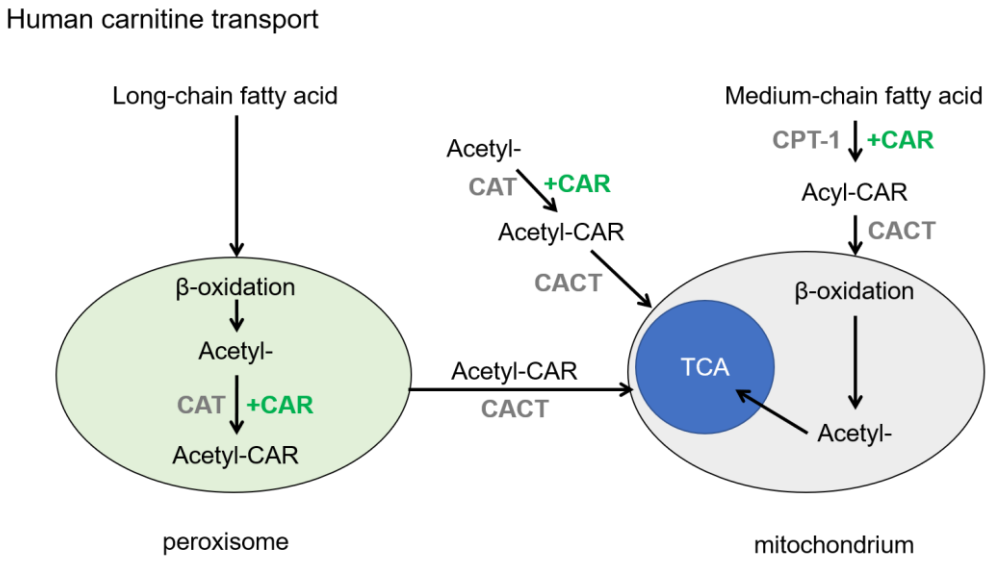


Figure 1-5: Carnitine shuttle scheme in mammalian cells. CAR – carnitine; CAT – carnitine acetyltransferase; CACT – acylcarnitine translocase; CPT-1 – palmitoyltransferase-1; for picture clarity, reactions occurring in mitochondria matrix are simplified.

To summarise, during the above biochemical conversions, carnitine not only appears as a free molecule but also bound to acetyl-, propionyl- and longer acyl groups. A tightly controlled equilibrium between free carnitine and its esters helps the organism to maintain energetic status and suggests additional roles that carnitine may play in the metabolism. For instance, by controlling the level of acyl-groups, carnitine prevents the build-up of an excess of acyl-CoA, which may be toxic for several enzyme activities. Furthermore, carnitine ensures that an excess of energy can be stored in the form of A-CAR, and plays a role in stress protection [74], [75].

1.2.3 Carnitine shuttle in yeast *S. cerevisiae*

In some eukaryotes including baker's yeast, fatty acid metabolism and carnitine utilisation differ. Regardless of the length, all fatty acids are primarily transported to peroxisomes and undergo degradation into acetyl-CoA, which is then transferred into A-CAR by carnitine acetyltransferase (Cat2p), and transported into mitochondria by mitochondrial carnitine transporter (Crc1p) [75].

Moreover, as some yeasts do not biosynthesise carnitine [76], they are able to transform acetyl-CoA molecules into succinate in the glyoxylate cycle by peroxisomal citrate synthase (Cit2p). Subsequently, succinate can be transported into mitochondria by the

succinate transporter (Acr1p) [74]. These processes are particularly important when yeasts do not have access to fermentable carbon sources like glucose, and acetyl-CoA needs to be shuttled into mitochondria (Figure 1-6).

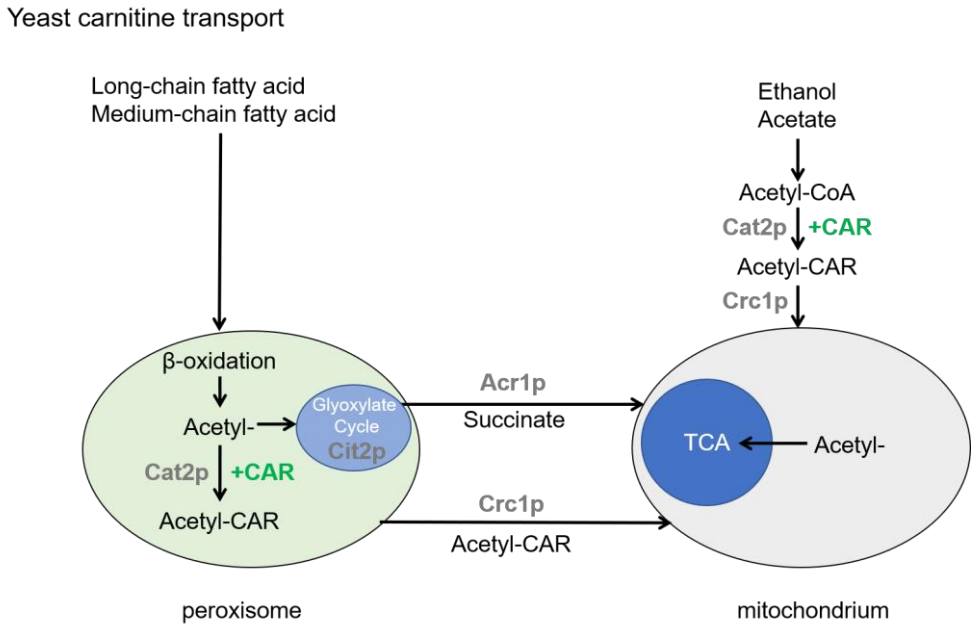


Figure 1-6: Carnitine shuttle scheme in yeast cells. CAR – carnitine; Cat2p – carnitine acetyltransferase; Crc1p – mitochondrial carnitine transporter; Acr1p – succinate transporter; Cit2p – peroxisomal citrate synthase.

1.2.4 Eukaryotic carnitine biosynthesis

There are two primary sources of carnitine in mammals, including humans: carnitine can be biosynthesised in the liver, kidney and brain, or be taken up from dietary sources. A healthy adult body requirement for carnitine is mainly (up to 75%) provided through a diet rich in meat and dairy products (2-12 µM/kg body weight/day). A vegetarian and vegan diet contains considerably less carnitine and may provide only 0.1 µM/kg body weight mg per day. Biosynthesis may deliver 1.2 µM/kg body weight of carnitine daily [70]. In the body, carnitine is not metabolised: carnitine is filtered in the kidneys and then reabsorbed, a process that helps maintain a steady carnitine concentration.

It was identified that carnitine biosynthesis is a conserved process from humans to mice and rats [77]. Further, the fruitfly *Drosophila melanogaster*, the round worm *Caenorhabditis elegans* and the yeasts *Neurospora crassa* and *Candida albicans* possess all conserved genes of carnitine biosynthesis [78]–[80].

In animal cells, trimethylated lysine is required as a precursor for carnitine biosynthesis. Except for some yeasts, free trimethyllysine (TML) cannot be produced from lysine [81].

In mammals, TML is exclusively obtained via lysosomal or proteasomal degradation of proteins that contain trimethylated lysine residues [75], [81], [82]. The main proteins containing trimethylated lysine residues include histones, actin, calmodulin, myosin, cytochrome c and eukaryotic translation elongation factor 2 (eEF2) [83]. These proteins contain the *N*-methylated lysines due to posttranslational methylations (see section 1.1.2).

After degradation of proteins containing trimethylated lysine, the biosynthesis of carnitine from TML requires four consecutive enzymatic steps (Figure 1-7). TML (6-*N*-trimethyllysine) is converted into 3-hydroxy TML (HTML) by TML dioxygenase (TMLH), which is a 2OG, O_2 and Fe^{2+} dependent enzyme. Afterwards, HTML is processed to 4-*N*-trimethylaminobutyraldehyde (TMABA) by HTML aldolase (HTMLA). TMABA undergoes a reaction with TMABA-dehydrogenase (TMABA-DH), leading to 4-*N,N,N*-trimethylaminobutyrate (γBB) production. Subsequently, γBB is converted into carnitine by another 2OG, O_2, Fe^{2+} dependent enzymatic reaction with γBB dioxygenase (GBBH).

Thus, carnitine biosynthesis in the body might be limited by several factors including availability of its precursor TML, and the activity of enzymes occurring in the pathway.

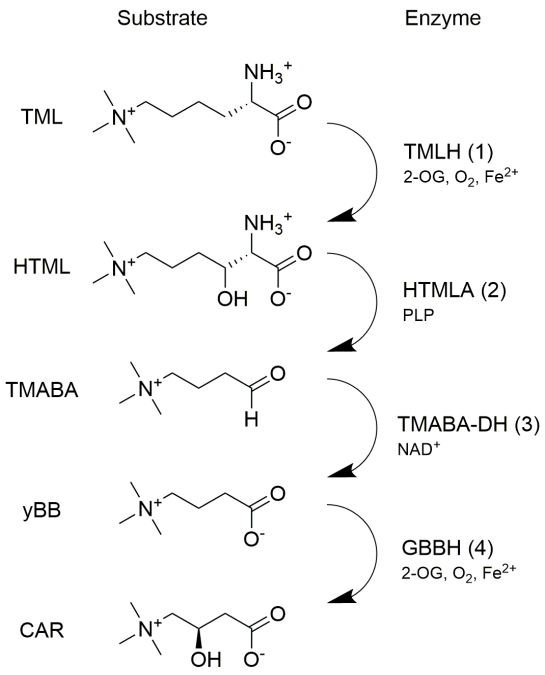


Figure 1-7: The biosynthesis of CAR from TML requires four consecutive enzymatic steps. 6-N-trimethyllysine (TML) is converted into HTML (3-hydroxy TML) by TMLH (TML dioxygenase), which is a 2OG, O_2 and Fe^{2+} dependent enzyme. Afterwards, HTML is processed to TMABA (4-N-trimethylaminobutyraldehyde) by HTMLA (HTML aldolase). TMABA undergoes reaction with TMABA-DH (TMABA-dehydrogenase) leading to γBB (4-N,N,N-trimethylaminobutyrate) production. Subsequently, γBB is converted into CAR by another 2OG, O_2 and Fe^{2+} dependent enzymatic reaction with GBBH (γBB dioxygenase); PLP – pyridoxal 5'-phosphate; NAD+ - nicotinamide adenine dinucleotide.

1.2.5 Diseases associated with carnitine deficiency

Proper carnitine homeostasis is kept by balancing carnitine endogenous biosynthesis, absorption from the diet, and renal reabsorption. However, carnitine deficiency still may occur during malnutrition, a vegan or unbalanced diet, kidney or liver disorders or due to the mutations of genes playing a role in carnitine activity. For instance, mutations in gene *SLC22A5* coding carnitine transporters OCTN (organic cation/carnitine transporter), that allow carnitine intake to cells, leads to primary carnitine deficiency [84]–[87]. As a result, patients are not able to accumulate most of the carnitine and their fatty acid oxidation is defective.

Carnitine deficiency may lead to myopathy (muscular weakness) and cardiomyopathy (heart muscle disease), arrhythmia and even death in a young age [75], [85], [88], [89]. Interestingly, carnitine supplementation is sufficient to prevent some of the mentioned complications, for instance, carnitine administration has been successfully used to treat heart failure [90].

Additionally, it was found that carnitine deficiency is correlated with risk of type 1 diabetes (T1D) and nervous system diseases, i.e. autism [91], [92]. One of the reported associations to autism is defects in carnitine biosynthesis enzyme *TMLHE* gene [93]–[95]. Therefore, recently more attention has been placed to the role of carnitine in other neurodegenerative disorders such as Alzheimer, Parkinson and schizophrenia [96]–[98]. Interestingly, carnitine esters have been linked with inhibition of histone deacetylases what may be beneficial for the treatment of neurodegenerative disorders, therefore, showing evidence of the association of a link between carnitine and epigenetics [96]–[98].

2. Aims and objectives

The aim of this thesis is to investigate to which extent the levels of protein lysyl trimethylation, an important epigenetic modification affects cellular carnitine levels, an essential regulator of fatty acid metabolism. This subject is important because an increased understanding on how epigenetic mechanisms link with basic cell metabolism can identify new approaches for pharmacological intervention, and contribute to a better understanding of associated diseases which include obesity, diabetic neuropathy and cardiomyopathy.

Specific objectives of this thesis include:

1. Selection of appropriate eukaryotic model organisms for studying the link between epigenetics and carnitine metabolism;
2. Development of rapid, sensitive and quantitative methodology for versatile and accurate determination of cellular carnitine levels and related metabolites;
3. Development of methodology for protein analysis to enable the investigation of the effect of *S. cerevisiae* genetic modifications and human cell line drug treatments on histone posttranslational modifications;
4. Genetic studies on *S. cerevisiae* that enable a correlation between epigenetics pathways, and those of cellular methylation enzymes in carnitine biosynthesis;
5. Small-molecule manipulation of a human cell line to build on the investigation of the role of cellular methylation and protein degradation pathways on carnitine biosynthesis;
6. Investigation of the importance of oxygenases in carnitine biosynthesis, including their inhibition with small molecules and the importance of Krebs cycle intermediates;
7. A study of the impact of clinically used energy metabolism modulators on carnitine biosynthesis, and products of fatty acid β-oxidation shuttle.

3. Materials and methods

3.1 Yeast Saccharomyces cerevisiae

3.1.1 Strains

All yeast strains used in this study are haploid derivatives of the *Saccharomyces cerevisiae* strains FY631 (Table 3-1), FY23 (Table 3-2) or BY4742 (Table 3-3).

3.1.1.1 FY631 strains

The FY631 strains were obtained from Bauer laboratory (Franken et al. 2015).

Table 3-1: Detailed genotypes of FY631 yeast strain used in this study.

Yeast strain	**Relevant genotype**	**Source**
FY631 WT	*MAT***a** *his4-917δ leu2Δ1 lys2-173R2 trp1Δ63 ura3-52*	Franken et al. 2015
FY631 *cit2Δ*	*MAT***a** *his4-917δ leu2Δ1 lys2-173R2 trp1Δ63 ura3-52 cit2::trp1*	Franken et al. 2015

3.1.1.2 FY23 strains

The FY23 strain was complemented with carnitine biosynthesis genes of *Neurospora crassa* [79] and, therefore, is capable of carnitine biosynthesis. The numbers behind strains names indicate with which genes of the carnitine biosynthesis pathway of *Neurospora crassa* the parent strain has been complemented (Table 3-2). The corresponding numbered enzymes are shown in *Figure 3-1*. Genomic deletions of strain FY23 1,3,4 were performed and described in this study.

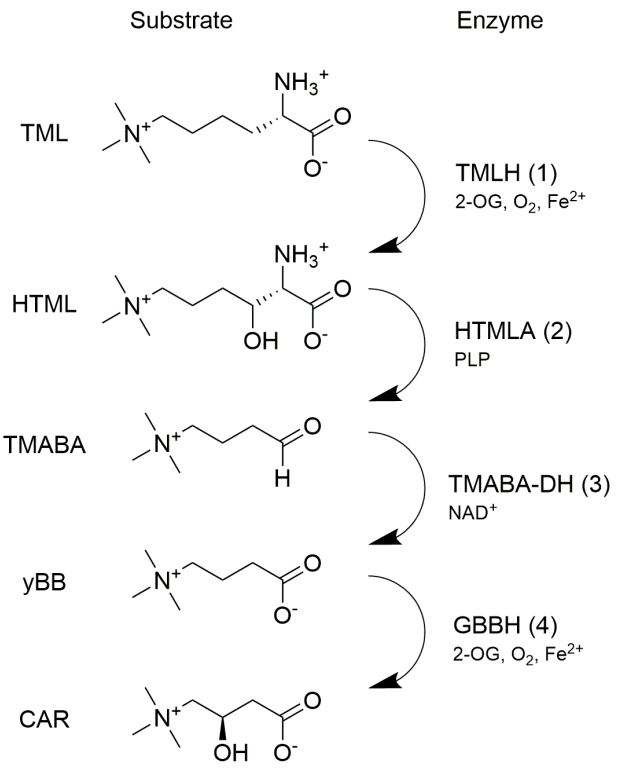


Figure 3-1: Four-step carnitine biosynthesis pathway: 1 – TMLH; 2 – HTMLA; 3 – TMABA-DH; 4 – GBBH; PLP – pyridoxal 5'-phosphate; NAD+ – nicotinamide adenine dinucleotide.

Table 3-2: Detailed genotypes of FY23 yeast strain used in this study.

Yeast strain	**Relevant genotype**	**Source**
FY23 1,4	*MAT***a** *ura3-52 trp1Δ63 leu2Δ1 TMLH BBH*	this work
FY23 1,2,4	*MAT***a** *ura3-52 trp1Δ63 leu2Δ1 TMLH HTMLA BBH*	Franken et al. 2015
FY23 1,3,4	*MAT***a** *ura3-52 trp1Δ63 leu2Δ1 TMLH TMABA-DH BBH*	this work
FY23 1,2,3,4	*MAT***a** *ura3-52 trp1Δ63 leu2Δ1 TMLH HTMLA TMABA-DH BBH*	Franken et al. 2015
FY23 1,3,4 *rkm2Δ*	*MAT***a** *ura3-52 trp1Δ63 leu2Δ1 TMLH TMABA-DH BBH rkm2::hphMX4*	this work
FY23 1,3,4 *rph1Δ*	*MAT***a** *ura3-52 trp1Δ63 leu2Δ1 TMLH TMABA-DH BBH rph1::hphMX4*	this work
FY23 1,3,4 *jhd2Δ*	*MAT***a** *ura3-52 trp1Δ63 leu2Δ1 TMLH TMABA-DH BBH jhd2::hphMX4*	this work
FY23 1,3,4 *set2Δ*	*MAT***a** *ura3-52 trp1Δ63 leu2Δ1 TMLH TMABA-DH BBH set2::hphMX4*	this work
FY23 1,3,4 *shm1Δ*	*MAT***a** *ura3-52 trp1Δ63 leu2Δ1 TMLH TMABA-DH BBH shm1::trp1*	this work

3.1.1.3 BY4742 strains

Strain BY4742 and its derivatives were obtained from yeast knockout consortium (Euroscarf) and their parental genotype is MAT**a** *his3Δ1 leu2Δ0 lys2Δ0 ura3Δ0* [99] (Table 3-3).

Table 3-3. Deleted genes in the BY4742 strain used in this study.

Yeast strain	**Systematic name of deleted gene**	**Relevant genotype**	**Source**
BY4742	*n.a*	MAT**a** *his3Δ1 leu2Δ0 lys2Δ0 ura3Δ0*	Euroscarf
BY4742 *set2Δ*	*YJL168C*	MAT**a** *his3Δ1 leu2Δ0 lys2Δ0 ura3Δ0 set2::kanMX4*	Euroscarf
BY4742 *dot1Δ*	*YDR440W*	MAT**a** *his3Δ1 leu2Δ0 lys2Δ0 ura3Δ0 dot1::kanMX4*	Euroscarf
BY4742 *rph1Δ*	*YER169W*	MAT**a** *his3Δ1 leu2Δ0 lys2Δ0 ura3Δ0 rph1::kanMX4*	Euroscarf
BY4742 *gis1Δ*	*YDR096W*	MAT**a** *his3Δ1 leu2Δ0 lys2Δ0 ura3Δ0 gis1::kanMX4*	Euroscarf
BY4742 *jhd1Δ*	*YER051W*	MAT**a** *his3Δ1 leu2Δ0 lys2Δ0 ura3Δ0 jhd1::kanMX4*	Euroscarf
BY4742 *jhd2Δ*	*YJR119C*	MAT**a** *his3Δ1 leu2Δ0 lys2Δ0 ura3Δ0 jhd2::kanMX4*	Euroscarf
BY4742 *ctm1Δ*	*YHR109W*	MAT**a** *his3Δ1 leu2Δ0 lys2Δ0 ura3Δ0 ctm1::kanMX4*	Euroscarf
BY4742 *efm2Δ*	*YBR271W*	MAT**a** *his3Δ1 leu2Δ0 lys2Δ0 ura3Δ0 efm2::kanMX4*	Euroscarf
BY4742 *efm3Δ*	*YJR129C*	MAT**a** *his3Δ1 leu2Δ0 lys2Δ0 ura3Δ0 efm3::kanMX4*	Euroscarf
BY4742 *efm5Δ*	*YGR001C*	MAT**a** *his3Δ1 leu2Δ0 lys2Δ0 ura3Δ0 efm5::kanMX4*	Euroscarf
BY4742 *efm6Δ*	*YNL024C*	MAT**a** *his3Δ1 leu2Δ0 lys2Δ0 ura3Δ0 efm6::kanMX4*	Euroscarf

3.1.2 Plasmids

All plasmids used in this study are listed in Table 3-4 and Table 3-5. *Escherichia coli* NEB-10β ultracompetent cells were used as a host for the construction and propagation of all plasmids.

Table 3-4: Plasmids used to amplify the hphMX (hygromycin) and trp1 genes.

Backbone	**Genotype**	**Source**
YEplac112	2μ TRP1	Gietz and Akio, 1988
pAG32	hphMX4	Goldstein and McCusker, 1999

Table 3-5: Plasmids used to provide carnitine biosynthesis capability.

	Backbone	Genotype	Info	Source
1	pRS305-TMLH	CEN6 LEU2 PGK1p-TMLH-PGK1t	TMLH (integrating vector targeting *LEU2* locus)	Franken et al. 2015
2	YCpLac22-PGK1pt-HTMLA	CEN4 TRP1 PGK1p-HTMLA-PGK1t	HTMLA (NcSHMT gene on centromeric *TRP1* plasmid)	Franken et al. 2015
3	pCEL13-TMABA-DH	2µ URA3 TMABA-DH	TMABA-DH (2µ plasmid)	Franken et al. 2015
4	pSP-PGK1pt-BBH	SMR PGK1p-BBH-PGK1t	BBH (integrating vector targeting *ILV2* locus)	Franken et al. 2015

3.1.3 Primers

Primer sequences used in this study can be found in Table 3-6 and Table 3-7. All were purchased from Sigma-Aldrich.

Table 3-6: Primers used for gene amplification.

Primer	Sequence
SHM1 fwd	AAAAATCATCAAGCCGACATTTCCACATCGAGTCTCATAGTCTTTCAATCATGTTTCCCAATGTCTGTTATTAATTTCACAGGTAGTTC
SHM1 rev	GTGGCTGTATATGTTAATACATAAAGTATTTGATTTTAAATCATAATTACCTATTTCTTAGCATTTTTGACGAA
CTM1 fwd	CCATCCTCATAACCACTGAAAAATCGAAGTTAACCAAAAGGAAAGTTGAAATGGGTAAAAAGCCTGAACTCAC
CTM1 rev	AGAAAGGACAACTAAAAACATTTATATACAAGATCGTAAGTGGTACTCATTTATTCCTTTGCCCTCGGACG
RKM2 fwd	ATACAGATTTTGAATAAATATCTACAAAAAAGTTACATAGTAAATTGCGAATGGGTAAAAAGCCTGAACTCAC
RKM2 rev	GGGCACTGGCACTTCCGAATTTAAAGTTATTTCTTGGACTTTACAAATACTTATTCCTTTGCCCTCGGACG
SET1 fwd	TAACATTCCTTATTTGTTGAATCTTTATAAGAGGTCTCTGCGTTTAGAGAATGGGTAAAAAGCCTGAACTCAC
SET1 rev	AGCAACGATATGTTAAATCAGGAAGCTCCAAACAAATCAATGTATCATCGTTATTCCTTTGCCCTCGGACG
SET2 fwd	AGTCGTGCTGTCAAACCTTTCTCCTTTCCTGGTTGTTGTTTTACGTGATCATGGGTAAAAAGCCTGAACTCAC
SET2 rev	CTTTGGGACAGAAAACGTGAAACAAGCCCCAAATATGCATGTCTGGTTAATTATTCCTTTGCCCTCGGACG
DOT1 fwd	AAGGAGGTCACCAGTAATTGTGCGCTTTGGTTACATTTTGTTGTACAGTAATGGGTAAAAAGCCTGAACTCAC
DOT1 rev	TATTTCTACTTAGTTATTCATACTCATCGTTAAAAGCCGTTCAAAGTGCCTTATTCCTTTGCCCTCGGACG
RPH1 fwd	GAAAAAAAGAATAAGACTGTCTTGGTGAGGATATTCAGTTGCGTGAAATCATGGGTAAAAAGCCTGAACTCAC
RPH1 rev	TTAAGAGCCTTCAAAATGAGAGATCTCGGTAAACAACTGGCAATCGTGAGTTATTCCTTTGCCCTCGGACG

JHD2 fwd	TCTAGATCATATTAACTAATCTCATCTTGCACAAAAAACGTATCACTATCA TGGGTAAAAAGCCTGAACTCAC
JHD2 rev	TGCCAAGTATTATTCTAAAAAATCATTACGCCATACACAAATATTGAAGAT TATTCCTTTGCCCTCGGACG
EFM3 fwd	AAGCAGAAAAATCGAGCTAGTAAAACTTGACCCTCCTCGTCAAAGATAACA TGGGTAAAAAGCCTGAACTCAC
EFM3 rev	TTTTTTTTTTAGTTATGTTTTATTTTTGAACTTGTACTTGCACATGTATCT TATTCCTTTGCCCTCGGACG

Table 3-7: Primers used for deletion verification.

Primer	**Sequence**
SHM1 fwd	GCCTCTTGGAGAAGAGCAAA
SHM1 rev	CAATGAACAGGGAAATATACTGGA
CTM1 fwd	GCAATGCTAGATCGTGTAAAGG
CTM1 rev	GGAAAAACGCGTCAGATTGT
RKM2 fwd	GCTAAAACTGGATGCGTCTACT
RKM2 rev	GCACATGTACTTGCGAAGAG
SET1 fwd	GTATTTATCTTTACCTTTTGCTGGA
SET1 rev	GCAACCCTCAACTTACGAGA
SET2 fwd	AGCTTTTCAAAGGGGCTTTC
SET2 rev	CGCAATTACAATTAAAGTACAAGAC
DOT1 fwd	TCGTCGTCTTAATTGCCTTG
DOT1 rev	GGCGCCTTATCCTTCTTTT
RPH1 fwd	CCACTTATTTTATAGATCTGCTGGA
RPH1 rev	ATTAGTGAATGTGGGTTTTCG
JHD2 fwd	CAACGCAGGCTCAATGTAGA
JHD2 rev	CGCTAAAAGTGGCGTGCTAA
EFM3 fwd	TCGCAAAAATGATGAAGAATG
EFM3 rev	GACTCGAGTGTCAGAAGATG

3.1.4 Stock solutions

The composition of the typical yeast stock solutions and other buffers used in assays is described in Table 3-8.

Table 3-8: Stock solutions were prepared as required.

Solution	Composition
Glycerol stock solution	65% (v/v) glycerol
	0.1 M $MgSO_4$
	0.025 M Tris HCl
TAE buffer	40 mM Tris
	20 mM acetic acid
	1 mM EDTA
LiTE buffer	0.1 M Lithium acetate
	10 mM Tris-HCl pH 7.9
	1 mM EDTA
PLATE buffer	40% (v/v) Polyethylene Glycol 3500
	0.1 M Lithium Acetate
	10 mM Tris-HCl pH 7.9
	1 mM EDTA
Yeast lysis buffer	20 µM Tris pH 8.0
	50 µM KCl
	2 µM DTT
	10 µM $MgCl_2$
	Protease inhibitor 1 tablet (SIGMAFAST, Sigma)

3.1.5 Yeast medium

For strain maintenance strains were cultured on autoclaved YPD medium (Table 3-9) supplemented with 2% (w/v) D-glucose; for experimental growth, BY4742, FY631 and FY23 strains were grown using autoclaved 10X SD (synthetic defined) minimal medium supplemented with amino acids according to genotype requirements (L-histidine, L-leucine, L-tryptophan and/or L-uracil). Normally, for growth on fermentable carbon source SD medium contained 2% (w/v) glucose. For studies on non-fermentable carbon source, instead of glucose, 1% (w/v) glycerol and 3% (v/v) ethanol were used in SD medium (SDEG medium). For agar plates, agar (2% (w/v)) was added to the otherwise identical medium. SD media content and amino acid supplements are listed in Table 3-10.

Table 3-9: YPD yeast media content

Buffer	Composition
YPD medium (1 L)	20 g peptone
	10 g yeast extract

Table 3-10: SD yeast media and amino acid supplements content

Buffer	Composition
12.5X Initial amino acid stock solution (1 L)	250 mg L-adenine sulphate
	250 mg L-arginine hydrochloride
	250 mg L-methionine
	375 mg L-tyrosine
	375 mg L-isoleucine
	375 mg L-lysine hydrochloride
	625 mg L-phenylalanine
	1250 mg L-glutamic acid
	1250 mg L-aspartic acid
	1850 mg L-valine
	2500 mg L-threonine
	5000 mg L-serine
10X Final SD medium (475 mL) pH 5.8	8.5 g yeast nitrogen base without amino acids and without ammonium sulphate
	25 g ammonium sulphate
	400 mL of the sterile 12.5X initial amino acid stock solution
20X uracil (100 mL)	40 mg uracil
20X L-tryptophan (100 mL)	40 mg L-tryptophan
100X L-histidine hydrochloride (100 mL)	200 mg L-histidine hydrochloride
100X L-leucine (100 mL)	1000 mg L-leucine

3.1.6 Yeast liquid cultures

Yeast liquid cultures were inoculated with cells from glycerol stock or a single colony selected from YPD-Agar or SD-Agar plate. The cultures were incubated overnight (approx. 16 h, 30 °C, 180 rpm) on appropriate YPD or SD medium. In order to control yeast growth, the optical density (OD) was monitored in selected time points. The cuvette with 100 µL of liquid culture diluted in 900 µL of Milli-Q water was placed in UV 1101 Biotech Photometer (WPA) and its absorbance was measured at 595 nm.

3.1.7 Glycerol stocks

For the purpose of long term storage, glycerol stocks were prepared from overnight yeast cultures which had been selected from individual colonies grown on YPD or SD agar plates. The glycerol stocks were prepared by combining 50% of overnight culture and 50% of glycerol stock solution (Table 3-8).

3.1.8 Plasmid MiniPrep purification

Zyppy Plasmid Miniprep Kit (D4036, D4019, D4020 & D4037) was used to extract plasmid DNA from *E. coli*. 5 mL of overnight culture was pelleted by centrifugation (1,000 g, 5 min) and resuspend in 600 µL of water. Next, 100 µL of 7X lysis buffer (provided with the kit) was mixed by inverting the tube 5 times and 350 µL of neutralisation buffer was added and again mixed by inverting the tube. Subsequently, the sample was centrifuged at 16,000 g for 3 min and the supernatant was transferred into provided Zymo-Spin IIN column placed in a collection tube and centrifuged for 15 s. The flow-through was discarded and the column was placed back into a collection tube. 200 µL of endo-wash buffer was added to the column and centrifuged for 1 min at 16,000 g. Subsequently, the column was transferred into a sterile 1.5 mL tube and 30 µL of autoclaved water was added onto the column membrane. After 1 min of incubation at RT, the column was centrifuged for 30 s to elute the plasmid DNA into an Eppendorf tube. The plasmid DNA product was stored at -20 °C.

3.1.9 PCR reactions

PCR reactions contained 1x One Taq Quick-Load 2X Master Mix with standard buffer (BioLabs), 100 ng template DNA and 0.5 nM of each forward and reverse primers (Table 3-11). The PCR was set up using thermal cycler (3Prime, Techne) (Table 3-12).

Table 3-11: Optimized PCR thermal cycler program for amplification and validation of genomic deletions.

Reagent	**Volume [µL]**
2x mix	12.5
Forward Primer	1 (0.5 µM final c.)
Reverse Primer	1 (0.5 µM final c.)
Template DNA	1 (4 ng/µL final c.)
Water	10.5

Table 3-12: Optimized PCR thermal cycler program for amplification and validation of genomic deletions.

Step		Temperature	Time
Stage I: Initial Denaturation		98 °C	1 min
Stage II: (40 cycles)	Denaturation	98 °C	30 s
	Annealing	55 °C	30 s
	Extension	68 °C	2 min
Stage III: Final extension		68 °C	5 min
Stage IV: Hold		10 °C	Hold

3.1.10 Agarose gel electrophoresis

Agarose gels were used for confirmation of amplification and validation of genomic deletions. A 1% (w/v) agarose gel was prepared by dissolving 0.9 mg agarose in 50 mL TAE buffer by heating in the microwave. Subsequently, 5 µL of SYBR Safe DNA gel stain (Invitrogen) was added and poured into the cast and the sample loading comb was inserted.

3.1.11 Transformation of yeast cells with LiOAc

To obtain the FY23 1,3,4 *ctm1Δ*, *rkm2Δ*, *set1Δ*, *set2Δ*, *dot1Δ*, *rph1Δ*, *jhd2Δ* and *efm3Δ* strains, the corresponding gene was replaced by the *hphMX4* gene utilizing homologous recombination method by LiOAc transformation of PCR products. For this purpose, the pAG32 plasmid was used to amplify *hphMX4* by PCR using suitable primers (Table 3-6). Then the 1185 bp disruption cassette containing the *hphMX4* gene with corresponding gene flanking regions was isolated and transformed into the FY23 1,3,4 strain. For this, 5 mL liquid culture of FY23 1,3,4 strain (at OD 1.0) was centrifuged, the pellet washed with water and resuspended in 1 mL LiTE buffer (Table 3-8). Then 5 µL of PCR product, 5 µL sheared, salmon sperm DNA, 50 µL of the cell suspension and 250 µL PLATE buffer (Table 3-8) were incubated for 15 min at 30 °C and subsequently at 42 °C for 60-90 min. The cell pellet was collected, washed, resuspended in 500 µL of YPD medium and incubated at 30 °C for 3-4 h to allow gene expression. After incubation, cells were washed and plated on fully supplemented SD medium agar plates containing 0.3 mg/mL hygromycin B.

To construct FY23 1,3,4 *shm1Δ*, the TRP1 auxotrophic marker was utilized. The *TRP1* gene containing cassette from the YEplac122 plasmid was amplified by PCR chain reaction using the *SHM1* primers (Table 3-6). The 675 bp (+100 bp) product containing *TRP1* gene with *SHM1* flanking regions was isolated and transformed into the appropriate single

gene deletion of FY23 1,3,4 and the original FY23 1,3,4 strain. Subsequent steps were performed as described above.

3.1.12 Genotype analysis of yeast deletion strains

In order to confirm the transformations, genomic DNA isolation was performed. Single colonies of transformants were chosen and cultured in 5 mL of appropriate medium. The cell pellet was collected, washed and resuspended in 500 µL of lysis buffer (Table 3-8). Acid washed glass beads were added up to 1.25 mL and vortexed for 2 min and next centrifuged. The liquid phase was collected, 275 µL of 7 M ammonium acetate pH 7.0 was added and incubated for 5 min at 65 °C and 5 min on ice. Subsequently, 500 µL of chloroform was added, vortexed and centrifuged. The top layer was collected, incubated with 1 mL of isopropanol for 5 min at RT and centrifuged. The obtained pellet was washed with 70% (v/v) ethanol, centrifuged and dissolved in 20 µL H_2O. The concentration of the DNA was measured on NanoDrop ND-1000 Spectrophotometer. The genomic DNA was initially analysed by PCR using corresponding checking primers (Table 3-7). Sanger sequencing was used for final verification of gene sequences.

3.1.13 Selection of plasmid with 5-fluoroanthranilic acid

To remove plasmid providing HTMLA enzyme FY23 1,2,4 and FY23 1,2,3,4 strains were plated as a mat on SD agar plates supplemented with 2% (v/v) glucose and 5-fluoroanthranilic acid (5-FAA) (1 mg/mL) and incubated at 30 °C for 3 d.

3.1.14 Carnitine dependency of *cit2Δ* strain

In order to investigate carnitine dependency of FY631 *cit2Δ* strain the overnight liquid culture of *cit2Δ* strain on SD medium supplemented with glucose was prepared. Then 20 µL of liquid culture was plated on SD with glucose or SDEG with ethanol and glycerol agar plates supplemented with 20 µg/mL of CAR. Plates were incubated at 30 °C for 6 d.

3.1.15 Carnitine requirement for *cit2Δ* strain

In order to investigate the FY631 *cit2Δ* strain carnitine requirements for non-fermentable growth, the overnight liquid culture of *cit2Δ* strain on SD medium supplemented with glucose was prepared. Then 2 µL of serial dilutions of liquid culture were plated on SDEG agar plates supplemented with different concentrations of CAR. Plates were incubated at 30 °C for 6 d.

3.1.16 Yeast carnitine complementation assay ("halo formation assay")

In order to phenotypically observe carnitine biosynthesis, an overnight liquid culture on glucose of carnitine-depended *cit2Δ* strain was prepared, washed and streaked on agar plate containing the desired carbon source (non-fermentable: ethanol and glycerol (SDEG) or fermentable: glucose (SD) and, as appropriate, supplemented with L-carnitine, TML and/or γBB. 5 µL drops of an SD liquid culture of FY23 1,3,4 mutant were placed on the prepared agar plates with a *cit2Δ* mat and incubated at 30 °C for 6 d to investigate whether *cit2Δ* growth was supported via the production of carnitine, creating a "halo" of cell growth around the drop.

To investigate the interaction with cellular metabolic pathways, the agar plates were additionally supplemented, list of supplements and their concentrations can be found in (Table 3-13).

3.1.17 Fluorometric detection of carnitine

To determine the amount of biosynthesised carnitine, a liquid culture of FY23 1,3,4 mutant strain was prepared in SD medium containing glucose with the addition of γ-butyrobetaine hydrochloride (γBB, Sigma-Aldrich) (200 mg/L) and was incubated for up to 48 h. Cell pellets were collected after 24 h and 48 h of growth, washed with phosphate buffered saline (PBS, Fisher), resuspended in 1 mL Assay Buffer (Abcam kit, ab83392) and homogenized by vigorous pipetting. Lysates were centrifuged at 12,500 g for 2 min and collected into new tubes. Next, ice-cold perchloric acid was added to a final concentration of 1 M and incubated for 5 min. Samples were centrifuged at 12,500 g for 2 min and supernatants were transferred into new tubes. The excess of perchloric acid was neutralised using 2 M KOH, and the pH was adjusted to 6.5-8.0 with 0.2 M KOH. Samples were again centrifuged at 12,500 g for 15 min and supernatants were collected into fresh tubes. After the deproteinization, CAR content was measured by an L-carnitine fluorometric assay by adding to the microplate 10 µL of sample and 50 µL of Reaction Mix and incubating it for 30 min protected from light (L-carnitine quantification Assay kit, Abcam, ab83392). Next, according to the manufacturer's protocol, the Ex/Em = 535/587 nm was measured on a microplate reader (Spark 10M, Tecan).

3.1.18 Yeast harvesting and sample preparation for HPLC-ESI-MS/MS analysis

In order to obtain yeast lysate, after the cultures reached an absorbance value at 595 nm of ~2.5, 10 mL of the 50 mL cultures were collected and centrifuged (1,000 g, 5 min, 20 °C). Supernatants were removed and the pellets were washed with water (1 mL). After centrifugation (73 g, 5 min, 20 °C), supernatants were removed and pellets were resuspended in 500 µL of yeast lysis buffer (100 mM Tris pH 8.0, 50 mM EDTA, 1% (w/v) sodium dodecyl sulfate (SDS)). The lysis was performed on a Precellys 24 homogenizer (Bretin Instruments), each sample was spun at a speed of 6,500 rpm for 15 s, then cooled on ice for 1 min and this process was repeated five times. The protein concentrations of the lysates were determined using Pierce bicinchoninic acid assay (BCA) (Thermo Scientific). Samples were normalized by diluting with water. Lysates were deproteinated by adding 75% by volume ethanol and heated at 95 °C for 5 min. The samples were then centrifuged (14,000 g, 10 min, 20 °C) and the supernatant was kept at -80 °C for 30 min to aid further precipitation of proteins. After centrifuging (14,000 g, 10 min, 20 °C) the supernatant was heated at 70 °C until all the ethanol had evaporated. The samples were resuspended in water (50 µL) and HPLC-ESI-MS/MS analysis was performed.

3.2 Human cell lines

3.2.1 Cell culture

HepG2 (human hepatocellular carcinoma cells), HeLa (human cervical epithelial adenocarcinoma) and HEK (human embryonic kidney 293T) cell lines were provided by Pritesh Mistry, Lia Blockpoel Ferreras and James Dixon from Wolfson Centre for Stem Cells, Tissue Engineering, and Modelling at University of Nottingham. HepG2 cells were cultured in Minimum Essential Medium Eagle medium (Lonza) and HeLa and HEK in Dulbecco's Modified Eagle Medium (Gibco), all containing 10% (v/v) foetal bovine serum (Sigma), 1% (v/v) antibiotic-antimycotic (Sigma), 1% (v/v) penicillin-streptomycin (Fisher), 1% (v/v) L-glutamine (Sigma) at 37 °C in a humidified incubator with 5% CO_2. Cells were passaged every 3-4 d using 0.25% (w/v) Trypsin (Sigma or Gibco).

3.2.2 Sample preparation for HPLC-MS/MS analysis

Cells were seeded onto 6-well plates (1 x 10^6 cells/well) or 12-well plates (0.5 x 10^6 cells/well) and were treated with a selected drug for the desired amount of time. Next, cells were washed twice with cold PBS and 200 µL of lysis buffer was added into growing cells on the well plate. Lysis buffer contained 20 mM Tris-HCl, 0.1% (v/v) Tween-20, 1x protease inhibitor cocktail (SIGMAFAST, Sigma; contains: AEBSF 2 mM, phosphoramidon disodium salt 1 µM, Bestatin hydrochloride 130 µM, E-64 14 µM, Leupeptin 1 µM, Aprotinin 0.2 µM, Pepstatin A 10 µM) and, where appropriated, DL-carnitine-(trimethyl-d_9) hydrochloride (CAR-d_9) isotope (1 µg/mL). Next, cells were lysed on ice for 10 min with gentle stirring, scraped and centrifuged at 6,500 g for 10 min at 4 °C. Cell pellet, where appropriate, was kept for histone extraction and cell supernatant protein concentration was determined using Pierce BCA assay (Thermo Scientific). Then, 1-2 µL of supernatant was diluted up to 50 µL in Milli-Q water and the sample was transferred into HPLC auto-sampler vials (0.3 mL TPX Snap Ring Micro-Vial with 11 mm PE Snap Ring Cap, Fisherbrand). Sample content was analysed by high-pressure liquid chromatography-tandem mass spectrometry (HPLC-MS/MS) using one of the methods developed for hydrophilic interaction liquid chromatography (HILIC) columns.

3.2.3 Sample preparation for histone analysis

3.2.3.1 Abcam histone extraction

Histone extraction was performed following the Abcam protocol [102]. Pellet obtained from HPLC-MS/MS cytoplasmic extraction was washed twice with 200 µL of Triton Extraction Buffer (TEB: 0.5% Triton X100 (v/v), 2 mM phenylmethylsulfonyl fluoride (PMSF), 0.02% (w/v) NaN_3 in phosphate-buffered saline (PBS)) and centrifuged at 6,500 g for 10 min. Then, the pellet was resuspended in 60 µL of 0.2 M HCl and histones were acid extracted overnight at 4 °C by gentle agitation. Next, samples were centrifuged at 6,500 g for 10 min at 4 °C. Protein concentration was determined using Pierce BCA assay (Thermo Scientific). Aliquots were stored at -80 °C.

3.2.3.2 Miller histone extraction

Histone extraction was performed following Miller extraction method [103]. HepG2 cells were seeded onto 6-well plates (1 x 10^6 cells/well). After overnight growth cells were washed twice with cold PBS and 200 µL of lysis buffer (50 mM Tris-HCl, pH 7.5, 25 mM KCl, 250 mM sucrose, 2 mM sodium butyrate, 1 mM sodium orthovanadate, 0.5 mM PMSF, protease inhibitor cocktail (SIGMAFAST, Sigma; containing: AEBSF 2 mM,

phosphoramidon disodium salt 1 µM, bestatin hydrochloride 130 µM, E-64 14 µM, leupeptin 1 µM, aprotinin 0.2 µM, pepstatin A 10 µM) was added. Next, cells were lysed on ice for 10 min with gentle stirring, scraped and centrifuged at 6,500 g for 10 min at 4 °C. Cytoplasmic supernatant was kept and stored at -80 °C and the cell pellet was resuspended in 60 µL of 0.4 N H_2SO_4 by gentle agitation in incubated on ice for 30 min. Histones extract was centrifuged at 14,000 g for 10 min at 4 °C. Protein concentration was determined using Pierce BCA assay (Thermo Scientific). Aliquots were stored at -80 °C.

3.2.4 Sample preparation for mitochondria analysis

Adapted mitochondria isolation protocol was utilised for HepG2 cell line [104]. HepG2 cells were plated on 6-well plate at cell density 1 x 10^6 cells/well and treated with a concentration range of metformin. Next, cells were washed twice with PBS. Next, 200 µL of lysis buffers was added (lysis buffer did not contain CAR-d_9 standard). Next, cells were strapped from the plate, transferred into a tube and cell membrane was destroyed by up and down pipetting. Next, the cell extract was centrifuged at 600 g for 10 min in 4 °C. Then, cell supernatant containing mitochondria was collected and spun at 7,000 g for 10 min at 4 °C. The obtained supernatant was a cytoplasmic extract, while pellet contained mitochondria. Next, the mitochondria pellet was washed in lysis buffer (no CAR-d_9 standard added), spun at 7,000 g for 10 min at 4 °C twice. Then, the cell pellet was resuspended in 20 µL of lysis buffer with CAR-d_9 standard added and freeze-thawed three times in liquid nitrogen in order to break the mitochondria membrane. Finally, the obtained extract was spun down at 7,000 g for 10 min at 4 °C and BCA assay was performed to find protein concentration. HPLC samples were prepared by adding 1 µL of mitochondria extract and 25 µL of water into HPLC vial.

3.2.5 Cytotoxicity assay

HepG2 cells were plated into 96-well plates at cell density 3 x 10^5 cells/well. Next, the test compound was added into the cells for 24 h. Next, 20 µL of colourimetric cytotoxicity assay solution (Abcam, ab112118) was added to the cell medium and plate was mixed gently and incubated for 3 h at 37 °C. Finally, the absorbance of each well at 570 nm and 605 nm was monitored with Spark 20M Multimode Reader (Tecan). The ratio of OD_{570}/OD_{605} was used to determine cell viability.

3.2.6 L-methionine and L-methionine-d_3 supplementation

3.2.6.1 Concentration curve

HepG2 cells were cultured in 12-well plate at starting concentration 4 x 10^5 cells/well in a cell culture medium containing L-methionine-d_3 concentration range (15-500 µg/mL). Control medium was supplemented with 15 µg/mL of regular L-methionine. HepG2 cells were cultured for 4 d.

3.2.6.2 Cell culture

HepG2 cells were cultured in T25 culture flasks at starting concentration 2 x 10^6 cells/flask in 6 mL culture media supplemented with L-methionine or L-methionine-d_3 at 500 µg/mL. Cells were split in a 1:2 ratio every second day (HepG2 doubling takes 48 h). Half of the cells amount (approximately 1 x 10^6) was added to a new culture flask containing L-methionine-d_3 and a remaining half (approximately 1 x 10^6) was spun down in Eppendorf tube for 5 min at 200 g and washed with PBS. The cell pellet was preserved in -80 °C for future cell lysis and HPLC sample preparation.

3.3 Small molecules

3.3.1 Materials

Small molecules (drugs, inhibitors, supplements) used for *S. cerevisiae* and HepG2 cells treatments can be found in Table 3-13.

Table 3-13: Small molecules used for S. cerevisiae and HepG2 cell line treatment.

Molecule	**Full name**	**Supplier**	**CAS number**
2OG	2-Oxoglutaric acid	Sigma-Aldrich	328-50-7
A-CAR	*O*-Acetyl-L-carnitine hydrochloride	Sigma-Aldrich	5080-50-2
AdOx	Adenosine-2′,3′-dialdehyde	Sigma-Aldrich	34240-05-6
Betaine	Trimethylglycine, TMG	Sigma-Aldrich	107-43-7
CAR	L-Carnitine, (*R*)-3-hydroxy-4-(trimethylammonio)butyrate	Sigma-Aldrich	541-15-1
CAR-d_9	DL-Carnitine-(trimethyl-d_9) hydrochloride	Sigma-Aldrich	1219386-75-0
CCT5-166	Dimethyl (*R*)-2-hydroxyglutarate	University of Oxford	103404-90-6
CCT5-168	Dimethyl (*S*)-2-hydroxyglutarate	University of Oxford	63512-50-5
Choline	(2-Hydroxyethyl)trimethylammonium chloride	Sigma-Aldrich	67-48-1
$CoCl_2$	Cobalt(II) chloride	Sigma-Aldrich	7646-79-9
DFO	Deferoxamine mesylate salt	Sigma-Aldrich	138-14-7

Dimethyl fumarate	Dimethyl fumarate	Sigma-Aldrich	624-49-7
Dimethyl succinate	Dimethyl succinate	Sigma-Aldrich	106-65-0
DMOG	Dimethyloxalylglycine	University of Oxford	89464-63-1
Fe^{2+}	Ammonium iron (II) sulfate hexahydrate	Sigma-Aldrich	7783-85-9
Folic Acid	Pteroyl-L-glutamic acid	Sigma-Aldrich	59-30-3
GSK-J4	Ethyl 3-((6-(4,5-dihydro-1H-benzo[d]azepin-3(2H)-yl)-2-(pyridin-2-yl)pyrimidin-4-yl)amino)propanoate	University of Oxford	1373423-53-0
IOX1	5-Carboxy-8-hydroxyquinoline	University of Oxford	5852-78-8
L-Methionine	(*S*)-2-Amino-4-(methylmercapto)butyric acid	Sigma-Aldrich	63-68-3
L-Methionine-d_3	L-Methionine-(methyl-d_3)	Sigma-Aldrich	13010-53-2
Metformin	1,1-Dimethylbiguanide hydrochloride	Alfa Aesar	1115-70-4
MG132	Z-Leu-Leu-Leu-al.	Sigma-Aldrich	133407-82-6
Mildronate	Meldonium dihydrate	Sigma-Aldrich	86426-17-7
Phenformin	Phenethylbiguanide monohydrochloride	Supelco	834-28-6
PMSF	Phenylmethylsulfonyl fluoride	Roche	329-98-6
SAHA	Suberoylanilide hydroxamic acid, vorinostat	Cayman Chemical Company	149647-78-9
TML	Trimethyllysine hydrochloride	Sigma-Aldrich	55528-53-5
Vitamin B_{12}	α-(5,6-Dimethylbenzimidazolyl)cyanocobamide	Sigma-Aldrich	68-19-9
Vitamin C	Sodium L-ascorbate	Supelco	134-03-2
γBB	(3-Carboxypropyl)trimethylammonium chloride	Sigma-Aldrich	6249-56-5

3.3.2 Iron chelation with metformin and DFO

The Fe^{2+} chelating ability of metformin was determined using a modified method described by Begium (Begum et al, 2015). 55 µL of reaction buffer (0.1 M Tris-HCl pH 7.5 in 50 mM NaCl), 10 µL of desired concentration of compound (metformin, EDTA, DFO) prepared in reaction buffer and 10 µL of 2 mM Fe(II) ammonium sulphate stock was added into each well of the reaction microplate (96-well, half-area, flat bottom, Corning). Next, the plate was incubated for 5 min and 25 µL of 20 mM 1,10-phenanthroline in the reaction buffer stock was added. The absorbance at 510 nm was measured on the Spark 10M plate reader.

3.4 Proteins

3.4.1 Protein concentration measurement

The protein concentrations of yeast and human cell lysates were determined using the Pierce BCA assay (Thermo Scientific). 5 µL of sample and 5 µL of bovine serum albumin (BSA, Thermo Scientific) stock dilution series were pipetted into 96-well plate and 95 µL of working reagent was added into each well. Then the plate was covered and incubated at 37 °C for 30 min and the absorption at 562 nm was measured on the Spark 10M (Tecan) plate reader. Data from the BSA stock dilution measurement were plotted and linear BSA concentration curve was created. The linear equation of the curve was used to calculate protein concentration in samples.

3.4.2 SDS-PAGE gel electrophoresis

SDS-PAGE gel samples were prepared by mixing 5-15 µg of proteins with 6x loading buffer and denaturated at 100 °C for 5 min. To prepare 10 mL of SDS-PAGE resolving gel (15%) 1.8 mL water, 5 mL 30% (v/v) acrylamide, 2.5 mL 1.5 M Tris-HCl pH 8.8, 0.5 mL 50% (v/v) glycerol, 0.1 mL 10% (w/v) SDS, 0.1 mL 10% (w/v) ammonium persulfate (APS) and 10 µL tetramethylethylenediamine (TEMED) were mixed. The 4% Stacking Gel (5 mL) was made by mixing 1.55 mL of water, 0.65 mL of 30% (v/v) acrylamide, 1.2 mL of 1.0 M Tris-HCl pH 8.8, 1.5 mL of 50% (v/v) glycerol, 0.05 mL of 10% (w/v) SDS, 0.05 mL of 10% (w/v) APS and 5 µL TEMED. Next, histone proteins were separated on 15% gel by SDS-PAGE in running buffer containing (per 1 L): 3 g Tris base, 14.4 g glycine, and 1 g SDS.

3.4.3 Western blotting

After electrophoresis, SDS-PAGE gels were transferred in a wet system (200 mA, 2 h) onto a 0.2 µm nitrocellulose membrane (GE Healthcare) in 20% transfer buffer containing (per 1 L): 200 mL methanol, 3 g Tris base, 1.44 g glycine. Membranes were prestained with Ponceau S and washed with tris-buffered saline (TBST) buffer containing (per 1 L: 9 g NaCl, 6 g Tris Base and 1 mL Tween-20) and blocked for 1 h in 5% (w/v) non-fat dried milk (Tesco) in TBST at room temperature. Next, membranes were washed three times for 5 min in TBST and incubated with chosen primary antibody (Table 3-14) diluted in 5% (w/v) BSA in TBST overnight at 4 °C. Next day, membranes were washed three times with TBST for 5 min, incubated for 1 h with horseradish peroxidase (HRP)-conjugated secondary antibody diluted in 5% (w/v) non-fat dried milk and again washed three times for 5 min with TBST. Membranes were incubated with chemiluminescence reagent

(Pierce ECL, Thermo Scientific) for 5 min and then scanned with Odyssey Fc imaging system (Li-Cor) and intensity of bands was measured by ImageJ software.

Table 3-14: Antibodies used in immunochemistry studies.

	Type	Antigen	Supplier and product no	Dilution
1	Primary	Rabbit Trimethylated lysine	Abcam ab76118	1: 1,000
2	Primary	Mouse Histone H4	Cell Signalling 2935S	1: 1,000
3	Primary	Mouse Trimethyl Histone H4K20	Santa Cruz sc-134216	1: 500
4	Primary	Mouse Acetyl-lysine	Santa Cruz sc-32268	1: 500
5	Primary	Mouse EF1 alpha 1/2	Santa Cruz sc-377439	1:1,000
6	Secondary	Goat anti-Rabbit IgG (HRP-conjugated)	ThermoFisher Scientific 31460	1:5,000
7	Secondary	Anti-Mouse IgGκ (HRP-conjugated)	Santa Cruz sc-516102	1:1,000-1:2,000

3.4.4 Protein in-gel digestion

After electrophoresis, SDS-PAGE gels were stained with Blue Safe Protein Staining Solution (Thermo Fisher Scientific). The bands of interest were excised and diced into 1 mm^3 cubes and transferred into a clean tube. To destain the band, 50 µL of 50:50 mixture of 100 mM ammonium bicarbonate and acetonitrile was added into the tube for 10 min. Next, 450 µL of acetonitrile was added and incubated for 3 min with occasional vortexing until the cubes were white and clumped together. To reduce the proteins, the supernatant was discarded and 50 µL of 10 mM dithiothreitol (DTT) in 100 mM ammonium bicarbonate was added and incubated for 30 min at 50-60 °C. Next, 450 µL of acetonitrile was added and incubated for 3 min with occasional vortexing. To alkylate proteins, the supernatant was discarded and 50 µL of fresh 55 mM iodoacetamide in 100 mM ammonium bicarbonate was added and incubated at room temperature for 30 min in the dark. Next, 450 µL of acetonitrile was added and incubated for 3 min with occasional vortexing. Next, to digest proteins, the supernatant was discarded and 50 µL of the appropriate protease at 10 ng/µL concentration (Sequencing Grade Trypsin or GluC (Promega)) in 100 mM ammonium bicarbonate was added and incubated overnight in 37 °C. Then, the supernatant was transferred into HPLC vial and 1 µL of formic acid was added to quench the reaction. The sample was analysed via HPLC-MS/MS.

3.5 Peptide mass spectrometry

3.5.1 HPLC-MS/MS peptide analysis

Protein digests analysis was carried out on a Dionex Ultimate 3000 Nano LC (Dionex, Thermo Fisher Scientific) system. The mobile phases A and B consisted of 95:5 water:acetonitrile and 5:95 water:acetonitrile, respectively, and both contained 0.1% (v/v) formic acid. Firstly, 2 µL of protein digest was injected in a load-trapping mode using a PepMap300 C18 pre-column (Thermo Fisher Scientific) and washed for 3 min with 5% A at flow rate of 0.3 mL/min. Then the pre-column was switched with a PepMap300 C18 nanocolumn (Thermo Fisher Scientific) and peptides were eluted using a gradient of 0% to 55% B for 35 min then 85% B for 5 min and 0% B for 20 min at a flow rate of 0.3 mL/min. HPLC system (Thermo Fisher Scientific) was coupled to a PicoTip (New Objective) and LTQ-FTICR Ultra mass spectrometer (Thermo Fisher Scientific) equipped with a commercial nanoelectrospray ionization source operating with a capillary voltage of 1.7 kV, and temperature set at 275 °C. Spectra were acquired in positive ion mode over a 400–2,000 *m/z* range. The instrument was controlled by Xcalibur software (Thermo Fisher Scientific). Identification of peptides was conducted using an automated data-dependent acquisition mode (DDA). For DDA, five most intense ions for each scan were isolated and subjected to collision-induced dissociation (CID) using nominal energy of 35.0 with any singly charged ions rejected. The data were searched with SEQUEST against a custom database using Bioworks software (Thermo Fisher Scientific). The search was performed for peptides with up to 3 modifications per peptide (lysine acetylation, methylation, demethylation or trimethylation).

3.6 Metabolite mass spectrometry

3.6.1 HPLC-ESI-MS/MS instrument and software

The HPLC-MS/MS system consisted of a Thermo Ultimate 3000 HPLC system (Thermo Scientific) and an Impact II (Bruker Daltonik) mass spectrometer with a qToF mass analyser and electrospray ionization (ESI) mode. The mass spectrometer was connected to the HPLC-system outlet via high-pressure tubing. The HPLC system was controlled by Thermo Scientific™ Chromeleon™ Chromatography Data System software. HyStar™ software (Bruker Daltonik) was used to coordinate the HPLC system with MS methods. Data acquisition and peak integration were performed using the Compass® Software

(Bruker Daltonik). Data could be further processed using DataAnalysis Software (Bruker Daltonik).

3.6.2 ESI-MS/MS parameters

After tuning the optimized source, transfer, quadrupole and collision parameters for CAR and TML detection on MS mode were as follows: End Plate Offset, 500 V; Capillary, 5000 V; Nebulizer, 3.0 Bar; Dry Gas, 12.0 L/min; Dry Temperature, 200 °C; Funnel 1 RF, 200.0 Vpp; Funnel 2 RF, 200.0 Vpp; In-Source Collision Induced Dissociation (isCID) Energy, 0.0 eV; Hexapole RF, 50.0 Vpp; Ion Energy, 4.0 eV; Low Mass, 110.0 *m/z*; Collision energy, 7.0 eV; Collision RF, 400.0 Vpp; Transfer Time, 30 µs; Pre Pulse Storage, 1.0 µs; Ion Polarity, positive; Mass Range, 50-500 *m/z*. Nitrogen was used as the nebulizer, auxiliary and collision gas.

MS/MS identification of ions was conducted using a multiple reaction monitoring (MRM) mode. For MRM assay the *m/z* +/-1.000 were isolated and subjected to CID using nominal energy of 19.3 eV for CAR, γBB, A-CAR and CAR-d_9, and 22.3 eV for TML.

3.6.3 HPLC columns

All HPLC columns used in this study for sample separation are listed in Table 3-15.

Table 3-15: HPLC columns used in this study.

Name	**Internal diameter [mm]**	**Column length [mm]**	**Particle size [µm]**	**Type**	**Supplier**
ZORBAX SB-Aq	4.6	150	5	Reversed-phase	Agilent Technologies
HILIC Silica Atlantis	2.1	50	5	Normal-phase	Waters
HILIC Silica Atlantis	2.1	150	5	Normal-phase	Waters

3.6.4 Zorbax mobile phase

1 mL of formic acid was added to 1 L of deionized Milli-Q water to achieve 0.1% (v/v) concentration and was used as the aqueous solvent of the mobile phase (solvent A). The same volume of formic acid was added to 1 L of acetonitrile that was used as the organic mobile phase (solvent B).

3.6.5 HILIC mobile phase

100 mM ammonium acetate (pH 3.5, 5.0 or 9.0) stock solution was prepared by dissolving 7.7 g of the salt in 1 L of deionized Milli-Q water, pH was adjusted with acetic acid and 5% acetonitrile was added to avoid bacteria growth. Then 10 mM ammonium acetate solution was prepared by dilution of 10x stock in Milli-Q water to obtain aqueous solvent of the mobile phase (solvent B). Acetonitrile was used as the organic mobile phase (solvent A).

3.6.6 Standard samples preparation

Standard stock solutions of L-carnitine inner salt (CAR, Sigma-Aldrich), ε-*N*-trimethyl-lysine hydrochloride (TML, Sigma-Aldrich), γ-butyrobetaine hydrochloride (γBB, Sigma-Aldrich), *O*-acetyl-L-carnitine hydrochloride (A-CAR, Sigma-Aldrich) and DL-carnitine-(trimethyl-d_9) hydrochloride (CAR-d_9, Sigma-Aldrich), L-glutamine (GLU, Sigma-Aldrich), L-isoleucine (ISO, Sigma-Aldrich), L-leucine (LEU, Sigma-Aldrich) and L-alanine (ALA, Sigma-Aldrich) were prepared by dissolving 10 mg of appropriate standard in 1 mL of Milli-Q water. The working standard solutions were prepared in serial dilution of the stock standard solutions with Milli-Q water. 50 µL of the sample dilution was transferred into auto-sampler vials.

3.6.7 HPLC method optimisation for Zorbax column

For Zorbax column a gradient of solvents was applied to separate molecules (Figure 3-2). Solvent A was 0.1% (v/v) formic acid in H_2O and solvent B was 0.1% (v/v) formic acid in Acetonitrile. The separation was performed at a flow rate of 0.500 mL/min. The injection volume was 5.0 µL. Prior to the analysis, the column was equilibrated with 30 column volumes of the mobile phase.

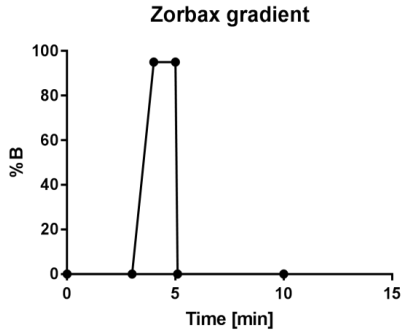


Figure 3-2: Mobile phase gradient used for Zorbax column. The mobile phase was: solvent A: 0.1% (v/v) formic acid in H_2O and solvent B: 0.1% (v/v) formic acid in acetonitrile. The adopted gradient was a linear gradient from 0% to 95% B in 3 to 4 min, constant at 95%

for 1 min and then the column was reconditioned in 5 min from 95% to 0% B and was constant at 0% from 5 to 10 min.

3.6.8 HPLC method optimisation for HILIC 50 mm and HILIC 150 mm columns

For 50 mm and 150 mm HILIC columns a gradient of solvents was applied to separate molecules (Figure 3-3). Solvent A was acetonitrile and solvent B was 10 mM ammonium acetate pH 5.0 in Acetonitrile. The separation was performed at a flow rate of 0.500 mL/min. The injection volume was 5.0 µL. Prior to the analysis, the columns were equilibrated with 30 column volumes of the mobile phase. A guard column (Waters) was used with each column.

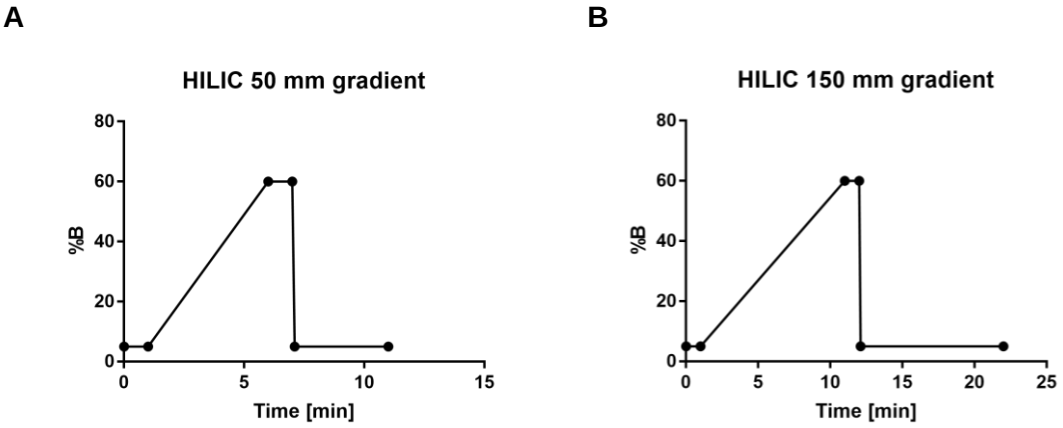


Figure 3-3: A) Adopted gradient for HILIC 50 mm column was a linear gradient from 5% to 60% B in 1 to 6 min, then constant at 60% B for 1 min, and then the column was reconditioned in 7 min from 60% to 5% B and was constant at 5% B from 7 to 11 min. B) Adopted gradient for HILIC 150 mm column was a linear gradient from 5% to 60% B in 1 to 11 min, then constant at 60% B for 1 min, then the column was reconditioned in 12 min from 60% to 5% B and was constant at 5% B from 12 to 22 min. The mobile phase was: solvent A: acetonitrile, solvent B: 10 mM ammonium acetate pH 5.0 with 5% (v/v) acetonitrile.

4. Establishing methods for metabolic studies

Carnitine (CAR) biosynthesis is a four-step enzymatic reaction of highly polar small molecule metabolites starting from ε-*N*-trimethyl-lysine (TML). Therefore, for a detailed investigation of CAR biosynthesis it was necessary to develop a rapid, sensitive and quantitative method for metabolite analyses. This chapter describes the development and optimisation of methods for the detection and quantification of CAR and related molecules (Figure 4-1).

Specific objectives of this chapter were to:

- Identify suitable model organisms to study the effect of cellular methylation levels on CAR biosynthesis;
- Optimise a phenotypical yeast assay based on "halo formation" upon complementation with CAR;
- Establish a fluorometric detection assay for CAR based on a coupled multi-enzymatic reaction, and determine its suitability;
- Develop an HPLC-ESI-MS/MS method to detect and quantify the levels of CAR and TML in cell lysates from yeast or human cells.

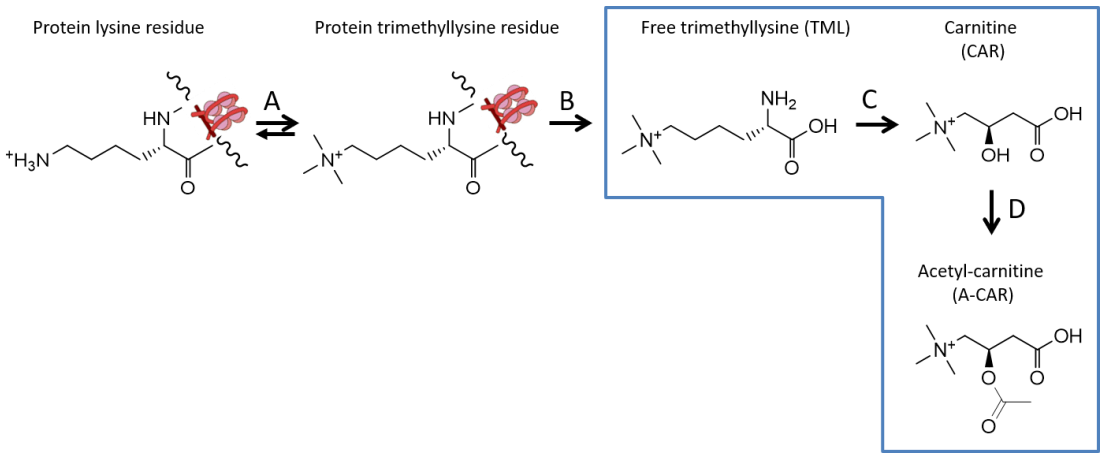


Figure 4-1: Optimized method for metabolites detection would enable for studies of CAR biosynthesis from TML (C) and levels of CAR conversion to A-CAR (D).

4.1 *S. cerevisiae* as a model organism

It has been established that carnitine biosynthesis is a conserved process across many eukaryotic species, based on work with the fruitfly *Drosophila melanogaster*, the round worm *Caenorhabditis elegans*, the yeasts *Neurospora crassa* and *Candida albicans* through mice, rats and finally in humans [77]–[80]. Recently, carnitine biosynthesis has also been reconstructed in yeast *S. cerevisiae* [79].

S. cerevisiae is one of the best investigated genetic model organisms and amongst the simplest eukaryotic organism that contains histones in their nuclei. As yeast shares over 20% homologous genes with humans, though, possess a smaller genome, choosing *S. cerevisiae* as a model organism allows for comparative biological studies. The well-established yeast methodology and rich knowledge on its genome make it ideally suited for an initial survey study and the selection of relevant genes to study carnitine biosynthesis [105], [106].

4.1.1 Carnitine dependency of the *S. cerevisiae cit2Δ* strain

S. cerevisiae yeast strains are capable of growing on both fermentable and non-fermentable carbon sources. Normally during non-fermentable growth, wild-type (WT) strain transport acetyl-CoA from the cytosol into peroxisomes where acetyl-CoA enters the glyoxylate cycle and is utilized for citrate production by the peroxisomal citrate synthase (cit2p) [107]. Subsequently, citrate can be shuttled into the Krebs cycle within mitochondria. After *cit2* gene deletion, the *cit2Δ* strain is not able to obtain the required citrate and CAR becomes required for transport of acetyl-CoA into the mitochondria, rendering survival on non-fermentable carbon sources dependent on CAR (Figure 4-2) [76]. However, as *S. cerevisiae* naturally does not possess the ability for CAR biosynthesis, CAR must be supplemented in the medium.

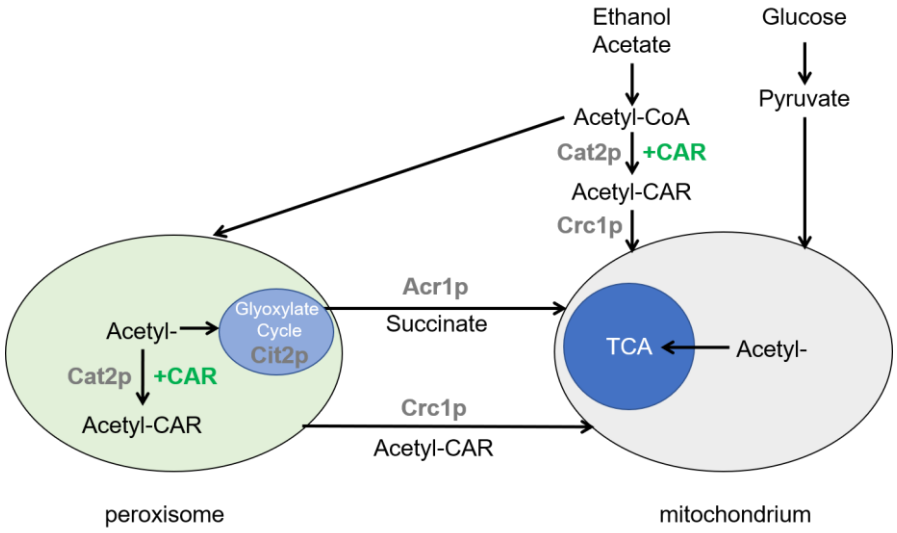


Figure 4-2: Yeast growth on fermentable (glucose) and non-fermentable (ethanol, acetate) carbon sources and carnitine shuttle. CAR – carnitine, CoA – coenzyme A; TCA – tricarboxylic acid cycle (the Krebs cycle).

Therefore, an initial attempt to study CAR biosynthesis in yeast was to utilize the dependency of yeast growth on non-fermentable carbon source on CAR, to determine optimal conditions allowing for the sensitive detection of CAR.

The *cit2Δ* strain is capable of growing without the addition of CAR only on SD medium with glucose [76]. This is due to the fact that glucose is fermented into pyruvate in the cytosol, which is transported into mitochondria, where it is metabolised to acetyl-CoA. This process shows that shuttling of acetyl groups via carnitine is not necessary for the Krebs cycle functionality. However, ethanol and glycerol, which do not undergo fermentation into pyruvate, are transformed via acetate into acetyl-CoA in the cytosol. Therefore, in this case, the transport of acetyl-CoA with carnitine across the mitochondrial membrane is crucial for the survival of *cit2Δ* strain (Figure 4-2) [76].

This carnitine dependency of FY631 *cit2Δ* strain was confirmed by culturing the strain in fermentable (SD with glucose) and non-fermentable (SDEG with ethanol and glycerol) medium with and without the addition of CAR. The results (Figure 4-3) were consistent with the data published in 2001 [76] that in the absence of *cit2* CAR is required for growth on non-fermentable carbon sources.

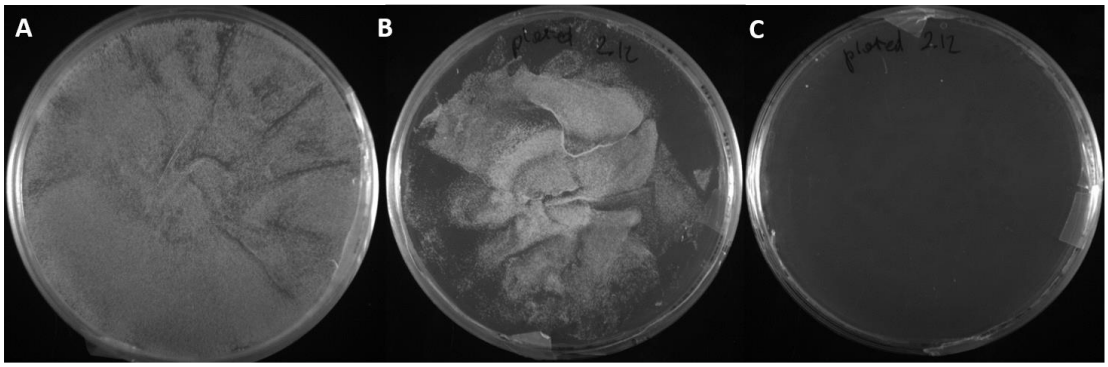


Figure 4-3: cit2Δ strain growth on agar plates with A: SD medium supplemented with 2% glucose; B: SDEG medium supplemented with 3% ethanol and 1% glycerol and CAR (20 µg/mL) C: SDEG medium supplemented with 3% ethanol and 1% glycerol with no carnitine; all plates were incubated for 6 d.

4.1.2 Carnitine requirement for *S. cerevisiae cit2Δ* strain

In order to investigate the required amount of carnitine, FY631 *cit2Δ* strain was grown on SD agar plates supplemented with non-fermentable carbon sources and different concentrations of CAR (Figure 4-4).

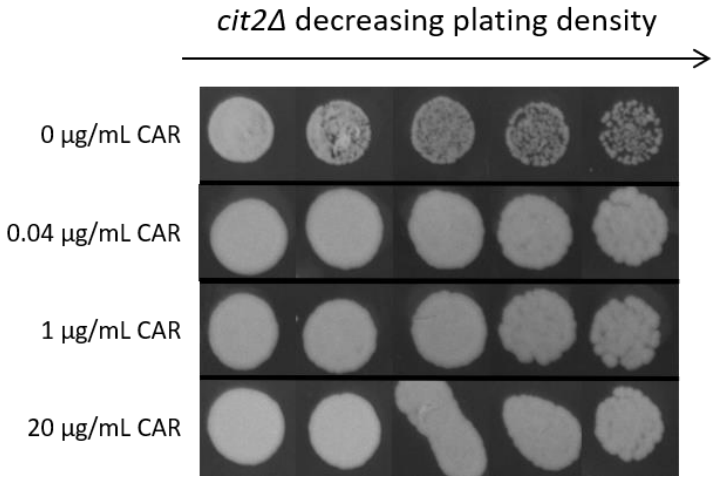


Figure 4-4: Different CAR concentrations (0 µg/mL, 0.04 µg/mL, 1 µg/mL, 20 µg/mL) tested by growing cit2Δ strain with decreasing plating density on SDEG agar plates for 6 d.

Figure 4-4 (line 1) shows that in the absence of CAR, the *cit2Δ* strain growth is inhibited. The visible growth is due to the remaining glucose in cells from overnight liquid culture. However, the plates with the addition of CAR support *cit2Δ* strain growth (line 2-4). Importantly, no noticeable changes between the highest and the lowest concentration were observed after 6 d of growth. At demonstrated plating density, a minimal concentration of 0.04 µg/mL CAR was sufficient for *cit2Δ* strain survival. Thus, even low

concentrations of CAR are sufficient to shuttle acyl groups, as CAR is not irreversibly consumed by yeast cells, providing efficient acetyl-CoA transport into mitochondria.

4.1.3 Carnitine biosynthesis reconstruction in *S. cerevisiae*

Natively, yeast *S. cerevisiae* is not able to produce L-carnitine. However, recently researchers at the Institute of Wine Biotechnology in South Africa engineered a strain producing carnitine by reconstructing the *Neurospora crassa* carnitine biosynthesis pathway [79]. They cloned all four *N. crassa* enzymes: TMLH, HTMLA, TMABA-DH and GBBH found to be necessary for carnitine production into *S. cerevisiae* (Figure 4-5). This achievement generated a carnitine producing *S. cerevisiae* strain for potential new industrial applications. In this chapter, the constructed strain (named as FY23 1,2,3,4 strain) was tested as one of the tools for investigation of the link between CAR and energy metabolism.

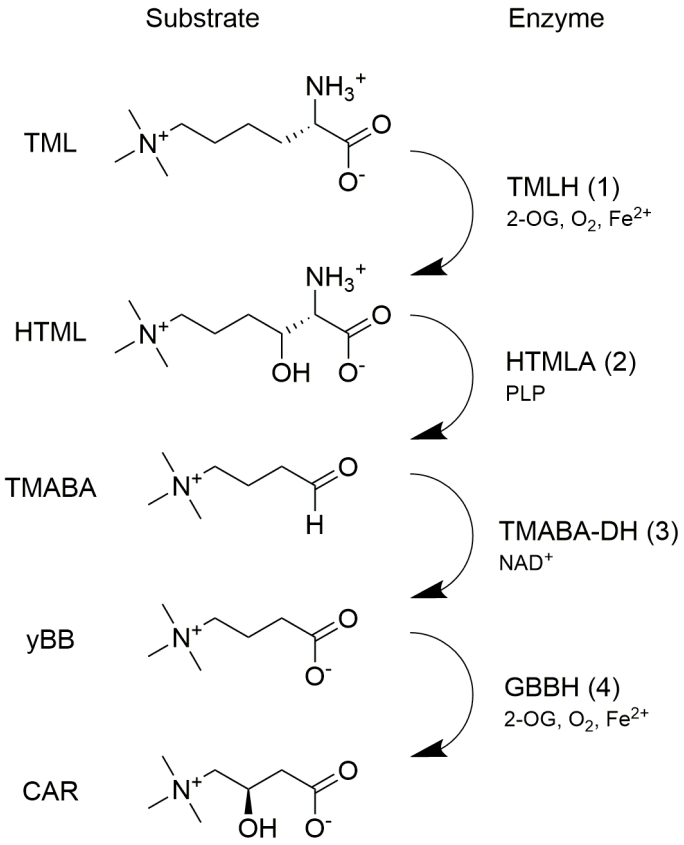


Figure 4-5: Four-step carnitine biosynthesis pathway. Enzymes reconstructed in FY23 1,2,3,4 strain: 1 – TMLH; 2 – HTMLA; 3 – TMABA-DH; 4 – GBBH.

4.1.4 Validation of *S. cerevisiae* FY23 1,2,3,4 strain capability of carnitine synthesis

To validate the capability of strain FY23 1,2,3,4 to produce carnitine, a small number of cells from that bioengineered strain were spotted on a plate covered with a highly diluted layer of cells from the FY631 *cit2Δ* strain growing on non-fermentable medium (SDEG). Additionally, exogenous TML was added to the agar plate as TML is the first substrate in CAR biosynthesis. Drops of a liquid culture of FY23 1,2,3,4 strain (capable of producing CAR) and FY631 WT strain for control (not producing CAR) were placed on the lawn of FY631 *cit2Δ* strain. After 6 d of agar plates incubation, the so-called "halo" effect (growth of *cit2Δ* yeast colonies around spot) could be observed around FY23 1,2,3,4 strain and not around WT strain (Figure 4-6).

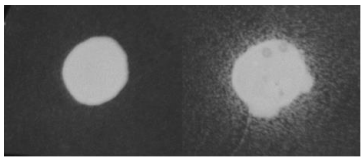


Figure 4-6: L-carnitine production by strain FY 1,2,3,4 on non-fermentable carbon source (SDEG) with the addition of TML (6.6 μg/mL) supporting the growth of cit2Δ lawn. "Halo" formation appears only for strain FY23 1,2,3,4 and not WT.

The "halo" formation appears due to CAR leaking into the medium and the supporting *cit2Δ* strain growth nearby. Thus, CAR is produced by strain FY23 1,2,3,4 but not by the WT strain. This is evidence that the FY23 1,2,3,4 strain is capable of catalysing the CAR biosynthesis from TML, while the FY631 WT strain does not possess this capability.

This "halo" formation assay can thus be regarded as a suitable tool for further studying the CAR biosynthesis pathway on using strain FY23 1,2,3,4. This method allows for the detection of carnitine biosynthesis in yeast at relatively low levels (40 ng/mL). Although this assay is advantageous in terms of quality and sensitivity, it quickly became apparent that it was not suitable for quantitative analysis of changes in carnitine biosynthesis levels. Thus, the development of a new quantitative and sensitive method for CAR determination was needed.

4.2 Fluorometric method for carnitine quantification

Another approach for CAR quantification was the utilization of a commercial fluorometric CAR detection system (Abcam). Such CAR detection kits are most probably based on the enzymatic reaction of CAR with acetyl-CoA releasing CoA. Then, CoA undergoes further reactions that result in oxidation of the fluorescent probe. The likely enzymatic reactions utilized in Abcam's commercial carnitine detection kit are presented in Table 4-1.

Table 4-1: Probable enzymatic reactions utilized by Abcam L-carnitine kit.

	Reaction	**Enzyme**	**Ref**
1	acetyl-CoA + carnitine --> acetyl-carnitine + CoA	carnitine acetyltransferase (CAT)	[108]
2	CoA + acyl --> acyl-CoA	acyl-CoA synthetase	[109]
3	acyl-CoA + O_2 --> *trans*-2,3-dehydroacyl-CoA + H_2O_2	acyl-CoA oxidase	[110]
4	H_2O_2 + OxiRed probe --> fluorescence	horseradish peroxidase (HRP)	[111]

In order to assess this fluorometric CAR detection assay, the FY23 1,3,4 strain that can produce CAR was cultured for up to 48 h with and without the addition of γBB (the last intermediate of the CAR biosynthesis pathway). The fluorometric analysis of the samples including a standard CAR curve are presented in Figure 4-7.

The fluorescent CAR detection method showed a near-linear standard CAR curve and, therefore, allowed for CAR quantification of the yeast samples described above. After 48 h the CAR production increased 6-fold compared to 24 h production regardless of the addition of γBB. Additionally, at each time point the addition of γBB increased the production of CAR by 3-fold. That result indicates that external supplementation with γBB supports CAR biosynthesis in yeast.

Therefore, the fluorometric CAR assay would be principally suited for further CAR studies. However, during experimental preparation, various limitations of the kit were observed.

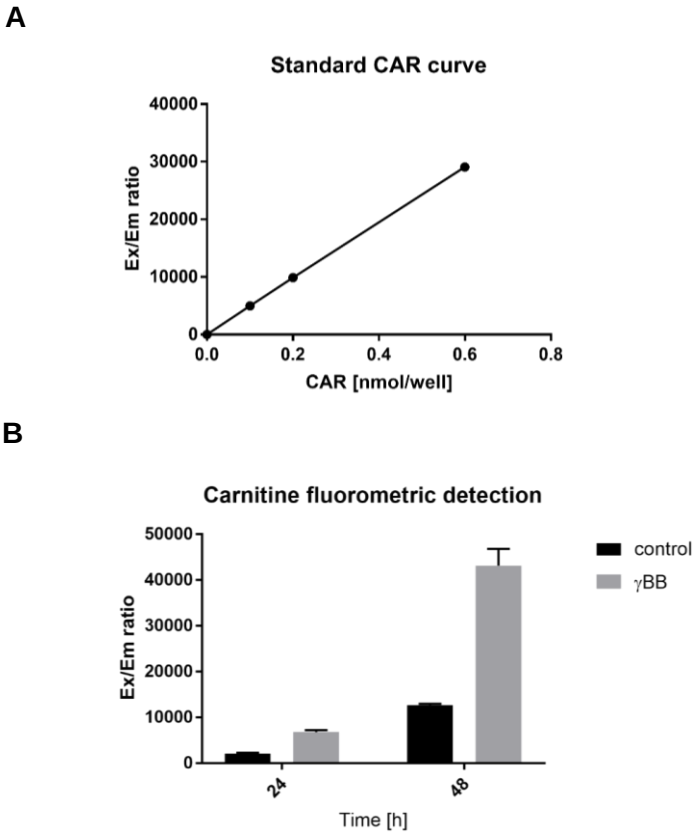


Figure 4-7: A) CAR standard curve in range 0 to 0.6 nmol/well; R^2=1, n=1; B) Fluorometric CAR detection in FY23 1,3,4 strain after 24 and 48 h growth with and without of γBB supplementation 200 mg/L; n=2.

Firstly, one of the steps of sample preparation for the fluorometric CAR assay is protein precipitation with perchloric acid and, subsequently, an adjustment of the pH. This procedure appeared to be a very time-consuming process that dilutes samples significantly. Additionally, handling concentrated perchloric acid and potassium hydroxide for pH adjustment of a large number of samples is concerning in terms of safety if the protein precipitation procedure is performed on a daily basis.

Secondly, pH adjustment introduces an additional error to the level of detected CAR that decreases the quality of analysis.

Thirdly, this Abcam assay limits the measure mostly to CAR levels only. Therefore, in case of subsequent interest in the analysis of related or other metabolites, other kits/methods of analysis would have been required.

Lastly, after careful consideration of the mechanism of action utilised in this fluorometric kit, the carnitine detection levels are likely to be a combination of background levels and other metabolites' interfering with the employed 4-step multi-enzymatic detection protocol. The fluorometric kit most likely detects free CoA from acetyl-CoA during the

transfer of the acetyl group to carnitine. Free CoA then undergoes multiple enzymatic reactions, which eventually result in oxidation of the OxiRed probe oxidation with concomitant release of fluorescence. It is likely that choline is also detected in addition to carnitine by this Abcam kit. Choline and its enzyme choline acetyltransferase can interfere with the first enzymatic step of the Abcam kit by producing acetyl-choline and CoA [112].

Thus, it was desired to establish a more specific detection methodology that allows the quantification of CAR and its related metabolites.

4.3 HPLC-ESI-MS/MS method

One of the analytical techniques for small molecules identification and quantification that has been developed and improved over the last decades is mass spectrometry (MS). The technique measures the mass-to-charge ratio (*m/z*) of molecules that have been ionized in the gas phase. One of the common ionization methods is electrospray ionization (ESI) during which molecules become positively or negatively charged [113]. Then, the electric field pulls the ions through the analyser separating them by their *m/z* ratio. Among popular analysers are the quadrupole, time-of-flight (ToF), ion traps, orbitraps and Fourier transform ion cyclotron resonance (FT-ICR) [113]–[117]. Lastly, the detector converts the detected ion signals into a mass spectrum of intensities of separated ions.

In case of complex biological samples, it is common to couple MS with liquid or gas chromatography systems (LC or GC). Chromatography allows for initial molecules separation by their polarity and size before they are injected to the MS. By this approach, the concentration of eluting molecules is being enhanced, therefore, enabling for increased MS selectivity and sensitivity. Then, for quantification, a common method is a measurement of peak area under the curve (AUC) of precursor ion's MS intensity [118].

In order to confirm the identity of the ion of interest, it can be fragmented by tandem mass spectrometry (MS/MS) [119]. The MRM mode is used to select "precursor ion" that then is isolated by its *m/z* ratio and fragmented by collision with an inert gas, for example, nitrogen [120]. Such collision results in creating "product ions" that belongs to the fragmentation pattern of "precursor ion". Fragmentation patterns may then be utilized for molecules identification in complex biological samples. One of the most widely used fragmentation techniques is collision-induced dissociation (CID) with a neutral gas [121].

4.3.1 Method optimisation workflow

Since it was previously reported that CAR biosynthesis can be quantified by HPLC-ESI-MS/MS [79], in this subchapter, it was investigated whether HPLC-ESI-MS/MS detection is suitable for the quantification of cellular TML and CAR levels in developed research conditions. Although this method requires considerable initial optimisation, its sensitivity may reach down to the ng/mL range for a large number of analytes and enable quantification.

In order to develop and optimise an HPLC-ESI-MS/MS method, the following workflow was utilized:

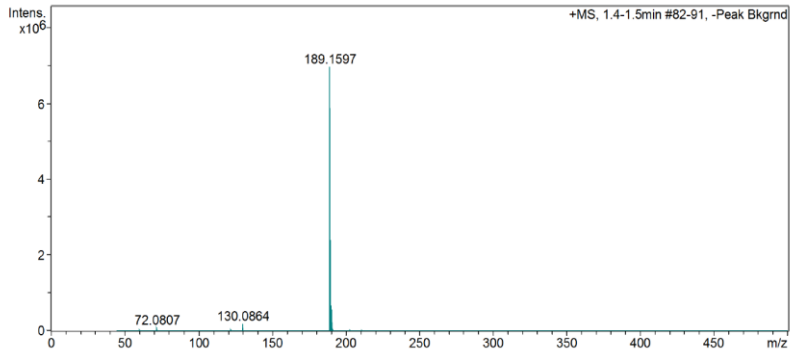
a) Mass spectrometry optimisation by injection of standards of molecules of interest;
b) Liquid chromatography optimisation by testing different separation conditions;
c) Method validation by testing molecules standards concentration ranges and analysis of their fragmentation patterns;
d) Method evaluation by testing complex matrices;
e) Automation of the analysis by establishing a Visual Basic script;
f) Method normalization by testing different standardization approaches.

4.3.2 Mass spectrometry optimisation

4.3.2.1 Mass spectrometry tuning

Firstly, the mass spectrometer was tuned by in-flow injection of a pure and concentrated mixture of CAR and TML at a concentration of 10 µg/mL each. That procedure allowed optimizing source, transfer, quadrupole and collision parameters for CAR and TML detection in single positive ion mode (MS) (Appendix Figure 11-1). At found parameters, TML $[M]^+$ ion was observed at m/z = 189.1597, while CAR $[M+H]^+$ ion was observed at m/z = 162.1123 (Figure 4-8).

A



B

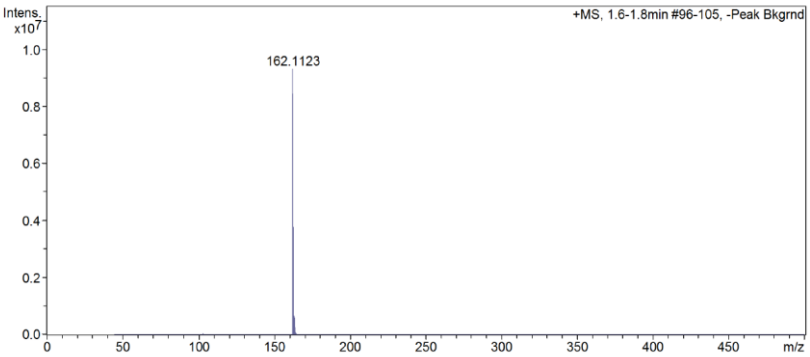


Figure 4-8: A) MS spectrum for TML; the detected ion m/z was 189.1597. B) MS spectrum for CAR; the detected ion m/z was 162.1123.

Successful detection of CAR and TML allowed for further method development.

4.3.2.2 Mass calibration

To assign the mass of peaks, a specific MS calibrant was needed as reference material. Proper calibration requires evenly spaced series of ions throughout the analysed mass range. In a developed method for this study, calibration was performed using sodium formate in the *m/z* range between 90.9766 and 1518.7125 before each sample injection (Appendix Figure 11-2).

4.3.3 Liquid chromatography optimisation

In order to achieve the best separation of molecules before injection and ionization in the mass spectrometer (MS) an HPLC method with applied solvents gradient was necessary. Additionally, that method was required to allow the direct analyses of whole cell lysate.

4.3.3.1 Reverse phase Zorbax column

To achieve optimal separation the appropriate HPLC column had to be chosen. Initially, a Zorbax (Agilent Technology) (Table 3-15) column was used and a 10 min

chromatography method with linear buffer gradient was adopted for TML and CAR molecules separation.

The Zorbax column appeared to separate CAR and TML well, however with very close retention times (CAR at 1.7 min and TML at 1.5 min). The observed masses were consistent with the masses noticed during initial in-flow MS analysis.

4.3.3.2 Normal phase HILIC column

Due to the high polarity of CAR and TML molecules, an HPLC method using a normal-phase hydrophilic interaction chromatography (HILIC) [122] column was developed and compared to the already tested reverse-phase column (Zorbax). Two lengths of HILIC columns were tested (50 mm and 150 mm) (Table 3-15).

The summary of CAR and TML elution times from all tested columns is presented in Table 4-2.

Table 4-2: CAR and TML elution times on Zorbax and HILIC columns.

	Retention time [min]		
Molecule	**Zorbax**	**HILIC 50 mm**	**HILIC 150 mm**
CAR	1.7	6.3	10.3
TML	1.5	7.2	13.0

Both HILIC columns and their gradients significantly improved CAR and TML separation. Applied normal-phase HILIC column additionally reversed the previous sequence of eluting molecules, eluting CAR first, and then TML. Therefore, HILIC columns were chosen for further investigation and HPLC-MS/MS method development.

4.3.3.3 Buffer pH optimisation on HILIC 50 mm

The pH of the mobile phase buffer may play an important role in the effectiveness of separation, elution and peak shape of investigated compounds. Therefore, three different pH values of Solution B (10 mM ammonium acetate) were tested on the 50 mm HILIC column: 3.5, 5.0 and 9.0. In outcome, pH 3.5 did not improve much molecules separation, while pH 9.0 worsened the detection and peaks shape (data not shown).

As altered pH of the aqueous mobile phase did not positively influence the separation method, the 10 mM ammonium acetate at pH 5.0 was utilized in further experiments.

4.3.4 Method validation for TML, γBB, CAR and A-CAR

In order to validate the accuracy of the developed method, concentration ranges and linearity of detection were necessary to investigate. At this stage of method development, more compounds of potential interest were included in the method validation. Serial dilutions were prepared for these molecules:

- TML – the first substrate in the 4-step CAR biosynthesis pathway;
- γBB – the last substrate in the 4-step CAR biosynthesis pathway;
- CAR – the final product in the 4-step CAR biosynthesis pathway;
- A-CAR – an acetylated form of CAR.

4.3.4.1 γBB and A-CAR addition to the method

Firstly, γBB and A-CAR were examined for HILIC 150 mm at 100 ng/mL concentration. The detected ions masses were covering expected ion masses (Appendix Figure 11-3). The appearance of additional peaks on the spectra was due to the very low concentration of samples and very low-intensity background molecules probably present in water used as a solvent of samples being detected.

4.3.4.2 Detection range and linearity for TML, γBB, CAR and A-CAR

To determine the detection range of the developed method, dilution series of standards were performed using HILIC 50 mm (Figure 4-9) and HILIC 150 mm columns (Figure 4-10). Peak areas of detected ions for each analyte were plotted against the nominal concentration of standard and linear equations were derived fitting to the y=ax+b equation.

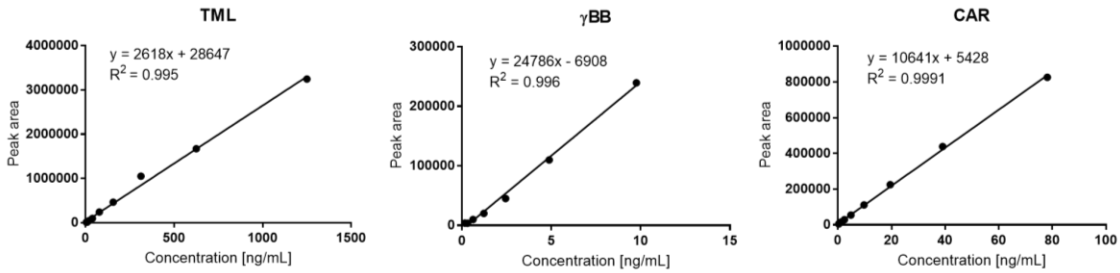


Figure 4-9: Detection range and linear fit for TML (1.22-1250 ng/mL), γBB (0.15-9.76 ng/mL) and CAR (0.15-78 ng/mL) performed on HILIC 50 mm column (n=1).

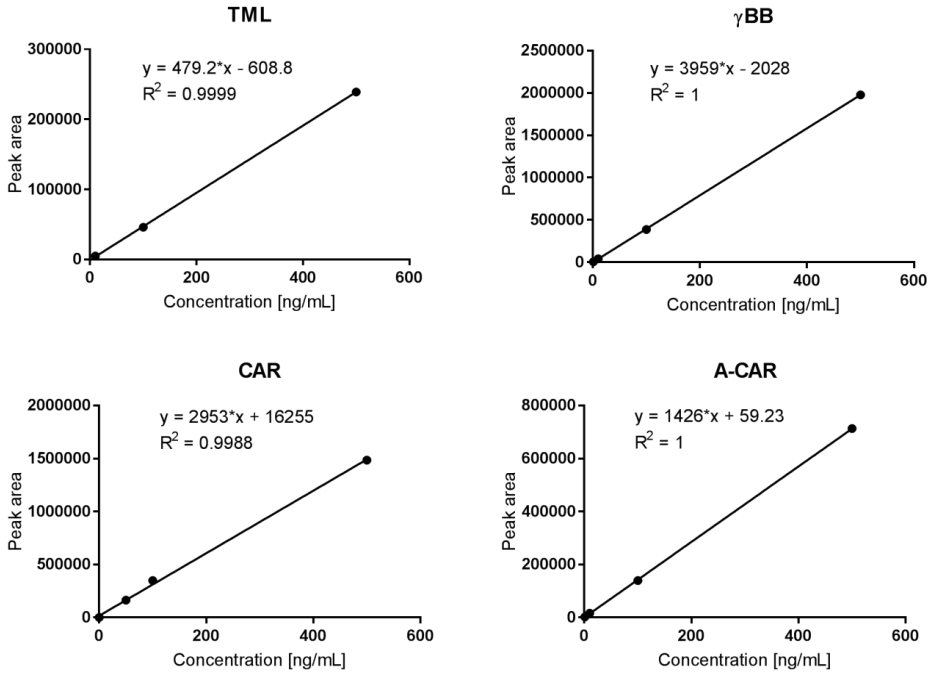


Figure 4-10: Detection range and linear equation for TML (10-500 ng/mL), γBB (1-500 ng/mL), CAR (0.1-500 ng/mL) and A-CAR (1-500 ng/mL) performed on HILIC 150 mm column.

In Table 4-3 and Table 4-4 are presented the lowest concentrations at which molecules were detectable. Developed method appeared to be very sensitive for both columns and able to detect concentrations of 1 ng/mL and below for most of the molecules of interest.

Table 4-3: Detection limits for each molecule separated on HILIC 50 mm.

HILIC 50 mm		
Molecule	**Retention time [min]**	**Limit of detection [ng/mL]**
TML	8.1	1.0
γBB	6.8	0.3
CAR	6.2	0.1

Table 4-4: Detection limits for each molecule separated on HILIC 150 mm.

HILIC 150 mm		
Molecule	**Retention time [min]**	**Limit of detection [ng/mL]**
TML	13.0	10.0
γBB	11.5	1.0
CAR	10.3	1.0
A-CAR	9.9	1.0

4.3.5 MS/MS analysis of TML, γBB, CAR, A-CAR and CAR-d_9

In order to confirm that the identity of the ions was correctly assigned the fragmentation patterns of these molecules needed to be analysed. This analysis is important for further investigation of the complex matrices, i.e. human or yeast whole cell lysates. For that purpose, MS/MS analysis was performed. In MS/MS only pre-defined *m/z* of precursor ions are selected and fragmented by CID [120]. Therefore, the *m/z* of TML, γBB, CAR and A-CAR was selected and the native fragmentation spectra for their standards were obtained in MS/MS mode. The applied method was acquired MS/MS spectra that are presented in Figure 4-11.

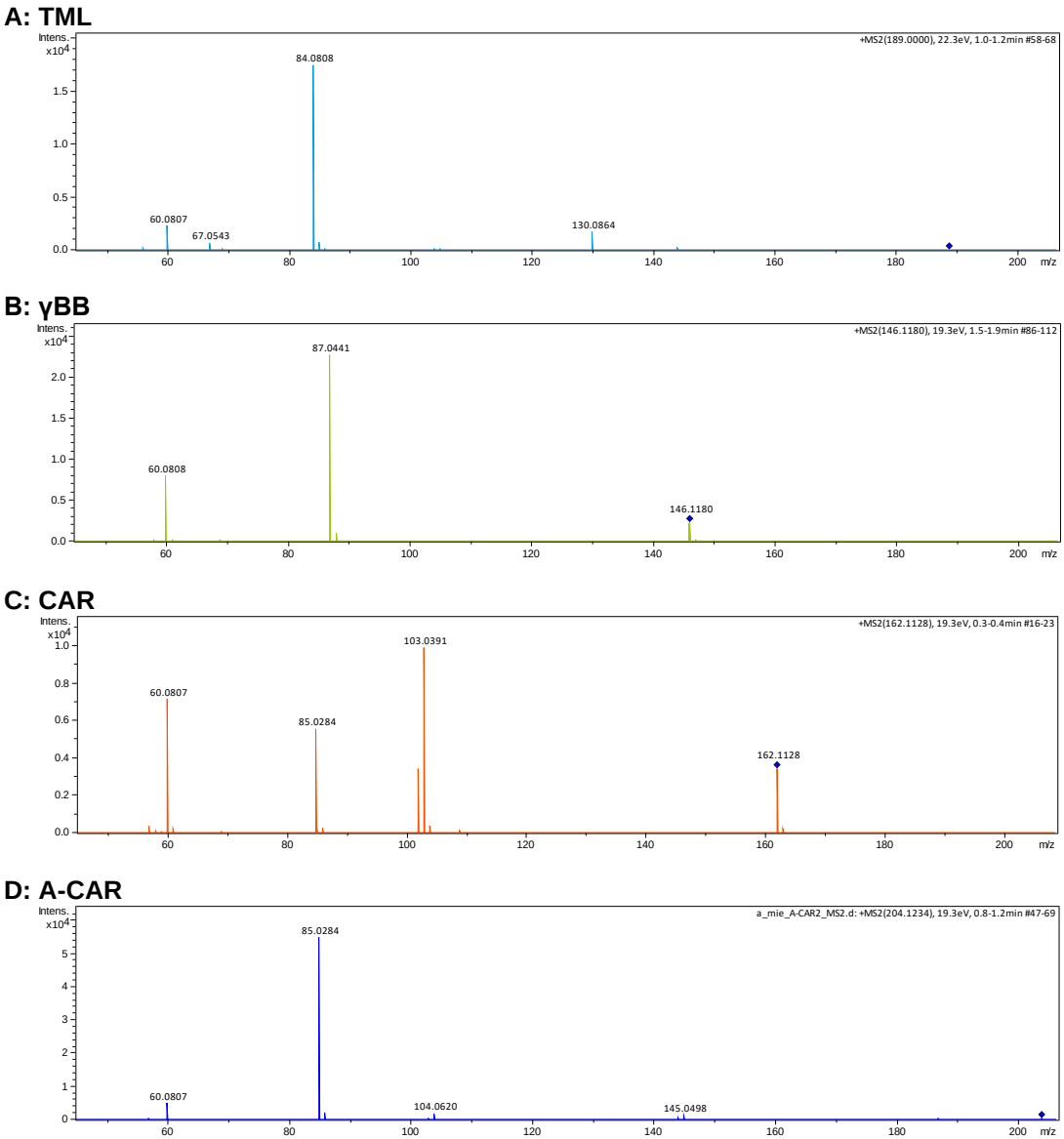


Figure 4-11: MS/MS spectrum for A) TML (light blue), B) γBB (green), C) CAR (red) and D) A-CAR (dark blue) at 1 µg/mL. Analysis performed by in flow injection, no solutions gradient and column was utilised. The collision energy for γBB, CAR and A-CAR was 19.3 eV and for TML was 22.3 eV.

Such direct in-flow injection allowed for pure sample fragmentation observation without any potential contamination from the mobile phase or/and elution from the column. Upon this fragmentation, for each molecule, several product ions were observed (Table 4-5) and matched to their computationally predicted fragmentation pattern obtained by ChemDraw Professional fragmentation tool (Figure 4-12).

Table 4-5: Detected positive ions from in-flow injection and fragmentation of TML, γBB, CAR and A-CAR at 1 µg/mL concentration in MS/MS mode. In yellow: positive ions that masses match to computational fragmentation prediction; In bold are highlighted most intense ions for a particular molecule.

Ions *(m/z)*	**TML**	**γBB**	**CAR**	**A-CAR**
Precursors	189.1597	146.118	162.1128	204.1234
Products	130.0664			145.0498
			103.0391	104.062
	84.0808	**87.0441**	85.0284	**85.0285**
	67.0541			
	60.0807	60.0808	60.0807	60.0807

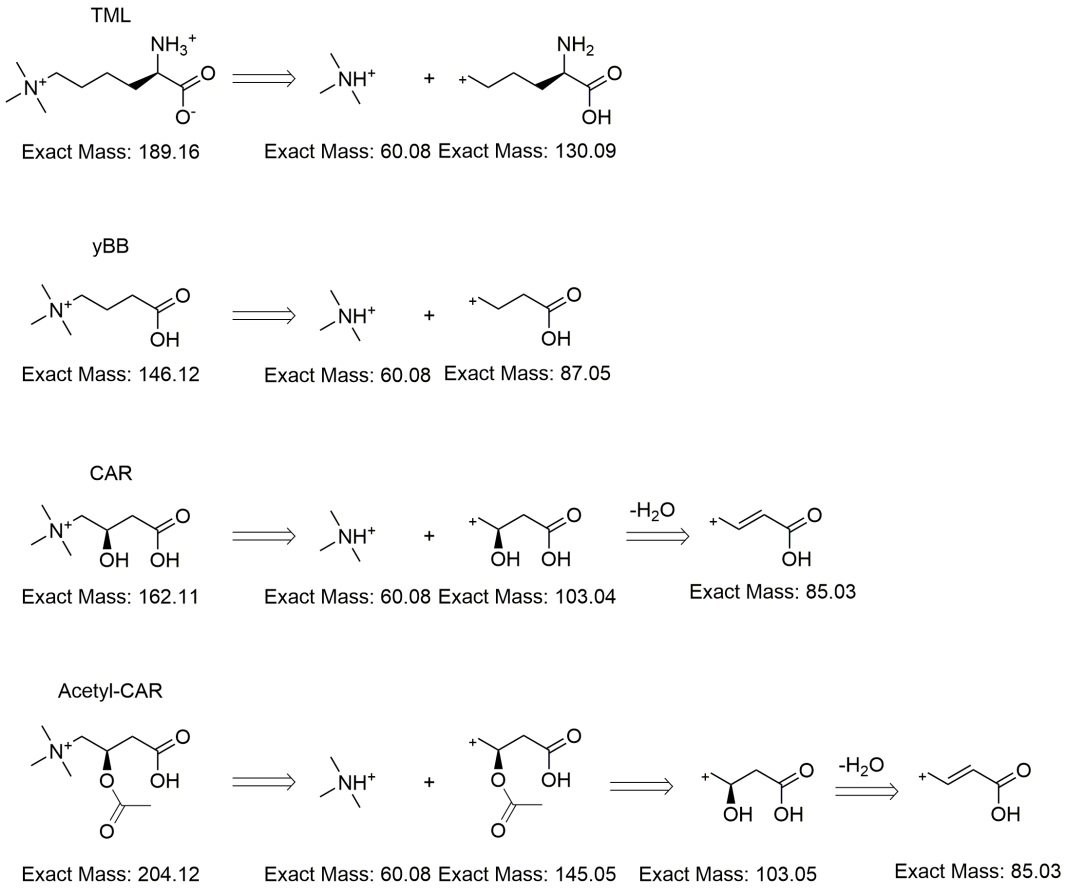


Figure 4-12: Computational fragmentation prediction for a positive ion of TML, γBB, CAR and A-CAR obtained by ChemDraw Professional fragmentation tool.

As all molecules of interest contain a carbon chain ending with a trimethylated amino group, MS/MS detects one common ion for TML, CAR, γBB and A-CAR: 60.0807 that is likely the $C_3H_{10}N^+$ ammonia fragment. Ammonia ion is a common product of fragmentation under CID condition resulting from an onium type fragmentation reaction. Additionally, for each molecule, MS/MS has found a remaining fragment of the substrate as well as other fragments belonging to the ionization pattern.

After obtaining fragmentation patterns of all molecules by in-flow injection, all compounds were fragmented followed by HPLC separation on HILIC 150 mm column to confirm whether detected previously product ions can be detected after developed HPLC separation methods (Appendix Figure 11-4).

Fragmentation patterns after HPLC separation appeared to be similar to these in MS/MS from the in-flow injection (Table 4-6). New ion appeared for a γBB ion with *m/z* = 121. These can be ions coming from HILIC column contamination or mobile phase.

Table 4-6: Detected positive ions from 150 mm HILIC separation and fragmentation of TML, γBB, CAR, A-CAR at 100 ng/mL concentration in MS/MS mode. In yellow: positive ions that masses match to computational fragmentation prediction; In bold are highlighted most intense ions for a particular molecule.

Ions *(m/z)*	**TML**	**γBB**	**CAR**	**A-CAR**
Precursors		146.1153	162.1095	
Products	130.0832	121.9638		145.0488
			103.0364	
	84.079	**87.0421**	85.026	**85.0278**
	69.0665			
	60.0791	60.079	60.0785	60.0798

Observed ionization patterns of TML, γBB, CAR and A-CAR can be utilized in biological tests and molecules identifications.

4.3.6 HPLC-MS/MS method evaluation in yeast and human cell samples

Next, the developed HPLC-MS/MS method was evaluated by testing complex biological matrices of cell extracts. The molecules were identified by comparison of the retention time, the MS and MS/MS spectra, with those of the previously analysed pure standards.

4.3.6.1 S. cerevisiae FY23 1,2,3,4 strain matrix

A sample containing the whole cell *S. cerevisiae* FY23 1,2,3,4 strain lysate was investigated by developed HPLC-MS/MS on HILIC 50 mm column (Figure 4-13). Among detected ions,

the ions with masses of TML, γBB, CAR and A-CAR were found to elute at the same time as observed for corresponding standards (Table 4-7). This result implied that the established method has sufficiently high sensitivity for the intended analysis.

Table 4-7 Comparison of the elution time for each molecule in S. cerevisiae FY23 1,2,3,4 strain lysate separated on HILIC 50 mm column to the standards separation.

Yeast matrix on HILIC 50 mm		
Molecule	**Retention time [min]**	**Expected retention time [min]**
TML	8.4	8.1
γBB	6.8	6.8
CAR	6.2	6.2
A-CAR	6.0	6.1

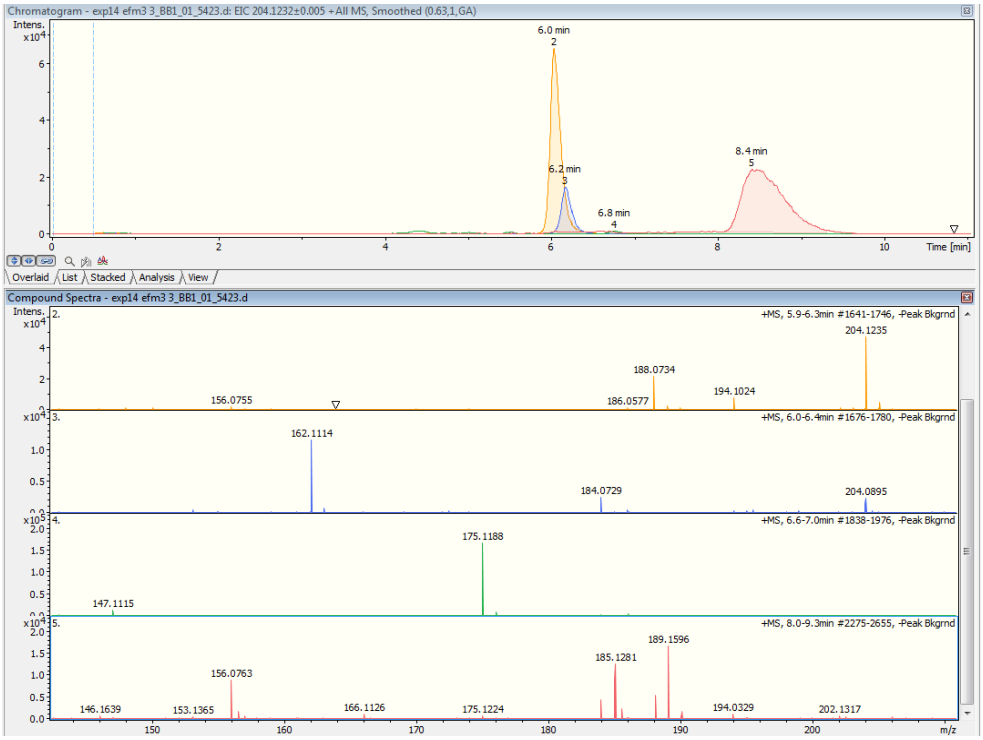


Figure 4-13: *Elution time and MS analysis of yeast extract: TML (on red) retention time was 8.4 min, detected ion m/z was 189.1596; γBB (on green) retention time was 6.8 min, detected ion m/z was 146.1181 (not visible on the picture); CAR (on blue) retention time was 6.2 min, detected ion m/z was 162.1114; A-CAR (on yellow) retention time was 6.0 min, detected ion m/z was 204.1235.*

However, after MS/MS analysis of detected ions, only the identity of TML was confirmed in *S. cerevisiae* cell extract. Fragmented TML ion resulted in product ions with *m/z* = 130.0849, 84.0803, 60.0827 that matched the standard fragmentation pattern (Figure 4-14).

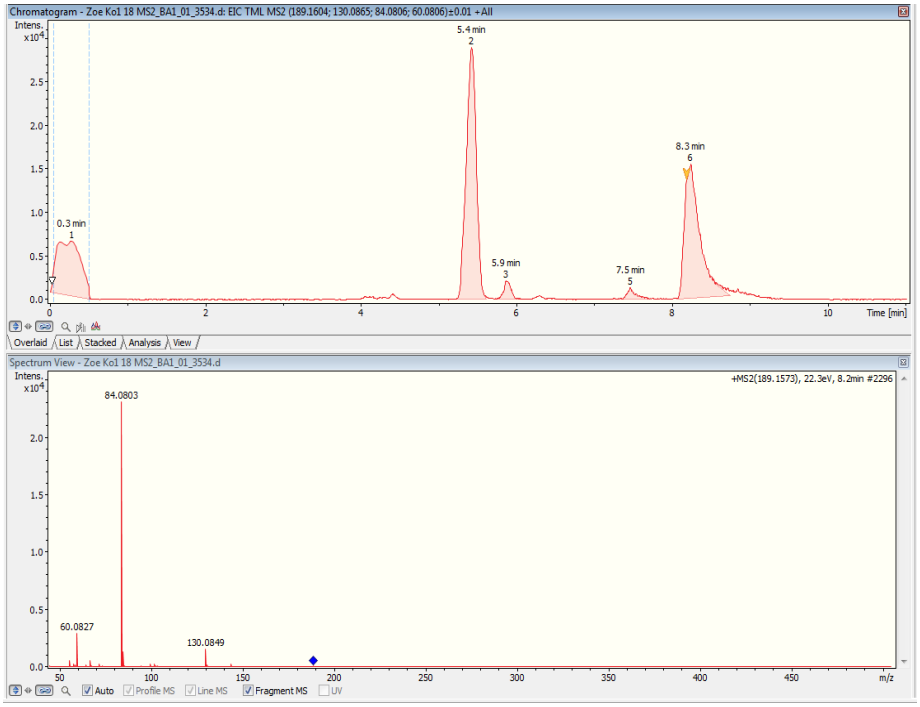


Figure 4-14: MS/MS analysis of yeast extract: TML retention time was 8.3 min; after its MS/MS fragmentation observed product ions m/z were 130.0849, 84.0803, 60.0827.

The identity of the observed molecules matching to *m/z* of γBB, CAR and A-CAR could not be confirmed by MS/MS fragmentation in yeast samples due to their low concentrations for MS/MS analysis. The only confirmed molecule was TML ion.

4.3.6.2 Human cell matrix

In order to further study the carnitine biosynthesis pathway in human cells, an established HPLC-MS/MS method was evaluated by analysis on human HepG2 cell line extract. The analysis was performed on both, HILIC 50 mm and HILIC 150 mm columns (Appendix Figure 11-5). Found ions and peaks elution times were matching to the corresponding standards of γBB, CAR and A-CAR (Appendix: Table 11-1 (for HILIC 50 mm) and Table 11-2 (for HILIC 150mm)). However, no TML *m/z* matching peak was found for both columns in human samples.

A lack of TML detection in the human samples may be a result of very low steady-state levels of TML, due to its dynamic conversion into carnitine, or other interfering pathways. Therefore, the levels of trimethylated lysine in human cell samples were measured by the western blotting method described further in section 5.

Accordingly to the previous yeast samples analysis, to confirm the identity of the found ions in the human samples the MS/MS analysis was performed for each molecule of interest (Appendix Figure 11-6). For each compound, at least one of the characteristic

ions from the fragmentation pattern was found (Appendix Table 11-3). Therefore, the identity of γBB, CAR and A-CAR in human cell extracts could be confirmed.

Above analysis confirmed that it is allowed to utilize developed HPLC-MS/MS method for analysis of TML in yeast samples and γBB, CAR and A-CAR in human cell lysates.

4.3.7 Analysis automation

After establishing the method of detection of the molecules of interest, a method for automated analysis was needed. Through collaboration with Bruker, a Visual Basic script for the automated data analysis of multiple metabolites in large batches of samples for Compass DataAnalysis software was incorporated into the analysis and adjusted to the particular analysis.

The developed script was automatically detecting peaks of the listed ions on the chromatogram. The relative peak area threshold was set as 1% while the absolute peak intensity threshold was set as 500 Abs. Peak minimum valley was set of 20%.

The chromatograms falling into those properties were extracted with a very high mass accuracy +/- 0.005 Da. Then, the extracted peaks on the chromatogram were smoothed, the baseline was subtracted and then the same was performed for the mass spectra of the ions to enable the effective peak area quantification (Appendix Figure 11-7).

Next, the developed script quantified peaks that appear in the expected retention time range on the chromatogram and exported obtained peak areas to an Excel file that can be easily utilized for data normalization and graphic illustrations.

The developed Visual Script allowed a considerable improvement in sample analysis time, being able to analyse ~ 100 samples in 1 h, while without such script manual analysis of 100 samples was taking 2 working days.

4.3.8 Method normalization

A challenging aspect of method development for metabolic analyses is to find an appropriate cellular standard for normalization of the obtained AUC data. Often an isotopically labelled external standard is added during sample preparation. However, this method is inconvenient due to the high cost of the isotopically labelled standards. Another approach is using as an internal standard a molecule whose level represents the amount of biological content in the prepared sample, for example, an amino acid. The difficulty of this method is to identify such a molecule whose levels are not affected by the analysed

cellular pathways and treatment during an experiment. Finally, another method for sample normalization is to utilize an external assay, for example, the protein Pierce BCA assay that measures a total amount of protein in the sample [123].

4.3.8.1 Amino acid as a standard

A molecule within the cell lysates that could serve as an internal standard was searched. Samples of amino acids were prepared and separated on developed HPLC-MS/MS method on HILIC 50 mm column. Among candidates that exposed good separation were L-alanine (ALA), L-isoleucine (ISO), L-leucine (LEU) and L-glutamine (GLU) (Appendix Figure 11-8). Then, four detected amino acid ions were searched in biological samples and only LEU or ISO ions with m/z = 132.1019 were found in biological human samples at the retention time of 5.1 min. Due to the fact that leucine and isoleucine are isomers, they could not be distinguished by MS and created one peak on the chromatogram. Nevertheless, peaks of LEU and ISO were selected for further detailed analysis as an internal standard candidate.

4.3.8.2 Isotopically labelled carnitine as a standard

The last investigated method was using an expensive isotopically labelled standard of carnitine: DL-carnitine-(trimethyl-d_9) hydrochloride (CAR-d_9) as an external standard candidate for MS analysis. CAR-d_9 is a stereochemical mixture of D-carnitine and L-carnitine isomers having 9 deuterium atoms allocated on epsilon-N-methyl groups of CAR.

Firstly, CAR-d_9 standard at 100 ng/mL concentration was separated by the developed method on HILIC 150 mm column to obtain its precise ion mass and elution time (Figure 4-15).

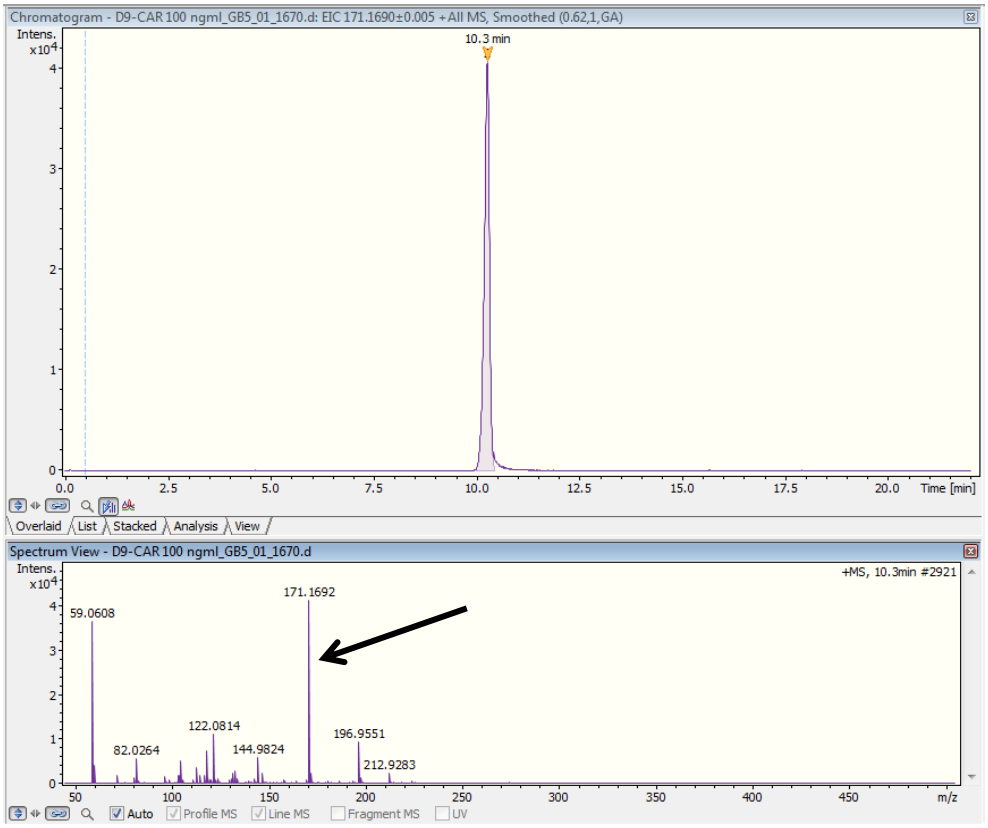


Figure 4-15: *CAR-d_9 retention time was 10.3 min, detected ion m/z was 171.1692.*

CAR-d_9 appeared to elute at the same time as CAR, however, the detected ion of CAR-d_9 was 9 Da heavier than CAR, as expected.

Next, the limit of detection of CAR-d_9 was established by performing dilution series test in concentration range 0.1-500 ng/mL (Figure 4-16 A).

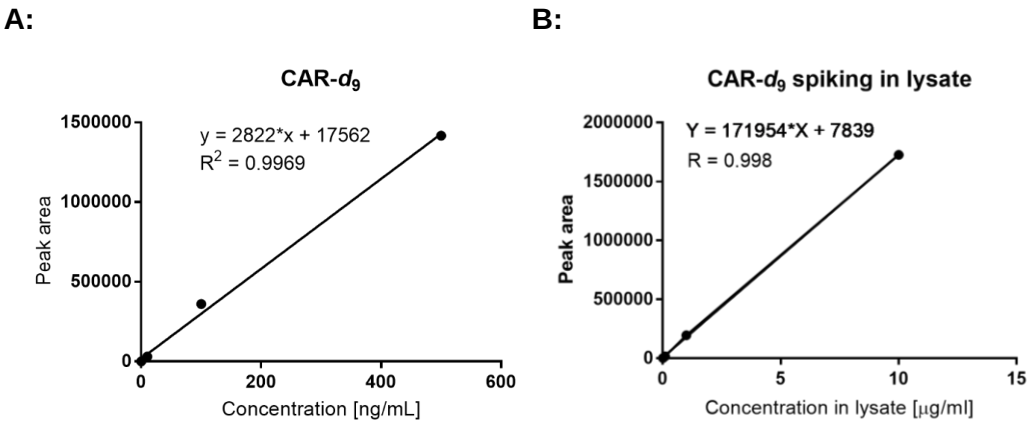


Figure 4-16: A) Linearity of CAR-d_9 detection in a concentration range 0.1-500 ng/mL. B) CAR-d_9 concentration range spiking in human cell lysate (0.01-10 µg/mL) (n=1).

The lowest tested and detectable CAR-d_9 concentration was 0.1 ng/mL. Obtained CAR-d_9 detection limit was even better than for CAR limit for that column. Therefore, CAR-d_9 could be used as a standard without concerns of lack of sensitivity for CAR-d_9 detection.

Next, the MS/MS tests of CAR-d_9 were performed by in-flow injection at 1 µg/mL (Figure 4-17). The obtained products ions are stated and compared to the CAR ionization pattern in Table 4-8.

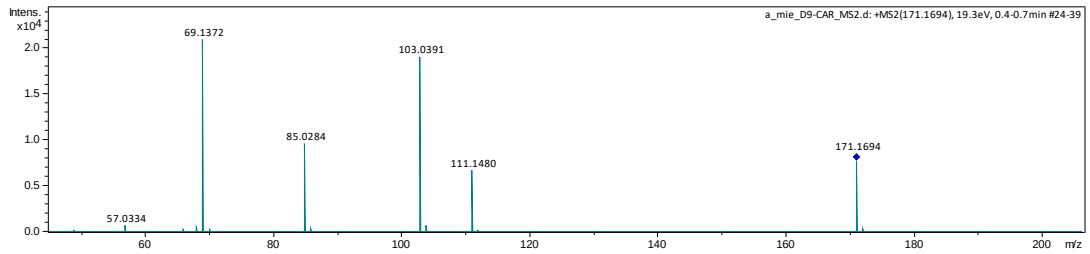


Figure 4-17: MS/MS in-flow injection analysis of CAR-d_9 at 1 µg/mL.

Table 4-8: Detected ions from in-flow injection and fragmentation of CAR-d_9 at 1 µg/mL concentration in MS/MS mode. In yellow: ions that masses match to computational fragmentation prediction; In bold are highlighted most intense ions for a particular molecule.

Ions *(m/z)*	**CAR**	**CAR-d_9**
Substrates	162.1128	171.1694
Products		111.1480
	103.0391	**103.0391**
	85.0284	85.0284
	60.0807	**69.1372**

The main difference in the fragmentation pattern of CAR-d_9 isotope to CAR is the lightest product ion mass. The CAR-d_9 isotope containing 9 atoms of deuterium on trimethylated amino group possess fragment m/z = 69.1372 indicating it is probably heavy isotope of ion $C_3H_{10}N^+$ with m/z = 60.0807 appearing in CAR fragmentation (Figure 4-18).

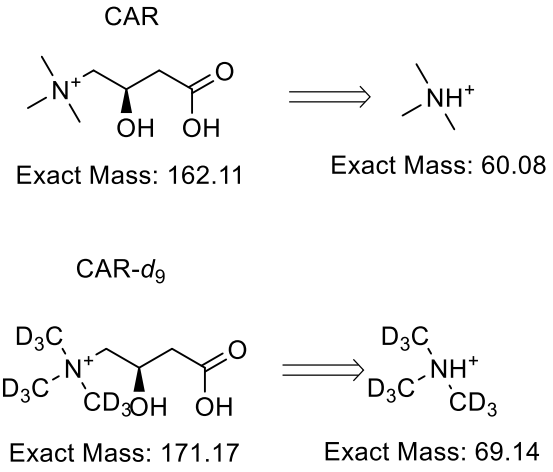


Figure 4-18: Positive ions obtained from computational fragmentation prediction for CAR and A-CAR.

Data obtained allowed testing of CAR-d_9 as an external standard for human samples normalization. CAR-d_9 stock serial dilution solutions were spiked into human sample lysate to establish a range of concentration where added CAR-d_9 isotope can be detectable in the human samples in a linear manner (Figure 4-16 B). The lowest detectable spiked CAR-d_9 concentration in a human cells sample was 10 ng/mL.

To confirm the detected peak identity in human samples, the MS/MS analysis of CAR-d_9 was performed. However, CAR-d_9 only at 1 µg/mL spiking concentration gave the characteristic m/z = 69.13 product ion allowing for the confirmation of CAR-d_9 standard appearance (Appendix Figure 11-9). Therefore, in further experiments, 1 µg/mL concentration of CAR-d_9 was added to the cell lysis buffer to be detected among other analysed molecules in human samples.

4.3.8.3 Protein concentration as a standard

To establish the protein concentration in human cell samples popular Pierce BCA assay was performed using BCA stock serial dilutions as a protein standard used for concentration calculations. Obtained protein concentrations were used as an internal standard candidate.

4.3.8.4 Methods comparison

Next, the above method for data standardization and normalization were tested in multiple data set. Below, the analysis of one of the data sets is presented. A set of 12 different samples grouped in 4 conditions was tested. The three first samples were controls (1-3), then treated with the obesity drug metformin at 1 mM (4-6), at 3 mM (7-9) and at 6 mM (10-12).

Firstly, the content of standard candidates: protein, CAR-d_9 and LEU in all 12 samples was measured and is shown in Figure 4-19.

Next, each group of samples was statistically tested using Student's t-test whether their standard content was significantly different against other sample groups (Table 4-9), for example, whether the protein content in the control (samples 1-3) is significantly different than the CAR-d_9 content in control samples. For that example, the result p=0.9416 is very close to 1.0 which means differences were not significant. Among tested groups only the protein to CAR-d_9 level for group 1 mM metformin was significantly different, as well as the protein to LEU level in group metformin 3 mM. For the rest of the analysis, the content was not significantly different. That test indicated that all of the candidates may potentially be used; however, the strongest result of significance was obtained for CAR-d_9 and LEU as "internal" standards.

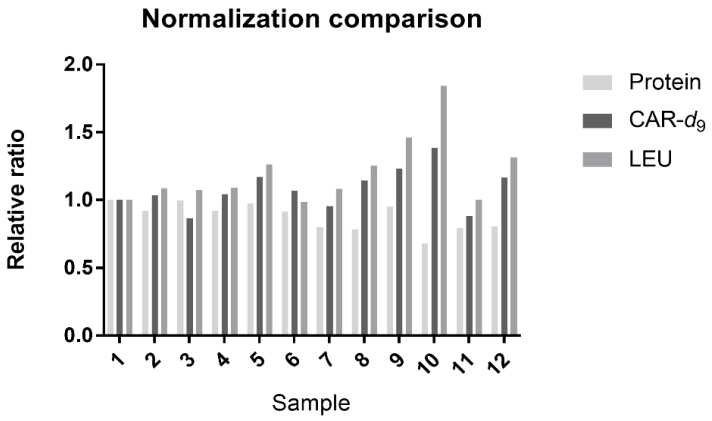


Figure 4-19: Content of each standard candidate in a 12-sample set. Protein: protein concentration in the sample; CAR-d_9: peak area of CAR-d_9 added to lysis buffer at 1 µg/mL; LEU: peak area of leucine/isoleucine. The content of each sample was normalized to the very first sample content for clearer figure formatting.

Table 4-9: Student's t-test of each group of samples. In yellow groups that were significantly different i.e, p<0.05.

Student's t-test			
Sample	**Protein vs CAR-d_9**	**CAR-d_9 vs LEU**	**Protein vs LEU**
1 to 3	0.9416	0.2343	0.0983
4 to 6	0.0348	0.8528	0.1556
7 to 9	0.0624	0.3297	0.0442
10 to 12	0.1093	0.4566	0.1215

Then, the CAR content in each sample was measured by HPLC-MS/MS and normalized to each standard's content. Then for each treatment condition (control, metformin 1 mM, 3 mM and 6 mM) average and error bars were calculated (Figure 4-20).

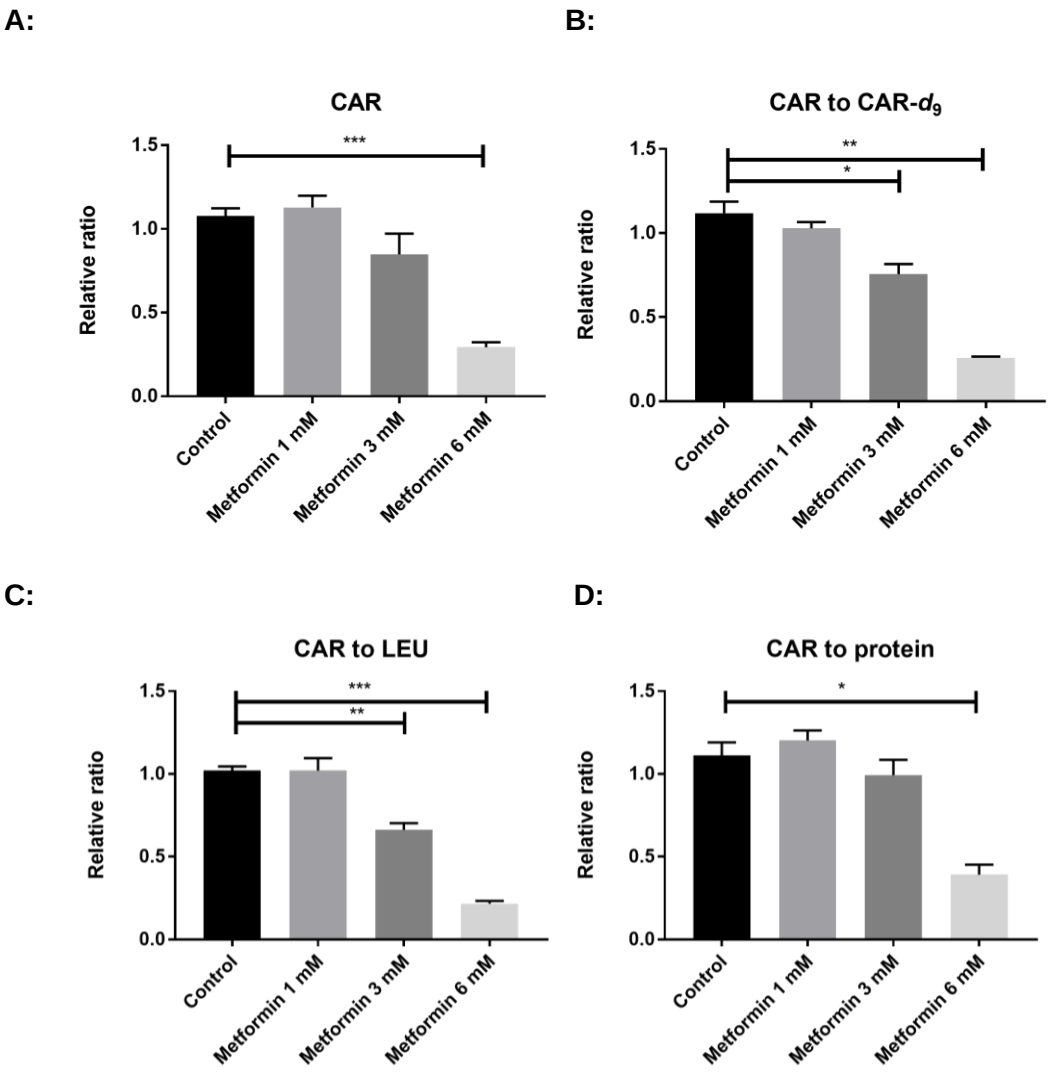


Figure 4-20: CAR level in metformin concentration range treatment. CAR level was A) not normalized, B) normalized to CAR-d_9, C) normalized to LEU, D) normalized to protein content. n=3, p=0.0003, 0.017, 0.006, 0.003, 0.0002, 0.015, respectively.

It can be observed that the results graphs differ from each other, however, preserving a similar pattern of response to metformin treatment. Knowing that metformin decreases CAR level (more results on this effect are described in section 9) the best-presented concentration range response on metformin treatment exhibited graph normalized to CAR-d_9 and LEU levels (Figure 4-20 C and D).

Statistical analysis of comparing each group of result did not show significant differences between groups of treatment (Table 4-10).

Table 4-10: Student's t-test of each group of treatments, p>0.05 mean no significance.

CAR Student's t-test	No normalization vs CAR-d_9	No normalization vs LEU	No normalization vs protein	CAR-d_9 vs LEU	CAR-d_9 vs protein	LEU vs protein
Control	0.6412	0.3660	0.7220	0.2872	0.9535	0.3685
Metformin 1 mM	0.3045	0.3579	0.4679	0.9251	0.0830	0.1355
Metformin 3 mM	0.8842	0.2736	0.4049	0.2832	0.1079	0.0530
Metformin 6 mM	0.3594	0.1096	0.2390	0.1061	0.1528	0.0919

In principal, CAR-d_9 content in the cell should remain at the same level. Therefore, taking into account the above analysis the adjustment of the data ideally should be performed to CAR-d_9 levels. However, due to the cost of CAR-d_9 isotope, other alternatives without normalization to CAR-d_9 were considered. However, each tested method is not ideal in principal. Leucine and isoleucine are amino acids that can change their level depend on the character of the experiment being performed and unintentional intervention of tested drug on LEU level. Protein concentration is measured by separated assay (BCA) that may introduce additional error to the adjustment as BCA assay is not as accurate as ESI-MS/MS. Additionally, protein normalization does not adjust the errors coming from MS sample pipetting and needle injection to the mass spec. The latter disadvantage also refers to the "no normalization" issues.

The presented Table 4-10 indicates that any of the methods exposed significant differences in obtained CAR quantification results. Therefore, whilst neither method lead to wrong conclusions, where possible, normalization to CAR-d_9 internal standard should be performed. For the experiments where such normalization was not possible, less reliable normalization methods (LEU, protein level) need to be utilized.

4.4 Discussion

In order to investigate the epigenetic link to carnitine biosynthesis, yeast *S. cerevisiae* strains were chosen as model organisms in this research study. Consequently, techniques suitable for CAR detection in both models were required.

In this chapter, two *S. cerevisiae* models were applied, modified and examined for further use. The first model is bioengineered FY23 1,2,3,4 strain that is capable of producing CAR and could be utilized for studies of CAR biosynthesis pathway. The second strain is genetically depleted FY631 *cit2Δ* strain that is fully depended on the CAR whilst growing on non-fermentable carbon sources.

Several methods of CAR detection in yeast were tested and optimized. The first method, yeast complementation assay with bioengineered *S. cerevisiae* strain capable of producing CAR appeared to be sensitive, however, not quantitative for CAR detection in yeast samples. The second method, fluorescent CAR detection kit allowed for quantitative CAR analysis. However, it exposed several technical and methodical limitations, i.e one metabolite analysis at the time, handling dangerous acids and not a convenient procedure for large batches of samples preparation. Lastly, the HPLC-MS/MS method was tested for qualitative and quantitate analysis of CAR and its associated metabolites.

An HPLC-MS/MS method, that development was described in this result chapter, enables to quantify relative levels of TML, γBB, CAR and A-CAR in biological samples. Due to the high polarity of these molecules, an HPLC method using a normal-phase HILIC [122] column was developed to separate molecules before injection and ionization in the mass spectrometer (MS). A real-time detection was performed allowing selection of mass and elution times of ions corresponding to the molecules of interest. For the confirmation of detected ions, a second ionization was utilized (MS/MS) and their fragmentation pattern was observed and compared to standards. Analysis of developed HPLC-MS/MS method accuracy and limit of detection for standards of TML, CAR, γBB and A-CAR was performed. The method was validated in complex matrices such as human and yeast cell extracts.

The developed method allows for the automated quantification of TML, CAR, γBB and A-CAR in yeast samples. Additionally, human HepG2 cell line extracts were tested on developed method and CAR, γBB and A-CAR were successfully detected in human cell samples. TML levels were difficult to measure in human cell lysates, probably due to its rapid transformation to hydroxytrimethyllysine (HTML) or other products in carnitine biosynthesis pathway [124].

The result of quantifications was tested against different standards and normalization methods, including the utilization of isotopically labelled CAR-d_9 standards.

5. Establishing a method for protein studies

To complement the methodology of analysis of the link between epigenetics and carnitine biosynthesis, an appropriate technique for histone proteins studies was required. The desired method should enable the investigation of the effect of the applied genetic modifications and drug treatments on histone PTMs, particularly level of the lysine methylation (Figure 5-1 A) and histone degradation (Figure 5-1 B). Importantly, such protein studies can supplement the HPLC-MS/MS method and particularly the problems arising from the lack of free TML detection in the human cell extract.

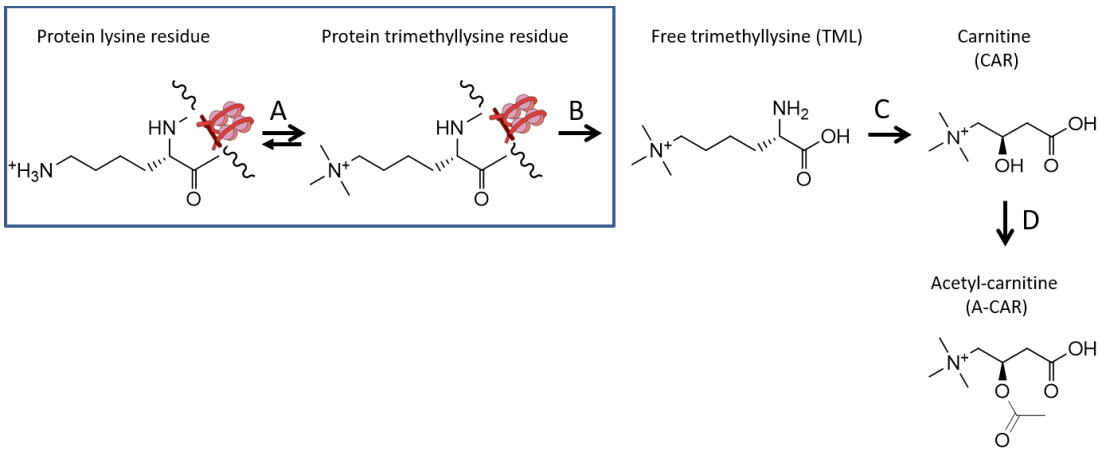


Figure 5-1: Optimized method of protein detection would enable for studies of histone lysine modifications (A) and protein degradation (B) role in carnitine biosynthesis.

Histone and non-histone proteins can be studied using immunochemistry methods that applies various antibodies detecting specific protein or specific protein modification. One of the most common immunochemical techniques is Western blotting that can be used for quantification of histone lysine modifications, including trimethylation and acetylation [125], [126]. Therefore, the western blotting technique was optimized and validated to study histone proteins.

5.1 Histone extraction method

Histones are proteins located in the nucleus, therefore, proper histone isolation technique was needed to be optimized. For that purpose, two protocols of histone extraction were tested on HepG2 cell line: Abcam (Abcam) and Miller [103] method (Figure 5-2). Both methods mainly differ from the composition of the cell lysis buffer and acid used for histone extraction. While Abcam method recommended using Triton X100 as a mild surfactant for cell lysis and 0.2 N HCl for histone acid extraction, Miller method did not

contain usage of any surfactant and utilized more concentrated 0.4 M H_2SO_4 for histone extraction.

Immunoblotting of the obtained samples with an antibody recognizing any (histone and non-histone) trimethylated lysine (TML) residues resulted in the detection of several proteins of different molecular weight. Using the Miller histone extraction method, the TML antibody was found to bind to proteins with ~30 kDa and 50 kDa size, whereas in the Abcam method, TML recognized proteins of size ~15 kDa. Also, as control, cytoplasmic fractions obtained by each extraction method were tested. In all cytoplasmic samples, the TML antibody detected a protein of ~50 kDa size.

The histone core protein (H2A, H2B, H3, and H4) masses range from 11-17 kDa. Therefore, the above experiment indicated that successful histone extraction was likely achieved by the Abcam method, whereas the Miller method contains predominantly cytoplasmic proteins.

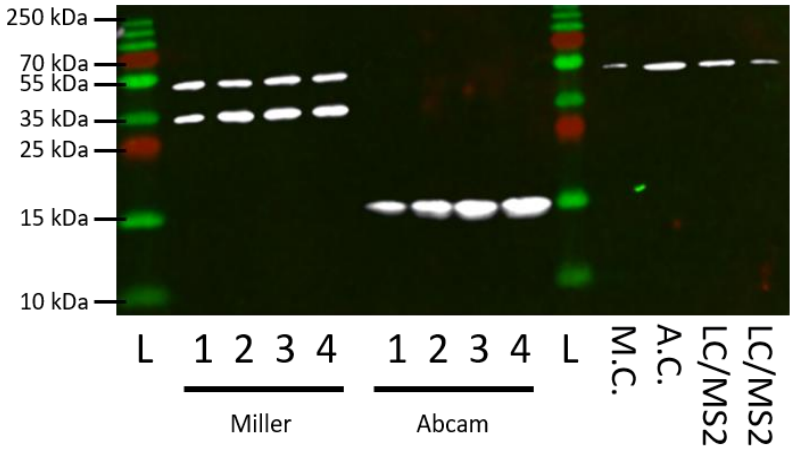


Figure 5-2: Comparison of Miller and Abcam histone extraction protocol by western blotting (WB) with trimethylated lysine antibody. L – protein ladder; 1-4 Miller: histones extracted with Miller protocol; 1-4 Abcam: histones extracted with Abcam protocol; M.C. – cytoplasmic protein fraction from Miller protocol; A.C. – cytoplasmic protein fraction from Abcam protocol; HPLC-MS/MS – cytoplasmic fraction used for HPLC-MS/MS analysis in the previous chapter.

5.2 Histones identification with HPLC-MS/MS

After the optimisation of the employed histone extraction method optimisation, it was necessary to confirm the identity of the proteins observed to bind to the TML antibody. The most common method for such an analysis is mass spectrometry. "Top-down" and "bottom-up" are two popular approaches to identify proteins by MS [127]–[129].

The “top-down” method [127], [130] relies on injecting the intact protein or a large fragment of protein into the mass spectrometer ion source. In this approach, usually the electron capture dissociation (ECD) or electron transfer dissociation (ETD) techniques are used for protein fragmentation in tandem mass spectrometry (MS/MS) [131]–[134]

In the “bottom-up” method [135], proteins are first digested into peptides using proteolytic enzymes. Then, the LC separates peptides before injecting them into the mass spectrometer (similarly to the method described in section 4). Next, the MS/MS fragmentation analysis is performed on the most intense eluting peptides. CID fragmentation is one of the commonly used techniques for fragmenting peptides [136]. Often, fragmentation is performed in DDA mode that selects the most intense precursor peptides for the MS/MS. Each of the fragmented peptides has its unique set of product ions called peptide mass fingerprint. Such fingerprint is compared to the available peptides databases and that approach enables peptide sequence identification and, consequently, determines protein identity [137], [138]. A commonly used software for proteomic database search is SEQUEST [138].

Unlike big multiply-charged proteins, small peptides generated in bottom-up analysis can be very efficiently separated with widely used LC methods. In this way, bottom-up experiments benefit from better fragmentation efficiency and, therefore, higher sensitivity than intact protein analysis. Top-down experiments are ideal for the single analysis of pure proteins rather than for complex biological samples. Therefore, for the histone analysis of this study, a bottom-up approach was chosen for further analysis.

5.2.1 In-gel histone digestion

Firstly, the digest was performed with the trypsin that is a member of the serine protease S1 family. As trypsin cleaves at lysine and arginine residues, it was considered suitable for histones that are rich in lysine residues [139]. Therefore, six bands from the histone fraction were selected for trypsin digest analysis. Additionally, one band from the cytoplasmic fraction was included to identify the cytoplasmic protein that also exposed trimethylation on lysine residues in the previous subchapter (Figure 5-3).

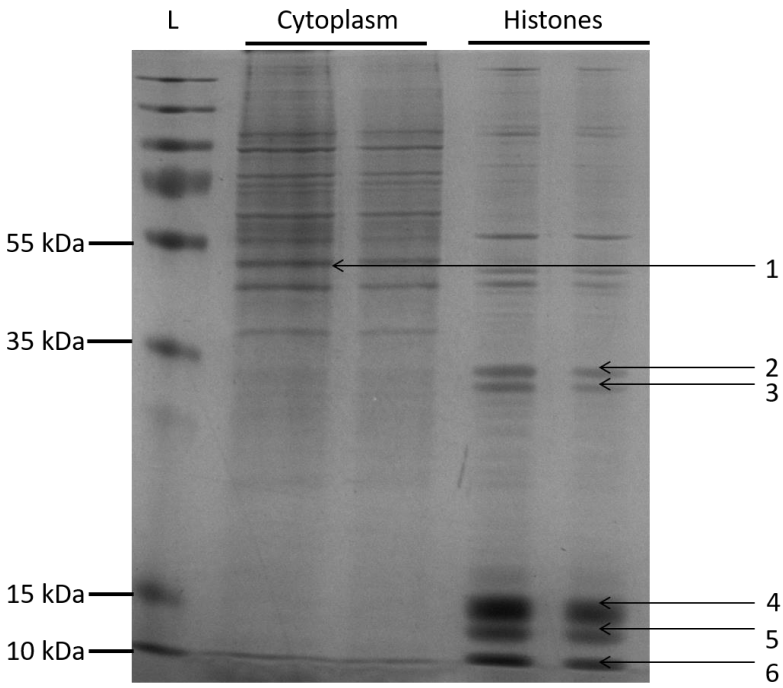


Figure 5-3: Selected bands for in-gel digestion with Trypsin. Band 1 belongs to the cytoplasmic fraction and bands 2-6 to an extract from the Abcam method without protein precipitation. Gel: 12.5% of 7 µg protein.

The products of trypsin digestion were injected into HPLC-MS/MS for analysis of peptides mixture. Sequences of peptides were then analysed with SEQUEST against a human protein database. Next, peptides that may belong to the same protein sequence were grouped and groups with the highest identity probability are summarised in Table 5-1.

Table 5-1: DDA analysis results for Trypsin digestion of bands 1-6. Band MW - approximated molecular weight of cut band; a number of found peptides – peptides covering part of the identified protein, DDA result – identified protein upon database search of found peptides, probability – the probability of appearance of found peptides in the identified protein sequence.

Band No.	Band MW (kDa)	No. of found peptides	DDA result	Probability	MW of DDA result (kDa)
1	50	6	Eukaryotic translation elongation factor 1 alpha 1	0.00001	50
2	34	1	H1 histone family, member 0	9.3E-08	32
	34	3	H1 histone family, member 2	1.20E-06	32
	34	1	H2A histone family, member A	1.30E-06	14
3	33	3	H1 histone family, member 2	2.1E-07	32
	33	3	H1 histone family, member 5	1.50E-05	32
	33	1	H2A histone family, member A	2.20E-04	14
4	14	2	Histone 2, H2bf	1.4E-08	14
	14	2	H2A histone family, member A	5.00E-08	14
	14	1	Histone 1, H2ad	5.60E-07	14
5	15	0	n/a	n/a	n/a
6	10	6	H4 histone	3.9E-08	11

The cytoplasmic band 1 was identified as the eukaryotic translation elongation factor 1 (EF1α) protein: the analysis found six peptides matching to the EF1α sequence. Immunoblotting of the same band with an antibody against EF1α supports this finding (Figure 5-4 A).

Analysis of the band 6 found six peptides matching to the H4 sequence. The analysis was additionally supported by western blotting of the histone fraction incubated with histone H4 antibody (Figure 5-4 B).

The band 4 was identified as a histone H2A. Several variants of this histone family were matched to the found peptides, including H2bf and H2ad. The identity of the band was also supported by the observed molecular weight of the band and histone H2A (14 kDa).

The bands 2 and 3 were identified as different variants of histone H1 or H2A. However, taking into account their theoretical molecular weights, it is more likely the observed bands belong to variants of H1 histone.

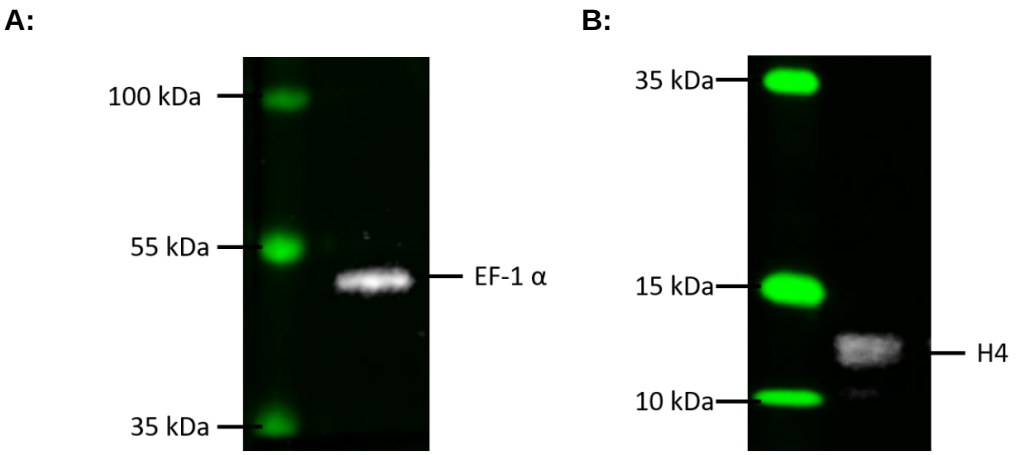


Figure 5-4: Western blotting of Abcam cytoplasmic fraction of HepG2 cells with A) EF1α antibody (1:1,000); B) H4 antibody (1:1,000) and anti-mouse secondary antibody (1:5,000).

The identity of the band 5 was not observed with trypsin digestion. However, this does not exclude the possibility of it belonging to the histone family.

To confirm the identity of additional histone proteins in the extract, the digestion with GluC enzyme was performed (Figure 5-5). GluC cleaves at the C-terminus of aspartic or glutamic acid residues and it is also widely used for histone digestion [139], [140].

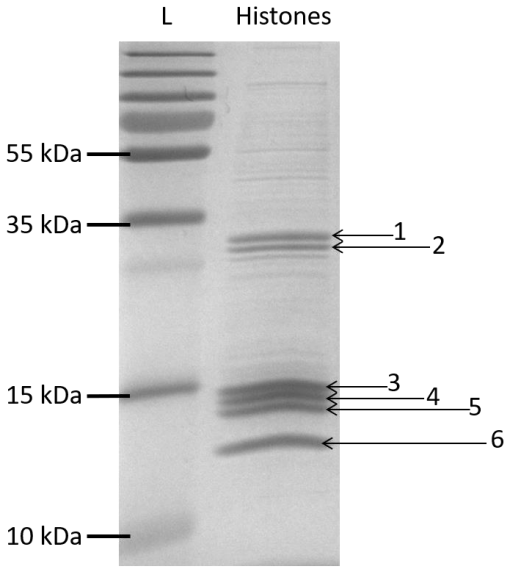


Figure 5-5: Selected bands for in-gel digestion with Gluc C. Band 1-6 from Abcam method extraction without protein precipitation. Gel: 12.5% of 5 µg protein.

After the digestion with GluC and HPLC-MS analysis, peptides were grouped as before and the proteins with the highest identity probability are presented in Table 5-2.

Table 5-2: DDA analysis result for GluC digestion of bands 1-6. Band MW - approximated molecular weight of cut band; a number of found peptides – peptides covering part of the

identified protein, DDA result – identified protein upon database search of found peptides, probability – the probability of appearance of found peptides in the identified protein sequence.

Band No.	Band MW (kDa)	No. of found peptides	DDA result	Probability	MW of DDA result (kDa)
1	34	1	Glutamate receptor, metabotropic 7 isoform c precursor	7.70E-04	102
2	33	0	n/a	n/a	n/a
3	14	3	Histone 2, H2Bf	7.30E-05	14
4	14	1	ZinC finger protein 641	3.00E-04	49
5	14	1	Histone 2, H2Bf	1.90E-04	14
6	12	1	H4, member J	1.20E-04	11

Among the six bands the identification probability for histones was high for band 3 (histone H2B), band 5 (also histone H2B) and band 6 (histone H4). All molecular weights of these bands match to the theoretical of the corresponding histone molecular weight, confirming their identity.

The appearance of ZinC finger protein peptides in band 4 was an interesting observation. One of the families of ZinC finger domain-containing proteins belongs to the MYST family of histone acetyltransferases (HAT) [141]. Therefore, a peptide from ZinC finger domain proteins possibly could have been bound to one of the histones appearing in the band 4 at the moment of digestion.

Additionally, GluC digestion did not confirm the histone H1 identity of band 1 and 2.

The difficulty of confirming the identity of all histones with both used enzymes may be the consequence of certain inherent problems with the applied bottom-up method. Firstly, long peptides (longer than 25 amino acids) tend to strongly bind to the employed C18 HPLC column. Secondly, some short peptides are very hydrophilic and are eluted immediately after injection, thus, with low detection sensitivity. These limitations cause decreased histone sequence coverage and result in a lack of protein identification. The H3 digestion with trypsin that targets lysine and arginine generates many short and hydrophilic peptides that cause difficulties in method sensitivity.

Moreover, one of the weaknesses of the search algorithms is the difficulty to identify peptides with multiple PTMs. In the used SEQUEST search engine, the employed method was limited to up to three modifications per peptide. In the case of PTM-rich histones,

such limitation may have excluded identification of some large histone sequences. Therefore, histone peptides that are rich in very stable and frequent modifications like methylation and acetylation, could not have been identified with utilized search tools. On the other hand, increasing the limit of PTMs per peptide in the searching options, besides the increased search time per peptide, typically results in obtaining false positive results [142].

Nevertheless, the bottom-up MS detected many peptides belonging to histone proteins H1, H2A, H2B, and H4 confirming the effectiveness of the employed histone isolation method.

5.3 Discussion

A method of histone extraction was optimized and validated by in-gel digestion with GluC and Trypsin followed by bottom-up MS. Several histone core proteins, such as H2A, H2B, and H4 were found in histone extracts. That finding allowed concluding that the observed western blot bands of lysine trimethylation correspond to histone proteins. Additionally, a non-histone protein that undergoes lysine trimethylation was found and identified as EF1α.

Therefore, this method allows for quantification of total lysine methylation levels on histone and non-histone proteins. Such a tool can be utilized for further studies on the link between the PTM of proteins, protein degradation, and CAR biosynthesis.

6. Epigenetic links to carnitine metabolism in *S. cerevisiae*

Genetic manipulation and biochemical laboratory methods are well established in *S. cerevisiae*. Additionally, *S. cerevisiae* has a relatively small genome, making it a useful eukaryotic model system for biological studies as discussed in section 4. *S. cerevisiae* has been exploited in this study to gain an initial understanding of the importance of cellular methylation in carnitine biosynthesis. The simplicity and genetic malleability of *S. cerevisiae* enable initial observations to be made which subsequently can be translated into the more complex human cell.

Therefore, this results chapter is dedicated to the investigation of the link between epigenetics and carnitine metabolism in *S. cerevisiae,* which includes:

- Validation of the enzymes required for CAR production in *S. cerevisiae*;
- Optimisation of the *S. cerevisiae* strain that fully complements CAR biosynthesis from TML;
- Selection of *S. cerevisiae* genes linked to cellular methylation and CAR biosynthesis;
- Gene deletions of protein KMTs and protein KDMs to alter TML levels;
- Utilization of the HPLC-MS/MS method for metabolic analysis of *S. cerevisiae* gene deletion strains;
- Identification of the KMTs and KDMs which significantly impact TML levels, followed by analysis of chemical inhibition of these enzymes;
- Studying the importance of the cellular methylation cycle on CAR biosynthesis using a methylation inhibitor.

6.1 Validation of the enzymes required for carnitine production

Previous studies have shown that the *S. cerevisiae cit2Δ* strain is carnitine-dependent when grown on non-fermentable carbon sources (section 4). These growth conditions can be complemented with the FY23 1,2,3,4 engineered strain capable of producing CAR. The constructed FY23 1,2,3,4 strain possesses all four carnitine biosynthesis enzymes and can utilize TML for CAR production (Figure 6-1). Therefore, the above FY23 1,2,3,4 strain can be used for studying the epigenetic link to energy metabolism in a simple eukaryotic organism with analytic methods developed in section 4.

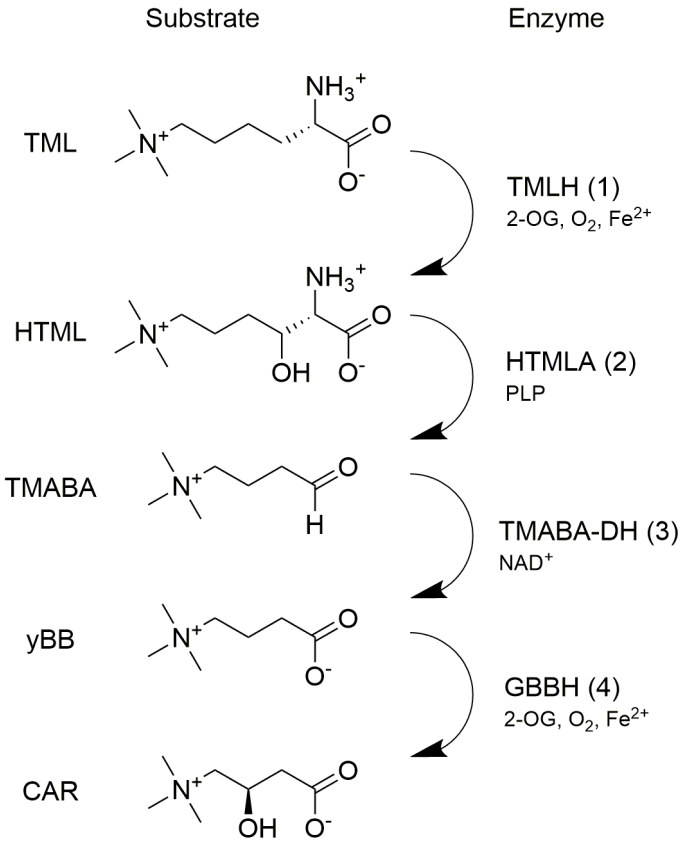


Figure 6-1: Four-step carnitine biosynthesis pathway: 1 – TMLH; 2 – HTMLA; 3 – TMABA-DH; 4 – GBBH.

6.1.1 Obtaining FY23 1,3,4 and FY23 1,4 strains

Recently researchers have identified several native genes of *S. cerevisiae* which may enhance the reconstructed carnitine biosynthesis pathway efficiency. For instance, the serine hydroxymethyltransferases Shm1p and Shm2p are possibly capable of catalysing the second step of the carnitine biosynthesis pathway, suggesting that the original *N. crassa* HTMLA enzyme is not required for carnitine biosynthesis [79].

To validate this hypothesis, the plasmid providing the HTMLA enzyme in strain FY23 1,2,3,4 and FY23 1,2,4 strain was genetically deleted (data not show). This plasmid utilizes TRP1 as an auxotrophic marker, thus it was possible to use the counterselection TRP1 with 5-FAA selection. Only strains lacking the *TRP1* gene were resistant against 5-FAA. This technique was used to obtain two new yeast strains FY23 1,3,4 and FY23 1,4 which enabled the study of the importance of the HTML coding gene for carnitine biosynthesis. Importantly, if HTML supplementation was not required for carnitine biosynthesis, then the TRP1 auxotrophic marker would be available for another genetic approach of manipulation carnitine levels in further studies.

6.1.2 Validation of the requirement of the second enzyme in CAR biosynthesis in FY23 strains

To validate the capability of the FY23 1,3,4 strain to produce carnitine, a complementation "halo" assay described in section 4. was utilized. A small amount of the strains FY23 1,4, FY23 1,2,4, FY23 1,3,4 and FY23 1,2,3,4 were introduced to the *cit2Δ* strain growing on a non-fermentable medium with the addition of an external TML source. After 6 days incubation, the "halo" effect could be observed around the FY23 1,3,4 and FY23 1,2,3,4 strains. Strain FY23 1,2,4 exposed a very weak "halo" formation and there was no growth support around the FY23 1,4 strain (Figure 6-2).

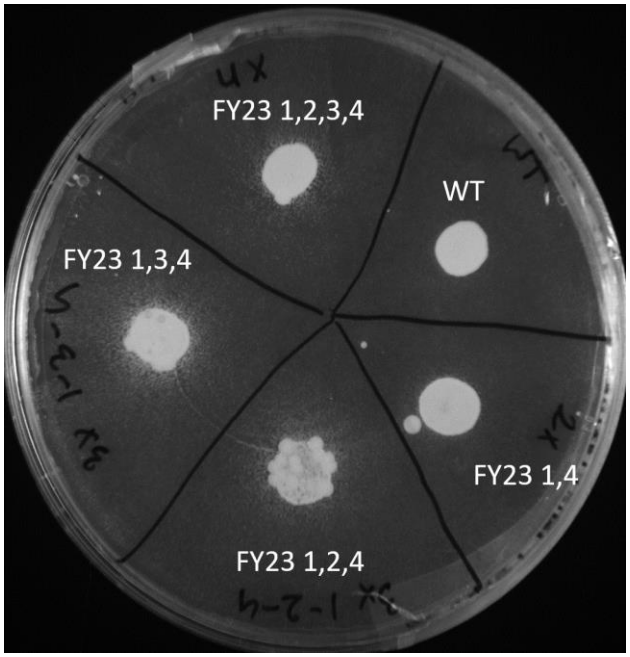


Figure 6-2: Validation of enzymes required for carnitine production on SDEG with TML supplementation. Strong "halo" formation appeared only for the strain FY23 1,3,4 and FY23 1,2,3,4. Pictures were taken after 6 d incubation.

The “halo” formation appears due to CAR leaking into the medium enabling *cit2Δ* strain growth. Thus, CAR is produced by strains FY23 1,3,4 and FY23 1,2,3,4 and to some extent by FY23 1,2,4 but not by the FY23 1,4 strain. This indicates that, as suggested in the literature, the HTML enzyme carried by the HTMLA plasmid (number 2) is not crucial for carnitine biosynthesis whereas all other enzymes (number 1, 3 and 4) are needed for this process. Therefore, as suggested previously, it is possible that *S. cerevisiae* natively possesses an enzyme catalysing the second step of CAR biosynthesis.

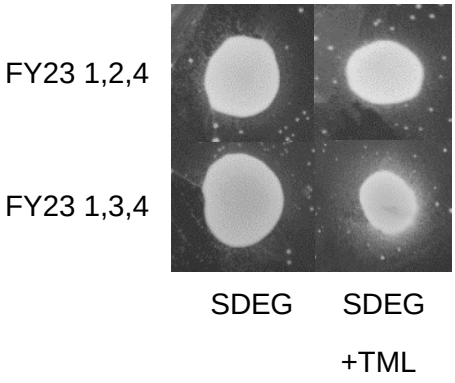


Figure 6-3: Effect of TML supplementation on FY23 1,2,4 and FY23 1,3,4 growth. The concentration of added TML was 6.66 µg/ml. Pictures were taken after 6 d of incubation.

Additionally, it was assessed whether TML supplementation is necessary for CAR production and complementation for *cit2Δ* strain growth. For that purpose, FY23 1,2,4 and FY23 1,3,4 strains were used in “halo” formation assay on agarose plates supplemented with and without TML. After 6 days incubation, strong halo formation around the FY23 1,3,4 strain was observed on plates only supplemented with TML (Figure 6-3). This result shows that the addition of TML is necessary to observe the CAR production effects which also confirms literature findings [79]. Additionally, this experiment highlights that the level of endogenous TML is insufficient for “halo” formation. Thus, for sufficient endogenous TML production and CAR biosynthesis, strains and/or experimental conditions must be further modified.

6.2 Optimisation of CAR biosynthesis in *S. cerevisiae*

The above experiments have provided evidence that *S. cerevisiae* possesses a native enzyme capable of catalysing the second step of carnitine biosynthesis from TML. According to recent findings, it is probable that Shm1p and Shm2p may play a role in carnitine production. This hypothesis may be supported by the research suggesting that HTML enzyme does not exist and that the reaction is performed by a serine hydroxymethyltransferase (SHMT) [143].

It was found that deletion of one of SHMT genes (mitochondrial *SHM1* or cytoplasmic *SHM2)* in *S. cerevisiae* increases the level of biosynthesised carnitine in *S. cerevisiae* and s*hm1Δ* elevates CAR levels up to 9-fold [79]. Both of these enzymes are serine hydroxymethyltransferases, which convert serine to glycine [144]. They probably compete for the substrate and, due to their different location, distribute their products to different metabolic pathways in such a way that they balance each other's activity. However, when one of the SHMT genes is deleted, their equilibrium is impaired resulting in enhanced CAR biosynthesis.

6.2.1 Deletion of SHM1 gene in FY23 1,3,4 strain

Data in the literature indicate that it may be possible to improve the production of carnitine by deleting the *SHM1* gene. To validate this idea, the *SHM1* gene was deleted on the parental FY23 1,3,4 strain using the TRP1 auxotrophic marker available from the HTML plasmid removal. The transformation was performed via homologous recombination of the genomic *SHM1* locus by the *TRP1* gene for which both positive and negative selection systems exist. The primers used for plasmid amplification are listed in (Table 3-6). Transformants were inoculated on SD-Ura-Trp agar plates and after 3 days of growth, the FY23 1,3,4 strain started to form colonies. After 7 days the leakage of tryptophan into the medium could be detected as "halo" growth for successfully transformed colonies, supporting the growth of surrounding non-transformed cells. The positive colonies were spotted onto new SD-Ura-Trp plates. After another 3 days of growth, liquid cultures of colonies were prepared, their genomic DNA isolated followed by PCR with checking primers (Table 3-7) to confirm the successful deletion. Visualized fragments of amplified DNA are shown in Figure 6-4. Among four potential depleted colonies, one colony had been successfully confirmed by Sanger sequencing.

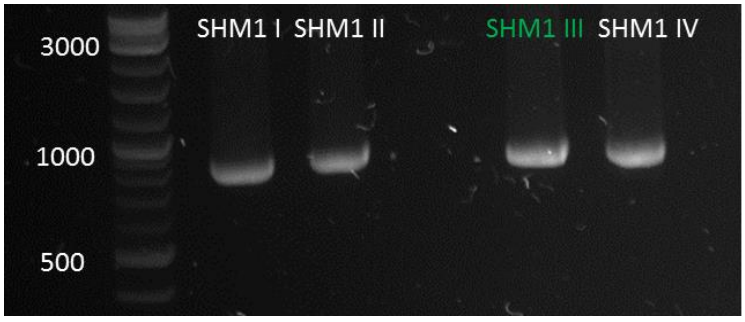


Figure 6-4: Separated DNA fragments of four colonies of FY23 1,3,4 strain with SHM1 deletion. The visible fragments represent the TRP1 gene (675 bp + 100 bp of flanking regions). The strain labelled on green (III) was confirmed by Sanger sequencing as a successful replacement.

6.2.2 HPLC-MS/MS analysis of *shm1*Δ strain

The "halo" formation assay appeared to be an excellent tool for visual selection of the depleted strains, however, it was not useful in quantitate CAR analysis. To investigate whether *SHM1* gene deletion influences carnitine levels, the "halo" complementation appeared to not be sufficiently sensitive for changes in CAR levels leaking to the agar plates and, therefore, failed in the comparative analysis of obtained depleted FY23 1,3,4 strains (data not shown).

Therefore, the HPLC-MS/MS method developed in section 4 was used for intended metabolites detection and quantification in FY23 1,3,4 *shm1Δ* strain cell extract. Firstly, cells were grown for 24 h in glucose-rich medium without adding TML. Next, cells were lysed and the lysate was analysed by HPLC-MS/MS. In these conditions, MS identified a small amount of carnitine biosynthesis for FY23 1,3,4 and FY23 1,3,4 *shm1Δ* strains and also detected A-CAR appearance in the extracts (Figure 6-5). Despite the fact that CAR levels seemed to be decreasing in the *shm1Δ* strain, the detection of CAR and A-CAR in the above growth conditions without external TML addition was a positive observation. Weak detection of CAR may be due to the strains being grown on glucose for only 24 h, therefore, glucose would not have been fully depleted. If glucose is still present in the media, yeast does not need to utilise non-fermentable carbon sources for survival. Thus, the production of carnitine, which shuttles acetyl groups to the mitochondria, is not necessary for cell growth.

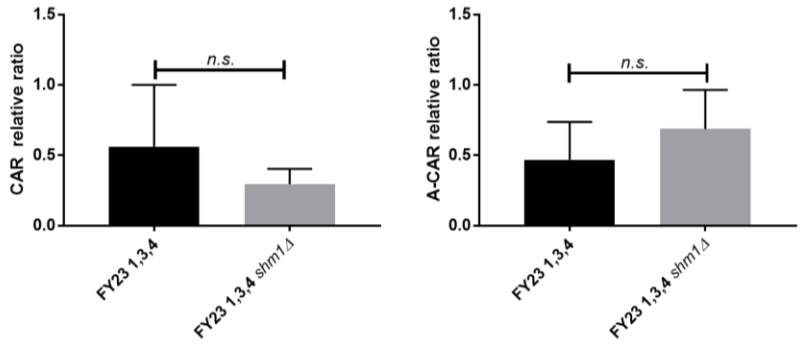


Figure 6-5: Relative CAR and A-CAR levels in FY23 1,3,4 cells and in shm1Δ strain after 24 h growth time (n=2, mean ±SEM).

Therefore, the growth of both strains was extended to 120 h that was sufficient to observe CAR production in both strains. The result of CAR quantitate analysis was consistent with the literature in that the depletion of *SHM1* caused an increase in CAR biosynthesis and consequently A-CAR levels compared to FY23 1,3,4 cells (Figure 6-6) [79]. The observed CAR level was elevated by 2.5-fold, while A-CAR by 5-fold.

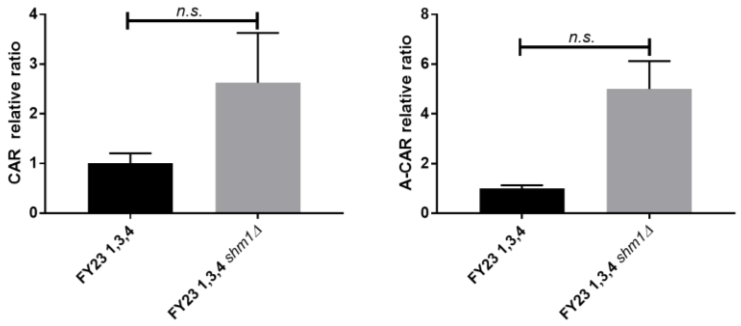


Figure 6-6: Relative CAR and A-CAR levels in FY23 1,3,4 cells and in FY23 1,3,4 shm1Δ strains after 120 h growth time (n=2, mean ± SEM).

Interestingly, the *shm1Δ* deletion significantly lowered TML levels by 35% compared to FY23 1,3,4 cells suggesting that the deletion of the *SHM1* gene also affects TML levels. Since SHMTs are involved in the methylation cycle 5,10-methylenetetrahydrofolate the deletion of *SHM1* may impair the distribution of the methyl groups on lysine residues consequently lowering free TML levels [145]. For instance, it was shown that s*hmt1-/-* mice displayed elevated levels of AdoMet, the direct methyl group donor molecule for lysine methylation, suggesting the potential blockage of the methyl group transfer onto lysine residues [145].

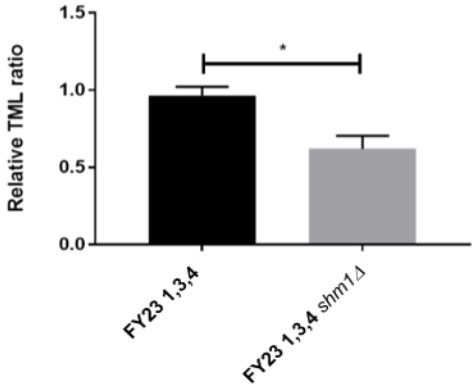


*Figure 6-7: Relative TML levels in FY23 1,3,4 cells and in shm1Δ strain after 96 h growth time (n=3, mean ± SEM); p-value: (p=0.034); (p<0.05) represent statistical significance marked with *.*

The above result, however, shows that the decreased level of TML does not impact the overall increased CAR in the *shm1Δ* strain (Figure 6-7). This may indicate a greater role of Shm1 in the second step of the CAR biosynthesis pathway than methyl transfer, supporting data in the literature [79]. Consequently, such change upraises the A-CAR cellular level suggesting the role of the Shm1 enzyme in acetyl group shuttle. Additionally, the result confirmed that produced CAR is utilized for shuttling acetyl groups in A-CAR

form, probably utilizing three known *S. cerevisiae* acetyltransferases (Cat2p, Yat1p) and carnitine translocase (Crc1p) [74], [76], [146].

6.3 Role of *S. cerevisiae* genes linked to the cellular methylation in CAR biosynthesis

The wide range of KMTs and KDMs regulate lysyl mono-, di- and tri-methylated states. Every methylation step requires AdoMet, a molecule providing a methyl group for the reaction (Figure 6-8). Usually, each KMT or KDM targets just a couple of lysine residues from the entire proteasome making these enzymes very specific. As proteins containing trimethylated lysine are the precursors for carnitine biosynthesis, it was investigated whether specific deletion of genes encoding KMTs or KDMs in *S. cerevisiae* may affect the intracellular level of TML and consequently carnitine. This insight may help to understand a single epigenetic enzyme contribution to the whole cellular metabolism.

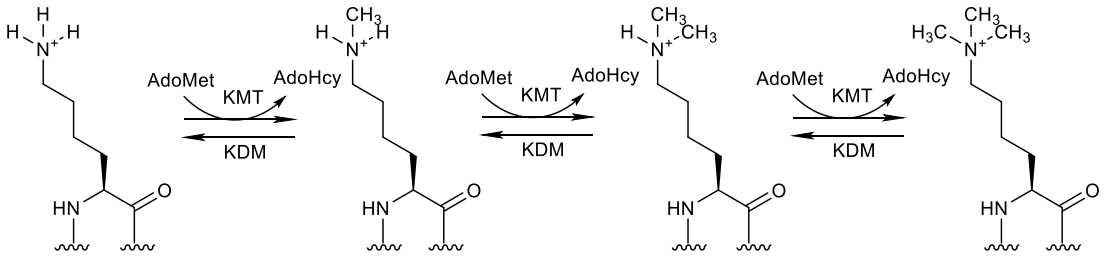


Figure 6-8: Lysine methylation states. Lysine residue can incorporate up to three methyl groups. Each of the methylation steps is regulated by specific KMT and KDM.

6.3.1 Selection of *S. cerevisiae* genes linked to the cellular methylation

To address the question, appropriate KMTs and KDMs were selected for this study using the Saccharomyces Genome Database (yeastgenome.com). The focus was mainly placed on KMT genes that can catalyse lysine trimethylation on the dimethylated substrate and on KDM genes that target trimethylated lysine residues for demethylation (Table 6-1) as these genes potentially have a direct effect on free TML levels. Selected genes code for enzymes that use histone and non-histone lysines as a substrate.

Table 6-1: Selection of KMTs and KDMs for further studies. Selected KMTs represent enzymes transferring methyl groups onto already dimethylated lysine residues, whereas selected KDMs demethylate trimethylated lysine residues. In substrate column, first is stated the substrate protein i.e H3 is histone 3, followed by lysine residue i.e. K36 means lysine residue 36 and finally, the methylation state of targeted lysine; i.e Me2 means demethylated lysine.

KMT (systematic name)	**Substrate**	**KMT abundance (number of molecules/cell)** [147]	**Substrate abundance (number of molecules/cell)** [147]	**Gene size (bp)**	**Reference**
Set2 (YJL168C)	H3K36Me1 H3K36Me2	217	461,000	2202	[36], [148]–[150]
Set1 (YHR119W)	H3K4Me1 H3K4Me2	172	461,000	3243	[151], [152]
Dot1 (YDR440W)	H3K79Me1 H3K79Me2	2160	461,000	1749	[36], [148], [153], [154]
Ctm1 (YHR109W)	Cytochrome c (K72Me2)	2940	7330	1758	[155]
Efm2 (YBR271W)	Elongation factors EF2 (K613Me1) and EF3 (K187)	217	1,031,800	1260	[156], [157]
Efm3 (YJR129C)	Elongation factor EF2 (K509Me1 K509Me2)	1550	160,800	1020	[156]–[159]
Efm5 (YGR001C)	Elongation factor eEF1A (K79Me1 K79Me2)	3060	827	902 (with introns)	[158], [160], [161]
Efm6 (YNL024C)	Elongation factor eEF1A (K390)	1760	827	741	[161], [162]
Rkm2 (YDR198C)	Ribosomal proteins Rpl12Ap and Rpl12Bp (K3Me2)	768	118,800	1440	[163]
KDM (systematic name)	**Substrate**	**KDT abundance (number of molecules/cell)**	**Substrate abundance (number of molecules/cell)**	**Gene size (bp)**	**Reference**
Rph1 (YER169W)	H3K36Me2 H3K36Me3	2230	461,000	2391	[148], [164], [165]
Gis1 (YDR096W)	H3K36Me1 (?) H3K36Me2 (?)	432	461,000	2685	[164], [166]
Jhd1 (YER051W)	H3K36Me1 H3K36Me2	784	461,000	3243	[148], [164]
Jhd2 (YJR119C)	H3K36Me1 H3K36Me2 H3K4Me1 H3K4Me2 H3K4Me3	290	461,000	2187	[152], [164], [167], [168]

6.3.2 Deletion of selected genes in *S. cerevisiae* strain capable of producing CAR

Next, to investigate the role of selected genes, it was necessary to generate a range of gene knockout *S. cerevisiae* strains.

Firstly, deletion of chosen genes was carried out using homologous recombination with FY23 1,3,4 as a parent strain. The adequate gene was replaced with the hygromycin gene (*hphMX*) as a selection marker. For this purpose, the plasmid pAG32 and amplification primers listed in Table 3-4 and Table 3-6 were used to obtain the *hphMX* gene with appropriate flanking sequences. Subsequently, *hphMX* was genetically introduced to the FY23 1,3,4 strain by transformation using the LiOAc technique. After 7 days of incubation, colonies of positive transformants were transferred onto new agar plates. Then, in order to confirm the genotype of each strain liquid cultures were prepared and their genomic DNA was extracted. Next, PCR with primers listed in Table 3-7 was performed. The separated and visualized DNA fragments are shown in Figure 6-9.

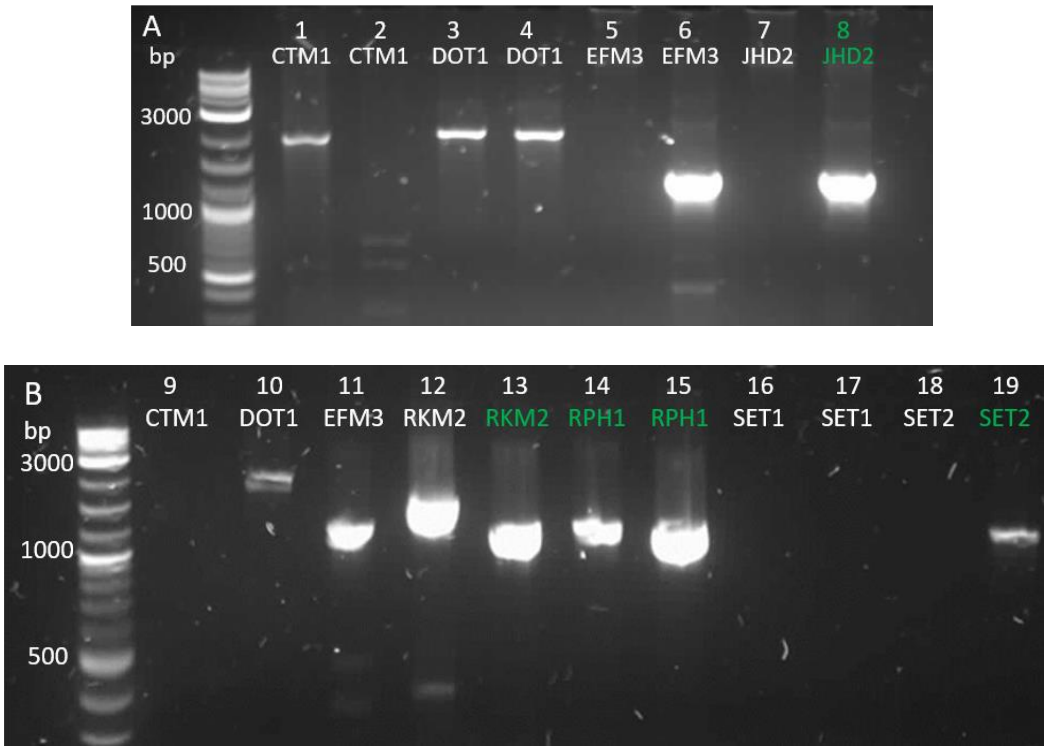


Figure 6-9: Separated DNA fragments from PCR of yeast strains containing the hphXM gene in place of the targeted gene. The hphMX fragment size is approximately 1185 bp, sizes of selected genes are listed in Table 6-1. A) Sample 1 (CTM1) and samples 3 and 4 (DOT1) represent WT of FY23 1,3,4 strain. Sample 8 (JHD2) represents a successful replacement with the hphXM gene. Sample 6 (EFM3) required further validation due to the similar size of EFM3 and hphXM gene. Sample 2 (CTM1), 5 (EFM3), 7 (JHD2) were repeated and their deletion was unsuccessful or could not be confirmed. B) Sample 11 (DOT1), sample 12 (RKM2) represent WT FY23 1,3,4 strain. Sample 13 (RKM2), 14, 15 (RPH1) and 19 (SET2) represents a successful replacement with the hphXM gene. Sample 11 (EFM3) required further validation. Sample 9 (CTM1), 16, 17 (SET1) and 18 (SET2) were repeated and their deletion was unsuccessful or could not be confirmed. Samples on green represent strains confirmed by Sanger sequencing as a successful replacement. Plasmid pAG32 and amplification primers listed in Table 3-4 and Table 3-6 were used to obtain the hphMX gene with appropriate flanking sequences.

The successful genomic replacement of *RKM2*, *RPH1*, *SET2* and *JHD2* genes with the *hphMX* resistance cassette in FY23 1,3,4 strain was confirmed by PCR and sequencing of genomic DNA. It was decided that this set of gene deletion strains represents a sufficient number to process with the subsequent analyses of FY23 1,3,4 strain in the context of CAR production.

Gene knockouts which were unsuccessful in strain FY23 1,3,4 were studied on strains obtained from Euroscarf yeast bank. To summarise, a range of knockout *S. cerevisiae* strains producing and not producing CAR was available and taken under further investigation (Table 6-2).

Therefore, obtained knockout strains may have an impaired level of protein trimethylated lysine residues that may result in changed levels of free cellular TML and, where applicable, CAR production.

Table 6-2: Straines used for analysis of TML and CAR level. Strains FY23 1,3,4 contains CAR production enzymes, while strains BY4742 are not capable of producing CAR. Depleted genes code enzymes responsible for posttranslational methylation of lysine residues on histone and non-histone proteins.

Yeast Strain	Source	The family of the deleted gene	Substrate type
FY23 1,3,4	this work	n/a	n/a
FY23 1,3,4 *rkm2Δ*	this work	KMT	Non-histone
FY23 1,3,4 *set2Δ*	this work	KMT	Histone
FY23 1,3,4 *rph1Δ*	this work	KDM	Histone
FY23 1,3,4 *jhd2Δ*	this work	KDM	Histone
BY4742 (WT)	Euroscarf	n/a	n/a
BY4742 *set2Δ*	Euroscarf	KMT	Histone
BY4742 *dot1Δ*	Euroscarf	KMT	Histone
BY4742 *ctm1Δ*	Euroscarf	KMT	Non-histone
BY4742 *efm2Δ*	Euroscarf	KMT	Non-histone
BY4742 *efm3Δ*	Euroscarf	KMT	Non-histone
BY4742 *efm5Δ*	Euroscarf	KMT	Non-histone
BY4742 *efm6Δ*	Euroscarf	KMT	Non-histone
BY4742 *rph1Δ*	Euroscarf	KDM	Histone
BY4742 *gis1Δ*	Euroscarf	KDM	Histone
BY4742 *jhd1Δ*	Euroscarf	KDM	Histone
BY4742 *jhd2Δ*	Euroscarf	KDM	Histone

6.3.3 HPLC-MS/MS analysis of depleted strains

Next, the total level of free TML and CAR biosynthesis were studied in obtained various *S. cerevisiae* knockout strains. For that purpose, strains were grown and their extracts were analysed by HPLC-MS/MS method.

6.3.3.1 HPLC-MS/MS analysis of KMT depleted strains

Firstly, the investigation focused on KMT strains that transfer methyl groups onto lysine residues. The KMT knockout strains were divided into 4 groups by the type of protein they target: histone (*set2Δ, dot1Δ*), ribosome (*rkm2Δ*), elongation factor (*efm2Δ*, *efm3Δ*, *efm5Δ*, *efm6Δ)* and cytochrome c *(ctm1Δ)*.

6.3.3.1.1 Histone targeting

SET2 and *DOT1* depleted BY4742 strains were grown for 24 h and the relative level of free TML in the obtained cell extracts was quantified by HPLC-MS/MS. After the analysis, the *SET2* knockout resulted in an approximate 50% decrease in free TML levels. The result was consistent with the expected effect of KMT deletion (Figure 6-10). However, the deletion of *DOT1* did not expose difference to the TML levels (data not shown).

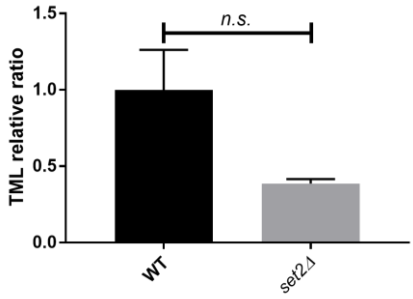


Figure 6-10: Relative TML level in SET2 depleted BY4742 strains after 24 h growth time (n=3, mean ± SEM).

These initial data may suggest that H3K79 methylation catalysed by DOT1 may not contribute to the overall TML level in the same extent as methylation of H3K36 catalysed by SET2.

Next, to observe the effect of *SET2* deletion on CAR biosynthesis, in contrast to BY4742 *set2Δ* cells that were grown only for 24 h on glucose, the FY23 1,3,4 *set2Δ* strain was grown for 120 h. The purpose of that extended growth was to enable cells to switch from fermentable to non-fermentable carbon source and utilize CAR biosynthesis genes for CAR production and possibly enhance acetyl group shuttle into mitochondria. After 120 h, cells were lysed and the relative levels of TML, CAR and A-CAR were quantified by HPLC-MS/MS.

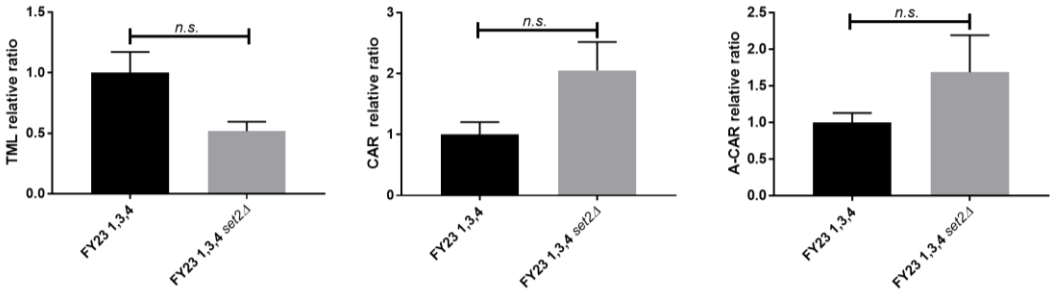


Figure 6-11: Relative TML, CAR and A-CAR levels in SET2 depleted FY23 1,3,4 strains after 120 h growth time (n=3, mean ± SEM).

After analysis, the observed 50% decrease of TML level in the cell lysate of the FY23 1,3,4 *set2Δ* strain was consistent with previous data using the BY4742 strain (Figure 6-11). Therefore, it was expected that CAR synthesis would decrease due to the decreased amounts of the precursor. However, surprisingly, *SET2* deletion resulted in the 100% and 50% upraise of CAR and A-CAR after 120 h growth, respectively.

It has been shown in the literature that *SET2* methylation plays an important role in nutrient stress response [36], [148]. Under nutrient stressed conditions the growth of *S. cerevisiae* cells lacking the *SET2* gene was disrupted. However, the proliferation of FY23 1,3,4 *set2Δ* strain under the stress growth conditions in this research chapter was not disturbed, suggesting that CAR biosynthesis could potentially rescue cell growth. FY23 1,3,4 *set2Δ* strain may increase the CAR biosynthesis from any available free TML and use it in the form of A-CAR to enhance acetyl group shuttling, potentially in response to nutrient stress.

Additionally, literature evidence indicates that the activity of some HAT complexes is essential for cell survival in nutrient stress conditions [150]. Therefore, increased A-CAR may also be linked with enhanced shuttling of an acetyl group for acetyltransferases activity. Especially it may be the case for *set2Δ* strain, where unmethylated histone lysine residues remain available for other PTMs, i.e acetylation what may play a role in the stress response.

6.3.3.1.2 Ribosome targeting

Next, the effect of ribosomal methylation was investigated in FY23 1,3,4 *rkm2Δ* strain. The cells were grown for 96 h and the relative levels of TML, CAR and A-CAR were quantified in their extract by HPLC-MS/MS.

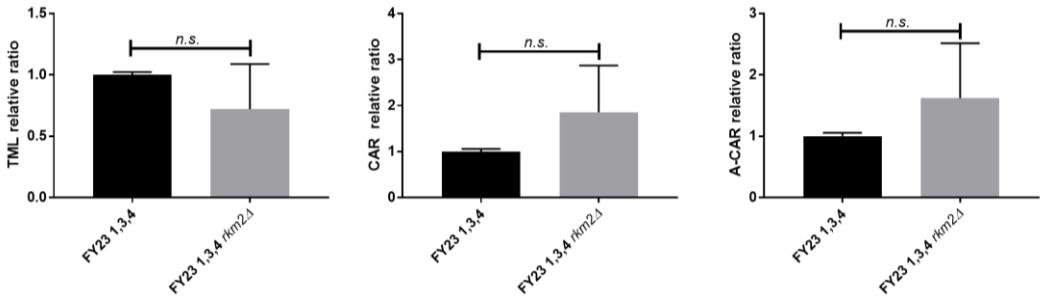


Figure 6-12: Relative TML, CAR and A-CAR levels in rkm2Δ depleted FY23 1,3,4 strains after 96 h growth time (n=3, mean ± SEM).

The *rkm2Δ* strain has a similar pattern to *set2Δ* in lowering TML and increasing CAR and A-CAR levels (Figure 6-12). However, the variations in molecule concentrations were

substantial, therefore, it was difficult to conclude whether the exposed pattern can be interpreted as general for KMTs, especially that both enzymes are responsible for methylation of two different targets. Set2's substrate is H3K36, while Rkm2 targets ribosomal proteins. However, evidence that ribosomes regulate stress response suggests that the observed in this study pattern may still be valid, indicating that *RKM2* depletion contributes to the lowered TML and increased CAR and A-CAR amounts, similarly to FY23 1,3,4 *set2Δ* strain [169].

6.3.3.1.3 Elongation factors targeting

Four elongation factor targeting KMT gene knockouts of the BY4742 strain were grown for 24 h and the relative levels of free TML in the obtained cell extracts were quantified by HPLC-MS/MS (*efm2Δ*, *efm3Δ*, *efm5Δ* and *efm6Δ*). Compared to the WT, the average levels of TML were reduced by >50% in cell lysates of three strains (*efm2Δ*, *efm3Δ* and *efm5Δ*) (Figure 6-13). *Efm6Δ* strains did not expose any change in TML levels (data not shown).

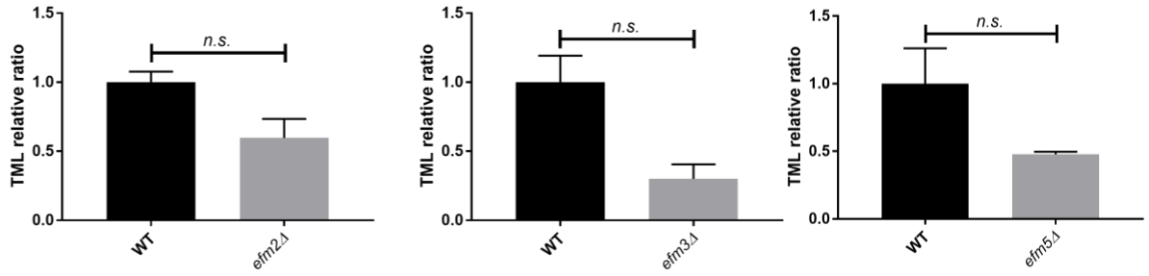


Figure 6-13: Relative TML level in elongation factor targeting KMTs (EFM2, EFM3, EFM5) depleted BY4742 strains after 24 h growth time (n=3, mean ± SEM).

The above result indicates an important role of methylation of the elongation factor proteins in carnitine biosynthesis and energy metabolism. In *S. cerevisiae*, Efm2 is a methyltransferase that targets elongation factor 2 (EF2) and potentially elongation factor 3 (EF3). Efm3 targets only EF2, while Efm5 methylates elongation factor 1 (eEF1A) [156]–[159]. These elongation factors (eEF1A, EF2 and EF3) are known for the ribosomal guidance of tRNA [157], [170].

However, the functions of their methylated lysine sites are not well known. It has been shown that EF2 methylation appears in close proximity of the EF2 contact side with ribosomal subunits [171], [172]. Therefore, the localisation of lysine methylation at EF2 suggests the role of this modification in ribosomal communication and translocation.

Also, little is known on elongation factor eEF1A methylation. It has been suggested that methylation of eEF1A by Efm5 plays a role in viral replication [161]. Except its ribosomal role eEF1A has been found to play role in the protein degradation as well as in hypoxia and therefore, lack of it methylation may potentially contribute to the cellular homeostasis [170].

In general, as elongation factors are involved in protein synthesis that is a highly energy-requiring process, the post-translational modifications of elongation factors may serve as one of the main mechanisms for regulating the energy consumption especially during stress [159]. Therefore, it is likely that elongation methylation may be linked with energy metabolism and CAR biosynthesis.

6.3.3.1.4 Cytochrome c targeting

Lastly, cytochrome c targeting gene depletion was investigated in BY4742 *ctm1Δ* strain grown for 24 h. Following the analysis of cell lysate samples, the deletion of *CTM1* responsible for cytochrome methylation was found to decrease TML relative levels by 50% (Figure 6-14).

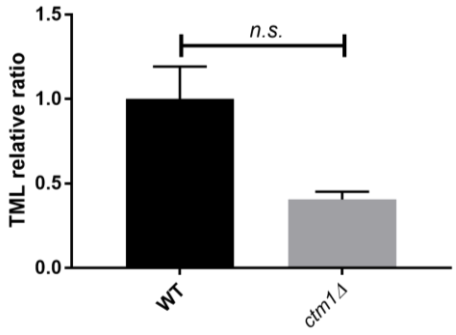


Figure 6-14: Relative TML level in cytochrome C targeting KMT depleted BY4742 ctm1Δ strain after 24 h growth time (n=3, mean ± SEM).

Cytochrome c methylation has been found to strengthen its binding to the mitochondria membrane and increases mitochondrial import [173], [174]. Therefore, the lack of cytochrome c methylation may not only affect a total free TML level but also the functionality of mitochondria, including CAR acetyl group transport. However, cytochrome c methylation has not been found in higher animals [175].

6.3.3.2 HPLC-MS/MS analysis of KDM depleted strains

Secondly, the impact of the depletion of enzymes demethylating lysine residues was taken into the investigation. Among five available KDMs deletion strains, all contain JmjC domain characteristic for histone targeting KDMs. The full description of the JmjC domain

mechanism of action can be found in section 1.1.2.2. Available strains were divided into two groups according to the structural similarity. Jhd1 and Jhd2 belong to the plant homeodomain (PHD) containing domain family while Rph1 and Gis1 possess a zinc-finger domain [164].

6.3.3.2.1 PHD domain containing Jhd1 and Jhd2

Firstly, *JHD1* and *JHD2* relationship to the free TML was studied using the BY4742 strain knockouts. After 24 h growth and HPLC-MS/MS analysis of cell extract, *jhd2Δ* strain appeared to slightly decrease TML (Figure 6-15), while deletion of *JHD1* did not expose the difference in TML levels (data not shown).

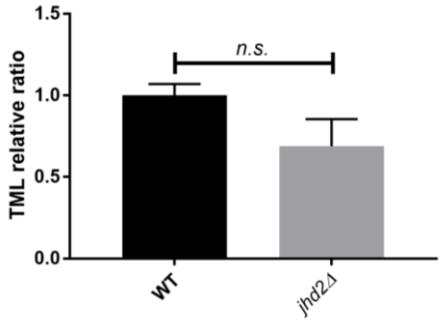


Figure 6-15: Relative TML levels in JHD2 knockout strains after 24 h growth (n=3, mean ± SEM).

The results of *JHD1* and *JHD2* gene knockouts revealed opposite outcomes to the expected rise of TML level due to the lack of demethylation caused by deletion of JHD enzymes and potential preservation of the lysine methylation states. However, the surprising result may be an effect of the growth conditions the strains were exposed to.

Therefore, the available FY23 1,3,4 *jhd2Δ* strain capable to produce CAR was analysed in a 120 h growth conditions similar to the previous subchapter dedicated for KMT deletion. Upon changed growth, HPLC-MS/MS data matched the expected result as such genetic manipulation increased free TML levels due to preserved methylation of trimethyllysine. Consistently with expectations, the average CAR and A-CAR levels were greater for the *jhd2*Δ strain (Figure 6-16).

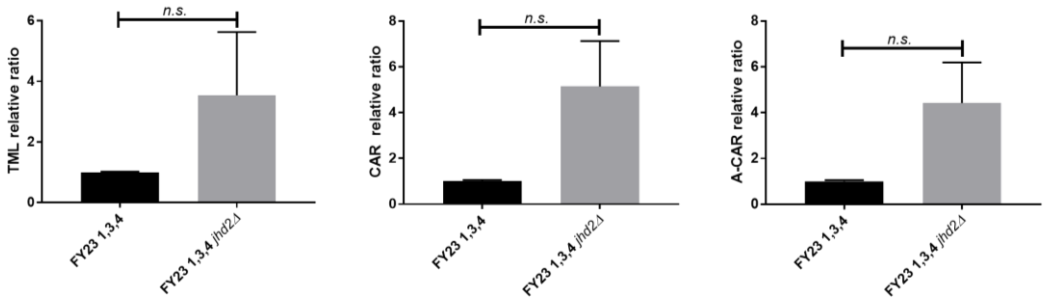


Figure 6-16: Relative TML, CAR and A-CAR levels in JHD2 depleted FY23 1,3,4 strain after 120 h growth time (n=3, mean ± SEM).

Nevertheless, two opposite results for TML analysis of BY4742 *jhd2Δ* and FY23 1,3,4 *jhd2Δ* strains may still be valid. It has been shown that the Jhd2 role in H3K4 demethylation depends on yeast growth conditions [152]; when cells were grown on fermentable carbon source the WT vs *jhd2Δ* did not expose the difference in H3K4Me3 level. However, cells grown on acetate exposed a significant difference with over 50% reduction for WT and almost 50% elevation of H3K4Me3 for *jhd2Δ* cells. This can be a possible explanation for the difference in detected TML level for FY23 1,3,4 *jhd2Δ* and BY4742 *jhd2Δ* in this result chapter. The FY23 1,3,4 cell line was grown for 120 h and during that growth was switched from fermentable to a non-fermentable carbon source, while BY4742 cells were grown only for 24 h in a glucose-rich medium. Therefore, the found Jhd2 impact on H3K4Me3 and its dependency on carbon source may contribute to the overall free TML level detected in cell extract [152]. The non-fermentable growth supported the H3K4 methylation, contributed to uprising TML levels and as an outcome increased CAR production in FY23 1,3,4 *jhd2Δ* strain. Possibly, CAR biosynthesis enhanced strain growth by shuttling acetyl groups to mitochondria during glucose depleted conditions.

6.3.3.2.1 Zinc-finger domain containing Rph1 and Gis1

Next, structurally similar Rph1 and Gis1 were taken under the investigation. The BY4742 knockout cells were grown for 24 h. Similarly to the *jhd2Δ* case, HPLC-MS/MS analysis of BY4742 *rph1Δ* strain did not expose the difference in TML levels (data not shown).

Next, according to the previous data showing an impact of the growth conditions, the FY23 1,3,4 *rph1Δ* strain was tested in prolonged growth time (120 h) (Figure 6-17).

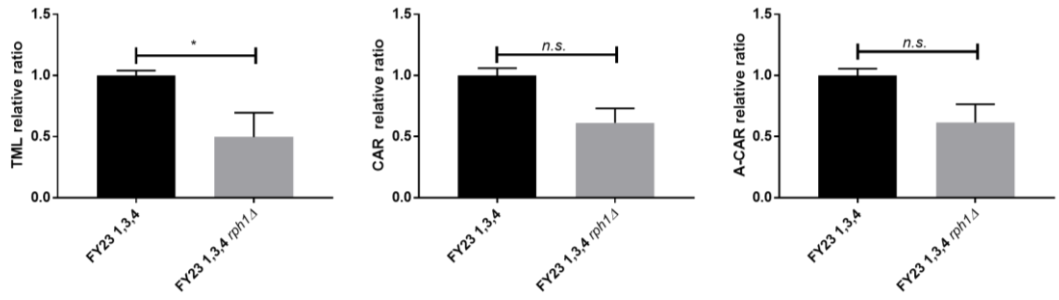


*Figure 6-17: Relative TML, CAR and A-CAR levels in RPH1 depleted FY23 1,3,4 strains after 120 h growth time (n=3, mean ± SEM); p-value: (p=0.04); (p<0.05) represent statistical significance marked with *.*

Surprisingly, in this case, the *rph1*Δ strain has shown lower free TML levels and consequently decreased levels of carnitine and acetylcarnitine.

It is suggested that *RPH1* play the role of the repressor responding to the DNA damage and environmental stress [176]. Therefore, the deletion of *RPH1* could potentially affect the methylation only during stress growth conditions. Due to this fact, the difference in the TML level in *RPH1* depleted strains is noticeable during 120 h experiment when cells switch their metabolism. However, the significant reduction of TML level in *rph1Δ* strain suggests that the role of *RPH1* during stress may be more complex and potential cross-talk with other signalling proteins may eventually lead to the decreased level of TML. Since there is little literature regarding an *RPH1* role in *S. cerevisiae* more investigation is needed to find a relation between Rph1 activity and histone methylation.

Interestingly, both Rph1 and Jhd2 target the same lysine residue on yeast histone H3. However, Rph1 demethylates di- and tri-methylated lysine, whereas Jhd1 utilizes mono- and dimethylated lysine as a substrate. Therefore, it would be expected to see *RPH1* depletion that directly enhances the TML preservation. However, instead, it was the *JHD1* that depletion increases free TML even though the Jhd1 is less abandoned in the cell compared to Rph1.

Nevertheless, both strains (*jhd2Δ* and *rph1Δ*) capable of CAR biosynthesis exposed consequential change of CAR and A-CAR to the change in TML level. However, only *JHD2* increased the TML level that can be explained by the mechanism of action of the depleted enzyme.

Next, *GIS1* that is structurally similar to *RPH1* was tested. In comparison to WT, the BY4742 *gis1Δ* strain exposed significant increase in TML levels (Figure 6-18). Interestingly, Gis1 does not directly target trimethylated lysine residues and, in general, there is little evidence of the activity of the JmjC domain in Gis1. Some resources claim

that Gis1 possess the mutations that disable its demethylation activity [165]. However, one study reveals possible Gis1 role in demethylation of mono- and dimethylated lysine residues [164]. Therefore, the obtained result suggests that the *GIS1* knockout may preserve mono- and di-methylated lysine residues on proteins and, consequently, promote these lysine residues to methylation by KMTs to produce trimethylated lysine residues, which may lead to an increase in free TML levels.

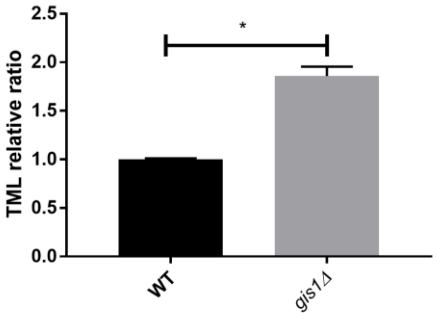


*Figure 6-18: Relative TML levels in GIS1 knockout strains after 24 h growth (n=3 mean ± SEM); p-value: (p=0.0161); (p<0.05) represent statistical significance marked with *.*

Interestingly, it is known that *GIS1*, as well as *RPH1*, regulates non-fermentable metabolism in yeast and that several genes involved in acetyl-CoA metabolism are down-regulated by *GIS1*. There is evidence that *GIS1* can act as a repressor and activator depending on the presence of glucose [177]. Unfortunately, the lack of the FY23 1,3,4 *gis1Δ* strain did not allow for further investigation of the changes in the TML and CAR level upon changing growth conditions tested for other strains.

Nevertheless, literature evidence combined with the result of this thesis confirms that Gis1 and Rph1 can regulate stress response and cell metabolism in glucose-depleted growth conditions [177].

6.3.4 Summary of deletion work and conclusions

Table 6-3: Overview of genes deletion impact on TML level in cell extract in strain FY23 1,3,4 and BY4742.

Yeast strain	The family of the deleted gene	Substrate type	The result on the TML level	The result on the CAR level
FY23 1,3,4	n/a	n/a	n/a	n/a
FY23 1,3,4 *rkm2Δ*	KMT	Non-histone	↓	↑
FY23 1,3,4 *set2Δ*	KMT	Histone	↓	↑
FY23 1,3,4 *rph1Δ*	KDM	Histone	↓	↓
FY23 1,3,4 *jhd2Δ*	KDM	Histone	↑	↑
BY4742 (WT)	n/a	n/a	n/a	n/a
BY4742 *set2Δ*	KMT	Histone	↓	n/a
BY4742 *dot1Δ*	KMT	Histone	-	n/a
BY4742 *ctm1Δ*	KMT	Non-histone	↓	n/a
BY4742 *efm2Δ*	KMT	Non-histone	↓	n/a
BY4742 *efm3Δ*	KMT	Non-histone	↓	n/a
BY4742 *efm5Δ*	KMT	Non-histone	↓	n/a
BY4742 *efm6Δ*	KMT	Non-histone	-	n/a
BY4742 *rph1Δ*	KDM	Histone	-	n/a
BY4742 *gis1Δ*	KDM	Histone	↑	n/a
BY4742 *jhd2Δ*	KDM	Histone	↓	n/a
BY4742 *jhd1Δ*	KDM	Histone	-	n/a

Among all tested depleted strains six KMT coding gene deletions resulted in decreased TML levels: *SET2* which targets histone 3 lysine 36 (H3K36), and *RKM2*, *CTM1*, *EFM2*, *EFM3*, *EFM5* that targets non-histone proteins including ribosomes, cytochrome C or elongation factors (eEF2 and eEF1A) (Table 6-3). Such observed decrease indicates a great contribution of tested enzymes to the protein methylation and highlights the importance of these KMTs for the total available free TML for CAR biosynthesis. While *SET2* is associated with stress response and *RKM2, EFM2*, *EFM3*, *EFM5* deletions may contribute to unpaired ribosomal activity and communication, the function of non-histone lysine methylation is still a very unexplored area of protein PTMs. Interestingly, the reduction of TML level in FY23 1,3,4 *rkm2Δ* and FY23 1,3,4 *set2Δ* strains, led to increased CAR biosynthesis levels under stress condition, indicating possible support of CAR for survival in glucose-depleted conditions. Taking into account an important CAR

role in acetyl group shuttling it may be possible that CAR biosynthesis was switched on just under the non-fermentable growth in FY23 1,3,4 strain utilizing all naturally appearing TML in cell extract resulting in decreasing TML and increase in CAR.

After analysis of all KDM depleted strains four resulted in an impaired level of free TML level in cell extracts (Table 6-3). However, again, the effect was depended on the strain growth condition. While growth on the glucose-rich medium decreased TML level for BY4247 *jhd2Δ* strain, the non-fermentable growth resulted in increased TML for the FY23 1,3,4 *jhd2Δ*. These opposite results indicate that together, Jhd2 and it targets H3K4 and H3K36, play an important role in stress response conditions. Elevated TML level for FY23 1,3,4 *jhd2Δ* and decreased TML level for FY23 1,3,4 *rph1Δ* accordingly resulted in the consequential change to the CAR biosynthesis. Surprisingly, the deletion of Gis1, the enzyme that JmjC domain activity is doubtful resulted in the most significant change to the TML levels in the BY4247 strain. The rise in the TML level in *gis1Δ* gives an interesting insight and again questions the Gis1 activity and role in the histone lysine demethylation.

From the obtained results in this research chapter, the observed behaviour of Jhd2 demethylase and Set2 methyltransferase depleted strains, both targeting H3K36, suggests the contribution of H3K36 to the overall free TML level. Therefore, H3K36 may have an important link to the CAR biosynthesis and energy metabolism, especially during the stress response.

Additionally, it is worth to point out that despite the fact that histone proteins are one of the most abundant substrates of KMTs the deletion impact of tested non-histone KMTs was comparable to SET2 deletion (Table 6-1). The effect may be due to different locations of deleted KMTs targets. Histones are located in the nucleus with DNA wrapped around them. Therefore, to obtain free TML from trimethylated lysine residues on histone proteins, they must first escape from the DNA and then exit the nucleus into the cytoplasm, where protein degradation takes place. Despite that, the abundance of tested non-histone proteins is much lower than histone 3; cytoplasmic location of these protein allows for the easier break down than histone proteins to the free TML. This could provide an explanation of why the knockout of non-histone targeting KMTs is comparable to histone targeting *SET2*.

Finally, an insight on yeast strains studied in this research subchapter can be translated into the investigation of the potential genes linked to the free TML levels and CAR biosynthesis in the human cell model. Table 6-4 summarises the human genes

orthologues corresponding to the yeast genes that have been found to potentially contribute to the CAR biosynthesis.

Table 6-4. Human orthologues corresponding to the yeast genes found to have an impact on TML levels in this research study and the diseases they are associated with (www.alliancegenome.org).

Yeast Gene	Systematic name	Type of gene	Human orthologues	Disease association
RKM2	YDR198C	KMT	SETD4	
SET2	YJL168C	KMT	SETD2 NSD1 NSD2 NSD3	acute myeloid leukaemia neuroblastoma
CTM1	YHR109W	KMT	n/a	
EFM2	YBR271W	KMT	n/a	
EFM3	YJR129C	KMT	FAM86A (EEF2KMT) FAM86B1 FAM86B2	
EFM5	YGR001C	KMT	EEF1AKMT1	
GIS1	YDR096W	KDM	KDM4A KDM4B KDM4C KDM4D KDM4E	alopecia areata AB urinary bladder cancer AB breast cancer B colorectal cancer B stomach cancer B nephroblastoma D E
RPH1	YER169W	KDM	KDM4A KDM4B KDM4C KDM4D KDM4E	alopecia areata AB urinary bladder cancer AB breast cancer B colorectal cancer B stomach cancer B nephroblastoma D E
JHD2	YJR119C	KDM	KDM5A KDM5B KDM5C KDM5D	alopecia areata A non-small cell lung carcinoma A breast cancer B malignant glioma B urinary bladder cancer B

6.4 Effect of small molecules accessibility on lysine methylation and carnitine biosynthesis

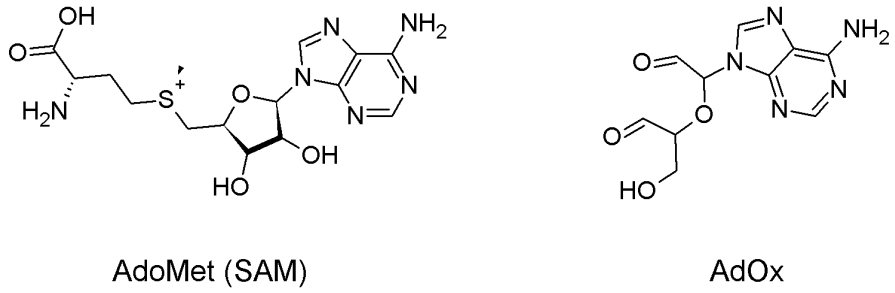
The level of cellular free TML is not only dependent on the activity of the KMT and KDM enzymes. One of the factors having a significant impact on this process is the availability of the small molecules associated with these enzymes, for example, of the methyl group donor for methyltransferases, or cofactors for the JmjC domain activity. Therefore, this

research subchapter investigates the impact of these small molecules on free TML and CAR biosynthesis.

6.4.1 Cellular methylation pathway inhibition

As mentioned before, AdoMet and AdoHcy are molecules involved in the cellular methylation pathway that is regulated by complex modifications (see section 1.1.2). Whereas AdoMet is a direct methyl group donor, the methyl group transfer onto lysine residue can be blocked by AdOx (adenosine-2',3'-dialdehyde) – an inhibitor of AdoHcy hydrolase (Figure 6-19 A) AdOx by its irreversible binding dysregulates a sensitive equilibrium between AdoMet and AdoHcy and, therefore, cellular methylation cycle [178]. The analysis of the FY23 1,3,4 strain after 4 h treatment with AdOx revealed decreased cellular TML levels by more than 50% (Figure 6-19 B).

A:



B:

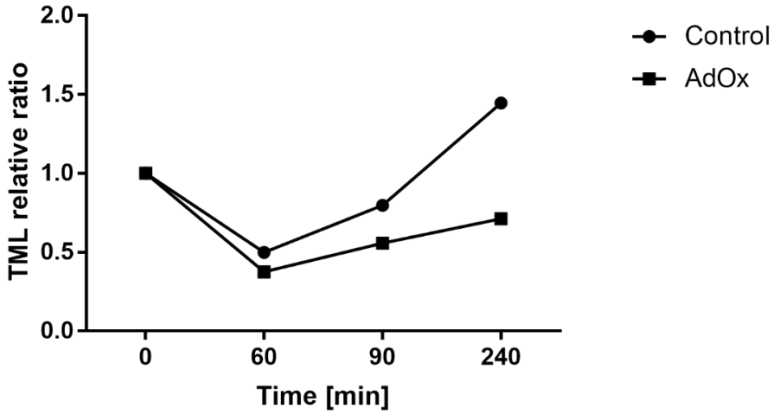


Figure 6-19: A) Structures of AdoMet and AdOx; B) FY23 1,3,4 strain treated with AdOx for up to 4 h (100 µM). The cellular extract was analysed by HPLC-MS/MS (n=1).

This treatment indicated an important role of the methylation pathway in the free TML level and, therefore, can have a significant role in KMTs activity, CAR biosynthesis and

energy metabolism. Consequently, the research related to cellular methylation cycle was one of the points in the further investigation in the human cell model.

6.4.2 JmjC-domain mechanism inhibition

The JmjC domain-containing KDMs are Fe^{2+} and 2OG dependent enzymes (see section 1.1.2.2). Dimethyl *N*-oxalylglycine (DMOG) is the cell-penetrating dimethyl ester, which inhibits 2OGXs [63]. Other available inhibitors of KDMs include $CoCl_2$, which replaces Fe^{2+} for Co^{2+} in the active site, and deferoxamine (DFO) that is a strong iron chelator [179].

The BY4247 strain was treated with DMOG, Co^{2+} and DFO and relative TML levels in the cell extract were quantified. The results for the $CoCl_2$, DFO and DMOG inhibitors all show an increase in TML levels compared to control cells (Figure 6-20), coming along with the expected result of KDM inhibition.

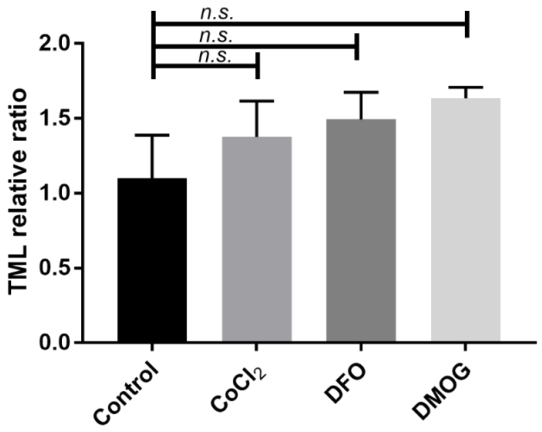


Figure 6-20: BY4247 strain treated with $CoCl_2$ (100 µM), DFO (100 µM) and DMOG (1 mM) for 24 h. The cell lysate was analysed by HPLC-MS/MS (n=3, mean ± SEM).

However, as discussed in the subchapter on KDM enzymes deletion, the impairment of the KDM activity may be more complex. It is important to consider that $CoCl_2$ and DFO may inhibit other iron-dependent processes in cells while DMOG may inhibit other 2OG-dependent processes.

The above *S. cerevisiae* strains treatment with inhibitors shows the importance of the cofactors and other small molecules on the activity of epigenetic enzymes. This preliminary data obtained from yeast gives an insight into TML for further research in human cell line models.

6.5 Discussion

S. cerevisiae is evolutionally programmed to primarily use glucose to perform alcoholic fermentation even in fully aerobic conditions. The so-called "Crabtree effect" allows yeast to produce ethanol, a non-fermentable carbon source, that is naturally aseptic to the other yeast species [180]. However, when glucose starts to be limiting, *S. cerevisiae* undergoes aerobic growth utilizing non-fermentable carbon sources produced earlier during the Crabtree effect. This switch from fermentable to non-fermentable growth, called diauxic shift, is oxygen independent and occurs even in fully aerobic conditions. Many metabolic signalling changes occur in the budding yeast during the diauxic shift and they involve regulation of gene expression and yeast differentiation, very likely also through epigenetic modifications [181], [182]. Therefore, in this research chapter, it was observed that nutrient availability affected free TML levels during *S. cerevisiae* growth. Possibly, the engineered FY23 1,3,4 strain induced CAR production upon diauxic shift, conditions that require utilizing non-fermentable carbon sources for the growth. Biosynthesized CAR could be used for shuttling acetyl groups in A-CAR form, probably due to known *S. cerevisiae* acetyltransferases (Cat2p, Yat1p) and carnitine translocase (Crc1p) activity [74], [76], [146].

Therefore, in such nutritionally restricted conditions, it was investigated whether it is possible to enhance reconstructed CAR biosynthesis by yeast genetic manipulations. Firstly, removal of HTML plasmid catalysing the second step of CAR biosynthesis appeared to not inhibit CAR production in reconstructed *S. cerevisiae* strain. Consequently, this result highly supports a hypothesis stating that *S. cerevisiae* possesses native enzymes, serine methyltransferases (SHMTs), that may catalyse the second step of CAR biosynthesis [79]. Additionally, this idea was tested by depletion of the *SHM1* gene that most probably impaired equilibrium between SHM1 and SHM2 enzymes activity and as an outcome increased CAR levels in reconstructed *S. cerevisiae* strain [79]. Interestingly, the *shm1Δ* also significantly lowered TML levels that seem to be an effect of the primary function of SHMTs being involved in the methylation cycle. Nevertheless, despite SHMT influence on cellular methylation, the *shm1Δ* appeared to play a great role in increasing CAR biosynthesis despite decreasing its substrate level.

Another advantage of cell growth during the diauxic shift was the possibility of studying budding yeast response to nutritionally-induced stress that is an important factor in the activity of many KMTs and KDMs [183]. The comparison between non-stressed cells

grown for 24 h versus stressed due to glucose depletion gave an important insight to understand the changes in free TML availability and CAR biosynthesis in yeast.

Firstly, it was observed that the depletion of lysine methylases (KMTs) in most cases led to a decrease in the free TML level. Nevertheless, that did not trigger the expected decrease in CAR production. Instead, CAR biosynthesis increased suggesting that cells may have reconstructed CAR enzymes for survival upon glucose-depletion. Interestingly, such an increase was also observed for A-CAR level indicating the enhanced shuttle of acetyl groups. The possible reason behind this activity is the fact that blockage of methylation may increase the lysine acetyltransferases that also are necessary for survival during stress and utilize acetyl groups for lysine modifications [183].

Secondly, histone, as well as non-histone targeting methyltransferases depletion, have, in most cases, let to decrease of overall free TML level. This observation raises the importance of non-histone lysine methylation in the availability of this substrate for CAR biosynthesis, especially in studies performed in human cell line model. However, functions of most of the methylation sides in the studied non-histone targets are not very well known and mainly discussed according to the general function of the protein, i.e. methylation of the Rpl12 or EF2 has been associated with their binding to the ribosomes [169], [171], [172]. Many of the methylation sides are probably associated with the response to stress that is again a factor that impacts the CAR biosynthesis in the first place. Therefore, it is still challenging to assess the importance of the depletion of particular methylation sides to the CAR biosynthesis and the role of the depletion of the whole protein on the CAR. Nevertheless, deletion of non-histones KMTs certainly leads to disturbed cell homeostasis and impacts the overall energy metabolism.

Among histone methylation sides it appears that methylation of the H3K36 may have a significant impact on CAR metabolism. Upon stressed condition, the deletion of SET2 that targets that side resulted in a decrease in the free TML level, while JHD2 increased it. This observation provides an interesting insight for further studies in the human cell model.

While investigating the gene knockouts in yeast cells was certainly a necessary and insightful approach, it would not be possible to achieve these gene knockouts in a human body. In clinics, research is limited to the use of external medication to inhibit molecular pathways and genes activity. Therefore, besides investigating the effect of yeast knockout onto overall TML level, it also was tested whether it is possible to obtain similar results by inhibition of KDMs and KMTs activity. Tested inhibitors of the methylation cycle and JmjC demethylases mechanisms revealed the possibility to manipulate the overall TML

level by using external drugs in yeast *S. cerevisiae.* Inhibitors such as AdOx, $CoCl_2$, DFO or DMOG will be further analysed in the human cell line model.

It is important to notice, that the KMTs and KDMs targeting histone proteins are involved in gene expression and regulate transcription of dozens of genes, which in turn can affect many biological pathways. For example, a histone targeting KMT/KDM deletion may result in a change in gene expression affecting proteolysis. As a consequence of this, there could be a decrease in the breakdown of proteins containing trimethylated lysine residues which would lead to a decrease in free cellular TML. Therefore, in some cases, it is challenging to predict the direction of deletion of histone targeting KMTs and KDMs on TML levels and CAR levels. Therefore, despite the fact that many analysed genes belong to the same family of proteins, their deletions have led to different effects. These opposing results give evidence for possible cross-talking of analysed epigenetic modifications and the complexity of this investigation. This would be also the case for small molecules targeting some of KDMs and KMTs that may also affect gene expression as well as TML abundance on proteins.

Additionally, it is important to point out that the abundance, half-life and location of studied KDMs, KMTs and their substrates in cell organelles may have also an impact on the free TML levels. For example, even if a targeted protein is less abundant in the cell, its shorter half-life and/or better accessibility to the cytoplasmic proteasomes may result in a greater level of free TML in the cell. On the other hand, very stable nuclear histones that are more abundant in the cell may have a similar or even lower contribution to the free TML level than non-histone proteins.

Although *S. cerevisiae* is easier to genetically manipulate compared to human cell model, the difficulty in consistently growing replicates in overnight cultures impeded obtaining statistically significant results in yeast. However, TML levels are difficult to study in human liver cells due to its very dynamic conversion during carnitine biosynthesis. Therefore, the results obtained in *S. cerevisiae* provide important guidance for experiments in human cells, despite the unresolved limitations from technical errors.

The challenges discussed for *S. cerevisiae* show that the selection of the genes contributing to the free TML in human cells without prior yeast studies could be even more challenging and time-consuming. Besides known associations of epigenetics to diseases like cancer, the future work on human cell lines may reveal an epigenetic link of the selected genes to CAR biosynthesis and energy metabolism.

7. Study of the role of protein methylation on carnitine biosynthesis in a human cell line model

To build on the investigations of a molecular link between epigenetic modifications and the abundance of free trimethylated lysine in the yeast, *S. cerevisiae* as a genetic model organism that is naturally capable of carnitine biosynthesis was chosen. For that, cultured human cell lines were found to offer good scope for ease of manipulation and physiological relevance, particularly the brain, kidney and liver cells [143], [184], as these organs produce the highest amounts of carnitine in the human body.

Research with cultured human cell lines allows for more in-depth investigation of the impact of protein methylation on carnitine biosynthesis, particularly their pharmaceutical manipulation by small molecules. Therefore, this thesis chapter's objectives include:

- Validation of carnitine biosynthesis and choice of the optimal human cell lines for further investigation;
- utilisation of the developed HPLC-MS/MS method for metabolic analysis and development of western blotting methodology for protein analysis in the human cell line;
- study of the importance of the cellular methylation cycle on carnitine biosynthesis using cellular methylation pathways inhibitors, methylation cycle augments and isotopically labelled metabolites;
- investigation of the role of the cellular protein degradation pathway in carnitine biosynthesis;
- examination of the role of other posttranslational modifications on carnitine biosynthesis.

7.1 Analysis of CAR biosynthesis in various cell lines

To corroborate literature reports [143], [184] and to identify a suitable human cell line for this investigation, I examined three human cell lines: the HepG2 cell line that derives from human hepatocellular carcinoma, HEK 293 cells obtained from embryonic kidney and the HeLa cell line from cervical epithelial adenocarcinoma [185]–[187]. All cell lines were cultured in similar growth conditions for 24-48 h (depending on the individual growth profiles), and next, were lysed and analysed via the developed HPLC-MS/MS method. The analyses resulted in the detection of the CAR peak in all three cell lines, with HepG2 having the highest content of CAR (Figure 7-1). Therefore, for these analyses, the HepG2 cell line was chosen for further investigations.

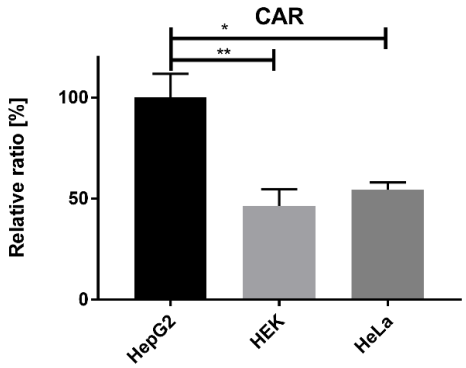


*Figure 7-1: HepG2, HEK and HeLa cells grown in 12-well plates at 0.5 x 10^6 cells/well; the cell lysate was analysed by HPLC-MS/MS (n=3, mean ± SEM); p-values: for HeLa p=0.015 and for HEK p=0.004, (p<0.05) represent statistical significance marked with *, (p<0.01) are marked with **.*

It is noteworthy that TML was not detected in any of these cell lines, confirming described in the section 4.3.6 difficulties of employed MS method to detect TML. Previous reports on liver and kidney tissues found that the abundance of several carnitine biosynthesis metabolites, including TML and HTML, is very limited in these tissues [184].

7.2 Role of methylation pathway on CAR biosynthesis

7.2.1 Treatment with methylation inhibitor

As summarised earlier (see section 1.1.2) cellular methylation pathway is regulated by a complex cycle of modifications that keeps that equilibrium stable. The direct methyl donor group is AdoMet that turns into AdoHcy after transferring the methyl group into acceptor. Next, AdoHcy turns into homocysteine with the assistance of AdoHcy hydrolase.

The balanced equilibrium between AdoMet and AdoHcy levels is essential for proper cellular methylation functionality (Figure 7-2) [188].

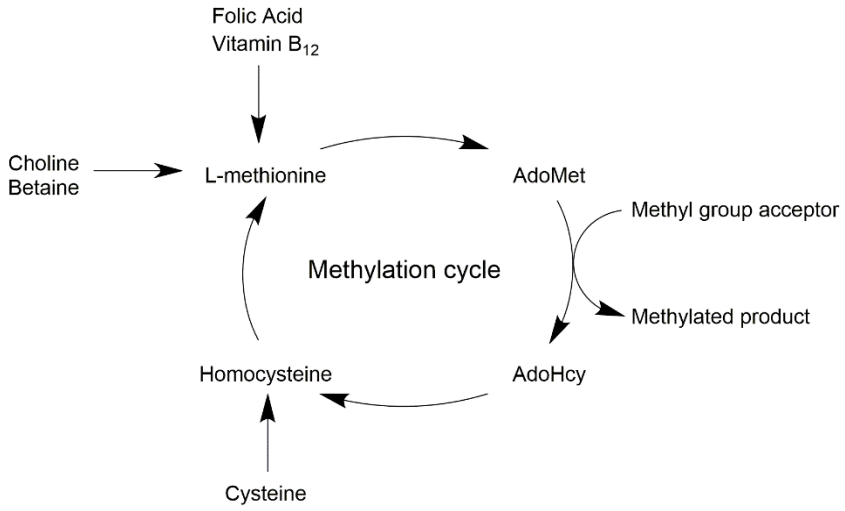


Figure 7-2: Cellular methylation cycle.

The cellular protein methylation pathways can be inhibited by AdOx, a compound which acts as an inhibitor of AdoHcy hydrolase leading to accumulation of AdoHcy. In turn, such accumulation cause impaired AdoHcy/AdoMet equilibrium, decrease AdoMet production and therefore inhibit cellular methylation [178]. Consequently, AdOx treatment is often used to induce hypomethylated state including proteins [178].

To investigate the effect of AdOx on carnitine biosynthesis, including its precursors, HepG2 cells were treated with 100 µM AdOx for up to 24 h. The obtained data (Figure 7-3) shows that γBB, CAR and A-CAR are all substantially affected by the treatment. The data also suggests that the influence of AdOx on CAR biosynthesis starts ~8 h after AdOx addition and the effect continues up to 24 h; at this time point CAR synthesis decreases significantly (by ~40%). Additionally, these results indicate that inhibition of cellular methylation levels does not affect CAR biosynthesis during the initial 8 h of treatment, presumably as a consequence of high initial CAR levels. Similar changes were observed for γBB and A-CAR levels in the tested time span.

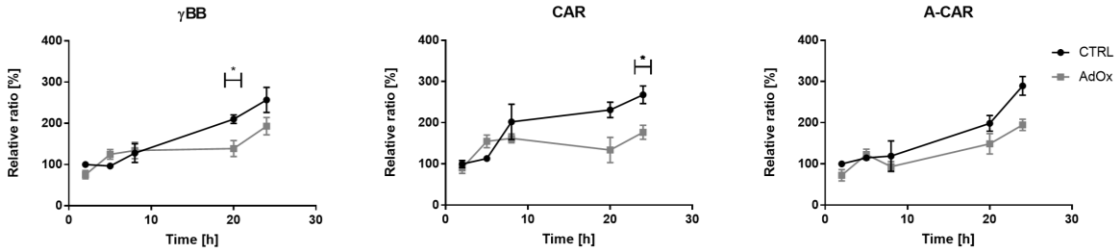


Figure 7-3: 100 µM AdOx treatment of HepG2 cells for 2 h, 5 h, 8 h, 20 h and 24 h (0.75 x 10^6 cells/well, n=3; mean ± SEM); p-values: γBB (p=0.045), CAR (p=0.031).

Next, the dose of AdOx was optimised and a range of concentrations (50 µM-200 µM) was tested for 20 h treatment on HepG2 cells (Figure 7-4); the strongest decrease of γBB, CAR and A-CAR was found at 200 µM AdOx concentration.

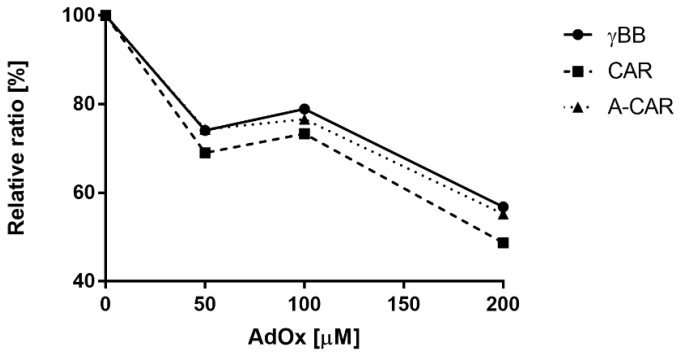


Figure 7-4: HepG2: 20 h treatment with AdOx at concentrations: 0 µM, 50 µM, 100 µM, 200 µM (n=1; 0.75 x 10^6 cells/well).

Finally, 200 µM AdOx treatment for 20 h was performed in triplicate leading to a significant decrease of almost 50% in CAR biosynthesis (Figure 7-5).

The result confirms that AdOx activity leads to an almost 40% reduction in CAR levels, implying that cellular methylation pathways play an important role in CAR biosynthesis. Given the findings in the earlier chapter (see section 6.4.1), by inhibiting protein lysine methylation and preserving hypomethylation states, AdOx likely leads to limited availability of free TML for use in CAR biosynthesis.

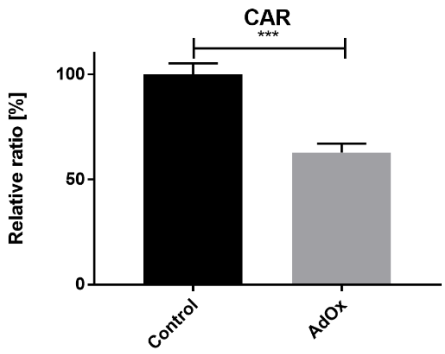


*Figure 7-5: HepG2 treatment with AdOx for 20 h at concentration 200 µM (n=3; 0.75 x 10^6 cells/well); p=0.0007; p<0.001 represent statistical significance marked with ***.*

Next, after the observation of the changes in metabolites level, it was examined whether AdOx introduces changes to the PTM of histone proteins. Since it was not possible to observe free TML levels in human cell lysates, western blotting analyses were used to investigate a link between events occurring on histones and carnitine.

Therefore, HepG2 cells were again treated with AdOx for up to 24 h, and next histones were extracted from the cell lysates and analysed by the western blotting technique optimised earlier. The analysis suggests that total histone H3 lysine methylation already decreased significantly after 8 h of AdOx exposure and continued to decline until the last time point (24 h). Interestingly, at the same time it was observed that levels of total histone H3 lysine acetylation drastically increased (Figure 7-6). This observation indicates significant epigenetic changes that appear during the perturbation of the cellular methylation cycle. Upon decreased lysine methylation level, it is possible that other PTMs are enhanced; apparently, the free histone lysine sides become available for other modifications such as lysine acetylation.

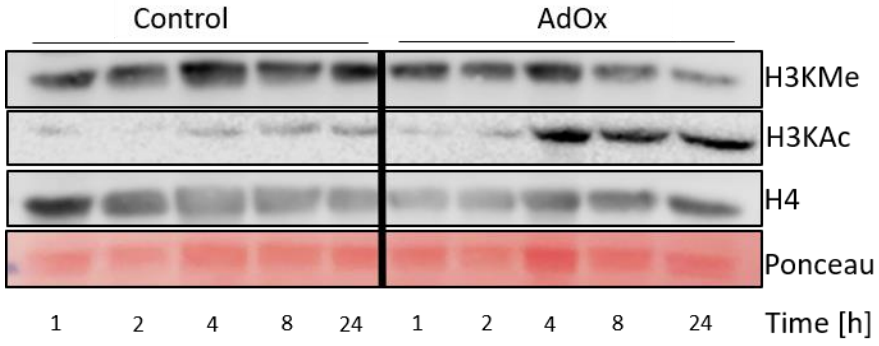


Figure 7-6: Western blotting analysis of total histone H3 lysine methylation (H3KMe) and acetylation (H3KAc) in HepG2 cells after 100 µM AdOx treatment over time (1 x 10^6 cells/well). As a loading control, histone H4 levels and ponceau stains are shown (n=1).

Importantly, lysine methylation does not only occur on histone proteins. There is reported evidence that many of the KMTs and KDMs occur to be active also on non-histone proteins i.e p53, G9a or NFκB [40]. Therefore, it is possible that non-histone lysine methylation also contributes to the CAR biosynthesis pathway. Thus, it was important to also investigate the level of non-histone cytoplasmic protein methylation and their role in overall TML precursor available for CAR biosynthesis.

During the investigation of the trimethylated lysine-containing proteins in HepG2 cell extract described in section 5.2, I identified that the cytoplasmic protein band that contains trimethylated lysine belongs to elongation factor EF1α. To examine the influence of methylation cycle on non-histone proteins. The cytoplasmic fraction of HepG2 cells treated with AdOx was analysed. After western blotting analysis, the experiment showed a noticeable decrease in EF1α methylation already after 3 h of AdOx treatment (Figure 7-7). The increased proteasomal turnover of cytoplasmic proteins probably causes this more rapid decrease of EF1α methylation compared to histones that are located in the nucleus. Therefore, the analysis confirmed that AdOx inhibits cytoplasmic methylation and suggests a potential role for non-histone proteins in providing precursors of trimethylated lysines for CAR biosynthesis.

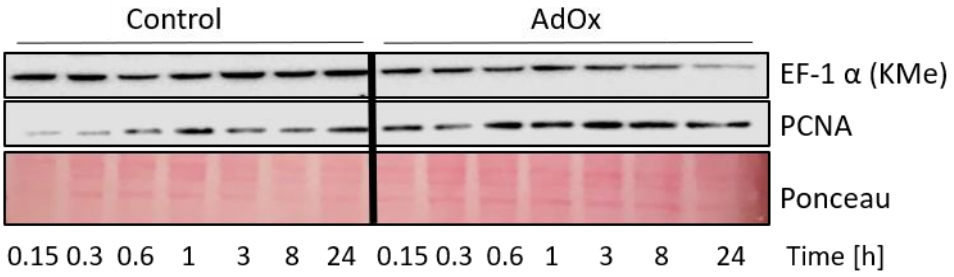


Figure 7-7: Western blotting analysis of cytoplasmic protein lysine methylation (EF1α) in HepG2 cells after 100 µM AdOx treatment over time (1 x 10^6 cells/well). As a loading control, PCNA and ponceau signals are shown (n=1).

The above data strongly suggest that the methylation inhibition with AdOx may affect carnitine biosynthesis through decreased availability of trimethylated lysine residues on histone as well as non-histone proteins. It was shown by western blotting and HPLC-MS/MS analysis that in a time-dependent manner AdOx administration lowers CAR biosynthesis.

AdOx has been reported for its capability to accumulate methyl-accepting proteins that are not a subject for rapid protein degradation [178]. Our study findings imply a slight increase of lysine methylation within the first hours of AdOx treatment (after 1 h for EF1α

and 4 h for H3), that later gets substantial reduced (Figure 7-6, Figure 7-7), consistent with literature reports. Indeed, that effect may explain a slight increase in CAR biosynthesis at the 5 h time point (Figure 7-3).

Interestingly, inhibition of H3 lysine methylation appeared to be correlated with increased lysine acetylation, providing evidence for a regulatory interplay between these two types of PTMs.

7.2.2 Treatment with methyl donors

AdOx is a molecule that directly affects the protein methylation by impairing the AdoMet/AdoHcy equilibrium. However, the cellular methylation pathway is regulated by a complex cycle of modifications that keeps that equilibrium stable. L-methionine is a precursor and methyl group donor and, in the methylation cycle, directly influences cellular AdoMet levels. In turn, methionine is regulated by homocysteine, betaine and 5-methyltetrahydrofolate in complex reactions involving the folate cycle and transsulfuration.

7.2.2.1 Folic acid, vitamin B_{12}, choline and betaine supplementation

In 2003, a group of researchers performed an experiment on yellow agouti mice where the methylation status of offspring was altered by methyl donor supplementation during the mother's pregnancy [189]. Mice nutrition with additional folic acid, vitamin B_{12}, choline and betaine (Figure 7-8) increased cytosine methylation within CpG sites of the offspring leading to changes in coat colour. This experiment has shown that a maternal diet during pregnancy may directly impact the child phenotype.

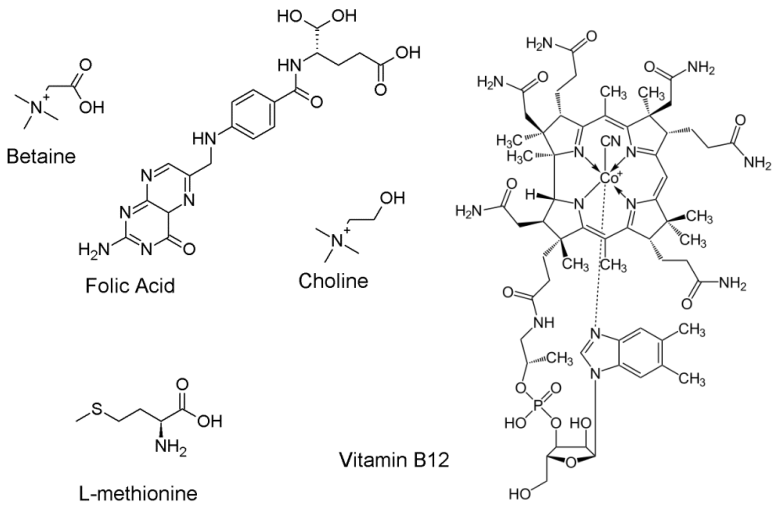


Figure 7-8: Structure of compounds used in the mice study: betaine, folic acid, choline, vitamin B12.

Therefore, to corroborate the previous results on AdOx, a supplement mixture consistent with that used in the above mouse study was added to the growth media of HepG2 cells, to analyse whether this affects the methylation state of lysine residues and, thereby, potentially influences CAR biosynthesis. HepG2 cells were treated with choline, betaine, folic acid and vitamin B_{12} for 24 h (Figure 7-9).

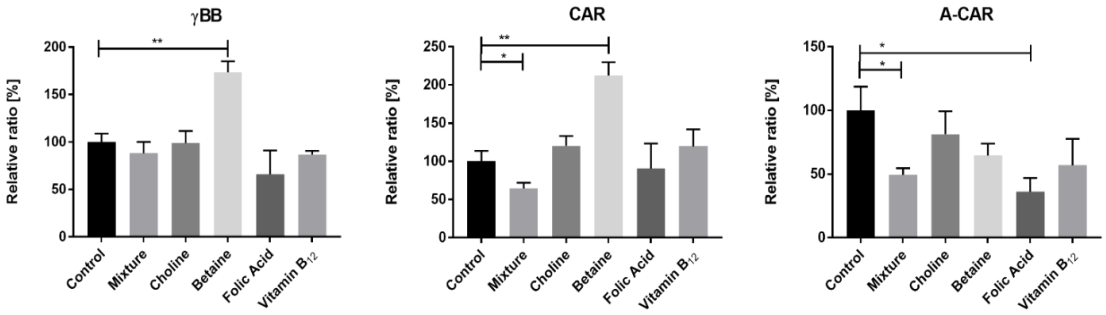


Figure 7-9. HepG2 treatment with a supplements mixture and/or each supplement individually: folic acid at 0.1 µM, vitamin B12 at 5 nM, choline at 0.5 mM, and betaine at 0.4 mM for 24 h (n=3; 0.75 x 10^6 cells/well); p values for: γBB (p=0.001), CAR (p=0.029 and p=0.001), A-CAR (p=0.035 and p=0.012); (p<0.05).

A significant decrease in CAR and A-CAR levels was observed by the complete supplementation, but not for γBB. HepG2 cells were also treated with each compound of supplement mixture individually. Interestingly, individually supplemented betaine increased γBB and CAR abundance significantly. However, that did not affect final A-CAR levels, which may have been distributed to another cellular pathway. Also, it is worth noticing that folic acid was individually capable of lowering all the tested metabolites, with significant impact on A-CAR, potentially explaining the observed effect of the total supplement mix.

Interestingly, the observed reduction in CAR levels was not consistent with the anticipated increase in CAR biosynthesis upon treatment with a mix of supplements. This result may be due to other roles on the methionine (methylation) cycle of the compounds utilised in the study. Dysregulation in the abundance of any of these compounds may lead to an impaired equilibrium between AdoMet and AdoHcy, the latter being a potent inhibitor of AdoMet and methylation level [188].

This study differs from the original mice study in several aspects: our analysis was performed on developed, non-stem cells with less dynamic epigenetic events i.e. histones and DNA methylation than in developing mice offspring stem cells and the growth

medium and the base level of AdoMet were likely very different. Therefore, pathways other than methylation may perturb the analysis in adult cells such as HepG2 line.

7.2.2.2 Isotope labelling with L-methionine-d_3

All above-tested compounds are involved in the regulation of L-methionine, a direct methyl donor for AdoMet. However, the previous experiment did not assess to what extent the supplementation with methyl donor has a direct impact on the methylation, and how much of it is an effect of the general metabolome alterations. Therefore, to ensure that the supplementation directly affects methylation levels and, consequently, CAR biosynthesis, an experiment was designed utilising isotopically labelled L-methionine-d_3.

For proteomic MS analyses, stable isotope labelling with amino acid (SILAC) type experiments are used for protein quantification [190]. Isotopically labelled amino acids, typically with heavy carbon or nitrogen isotopes, are added to cultured cells [191] or living animals [192] to observe tagged proteins and then perform precise quantification to exclude any technical variations coming from sample preparation. Usually, the complete labelling of all protein is achieved after at least six cell passages in cell culture [191].

However, in this experiment, isotope labelling was utilised to detect and potentially quantify isotopically labelled γBB and subsequently CAR and/or A-CAR. The observation of heavy CAR would allow testing whether the methylation pathway is directly influencing CAR biosynthesis. Furthermore, if isotopically labelled CAR would be observed of a stable level, that assay could be used to alter CAR biosynthesis in more controlled conditions allowing for precise quantification of the CAR-d_9 and outcome of biological treatments. Furthermore, the isotope labelling could be potentially beneficial for future mapping of the histone PTMs that contribute to CAR biosynthesis, for example through a top-down approach. Therefore, despite the high cost of isotopically labelled amino acids, the distinct advantages justify these experiments.

L-methionine containing deuterium labels at the terminal methyl group was used. This methyl group is directly transferred in the methylation cycle and is used for lysine methylation. Cell media were supplemented with L-methionine-d_3 and such media was utilised in HepG2 culture until the sixth experimental passage was reached. Cell samples from second to sixth passage were collected and the cell extracts analysed by HPLC-MS/MS. No differences were observed in the growth of cells when exposed to labelled L-methionine-d_3 i.e. there was no change in cell division time and morphology as observed

via microscopic technique. Initial observations revealed that the addition of L-methionine, as the direct substrate for AdoMet, decreases γBB and CAR biosynthesis (Figure 7-10).

Moreover, within increasing cell passages the level of γBB and CAR in control cells was rising, indicating a rising cell number in the flask after each passage. Nevertheless, such passage-dependent increase was not noticed in the flasks with added L-methionine or L-methionine-d_3. Taking into account that the cell morphology and growth was not impaired during the experiment, this may suggest that changes to γBB and CAR biosynthesis that occurred within the first passages have been preserved. In such a scenario, L-methionine supplementation may have caused epigenetically induced changes by decreasing methylation level and such changes could have been preserved in the further cell generations.

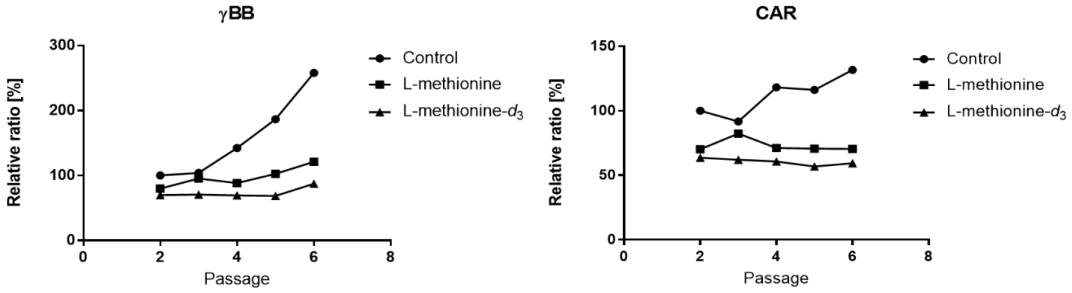


Figure 7-10: Impact of L-methionine and L-methionine-d_3 on γBB and CAR biosynthesis (cell number 1 x 10^6/flask, L-methionine and L-methionine-d_3 at 500 µg/mL).

For the HPLC-MS/MS analysis of isotopically labelled γBB, CAR and A-CAR, the detection of the corresponding compound masses in the HPLC-MS/MS script were increased by 3 Da, 6 Da and 9 Da adequately to labelling of one, two or all three terminal methyl groups of the investigated metabolites. Therefore, the analyses included four masses for each of the three investigated compounds. Among twelve tracked isotopic masses, one peak corresponded to the mass of isotopically labelled γBB-d_9 (4-*N*,*N*,*N*-trimethylaminobutyrate-(trimethyl-d_9)).

This peak appeared in all cell extracts treated with L-methionine-d_3 and showed increased intensity with each additional cell passage (Figure 7-11). However, the employed HPLC-MS/MS method did not detect peak masses corresponding to any of the isotopically labelled forms of CAR, nor A-CAR.

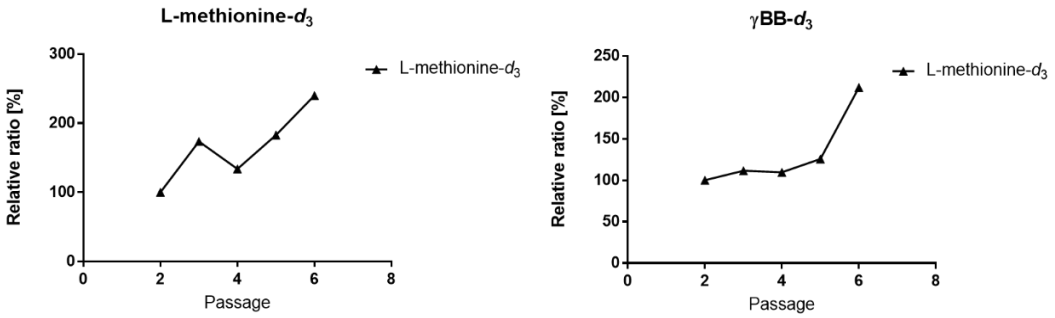


Figure 7-11: Peak intensities of L-methionine-d_3 and the potential γBB-d_9 ion in each cell passage. Both molecules were not detected in control and L-methionine treated cells.

To corroborate the identity of the potential γBB-d_9 ion, MS/MS analysis was performed using the previously established fragmentation patterns of γBB, CAR and CAR-d_9 as standard. As discussed in section 4.3.5, γBB and CAR share the common fragment $C_3H_{10}N^+$ with m/z = 60.0807; while CAR-d_9 contains fragment with m/z = 69.1372 (Figure 7-12). Therefore, above common heavy ion was investigated in the method of γBB-d_9 identification.

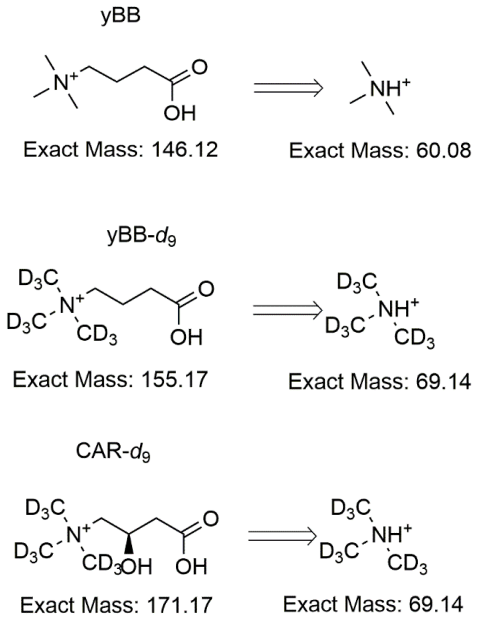
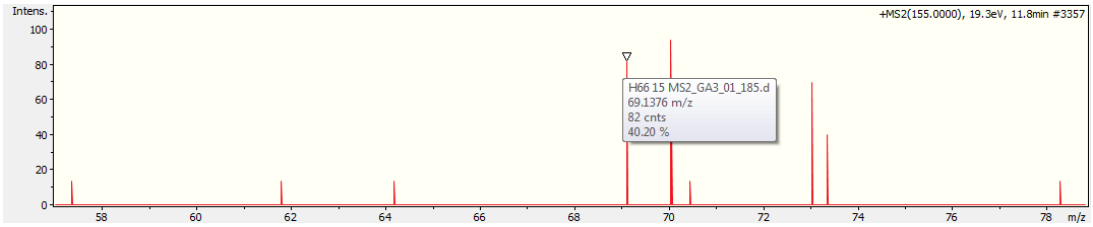


Figure 7-12: Positive ions obtained from computational fragmentation prediction for γBB, γBB-d_9 and CAR-d_9.

For this comparative analysis of the identity of potential γBB-d_9, a cell extract obtained in the final cell passage was investigated. The MS/MS method was adjusted for the search of a peak of the m/z = 146+9 = 155 (γBB-d_9). MS/MS fragmentation analysis of that peak revealed a heavy methyl fragment with m/z = 69.1372, clearly identifying the peak as isotopically labelled γBB-d_9 (Figure 7-13).

A



B

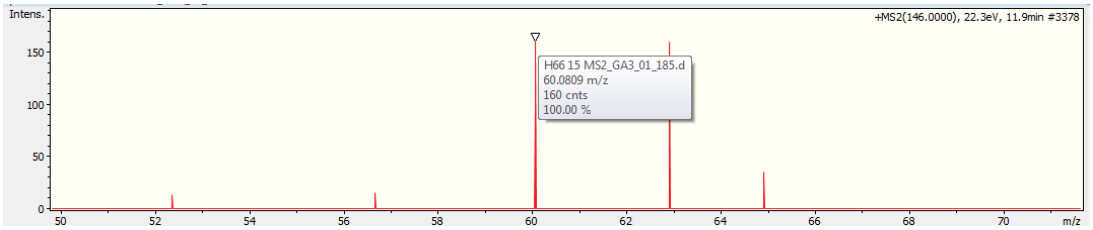


Figure 7-13: MS/MS analysis of the γBB-d_9 peak in the cell extract obtained from the sixth HepG2 passage. A) appearance of the 69.1376 ions after fragmentation of the molecule with m/z = 155 at elution time 11.8 min; B) the presence of the 60.0809 ions after fragmentation of the molecule with m/z = 146 at elution time 11.9 min.

However, the absence of the detectable isotopically labelled CAR and A-CAR was unexpected. It may be possible that the method was not sensitive enough for the small amounts of labelled compounds or that isotopically labelled CAR intermediates where not well recognized by their corresponding enzymes.

Consistently, the detected amounts of γBB-d_9 were minimal (~10-fold lower than γBB). Reduced γBB production might also be a consequence effect of the cells being treated with L-methionine. Furthermore, the experiment already required six cells passages (12 days) and high amounts of L-methionine supplementation (after concentration optimisation (data not shown)) to achieve γBB levels sufficient for MS/MS analysis. These technical challenges and the lack of detection of isotopically labelled CAR in the above time frame demonstrated that the isotope feeding is not suitable for routine experiments.

Nevertheless, the SILAC-like method allowed observing isotopically labelled γBB, confirming that cellular L-methionine is converted into γBB. Together with the analysis of AdOx inhibition and methyl donor treatment, it can be concluded that the methylation cycle has a direct impact on CAR biosynthesis through protein methylation.

7.3 Role of protein degradation on CAR biosynthesis

In mammalian cells, the carnitine precursor TML cannot be produced from free lysine [81]. A protein source of trimethylated lysine is required for carnitine biosynthesis. TML is exclusively generated via lysosomal or proteasomal degradation of proteins that

contain trimethylated lysine residues [75], [81], [82]. Degradation of proteins in human cells can take place in multiple ways: by the ubiquitin-proteasome pathway and by enzymatic proteolysis [193], [194]. The ubiquitin-proteasome pathway utilises ubiquitin which attaches to lysine residues. Subsequently, more ubiquitins are added and form a multiubiquitin chain which is recognised by proteasomes, where polyubiquitinated proteins undergo degradation [195]. Enzymatic proteolysis may take place in lysosomes containing proteases which can digest proteins taken up by endosomes, cytosolic proteins, and organelles [195]. To study the cellular source of free TML used for CAR biosynthesis, the inhibition of protein degradation pathways was investigated.

7.3.1 Inhibition of serine proteases using PMSF

The first focus of the study was an investigation of the inhibition of serine proteases, which mainly occur in lysosomes, by the widely-used protease inhibitor phenylmethanesulfonyl fluoride (PMSF, Figure 7-14).

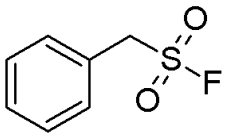


Figure 7-14: Structure of PMSF.

An analysis performed in HepG2 cells with 500 µM PMSF (Figure 7-15) did not show any significant difference, indicating that degradation of proteins containing trimethylated lysine residues was not inhibited. Several reasons may account for the lack of inhibition.

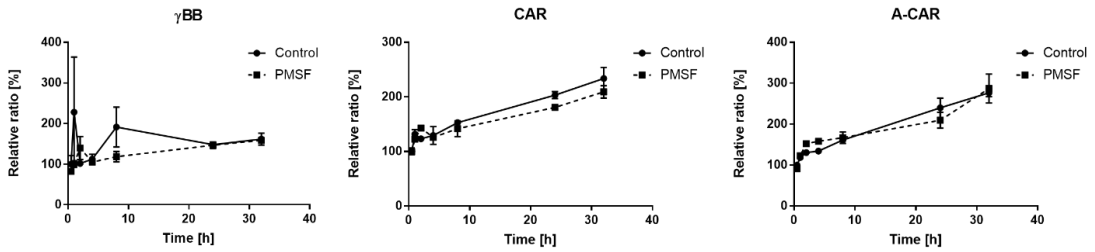


Figure 7-15: HepG2 treatment with 500 µM PMSF for 0.5, 1, 2, 4, 8, 24 and 32 h (0.75 x 10^6 cells/well, n=3, mean ± SEM).

Firstly, PMSF is unstable in water [196], and thus to prevent its degradation the PMSF stock solution was prepared in ethanol. Nevertheless, PMSF might have also degraded during exposure to the aqueous cell culture media, lowering its effective concentration.

Secondly, the lack of CAR biosynthesis inhibition could also suggest that for the degradation of lysine trimethylated proteins, serine proteases are not important.

7.3.2 Inhibition of the proteasomes using MG132

Based on the previous result, the next focus of protein degradation was an examination of the polyubiquitination pathway which can be inhibited by the peptide aldehyde MG132 (carbobenzoxy-Leu-Leu-leucinal) (Figure 7-16). Its mechanism of action relies on blocking the catalytic core of proteasomes, which prevents degradation of targeted proteins [197].

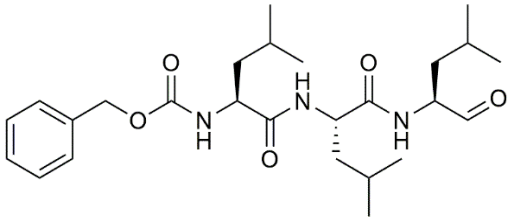


Figure 7-16: MG132 structure.

HepG2 cells were treated with 10 µM of MG132, resulting in a significant decrease in CAR biosynthesis after 8 h (Figure 7-17). Moreover, after 24 h almost complete loss of γBB, CAR and A-CAR production was observed.

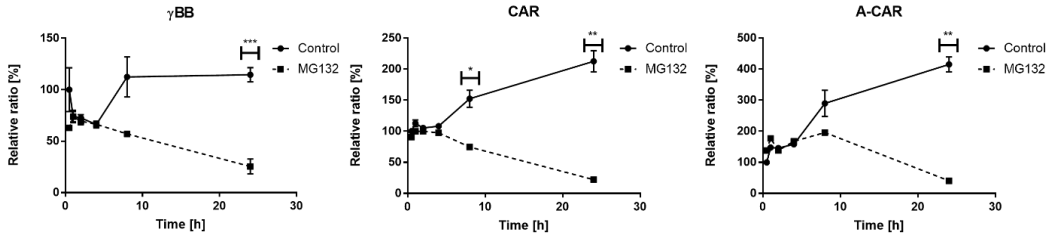


Figure 7-17: HepG2 cells treatment with 10 µM MG132 for 0.5, 1, 2, 4, 8 and 24 (n=3; 0.75 cells/well); p-values γBB (p=0.0009), CAR (p=0.0276, p=0.0058), A-CAR (p=0.0041).

Therefore, these results indicate that inhibition of proteasomal protein degradation results in decreased TML levels, which subsequently appear to significantly reduce γBB, CAR and A-CAR levels.

These findings are potential evidence for the importance of the protein degradation pathway in CAR biosynthesis. Additionally, at least in cellular cells, the source of free TML appear to be predominantly derived from proteasomal protein degradation, rather than serine protease activity.

Next, a more detailed investigation of these effect of MG132 was conducted by combination with AdOx. The idea behind this experiment was to link findings from protein methylation and degradation activity to CAR biosynthesis. Human cells were treated with 100 µM AdOx to inhibit the process of protein methylation, and after 30 min additionally 10 µM MG132 was added to the medium to inhibit protein degradation. Samples of cells were collected for up to 12 h of treatment and proteins analysed in the cell extract by western blot (Figure 7-18 and Figure 7-20).

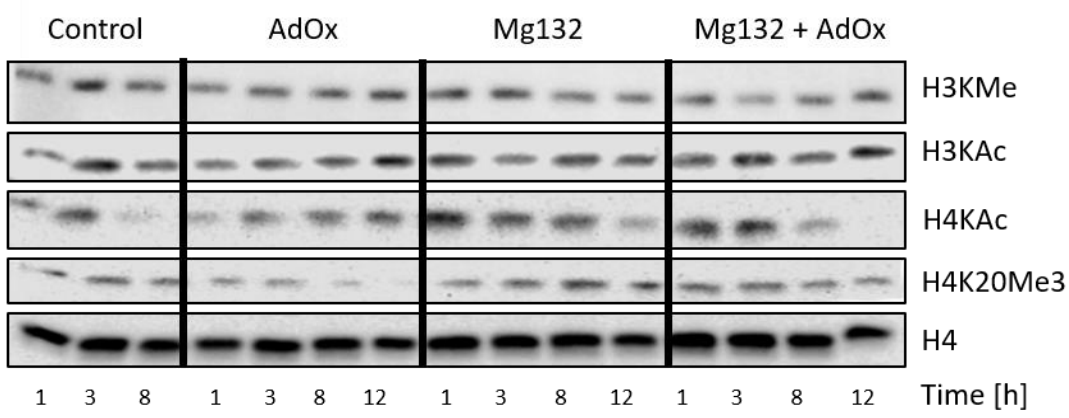


Figure 7-18: Western blot analysis of HepG2 histone extract treated with 10 µM MG132, 100 µM AdOx and with a combination of both. MG132 was added 30 min after addition of AdOx. Cells were collected after 1 h, 3 h, 8 h and 12 h of treatment (1 x 10^6 cells/well, n=1).

Histone extract analysis revealed a small increase in histone H3 methylation after 3 h of treatment with MG132. Treatment with AdOx alone over this time-frame did not show measurable effects on lysine methylation levels. Treatment with MG132 alone resulted in an unexpected decrease in observed total H3 lysine methylation. Interestingly, combined AdOx and MG132 treatment showed a rapid decrease in methylation level over the first few hours, followed by an increase in lysine methylation. Additionally, after the addition of AdOx, lysine acetylation was again found to accumulate. This effect on lysine acetylation was also observed upon combined treatment with both AdOx and MG132.

Importantly, H4 appeared to be a well-suited loading control that showed stable histone levels and long protein half-life. MG132 did not cause histone H4 accumulation, demonstrating that the H4 protein does not undergo rapid degradation.

However, interestingly, when an H4K20Me3 specific antibody was used for WB analysis, the results of the experiments became clearer. For this particular PTM, clear accumulation H4K20 trimethylation was noted after treatment with MG132 alone, whereas a significant reduction of methylation occurred after treatment with AdOx alone. In combined

treatment, a decrease of methylation was observed, implying that MG132 might only lead to accumulation of the smaller levels of methylated H3 after AdOx treatment.

To confirm these observations, the treatment was repeated for 12 h in triplicates (Figure 7-19). MG132 slightly increased the level of total methylation of lysines on histone H3 (by ~10%), whereas H4K20 trimethylation increased strongly (by almost 50%). AdOx significantly decreased methylation for both generic H3 lysine and H4K20Me3 (by ~15% for total H3KMe and by ~50% for H4K20Me3). However, on average the combined 12 h treatment of both AdOx and MG132 in the triplicate experiment decreased H4K20 methylation by 40% but increased total H3 lysine methylation by ~20%.

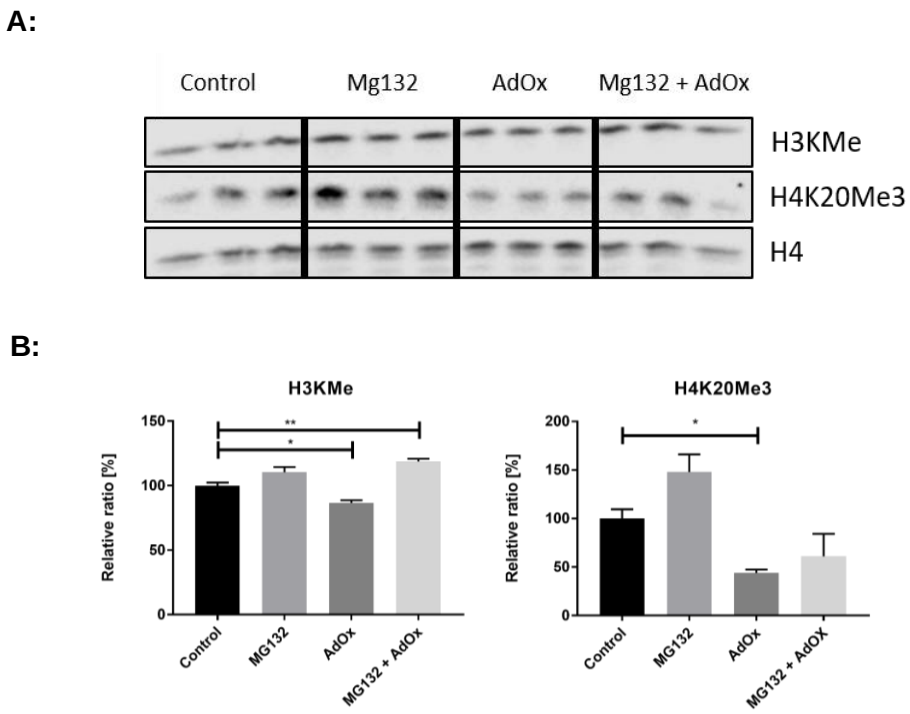


Figure 7-19: Western blot analysis (A: visual and B: quantitative) of HepG2 histone extract treated with 10 µM MG132, 100 µM AdOx and with a combination of both. MG132 was added 30 min after addition of AdOx. Cell were collected after 12 h of treatment (1 x 10^6 cells/well; n=3; mean ± SEM;); p-values: H3KMe (p=0.013 and p=0.005), H4K20Me3 (p=0.017).

A cytoplasmic cell extract was additionally analysed by western blotting for investigation of changes in lysine methylation for non-histone proteins. These analyses showed a much more rapid accumulation of EF1α methylation compared to histone methylation (Figure 7-20). Already after 3 h of treatment with MG132, an increased level of EF1α lysine methylation was observed. Additionally, as expected, AdOx reduced methylation of this elongation factor. Combined treatment with both MG132 and AdOx resulted in almost complete loss of lysine methylation on EF1α.

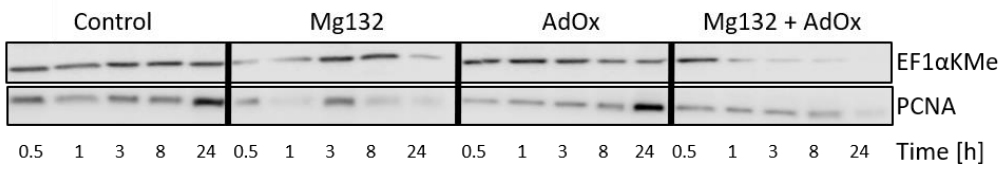


Figure 7-20: Western blot analysis of HepG2 cytoplasmic extract treated with 10 µM MG132, 100 µM AdOx and with a combination of both. MG132 was added 30 min after addition of AdOx. Cells were collected after 0.5 h, 1 h, 3 h, 8 h and 24 h of treatment (1 x 10^6 cells/well; n=1). PCNA was measured as a loading control.

To study the level of metabolites upon combined treatment with MG132 and AdOx, HPLC-MS/MS analysis of their cell lysates was performed (Figure 7-21). Treatment with MG132 and AdOx slightly rescued reduction of the CAR and A-CAR compared to MG132 alone. This might be due to the effect of slightly increased H3KMe levels with AdOx observed in the first hours of AdOx treatment.

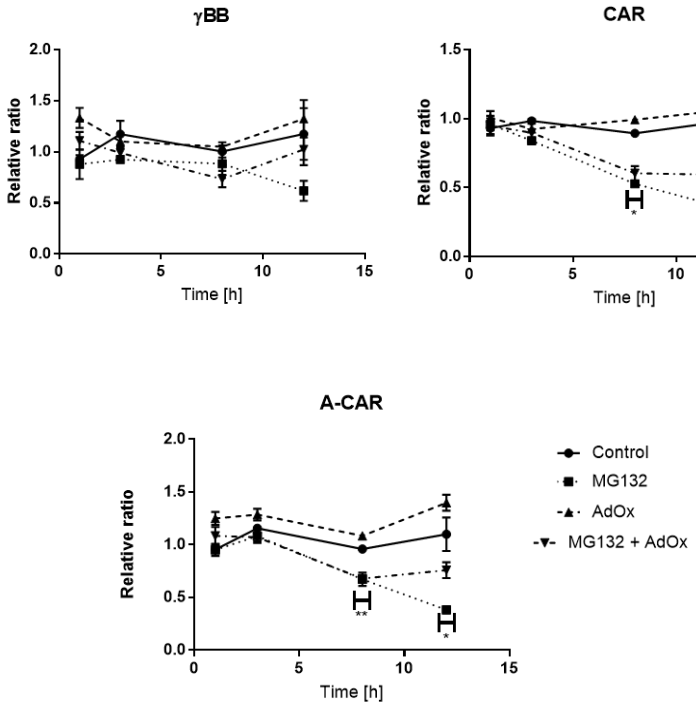


Figure 7-21: Mass spectrometric analysis of HepG2 cell lysate treated with 10 µM MG132, 100 µM AdOx and with a combination of both. MG132 has been added 30 min after addition of AdOx. Cell were collected after 1 h, 3 h, 8 h and 12 h of treatment (0.75 x 10^6 cells/well; n=3; mean ± SEM); p-values for 8 h treatment: γBB to MG132 p=0.038; CAR to MG132 p=0.007; CAR to AdOx+MG132 p=0.017; A-CAR to MG132 p=0.003; A-CAR to AdOx+MG132 p=0.0005; p-values for 12 h treatment: CAR to MG132 p=0.014; A-CAR to MG132 p=0.041.

In summary, the experiment showed that combined proteasome inhibition and hypomethylation result in reduced CAR biosynthesis. This is consistent with a molecular link between carnitine and the methylation and degradation of both histone and non-histone proteins.

Nevertheless, it is worth to note that the overall effect of methylation and degradation inhibition is an average of all changes occurring to PTMs on proteins. It is important to emphasise that inhibition of individual PTM may have different, sometimes opposite effect to the expected due to its localisation on the histone tail and related epigenetic consequence. The experiment revealed a potentially important role of the total H3 and the H4K20 methylation state to overall CAR biosynthesis. The observed changes in H4K20 methylation to the treatments were significant and consistent with the working hypothesis.

7.4 Role of PTMs cross-talk on CAR biosynthesis

Interventions in the cellular methylation cycle lead to various consequences in cellular metabolism. The above analyses of CAR biosynthesis also underline the importance of the methylation cycle in cell metabolism. However, during these studies, it was observed that manipulation of the methylation pathway also leads to an altered level of other PTM such as lysine acetylation. These are however precedent for this finding, as evidence for PTM cross-talk has already been reported [1], [198]. Therefore, this data also allows the hypothesis that should be feasible to link other PTMs to CAR biosynthesis. For instance, acetylation of lysine residues blocks their availability for methylation, and hence the level of trimethylated lysine residues should be altered. Therefore, it was a logical follow-up to study how histone lysine acetylation and its inhibition, e.g. via histone deacetylases (HDAC), affects CAR biosynthesis.

In 2006, SAHA was approved by the FDA as a histone deacetylase inhibitor and is currently used in patients with cutaneous T-cell lymphoma (CTCL) [199]. The mechanism of action for SAHA involves binding to the active site of histone deacetylases through chelation of zinc ions (Figure 7-22) [63], [199].

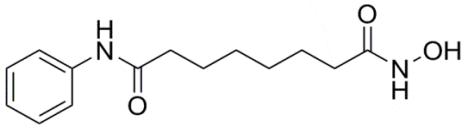


Figure 7-22: Structure of suberanilohydroxamic acid (SAHA, vorinostat).

HepG2 cells were treated with 5 µM SAHA (Figure 7-23). This resulted in a reduction of γBB, CAR and A-CAR levels after 24 h of treatment by 18%, 24% and 38%, respectively. This result suggests that histone deacetylation may influence CAR biosynthesis. SAHA may have decreased the lysine methylation state by inhibition of lysine deacetylation, and thus maintenance of a hyperacetylated and hypomethylated state, consistent with the hypothesis of the influence of epigenetic modification cross-talk on CAR biosynthesis.

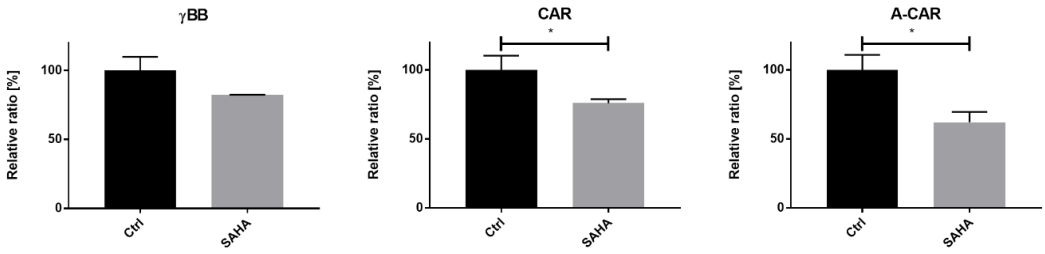


Figure 7-23: HepG2 treatment with 5 µM SAHA for 24 h (n=3; 0.75 x 10^6 cells/well); p-value for CAR (p=0.045), for A-CAR (p=0.010).

7.5 Discussion

This research chapter focused on two main objectives.

The first objective was to find an appropriate human cell line model for CAR biosynthesis studies. Human hepatocellular carcinoma (HepG2) cell line, which showed the highest level of carnitine. However, successful detection of CAR in all tested cell lines (HepG2, HEK and HeLa) suggests that its biosynthesis may be conserved in more types of human tissues than reported in the literature. The widely used HEK and HeLa cell lines are generally well known as suitable cellular models for genomic studies. Therefore, analysis of CAR biosynthesis in HEK and HeLa cell lines may be suitable for future studies i.e. transfection or overexpression of KMTs and KDMs enzymes.

The second objective of this chapter was an examination of the link between protein methylation and carnitine biosynthesis. For this purpose, various small molecules were utilised to interfere with the cellular methylation cycle as well as with protein degradation pathways.

As an outcome, AdOx, a competitive inhibitor of the methyl donor AdoMet, was found to be capable of reducing lysine methylation levels of both histone and non-histone proteins, thereby reducing the availability of CAR precursors and resulting in reduced CAR biosynthesis. This response was more rapid for cytoplasmic EF1α elongation factor rather than nuclear histone H3, which may be due to the different localisation of these two

proteins. Moreover, there is evidence that AdOx may interfere with the expression of genes regulating lipid metabolism in HepG2 cells including genes coding enzymes like carnitine palmitoyltransferase I [200].

The cellular methylation cycle plays a critical role in the action of methyltransferases. The direct impact of this cycle on CAR biosynthesis was confirmed by identification of γBB-d_9, an isotopically labelled CAR precursor, in cells supplemented with L-methionine-d_3. However, supplementation with the molecules involved in the methylation cycle was found to impact CAR biosynthesis both positively (like betaine) or negatively (as folic acid or L-methionine). The methylation cycle is known to be highly regulated by several interacting pathways including other metabolomic factors and the addition of one of the cycle intermediates does not necessarily lead to the desired outcome.

Interestingly, dietary supplementation with folic acid is a common practice during pregnancy to prevent from neural tube [201], [202]. The obtained results indicate that this practice may by analogy lower carnitine biosynthesis in maternal liver cells. This hypothesis would be supported by previous clinical studies showing a reduced plasma carnitine concentration in pregnant women [203]. The mentioned study states that the reasons for that reduction were unknown. Therefore, our findings may potentially contribute to the research on the causes of such effects. Since carnitine deficiency can lead to serious complications, it may be beneficial for pregnant women to supplement folic acid together with carnitine.

Also, L-methionine is one of the essential amino acids that the body cannot produce and must be taken up from the diet. Interestingly, L-methionine dietary restriction (MR) has been reported to improve lipid profiles, increase fat oxidation in obese humans with metabolic syndrome and even increase lifespan in mice [204]–[206]. Therefore, together with the results presented in this chapter, showing L-methionine supplementation downregulates CAR biosynthesis in HepG2 cells, one can hypothesise a role for L-methionine diet restriction via CAR biosynthesis, related to human fat metabolism.

It is worth noting that the only methylation cycle compound that individually increased CAR levels was betaine. Betaine supplementation has been found to be beneficial for regulating fatty acid and lipid metabolism and even improve insulin resistance in obese mice [207], [208].

The analyses of where TML is derived from confirmed that proteasomal protein degradation plays a crucial role in the source of free TML necessary for CAR biosynthesis; however, such a role was not found for serine proteases. Observations from blocking

proteasomal degradation pointed out that many individual PTMs may contribute differently to the overall effect of methylation and degradation on CAR biosynthesis. H4K20Me3 was found to be playing a potentially important role in that process as its cumulative response to MG132 was very significant.

During the investigation of protein methylation levels, changes in the degree of histone acetylation upon treatment with small molecules were also studied. This has allowed observation of the regulation between these two types of PTMs. Such cross talk was noticed during AdOx treatment when reduced H3 lysine methylation led to increased H3 lysine acetylation. Additionally, inhibition of proteasomal degradation induced changes in H3 and H4 acetylation. The inhibition of histone lysine deacetylases with SAHA reduced CAR biosynthesis. A possible reason for this observation was the preservation of acetyl groups on lysine residues and, therefore, decreasing the availability of lysine acceptors for methylation. This demonstrates the importance of crosstalk between PTMs in regulating CAR biosynthesis.

In summary, this research chapter provides new insights towards an understanding of the role for histone and non-histone protein methylation and their degradation on the level of CAR biosynthesis and, subsequently, overall fatty acid metabolism.

8. Study of the role of oxygenases in carnitine biosynthesis in human cell line model

Oxygenases belong to a broad and diverse superfamily of enzymes that transfer molecular oxygen into the substrate. One of the subfamily, consisting of more than 60 enzymes, are human 2OGXs that play multiple roles in the human body, including hypoxic sensing, demethylation of DNA, histone lysyl demethylation and carnitine biosynthesis [209]. Currently, researchers perform extensive studies on hypoxia sensing system and hydroxylation of hypoxia-inducible factor (HIF) enzymes carried through PHD 2OGXs.

The mechanism of action of 2OGXs relies on the coupling of the two-electron substrate oxidation with the oxidative decarboxylation of 2OG. This catalysis requires Fe^{2+} as a cofactor that binds to facial oxygenases amino acid triad (His-Asp/Glu-His) of a common double-stranded β-helix core (also referred to as a "jelly-roll" motif). During the catalytic reaction, the molecular oxygen is split, and one atom is transported into the substrate residue, while the second oxygen atom is incorporated into succinate. This reaction, which occurs on a range of substrates (i.e. proteins, lipids, nucleic acids, small molecules), also releases carbon dioxide as a by-product (Figure 8-1). Hydroxylation is the most common reaction catalysed by 2OGXs and, if carried by JmjC domain-containing 2OGX may lead to demethylation [26]–[30].

2OGXs are also involved in energy metabolism and carnitine biosynthesis [30], [75]. Firstly, carnitine biosynthesis starting from TML is a four-step enzymatic reaction catalysed by two 2OGXs: TMLH and GBBH (Figure 8-2) [30], [75]. Structural studies of GBBH and sequence analysis of TMLH reveal that both enzymes form homodimers with similar active sites in the 2OG-dependent catalytic reaction [210]. The substitution of Cys40 and Asn191 in BBOX to serine and Asp131 in TMLH is likely responsible for their altered specificity [210].

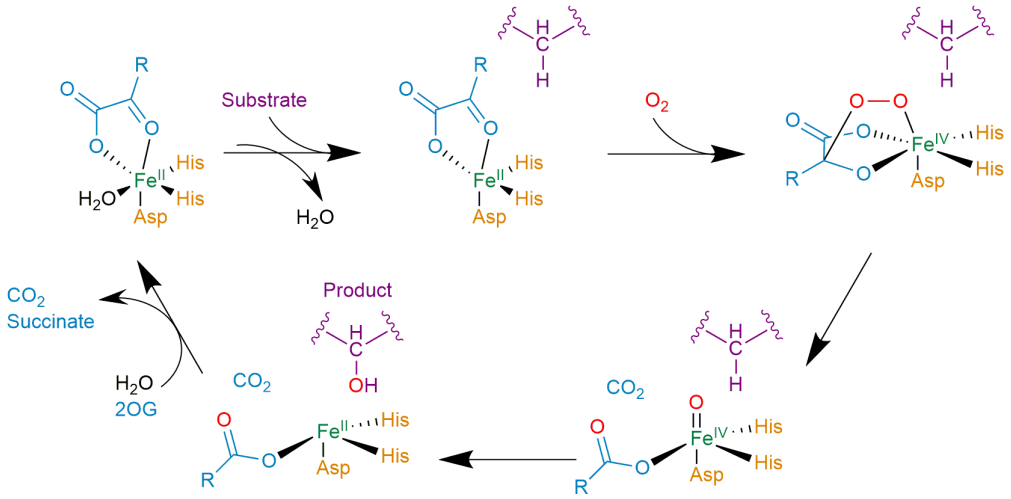


Figure 8-1: Mechanism of action of 2OG, Fe^{2+}, O_2 dependent oxygenases relies on coupling the two-electron substrate oxidation with the oxidative decarboxylation of 2OG. This catalysis requires Fe^{2+} as a cofactor that binds to facial oxygenases amino acid triad (His-Asp/Glu-His) of a common double-stranded β-helix core ("jelly-roll"). During the reaction, the molecular oxygen is split, and one atom is transported into substrate residue, while the second oxygen atom is incorporated into succinate. The reaction also releases carbon dioxide as a by-product. Colours on red indicate incorporated oxygen; green: Fe^{2+} ion; blue: 2OG/its products; orange: oxygenase amino acid triad; purple: substrate undergoing hydroxylation/product.

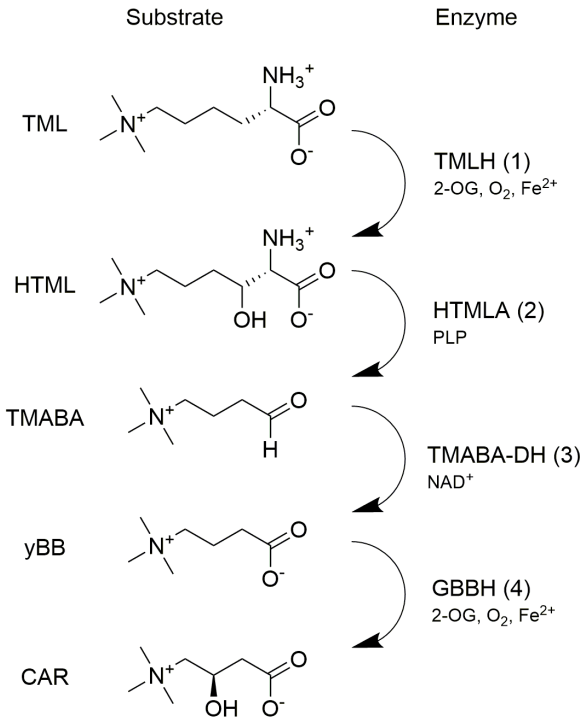


Figure 8-2: The biosynthesis of carnitine from TML requires four consecutive enzymatic steps. TML is converted into HTML by TMLH, which is a 2OG, O_2 and Fe^{2+} dependent enzyme. Afterwards, HTML is processed to TMABA by HTMLA. TMABA undergoes reaction with TMABA-DH leading to γBB production. Subsequently, γBB is converted into L-carnitine by another 2OG, O_2, Fe^{2+} dependent enzymatic reaction with GBBH.

Secondly, one class of KDMs also belongs to the 2OGXs family. These KDMs contain JmjC domain that, via hydroxylation state, demethylates tri-, di- and monomethyl lysine residues. These enzymes are involved in the demethylation of protein lysine residues which eventually has an effect on the availability of trimethyllysine for carnitine biosynthesis. Interestingly, recent findings demonstrate that JmjC domain function is not limited exclusively to histone demethylation, but can also be involved in non-histone proteins, thus suggesting that the JmjC domain may also play a role in actual hypoxia sensing, rather than just in epigenetic regulations [29].

Finally, the role of 2OGXs in energy metabolism is probably not only limited to CAR biosynthesis. These oxygenases regulate the consumption of 2OG, which may also have an impact on the Krebs cycle, in which 2OG is involved. Consequently, 2OGXs can interfere with the Krebs cycle metabolites and may regulate energy production [211].

This research chapter is dedicated to the investigation of the role and importance of the 2OGXs in the link between epigenetics and carnitine metabolism, which includes:

- Study of the impact of 2OG and Fe^{2+} supplementation on 2OGXs activity and CAR biosynthesis in HepG2 cell line;
- Examination of the effect of 2OG and Fe^{2+} limitation on hydrogenases activity and CAR biosynthesis;
- Investigation of the importance of the Krebs cycle enzymes on CAR biosynthesis
- Study of the selectivity and efficiency of KDM inhibitors towards CAR biosynthesis.

8.1 Investigation the iron-dependent oxygenases mechanism of action

8.1.1 Supplementation of Fe^{2+} and vitamin C

The activity of 2OGXs is largely dependent on 2OG, O_2 and Fe^{2+} availability. However, it was found that many 2OGXs, including GBBH, also require a presence of ascorbate (vitamin C) for their enzymic activity [210], [212], [213]. The exact functions of vitamin C and mechanisms by which the iron abundance is sensed are not yet well understood, however, it is envisaged that ascorbate plays a role in maintaining the iron in the ferrous state during the 2OGXs catalysis [143], [214].

Firstly, it was investigated how iron and ascorbate impact carnitine biosynthesis. HepG2 cell medium was supplemented with ammonium iron sulphate to increase the availability of Fe^{2+} ions, and with sodium ascorbate to increase the concentration of vitamin C (Figure 8-3).

The above conditions resulted in a slight increase in γBB and CAR abundance for individual treatments (10-20%). However, such an increase was not observed for combinational supplementation of vitamin C together with Fe^{2+}.

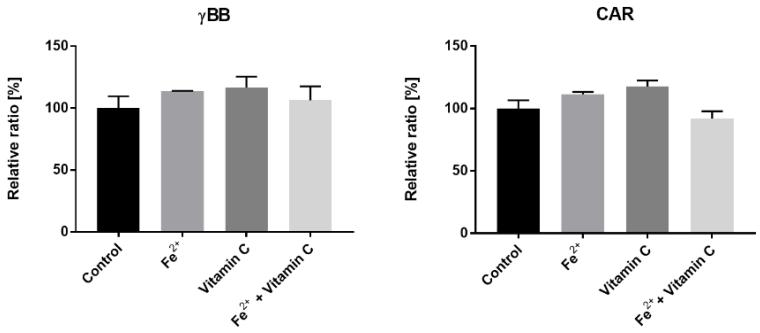


Figure 8-3: HepG2 treatment with 100 µM ammonium iron sulphate (Fe^{2+}) and 1 mM ascorbate (Vitamin C) for 24 h (0.3 x 10^6 cells/well; n=3; mean ± SEM).

These results confirmed that the activity of 2OGXs is related to the abundance of its cofactors which then, in turn, impacts the CAR biosynthesis. A comparable increase in γBB and CAR levels may indicate that the supplementation of Fe^{2+} ions and ascorbate may have enhanced the activity of TMLH in the first step of CAR biosynthesis (from TML to HTML) and ultimately such enhancement affected γBB levels. These results are consistent with studies previously performed on HIF whereas the presence of ascorbate increased the extent of hydroxylation by 2OGXs possibly by promoting the migration of Fe^{2+} to the active site of the enzyme [213], [215].

The reducing effect which was observed in the case of combined treatment with ascorbate, as well as $Fe^{2+,}$ is somewhat more challenging to interpret, as the exact role of the ascorbate in the mechanism of the 2OGX catalysis is not well understood. However, since ascorbate probably regulates the ferrous state of iron, it is possible to argue that in case of the extent of iron ions, ascorbate may have downregulated its ferrous states for 2OGX catalysis.

In addition, these preliminary data do not suggest that the enhancement of KDMs activity towards histones is due to the increase of ascorbate and Fe^{2+} levels; the latter could potentially reduce free TML levels leading to a decrease in γBB abundance.

8.1.2 Inhibition studies with iron chelators

Next, it was interested in whether the limitation of Fe^{2+} availability can inhibit the activity of oxygenases in CAR biosynthesis. Additionally, if possible, I wanted to examine the specificity of the inhibitors used.

Iron chelators can readily inhibit many 2OGXs. However, this approach does not provide high specificity. For generic inhibition of iron-dependent enzymes, the following molecules were analysed: deferoxamine (DFO) (Figure 8-4) and cobalt chloride ($CoCl_2$). DFO is widely used in iron poisoning, blood transfusions, and dialysis [216]. $CoCl_2$ substitutes iron active-site and thus disables the support of the catalytic reaction [217]. In some reported studies, DFO and $CoCl_2$ are used to induce hypoxic environment [218].

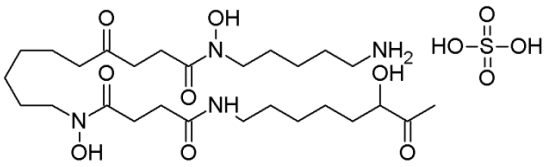


Figure 8-4: Structure of deferoxamine (DFO).

In our research study, firstly, HepG2 cells were treated with a range of concentrations of both $CoCl_2$ and DFO (Figure 8-5).

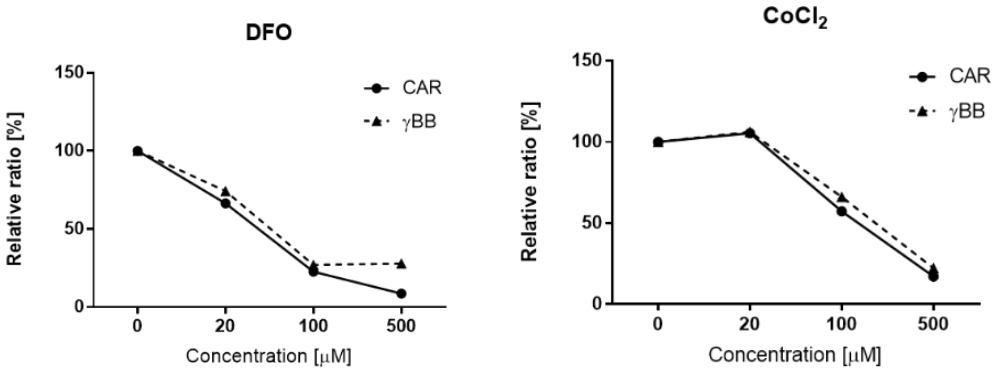


Figure 8-5: HepG2 cells treated with concentration range of DFO and $CoCl_2$ (20, 100, 500 μM) for 24 h (n=1; 0.75 x 10^6 cells/well).

DFO was found to decrease γBB and CAR by 70-90% at higher concentrations (100-500 μM). This data highlight the role of DFO in the inhibition of CAR biosynthesis. $CoCl_2$, which plays a similar role as DFO, acting as an inhibitory function in cell metabolism, showed the same effect as observed for DFO by decreasing levels of γBB and CAR by 40-80% in high concentration (100-500 μM). Interestingly, a small concentration of $CoCl_2$ (20 μM) seemed to exhibit the opposite effect by slightly elevating γBB and CAR levels.

Subsequently, optimised DFO and $CoCl_2$ treatments were repeated in triplicates (Figure 8-6). 150 μM DFO treatment resulted in a significant decrease in γBB and CAR levels by 60%.

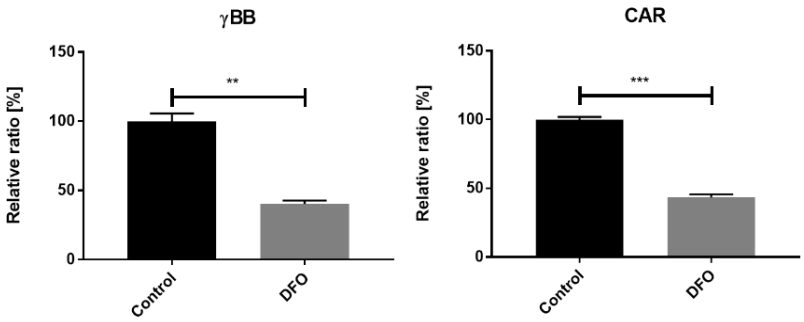


Figure 8-6: HepG2 treatment with 150 μM DFO for 24 h (1 x 10^6 cells/well; n=3; mean ± SEM); p-values: γBB (p=0.003), CAR (p=0.0001).

A similar outcome was observed in a 100 μM treatment with $CoCl_2$, where γBB and CAR levels were reduced by 40% (Figure 8-7).

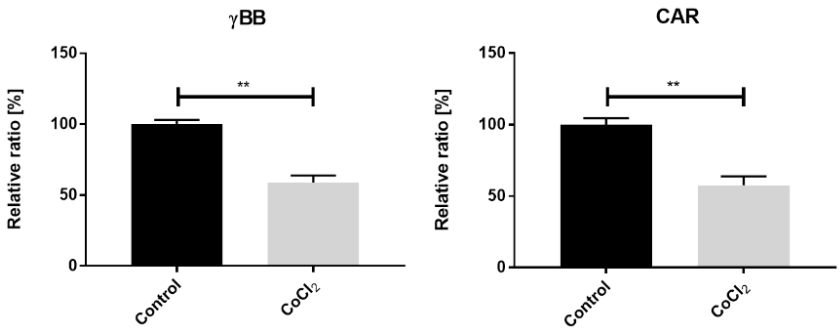


Figure 8-7: HepG2 treatment with 100 µM $CoCl_2$ for 24 h (0.3 x 10^6 cells/well; n=3; mean ± SEM); p-values: γBB (p=0.004), CAR (p=0.007).

The above observations suggest that Fe^{2+} chelation by DFO and $CoCl_2$ affects the early stages of CAR biosynthesis, most probably the TMLH enzyme activity (first step of CAR biosynthesis from TML to γBB). The decrease of CAR may be just the consequence of the limited availability of γBB for further biosynthesis. Stronger inhibition by DFO compared to that of the $CoCl_2$ may be due to the structural differences in both molecules. DFO with high-affinity chelates Fe^{2+} ions, while Co^{2+} as a single ion just competitively replace Fe^{2+} in reaction.

To further investigate the role of the iron chelation in γBB reduction and its potential involvement in the inhibition of KDMs, western blot analyses of DFO treated HepG2 cells were performed(Figure 8-8).

Interestingly, western blot analyses and antibody signal quantifications in histone extracts showed that 150 µM DFO did not significantly affect the protein methylation levels and for histone H3 exhibited a decreased level of histone trimethylation.

In cytoplasmic fraction analysis, EF1α methylation did not change, thus indicating that DFO did not target specific to EF1α demethylases, or that such activity of demethylases is not potent. Therefore, the observed decrease of γBB could be a result of the inhibition of the TMLH enzyme.

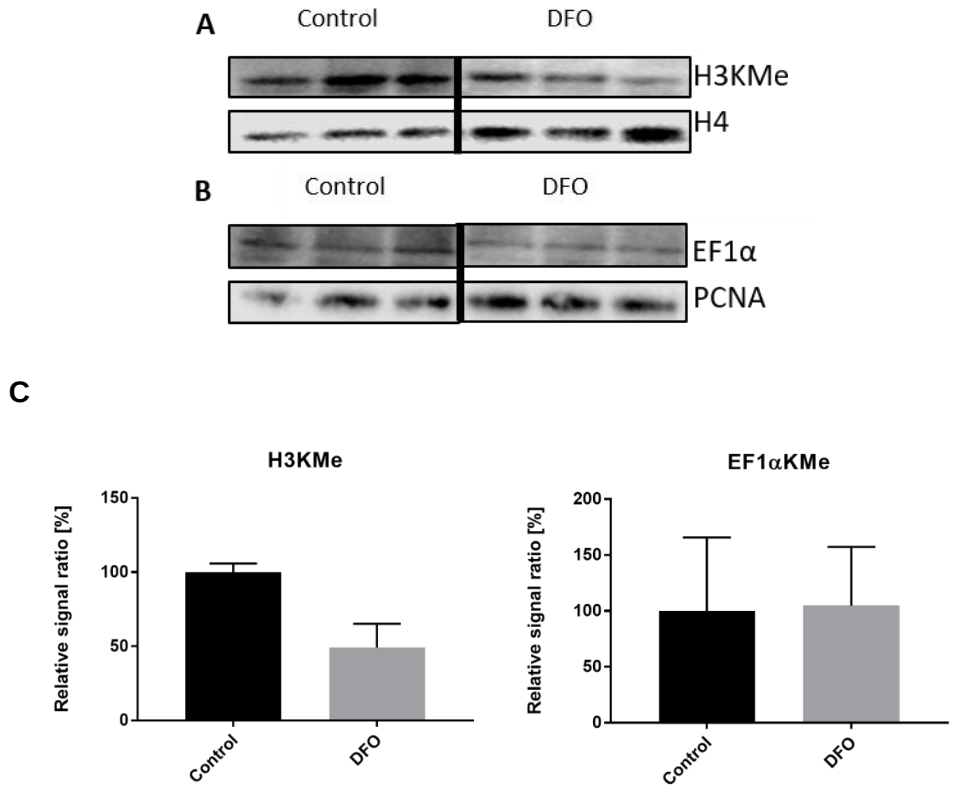


Figure 8-8: Western blot analysis (A and B: visual and C: quantitative) of HepG2 histone (A) and cytoplasmic extract (B) after treatment with 150 µM DFO for 24 h); (C) relative signal ratios; (1 x 10^6 cells/well; n=3; mean ± SEM); p-value for histones (p= 0.07).

The observed decrease in histone H3 methylation was contrary to those reported in the recent literature [219], [220]. However, these reports examine the individual lysine methylation states levels. Our study was an analysis of global histone H3 lysine trimethylation states, which were on average reduced compared to the control runs. Therefore our data may suggest that there might be an additional adverse influence of DFO on histone methylation, other than the inhibition of the KDMs activity. Possibly, DFO may have an impact on the metabolic pathways that may have induced changes to the epigenetic gene regulation. Such reducing DFO impact on the epigenetic methylation may be a reason behind a decreased γBB availability observed.

DFO is an FDA approved drug used to clean iron during haemodialysis [221]. Therefore, our data suggest that the supplementation of carnitine may be necessary for the patients having inhibited CAR biosynthesis for maintaining their energy metabolism. Recent studies report carnitine deficiency in patients receiving haemodialysis and CAR supplementation trial in such individuals has been conducted [222]. Interestingly, the trial revealed that CAR supplementation helps to maintain physical functions and lean body mass in people on haemodialysis with observed CAR deficiency [222].

8.2 Investigating the mechanism of action of 2-oxoglutarate-dependent oxygenases

8.2.1 Supplementation with 2-oxoglutarate

2-oxoglutarate is one of the fundamental metabolic regulators that has numerous biological functions and roles, including those in cellular signalling, metabolism and gene expression. 2OG is a Krebs cycle intermediate [223], which occurs after isocitrate and is then transformed into succinyl-CoA, ultimately yielding succinate [211].

It is not known whether the cellular availability of 2OG could ever be naturally limited. However, the next objective of this chapter's investigation was to study the impact of 2OG availability on 2OGXs involved in CAR biosynthesis. Firstly, it was studied the effects of 2OG supplementation in cell medium for HepG2 cells (Figure 8-9).

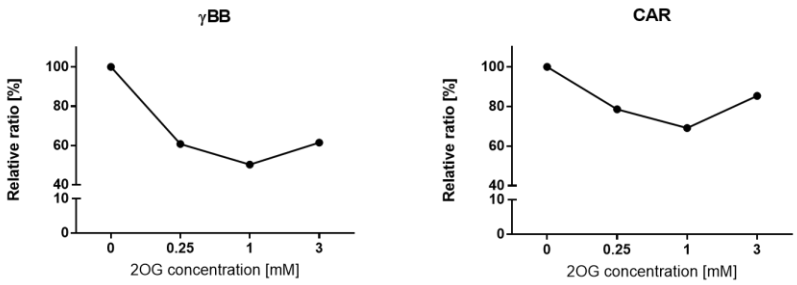


Figure 8-9: HepG2 treatment with concentration range of sodium 2OG (0.25 mM, 1 mM, 3 mM) for 24 h (n=1; 0.75 x 10^6 cells/well);

The performed experiments showed that 2OG supplementation (up to 1 mM) reduces γBB and CAR biosynthesis by 50% and 30%, respectively. However, higher concentrations may potentially reverse such effect.

Since 2OG is involved in the Krebs cycle, which in turn additionally regulates 2OG consumption, potentially, increased 2OG availability could interfere with the Krebs cycle and cell energy metabolism thus resulting in impaired CAR biosynthesis.

8.2.2 Competitive inhibition with dimethyloxalylglycine

Next, it was investigated whether the reduction of 2OG availability would inhibit oxygenases activity. For this purpose, DMOG, a prodrug form of *N*-oxalylglycine (NOG), which acts as a cell-penetrable competitive inhibitor of 2OGXs was used (Figure 8-10)

[224]. DMOG is also known for its upregulating effect on the HIF by blocking PHD domain activity [179], [225].

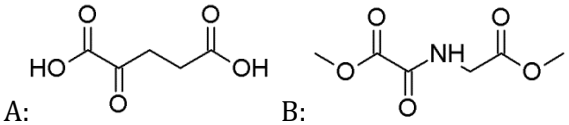


Figure 8-10: Structures of 2-oxoglutarate (2OG) (A) and dimethyloxalylglycine (DMOG) (B).

After a 24 h treatment with DMOG (with a concentration range of 1-15 mM), I observed linearly reduced CAR biosynthesis levels. However, γBB abundance did not drop to the same extent as CAR in case of 1 mM and 5 mM treatments. DMOG treatment at 1 mM dose did not change γBB levels, however, it did decrease CAR levels by 23%. At 5 mM, DMOG slightly decreased γBB and again CAR by 23% in comparison to γBB abundance (Figure 8-11).

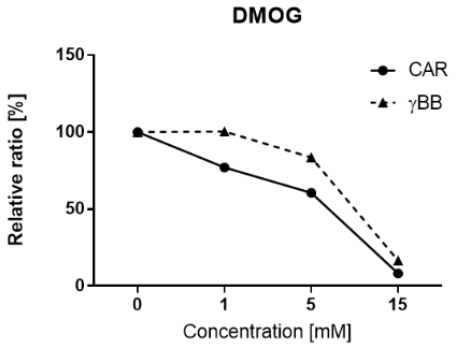


Figure 8-11: HepG2 cells treated with concentration range of DMOG (1, 5, 15 mM) for 24 h (n=1; 0.75 x 10⁶ cells/well).

Next, HepG2 cells were treated with 1 mM DMOG in triplicates and a significant decrease for both molecules (γBB and CAR) was observed (Figure 8-12).

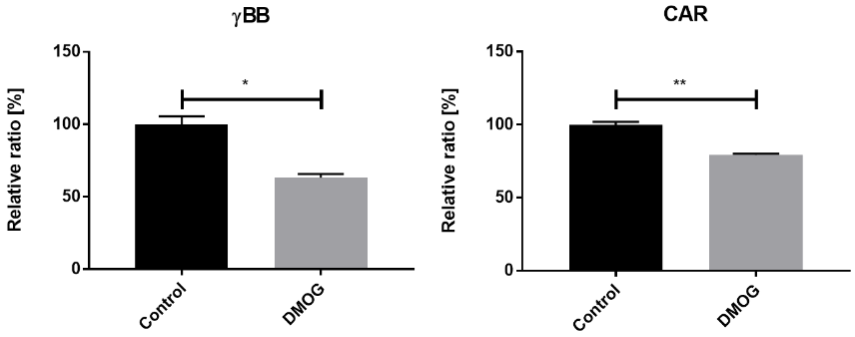


Figure 8-12: HepG2 treatment with 1 mM DMOG for 24 h (1 x 10⁶ cells/well; n=3; mean ± SEM); p-values: γBB (p=0.011), CAR (p=0.003).

The results above were not clear in terms of DMOG specificity. The concentration range results suggested that the DMOG mostly inhibits the GBBH enzyme. However, the triplicate data showed that DMOG possibly inhibits both TMLH and GBBH.

The previous studies conducted on GBBH have shown that this enzyme may accept a wide range of substrates that are structurally analogous to 2OG, including NOG. Taking into account that DMOG is a precursor for NOG, the above observations supports the claim that GBBH is inhibited by DMOG [210].

Next, to better understand the role of DMOG in inhibition of 2OGXs, a western blot analysis was performed on DMOG treated cell extracts including histone and cytoplasmic fraction (Figure 8-13). Interestingly, analyses and antibody signal quantification showed that 1 mM DMOG significantly increased the levels of methylation on EF1α lysine residue but has no effect on global histone lysine methylation.

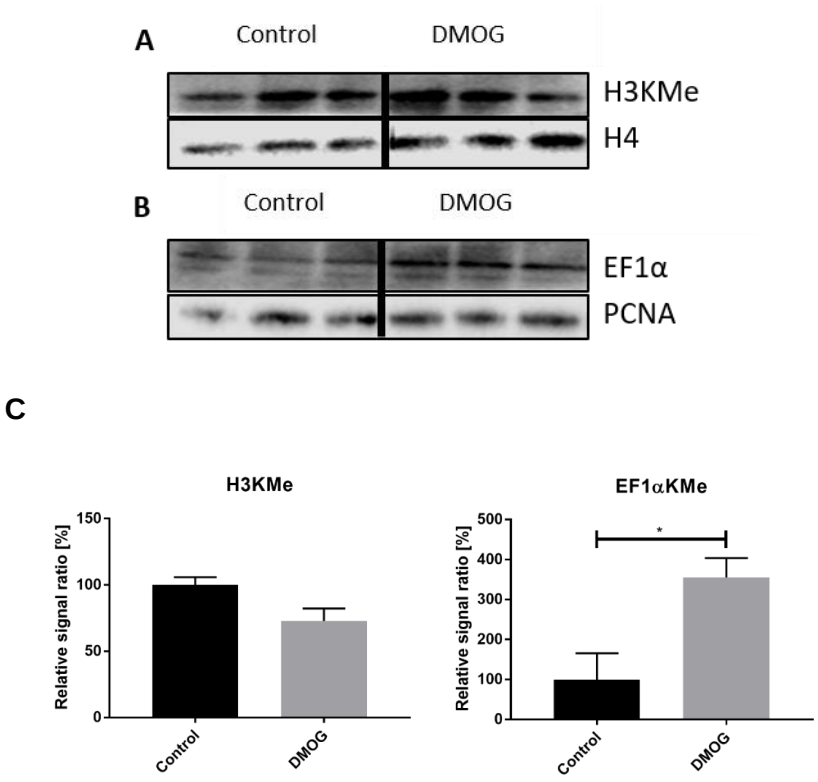


Figure 8-13: Western blot analysis (A and B: visual and C: quantitative) of HepG2 histone (A) and cytoplasmic (B) fraction after treatment with 1 mM DMOG for 24 h (1 x 10^6 cells/well; n=3; mean ±SEM); p-values: EF1aKMe (p=0.04), H3KMe (p=0.07).

Interestingly, an increase of EF1α lysine methylation did not trigger a raise in γBB levels giving two possible explanations: either (i) EF1α lysine trimethylation does not have a great impact on global free TML levels, or (ii) if it does significantly upraise TML levels, then the TMLH enzyme inhibition prevented the γBB increase observation. The decrease

in average histone H3 lysine trimethylation, similarly to DFO, may suggest that, in general, DMOG may negatively regulate the epigenetic methylation.

The above results indicated that DMOG might act in a very general and rather unspecific way, competitively inhibiting most of 2OGXs involved in the CAR biosynthesis, which is supported by evidence for broad-spectrum DMOG inhibition. Nevertheless, some studies revealed a potential for a therapeutic role of DMOG that might selectively kill some types of cancers cells [224].

8.2.3 Investigation the role of the Krebs cycle

As mentioned before, 2OG plays an essential role in energy metabolism as it is one of the intermediates of the Krebs cycle (Figure 8-14). 2OG, which is produced from isocitrate, transforms into succinyl-CoA, which is then converted into succinate and next to fumarate [211]. Mutations of enzymes which play a role in the Krebs cycle happen in some types of cancers. For instance, isocitrate dehydrogenase (IDH1) mutation can be found in gliomas or acute myeloid leukaemia [226]–[228]. Moreover, some cancers like paraganglioma or melanoma are caused by succinate dehydrogenase (SDH) and fumarate hydratase (FH) mutations [229]–[234]. The aforementioned mutations lead to accumulation of 2-hydroxyglutarate (2-HG), succinate and fumarate. In turn, as 2OG is a co-substrate of 2OGXs, the turnover of Krebs cycle intermediates likely causes overall endogenous 2OGXs inhibition. That also includes inhibition of JmjC domain-containing KDMs and metabolic disturbance to histone and DNA methylation [229], [235]–[237]. In cellular functional studies, the ester derivatives of Krebs cycle intermediates are often used as prodrugs due to their excellent cell penetration abilities [238].

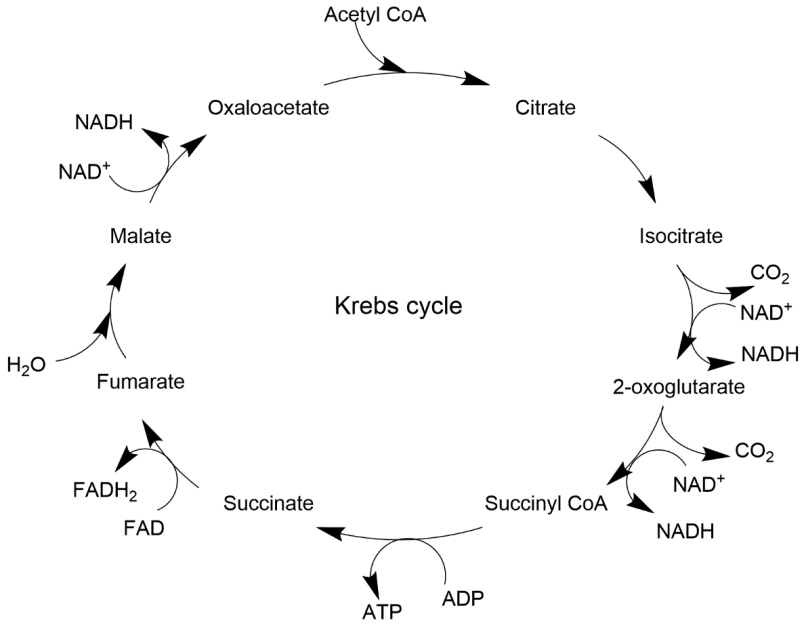


Figure 8-14: Scheme of the Krebs cycle and its intermediates.

8.2.4 Treatment with 2-hydroxyglutarate

Dysfunction in the IDH activity leads to a loss of 2OG production and increased production of *R*-2-hydroxyglutarate (*R*-2-HG) and *S*-2-hydroxyglutarate (*S*-2-HG) [227]. Literature reports that when present at elevated levels, *R*-2-HG acts as a competitive inhibitor of 2OGXs (including histones demethylases) [227]. Additionally, recent studies show that the *S* form of 2-HG is more potent than the *R* form in inhibiting H3K4 specific demethylases (Figure 8-15) [226], [236].

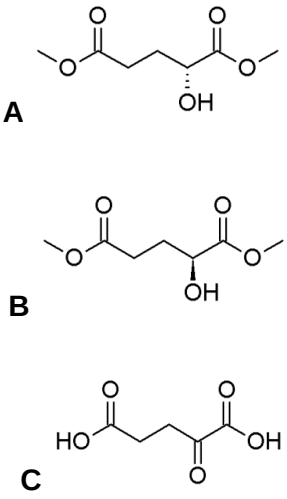


Figure 8-15: A) Dimethyl R-2-hydrogyglutarate (R-2-HG) (CCT5-166), B) dimethyl S-2-hydrogyglutarate (S-2-HG) (CCT5-168), C) 2-oxoglutarate (2OG) structure.

To investigate the effect of 2-HG on CAR biosynthesis, both ester forms of 2-HG, dimethyl *R*- and *S*-2-hydroxyglutarate (CCT5-166 and CCT5-168, respectively), were tested on HepG2 cell line for 24 h at 1 mM concentration (Figure 8-16). Both molecules did not affect γBB and A-CAR levels, however, both 2-HG stereoisomers significantly reduced CAR biosynthesis by 20%.

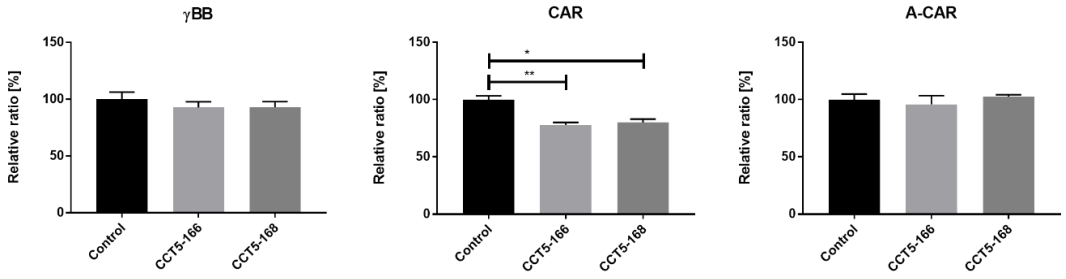


Figure 8-16: HepG2 treatment with 1 mM dimethyl R-2-HG (CCT5-166) and 10 mM dimethyl S-2-HG (CCT5-168) for 24 h (0.75 x 10^6 cells/well; n=3; mean ± SEM); p-value for CCT-166 CAR (p=0.006), for CCT-168 CAR (p=0.01).

To gain more understanding of the observed specificity of 2-HG towards CAR biosynthesis inhibition, HepG2 cells were treated with an increased concentration of *S*-2-HG and *R*-2-HG (10 mM) (Figure 8-17).

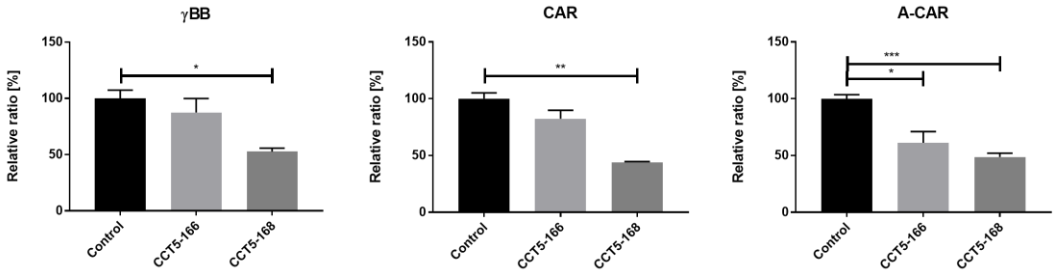


Figure 8-17: HepG2 treatment with 10 mM dimethyl R-2-HG (CCT5-166) and 10 mM dimethyl S-2-HG (CCT5-168) for 24 h (0.75 x 10^6 cells/well; n=3; mean ± SEM); p-value for CCT-166 A-CAR (p=0.046), for CCT-168 γBB (p=0.013), CAR (p=0.008), A-CAR (p<0.001).

Interestingly, cells treated with 10 mM *S*-2-HG (CCT5-168) showed a significant decrease in γBB (by 50%) and CAR levels (by 55%), whereas *R* isomer (CCT5-166) only exhibited mild reduction (only 15% for γBB and CAR, as previously); this is consistent with literature data showing better general inhibition of 2OGXs for *S* form of 2-HG [226]. In terms of CAR's ability to bind to acetyl groups, both inhibitors decreased A-CAR levels to a similar extent (by 40-50%).

The data above suggest that the *S* form of 2-HG is a more potent inhibitor of GBBH and TMLH enzymes in CAR biosynthesis. This finding can be further supported by the recent *in vitro* assay studies showing that the *S* form is indeed more potent towards GBBH than *R* form (IC_{50} 142 µM for *S* vs 13200 µM for *R*) [236]. This additional finding of significant inhibition of TMLH by *S* form of 2-HG may provide new insight into the development of 2OGXs specific inhibitors. Moreover, from a pharmacological standpoint, our data suggest that mutations in *IDH1* may require special attention in relation to the CAR abundance in the human body and potential supplementation.

8.2.5 Treatment with dimethyl-succinate and dimethyl-fumarate

The accumulation of succinate, a by-product of enzymatic hydroxylation, is often rate-limiting for 2OGXs activity, and when in high concentration, can exert inhibitory activity. Previously reported studies suggest that the accumulation of succinate can inhibit JmjC histone demethylation, thus particularly linking JHD2 activity with energy metabolism [229]–[231], while fumarate inhibits H3K36 demethylation [229].

SDH and FH mutations can be chemically mimicked via utilisation of ester forms of both succinate and fumarate, as prodrugs. Therefore, dimethyl-fumarate and dimethyl-succinate treatment (Figure 8-18) was the focus of this study.

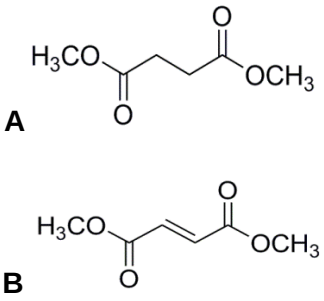


Figure 8-18: Dimethyl-succinate (A), dimethyl-fumarate (B).

A range of concentrations for both compounds of interest was analysed for 24 h (Figure 8-19, Figure 8-20). Upon treatment with 10 mM dimethyl-succinate, HPLC-MS/MS analysis showed a significant decrease in the levels of γBB (by 30%), CAR (by 40%) and A-CAR (by 60%). Additionally, a decrease in A-CAR was observed already at conditions employing only 1 mM succinate.

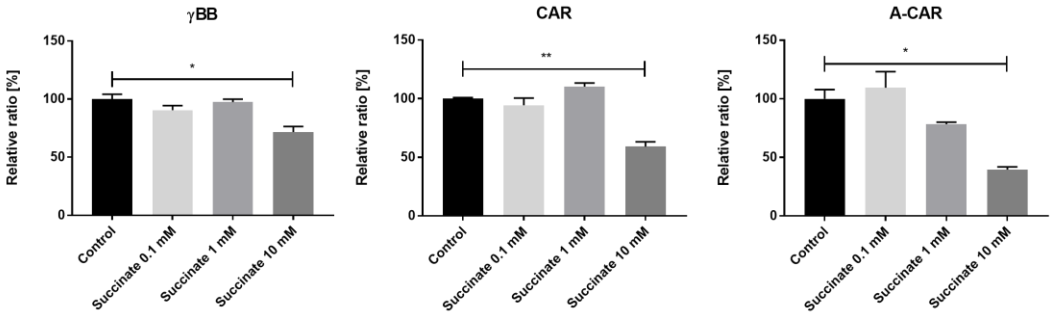


Figure 8-19: HepG2 treatment for 24 h with dimethyl-succinate concertation range (0.1 mM-10 mM) (0.75 x 10^6 cells/well; n=3; mean ± SEM); p-value for 10 mM dimethyl succinate γBB (p=0.011), CAR (p=0.008), A-CAR (p=0.011).

Dimethyl-fumarate was lethal for cells at 10 mM and was thus tested at 10 µM and 100 µM. Both of the aforementioned concentrations of fumarate exposed a significant decrease in γBB (by 40% and 25%), a slight reduction in CAR (by 15% and 5%) and a decrease in A-CAR levels (by 25% and 13%).

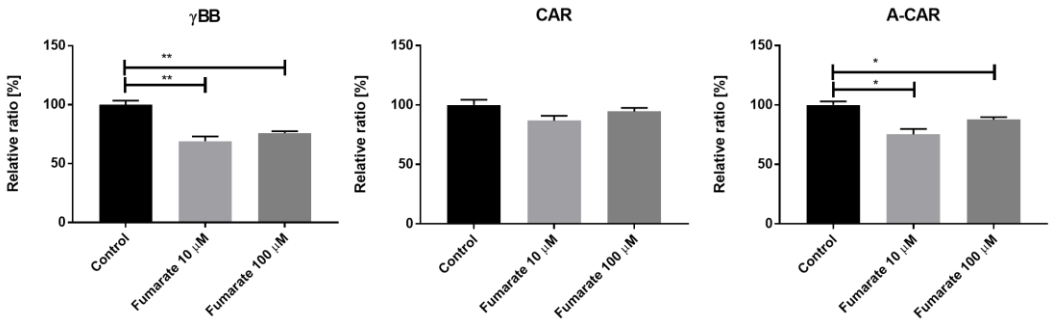


Figure 8-20: HepG2 treatment for 24 h with dimethyl-fumarate concertation range (10 µM-100 µM) (0.75 x 10^6 cells/well; n=3; mean ± SEM); p-value for 10 µM dimethyl fumarate γBB (p=0.004), A-CAR (p=0.015); p-value for 100 µM dimethyl fumarate γBB (p=0.009), A-CAR (p=0.034).

Both analyses suggest that SH and FH mutations may indeed lead to a reduced CAR biosynthesis, which was also confirmed by 2OG analogy studies showing that succinate is acting as a GBBH inhibitor [210]. Moreover, a decrease in A-CAR levels at 1 mM succinate may suggest that the succinate may have an effect on the energy metabolism already at lower concentrations.

8.3 Investigating the role of specific inhibitors

General 2OGXs inhibitors (i.e DMOG) in many cases significantly decreased CAR biosynthesis mostly by acting on TMLH and GBBH enzymes. Therefore, their potential impact on upraising TML levels by inhibiting KDMs was probably masked by their strong potency towards the key enzymes of CAR biosynthesis (TMLH and GBBH). Therefore, inhibitors with much greater specificity are desired to potentially upregulate CAR production via the inhibition of JmjC KDMs without having an effect on TMLH and GBBH.

JmjC domain-containing KDMs comprise a diverse group of 2OGXs. Although most of them demethylate histone lysine residues, there is evidence for non-histone JmjC domain activity that can lead to hydroxylation [29]. FIH (factor inhibiting 2OG-dependent HIF) is an example of such JmjC domain-containing hydroxylase [239]. Presently, JmjC KDMs are considered the largest family of JmjC enzymes and are divided into six human subfamilies. Among them, three subfamilies target trimethyllysine in histones: KDM4, KDM5, KDM6 [240], [241]

The activity of JmjC KDMs is associated with a certain type of tumour proliferation; currently, these enzymes are potential targets for cancer therapies (especially some forms of KDM4 and KDM5 subfamilies) [242]–[244]. However, highly selective and potent inhibition of 2OG-dependent oxygenases is a challenging task which demands development of appropriate strategies and techniques, that would enable the screening of multidomain 2OGXs (in particular large JmjC KDMs). The majority of the current approaches are based on a combination of crystallographic analyses, *in vitro* enzymatic assays and antibody-based methods. In the future, promising results may be obtained from mass spectrometry protein analysis that is increasingly playing a significant role in proteomic methodology. Many generic 2OGXs inhibitors served as templates in the development of more selective inhibitors. However, thus far very few specific JmjC 2OGXs inhibitors have been developed, and currently, more extensive work is being performed to address this [244], [245].

Among KDMs inhibitors with high target specificity are small molecules that target both active and non-active enzymatic sites as well as auxiliary domains [63]. The structural difference between hydroxylases such as GBBH and many other 2OG-dependent demethylases is that in demethylases, the binding site is less hydrophobic which in turn enables the methyl group to be closer to the iron centre [246]. Therefore, some of the developed inhibitors rely on the ability to translocate the active site metal ion, i.e. GSKJ-1, GSK-J4 and IOX1 (Figure 8-21).

IOX1 (5-carboxy-8-hydroxyquinoline) was found to exhibit moderate selectivity towards KDM2, KDM3, KDM4 and KDM6 families; however, it also manifested the inhibition of other 2OGXs (HIF, GBBH) [247]. IOX1 inhibition occurs in the active site of the enzyme where IOX1 chelates Fe^{2+} in a bidentate manner, utilising its phenolic oxygen and quinoline nitrogen atoms. The carboxylate motif at the 5-position interacts with the enzyme amino acid in a similar way to the 2OG, and likely plays an important role in efficient binding [63].

GSK-J4 is a precursor of GSK-J1 that inhibits histone demethylation catalysed by KDM6 subfamily oxygenases (IC_{50} = 60 nM) [248]. GSK-J1, similarly to IOX1, induces a movement of the active site metal by chelating to Fe^{2+}. A propanoic acid side chain mimics the 2OG binding [63].

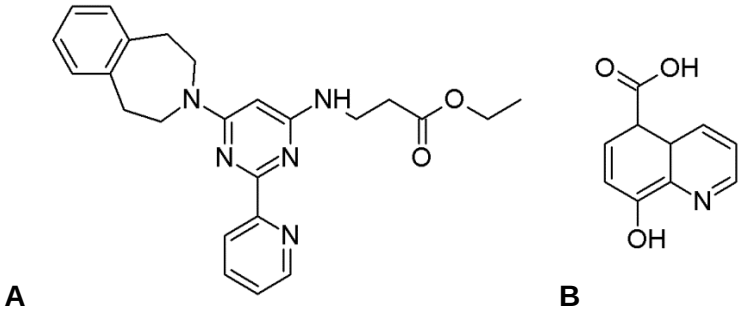


Figure 8-21: GSK-J4 (A) and IOX1(B) structures.

To test GSK-J4 and IOX1 specificity in CAR biosynthesis, inhibition compounds were analysed at 30 µM and 300 µM, respectively. A decrease in the levels of γBB and CAR was observed for IOX1 (by 35% and 40%), as well as a slight increase of both upon GSK-J4 treatment (by 10%) (Figure 8-22).

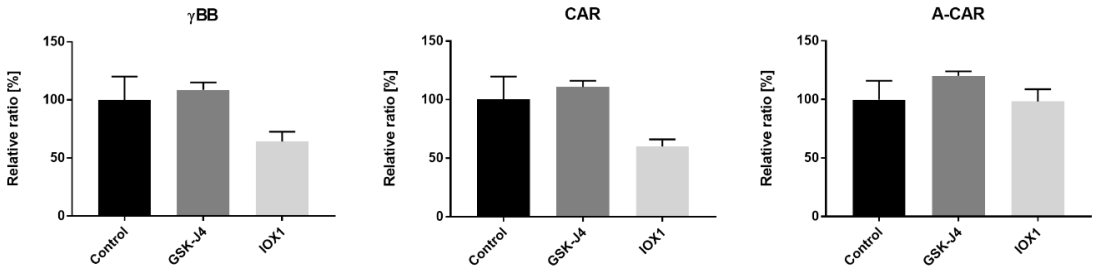


Figure 8-22: HepG2 treatment with 30 µM GSK-J4 and 300 µM IOX1 for 24 h (0.75 x 10^6 cells/well; n=3; mean ± SEM).

These results suggest a non-selective general inhibition of 2OGXs by IOX1, whereas the role of GSK-J4 remained unclear.

Based on the above result, an additional experiment was performed utilising higher concentration of GSK-J4 (250 µM, Figure 8-23).

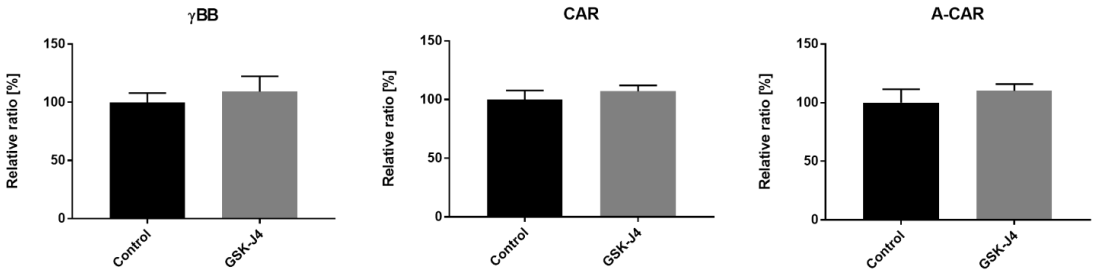


Figure 8-23: HepG2 treatment with 250 µM GSK-J4 for 24 h (0.75 x 10^6 cells/well; n=3; mean ± SEM).

Increased GSK-J4 concentrations did not lead to an increase in the inhibitory effect of GSK-J4. Nevertheless, a slight rise in γBB, CAR and A-CAR levels (by 10%) at both tested concentrations may indicate that GSK-J4 may indeed be a selective inhibitor of KDMs, resulting in elevated levels of lysine methylation and subsequently leading to an increased γBB availability for CAR biosynthesis. Unfortunately, due to the limited availability of GSK-J4, it was impossible to perform a WB analysis of histone H3 lysine methylation levels.

Nevertheless, GSK-J4 showcased the potential role of KDM specific inhibitors in improving energy metabolism. Interestingly, it has been reported that GSK-J4 together with anti-diabetic drug metformin can also be beneficial in cancer treatment [248].

8.4 Discussion

2-oxoglutarate dependent oxygenases comprise a diverse family of enzymes which target various substrates: proteins, lipids, nucleic acids and small molecules. In general (but not in all cases), they are transforming the substrates to the hydroxylated product via 2OG and Fe^{2+}-dependent mechanism of action. Cellular carnitine biosynthesis is highly reliant on 2OGXs activity as well as an abundance of the involved co-factors. In this research chapter, the importance of 2OGXs (TMLH, GBBH and JmjC containing KDMs) in carnitine metabolism was examined. This investigation used several small molecules capable of interfering with the 2OGXs mechanism.

Inhibitors of 2OGXs appeared to decrease CAR biosynthesis. All combined data obtained from inhibitors chelating iron ions ($CoCl_2$, DFO) or inhibitors competing with 2OG (DMOG, 2-HG, succinate and fumarate), exposed their highly generic nature towards the inhibition of 2OGXs. Due to their very high potency towards enzymes occurring in the late stage of

CAR biosynthesis (TMLH and GBBH), their inhibitory abilities towards KDMs have been most probably masked in the CAR quantification studies. This observation showed that there is potential for the modulation of CAR biosynthesis through inhibition of KDMs, and that is likely impossible to increase the TML levels with generic 2OG inhibitors. In HepG2 cell model, the only increase of CAR production through general 2OG mechanism was observed after a cell medium supplementation with both Fe^{2+} and ascorbate (vitamin C).

The issue of low selectivity of 2OGX inhibitors was recognised a long time ago. The therapeutic potential of 2OGXs inhibition in several cancer models and anaemia has been observed [63], [249]–[251]. However, the development of selective and potent molecules targeting 2OGXs with a high degree of target specificity is highly challenging in terms of selectivity tuning, mostly because the biological functions of 2OGXs are crucial in many other metabolic processes. IOX1 and GSK-J4 are molecules that have been well known for their potency towards some KDM families. However, after tests on HepG2 cells, only GSK-J4 showed a slight increase in CAR biosynthesis, thus showing some potential for the future KDM specific inhibitors, which may be able to also modulate CAR production.

Nevertheless, some previously reported studies suggest that there can be a positive impact on CAR biosynthesis inhibition. They argue that pharmacologically used GBBH inhibitor (mildronate) induces cardioprotective effects [210], [252]. Additionally, a study in rats with myocardial ischemia indicated that CAR biosynthesis inhibition protects left ventricular dysfunction [253].

However, it is worth to consider that since many 2OGXs play multifunctional roles and are very flexible towards their substrates, their therapeutic inhibition has to be very carefully considered. For example, extended research demonstrated that the accumulation of HIF proteins, which degrade via the action of 2OGXs, is linked with hypoxia state and is observable in proliferating [254]. One of the HIF hydroxylases is FIH protein, an example of an enzyme possessing JmjC domain. Finding the JmjC domain on non-histone targeting 2OG has revealed that the biological role of the JmjC domain is not limited exclusively to histone demethylation [239]. That implied that other JmjC enzymes (including KDMs) may play a role in a non-histone hydroxylation and hypoxia sensing. Additionally, FIH was found to hydroxylate HIF asparagine, histidine and aspartate residues, thus demonstrating JmjC's activity beyond lysine [29], [255]. Furthermore, one of the HIF target genes is carnitine palmitoyltransferase 1A (*CPT1A*), which reduces fatty acid shuttle into mitochondria and drives lipid storage when downregulated. *CPT1A* suppression has also been linked with tumour growth [256]. Lastly, a previously reported study on obesity-associated *FTO* gene found that *FTO* encodes a 2OGXs nucleic acid

demethylase [69]. Therefore, above 2OGXs examples suggests that even a highly selective inhibition of specific catalytical sites in 2OGXs may involve many undesired effects in the secondary metabolism and epigenetic changes, therefore leading to a downregulation in gene expression.

9. Investigating the impact of metabolic modulators on CAR biosynthesis and function

Cell metabolism consists of a very complex and sensitive net of protein-metabolite interactions that can be easily impaired by numerous factors. Currently, the pharmacological market offers a wide range of medications that interfere with metabolism affecting cellular energy metabolism. The developed therapies are targeted against obesity, diabetes and cardiovascular diseases (Dambrova, Liepinsh, & Kalvinsh, 2002; Edgars Liepinsh et al., 2011, Knowler et al., 2002; Turner, 1998, Shitara et al., 2013). One example of such a molecule is mildronate, clinically used as a cardioprotectant, which has recently been found to inhibit CAR biosynthesis [240], [259].

In this thesis chapter, I have further explored the role of mildronate and other energy metabolism modulators in carnitine production and activity. Moreover, selected molecules have also been tested for their potential link to epigenetic PTMs.

The specific objectives of this chapter include:

- A study of the impact of metabolic modulators (mildronate, metformin and phenformin) on carnitine biosynthesis in HepG2 cells;
- An examination of the mechanism of action of selected modulators with an iron chelation assay;
- A study of the influence of chosen modulators on acetyltransferases by utilising isotopically labelled CAR;
- An investigation of the impact of chosen modulators on carnitine transporter receptors by CAR, γBB and A-CAR supplementation, and an examination of mitochondrial content and study of acyl-CAR levels;
- An examination of HepG2 cell line viability treated with selected metabolic modulators and impact of CAR on cell homeostasis;
- An investigation of the influence of selected metabolic modulators on epigenetic modifications utilising Western blotting technique on HepG2 cell line and HPLC-MS/MS in *S. cerevisiae* protein extract.

9.1 Impact of selected metabolic modulators on CAR levels

9.1.1 Mildronate

Mildronate (meldonium) is a cardioprotective and antiatherosclerotic drug regulating energy metabolism [260], [261]. Due to this, currently mildronate is added to the World Anti-Doping Agency list as a prohibited substance [262]. The mildronate mechanism of action is based on competitive inhibition of γBB, which impairs the final step of carnitine biosynthesis by blocking the docking pocket of γBB hydroxylase (GBBH) (Figure 9-1) [240], [259]. Moreover, a recently published study shows that mildronate also acts as a GBBH substrate yielding in, i.e. formaldehyde as a catalysis product [210]. Another study shows mildronate's ability to bind to carnitine acetyltransferase, lowering the shuttle activity of the β-oxidation products of the carnitine transport [71].

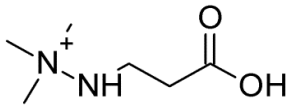


Figure 9-1: Structure of mildronate (meldonium).

In this study, HepG2 cells were treated with the previously optimised mildronate concentration of 50 µM for 24 h. HPLC-MS/MS analysis of the cell extract revealed that γBB, CAR and A-CAR were significantly decreased by 51%, 63% and 52%, respectively (Figure 9-2).

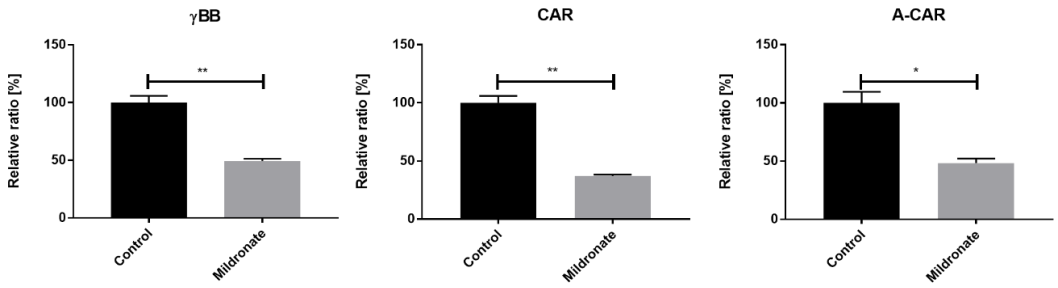


Figure 9-2: HPLC-MS/MS analysis of HepG2 cell treated with mildronate (50 µM) for 24 h. Analysis for γBB, CAR and A-CAR level (p=0.007; p=0.007; p=0.021, respectively); (1 x 10^6 cells/well; n=3; mean ± SEM).

This result confirms the previous reports of mildronate being a competitive substrate towards GBBH [210]. Also, the observed lower levels of γBB indicate that mildronate probably inhibits other enzymes in CAR biosynthesis, i.e TMLH or TMABA-DH. The impact of mildronate on TMLH enzyme may be due to the structural similarity between TMLH and GBBH enzymes, which could allow mildronate to bind to the TMLH docking pocket.

Also, the structural similarity of the TMABA product to mildronate may affect the TMABA-DH activity.

The lowered A-CAR levels observed are probably the accumulated effect of mildronate inhibiting CAR biosynthesis and the simultaneous inhibition of carnitine acetyltransferase (CAT) [71].

9.1.2 Metformin

Metformin is a metabolic disruptor widely used for T2D treatment (Figure 9-3) [257], [258]. This drug is capable of lowering blood glucose without disturbing the insulin levels, thereby, inhibiting hepatic gluconeogenesis, improving lipid profile, preventing body weight gain and reducing insulin resistance [261], [263]–[265]. Moreover, there is additional evidence that metformin interferes with cell metabolism, i.e. by decreasing Krebs cycle intermediates (2OG, citrate, malate, fumarate, succinate) [266]. By preventing diabetes, metformin also may contribute to lowering the risk of cardiovascular morbidity and mortality [267], [268]. Also, a recent study shows that metformin prevents pancreatic cancer, reverses fatty liver diseases and even has an influence on the gut microbiome [269], [270]. However, the precise mechanism of metformin action is still not elucidated.

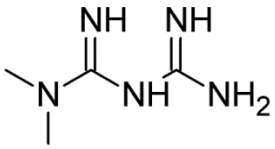


Figure 9-3: Metformin structure.

In this study, HepG2 cells were initially treated with metformin (1 mM to 5 mM) for 24 h. HPLC-MS/MS analysis of cell extract revealed that CAR decreases with rising metformin concentration, whereas levels of A-CAR increase, and γBB abundance does not appear to change (Figure 9-4).

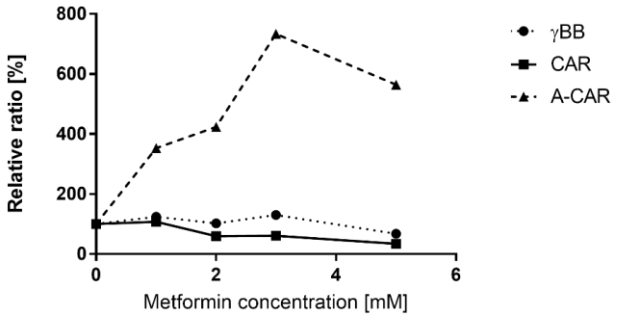


Figure 9-4: HPLC-MS/MS analysis of HepG2 cells treated with metformin (1 mM, 2 mM, 3 mM, 5 mM) for 24 h. Analysis for γBB, CAR and A-CAR level (n=1; 1 x 10^6 cells/well).

Next, to test the significance of the observed changes, three different metformin concentrations (0.1 mM, 1 mM, 10 mM) were tested on HepG2 cells (Figure 9-5). At the highest dose (10 mM), metformin reduces CAR levels by 70%, γBB by 35% and increases A-CAR levels by 35%. At lower concentrations, γBB and A-CAR do not change significantly, whereas CAR decreases by 40% at 1 mM metformin concentration.

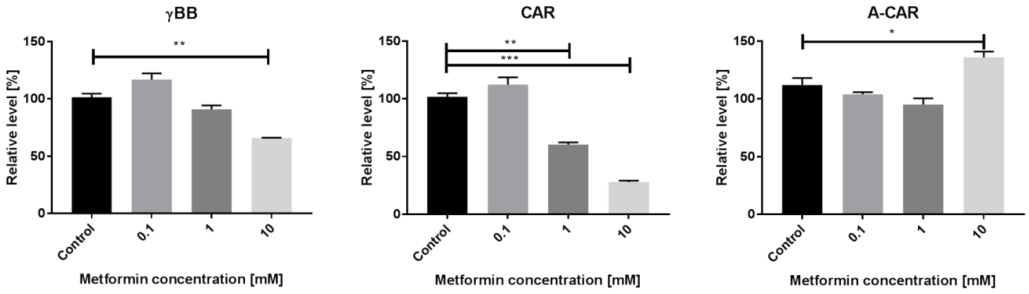


Figure 9-5: HPLC-MS/MS analysis of HepG2 cells treated with metformin at 0.1 mM, 1 mM, 10 mM concentrations for 24 h (1 x 10^6 cells/well; n=3; mean ± SEM); analysis for γBB, CAR and A-CAR level; p-values for γBB (p=0.008); for CAR (p=0.001) and (p=0.0007), respectively; for A-CAR (p=0.041).

Based on these results, it is possible that metformin directly inhibits CAR biosynthesis through GBBH inhibition. The increase of A-CAR abundance in higher concentration was also an interesting observation that is going to be further investigated. To corroborate the observed inhibition of CAR levels, the CAR level in HepG2 cell extract was additionally determined with the L-carnitine quantification Assay kit (Abcam) (Figure 9-6).

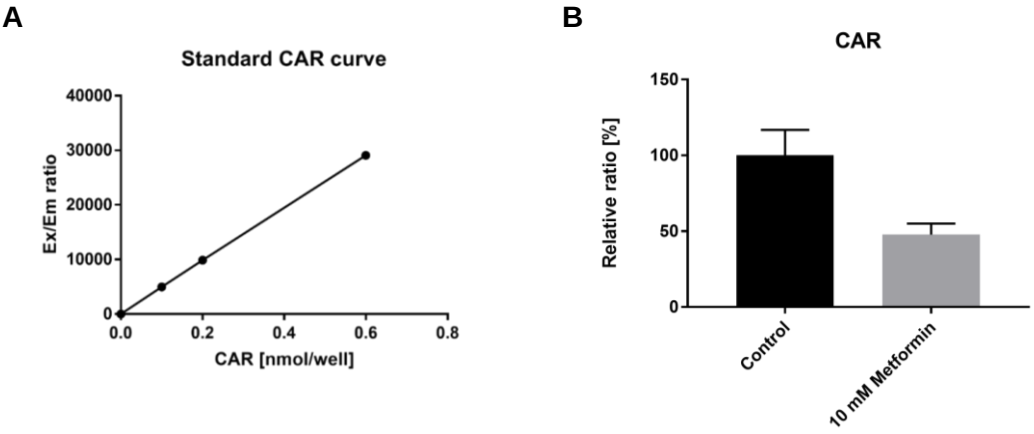


Figure 9-6: Fluorometric measurement of CAR concentration: A) standard CAR concentration curve (0, 0.1, 0.2, 0.6 nM per well) in lysis buffer (n=1); B) CAR concentration in HepG2 cell lysate treated with 10 mM metformin for 24 h (1 x 10^6 cells/well; n=3; mean ± SEM); p-value: (p=0.073).

After plotting of a standard CAR curve and analysing the CAR concentration, the L-carnitine quantification Assay kit revealed that a concentration of 10 mM metformin decreases CAR levels by 50%, as confirmed by previous observations using the HPLC-MS/MS method.

Using metformin in such a high dosage (10 mM) in further research is justifiable because in human therapies metformin is used in very high doses of 1.5-2.5 g/day, which equals approximately 9-15 mM/day/whole body mass [271].

9.1.3 Phenformin

Phenformin, as well as metformin, belong to the family of biguanides that are used to treat hyperglycaemia in patients with T2D (Figure 9-7) [272]. However, phenformin has been withdrawn from the market due to cases of high lactic acidosis (40-64 cases per 100,000 persons for phenformin) [271]. Metformin also induces lactic acidosis, but to a lower extent (0-9 cases / 100,000 persons) making metformin safer. The excess of lactate is used as a substrate to sustain gluconeogenesis which also prevents metformin from lowering the glucose to unsafe levels.

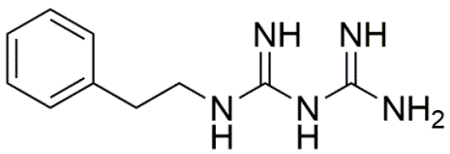


Figure 9-7: Phenformin structure.

To study whether the impact of metformin is relevant to the general class of biguanide antidiabetics, the effect of phenformin on CAR biosynthesis was tested by HPLC-MS/MS.

First, HepG2 cells were treated with concentration range of phenformin (20 μM, 60 μM and 200 μM) for 24 h. The lower concentration range was due to phenformin toxicity on cells. HPLC-MS/MS analysis of cell extract revealed that CAR and A-CAR decreased at the highest concentration by 43% and 60%, respectively, while levels of γBB abundance seemed not to change (Figure 9-8).

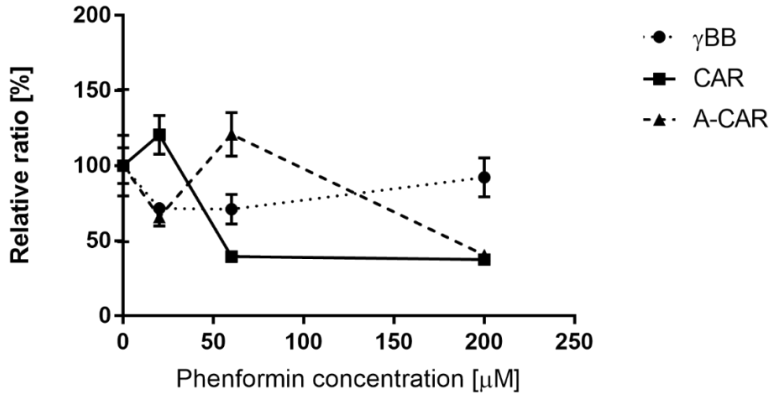


Figure 9-8: HPLC-MS/MS analysis of HepG2 cells treated with phenformin concentration range 20 μM, 60 μM, 200 μM for 24 h. Analysis for *γBB, CAR and A-CAR level; (1 x 10^6 cells/well; n=3; mean ± SEM).*

Next, to obtain more detailed data, HepG2 cells were treated at 100 μM concentration of phenformin for 24 h in triplicates (Figure 9-9). HPLC-MS/MS analysis revealed that γBB decreased by 54%, CAR by 65%, while A-CAR levels did not change.

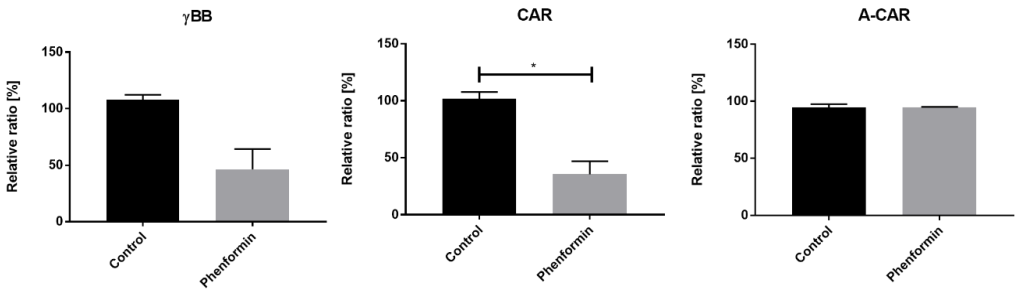


Figure 9-9: HPLC-MS/MS analysis of HepG2 cells treated with 200 μM phenformin for 24 h. Analysis for γBB, CAR and A-CAR level (p=0.043); (*1 x 10^6 cells/well; n=3; mean ± SEM).*

Phenformin appeared to lower the abundance of γBB and CAR. However, the lack of effect on A-CAR abundance indicated that potency of phenformin towards acetyl group shuttle is different.

9.1.4 Combined treatments

9.1.4.1 Metformin with mildronate

The combined supplementation with metformin and mildronate was a subject of study on the Zucker rat model [261]. Mice treated for four weeks with mildronate (200 mg/kg) and metformin (300 mg/kg) had decreased weight gain by 19%. Each drug reduced the blood glucose concentration during the fed and fasted states by 1-2 mM. Additionally, mice insulin concentration decreased by approximately 30% and 47% in a combination of drugs. These results brought new insight for metabolic effects of combining treatment of mildronate with metformin on obesity and impaired glucose tolerance.

Therefore, net the combination of mildronate and metformin was tested on HepG2 cells (Figure 9-10). Each drug, separately and in combination, significantly decreased γBB (by 45%, 30% and 65%, respectively) and CAR (58%, 80%, 90%, respectively). Additionally, a decrease of γBB and CAR level in the combination of drugs was due to their additive effect. Mildronate also significantly decreased A-CAR (by 50%), while metformin increased A-CAR (by 92%). Combined treatment decreased A-CAR by 25%.

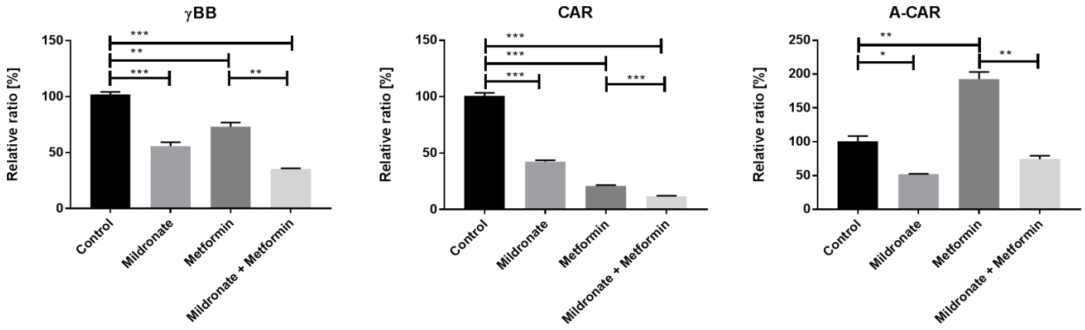


Figure 9-10: HPLC-MS/MS analysis of HepG2 cells treated with mildronate (50 μM) and metformin (10 mM) for 24 h (1 x 10^6 cells/well; n=3; mean ± SEM); analysis for γBB, CAR and A-CAR level; p-values: for γBB (p=0.0007, p=0.005, p=0.0006, p=0.008, respectively); for CAR (p=0.0005, p=0.0006, p=0.0007, p=0.0009, respectively); for A-CAR: (p=0.023, p= 0.003, p=0.003, respectively).

These results suggest that both drugs play a role in competitively inhibiting γBB and CAR biosynthesis; however, only mildronate lowers A-CAR, while metformin addition rescues it. The reduced levels of A-CAR indicated that both drugs have a different impact on handling the shuttling of acetyl groups.

9.1.4.2 Phenformin with mildronate

Next, to examine whether the observed combined effect is representative for compounds from the biguanide family, phenformin and mildronate combination was tested on HepG2 cells (Figure 9-11). Each drug separately and in combination decreased γBB (by 54%, 25% and 63%, respectively) and CAR (65%, 47% and 80%, respectively). Additionally, a reduction of γBB and CAR level in the combination of drugs was due to their addictive effect. Mildronate also significantly decreased A-CAR (by 48%), whereas phenformin did not change A-CAR levels. The combined treatment decreased A-CAR by 30%.

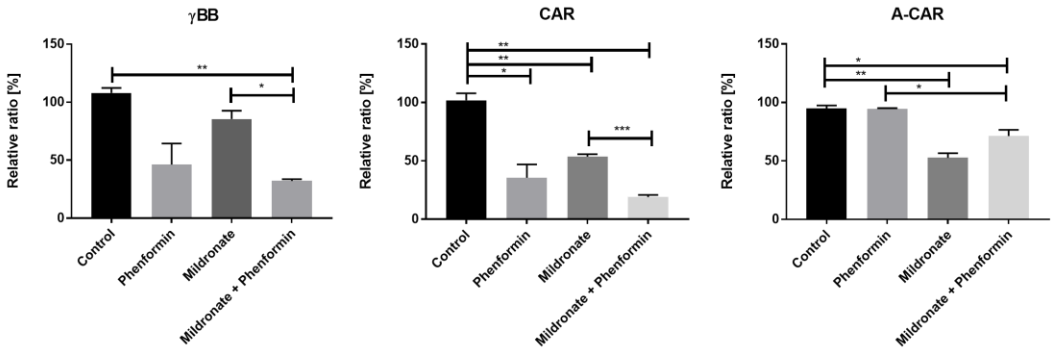


Figure 9-11: HPLC-MS/MS analysis of HepG2 cells treated with phenformin (100 µM) and mildronate (50 µM) for 24 h (1 x 10^6 cells/well; n=3; mean ± SEM); analysis for γBB, CAR and A-CAR level; p-values for γBB: (p=0.0015, p=0.00145, respectively); for CAR: (p=0.0143, p=0.0092, p=0.0030, p=0.0002, respectively); for A-CAR: (p=0.0017, p=0.0303, p=0.0468, respectively).

The results above suggest that phenformin plays a similar role to metformin in singular and combinational treatment with mildronate. Whereas, single phenformin alone does not show the increasing A-CAR effect observed with metformin treatment, in combination with mildronate, phenformin similarly to metformin rescues the decrease of A-CAR caused by mildronate.

Therefore, this shows that indeed biguanide family of compounds reduces CAR biosynthesis; however, they act differently to mildronate with respect to affecting cellular A-CAR levels.

9.2 Examination of metformin mode of action

Since it is known that mildronate is a competitive inhibitor of GBBH (and most likely TMLH) [240], [259] and carnitine acetyltransferase inhibitor, the observed reduced levels of γBB, CAR and A-CAR can be explained. Metformin and phenformin show similar effects to the γBB and CAR abundance. However, lowering CAR does not translate to expected decrease of A-CAR. Therefore, in this chapter, potential metformin mechanism of action will be examined. Due to multiple roles and benefits of metformin playing in the human body, it is likely that this molecule might impact the level of CAR via several independent mechanisms.

9.2.1 Investigation of iron chelation ability of metformin

First, I investigated whether metformin lowers CAR by inhibition of 2OGXs via chelation of the active site metal.

The Fe^{2+} chelating ability of metformin was determined by using a modified method described by Puntel in 2015 [273]. EDTA and DFO were utilised as chelating control [274]. A concentration range of metformin, DFO and EDTA was used (1 nM to 10 mM). EDTA and DFO demonstrated strong Fe^{2+} chelation abilities at 10 µM and 100 µM, respectively, and continued to increase with the increase of chelator concentration. However, metformin did not show any Fe^{2+} chelation within the tested concentration range (Figure 9-12).

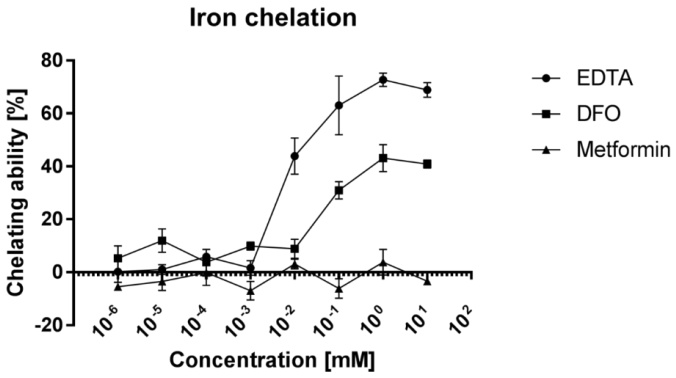


Figure 9-12: Iron chelation assay. EDTA, DFO and metformin chelating ability at concentration range (1 nM, 10 nM, 100 nM, 1 µM, 10 µM, 100 µM, 1 mM, 10 mM). Iron concentration was used at 200 µM. Phenanthroline (8 µM) absorbance was measured at 510 nm (n=3; mean ± SEM).

The above result indicates that metformin does not significantly chelate iron. The finding is also supported by the fact that metformin did not change the pH of the reaction buffer.

Nevertheless, these results did not exclude the possibility that metformin is a substrate or competitive γBB/CAR inhibitor of 2OGXs. An additional study was done in collaboration with the University of Freiburg where metformin was used in NMR analysis of succinate formation in the catalytic reaction of purified GBBH enzyme (data not shown). Succinate formation was decreased 5-fold in the presence of metformin, which indicated that metformin possibly inhibits GBBH. Also, the reaction did not show metformin modification which suggests that metformin is not an active GBBH substrate (data not shown). As metformin is a potential inhibitor of GBBH, it is highly possible that similarly to mildronate, it blocks either TMLH or TMABA-DH enzymes, which may explain how metformin also decreases levels of γBB.

9.2.2 Impact of metformin on carnitine acetyltransferases

The inhibitory role of metformin in CAR biosynthesis does not provide an explanation for the increase of A-CAR in HepG2 cellular extract. Therefore, it indicates an additional role of metformin in acetyl-group shuttling and CAR/A-CAR equilibrium. One of the possibilities is manipulation of the carnitine acetyltransferases (CAT) activity that are responsible for exchange CoA group for carnitine in binding to acetyl groups.

For further investigation of metformin, the activity of CAT was tested in the presence of metformin with the utilisation of isotopically labelled CAR. This approach would potentially allow for isotopically labelled A-CAR formation and the observation of the changes in levels of this isotopically labelled substrate upon metformin treatment.

Therefore, the HepG2 cell line was treated with 3 mM metformin, and a concentration range (2.5 µM to 40 µM) of CAR-d_9 was added to the cell medium (Figure 9-13). After 24 h of treatment, CAR-d_9 decreased the level of γBB to 75% and CAR to 50% (Figure 9-13 A: control and Figure 9-13 B: control). The inhibitory effects of CAR-d_9 and metformin combined in co-treatment, almost entirely reducing CAR biosynthesis in the highest CAR-d_9 concentrations (Figure 9-13 B: control vs metformin). Interestingly, CAR-d_9 also reduced levels of A-CAR which was not rescued by 3 mM metformin (Figure 9-13 C). HPLC-MS/MS analysis revealed that CAR-d_9 led to the formation of A-CAR-d_9 (acetyl-carnitine-(trimethyl-d_9)), whose abundance was increasing with CAR-d_9 concentration (Figure 9-13 D: control). However, the addition of metformin did not increase the level of isotopically labelled A-CAR (Figure 9-13 D: control vs metformin). Moreover, 3 mM metformin appears to decrease CAR-d_9 uptake (Figure 9-13 E: control vs metformin).

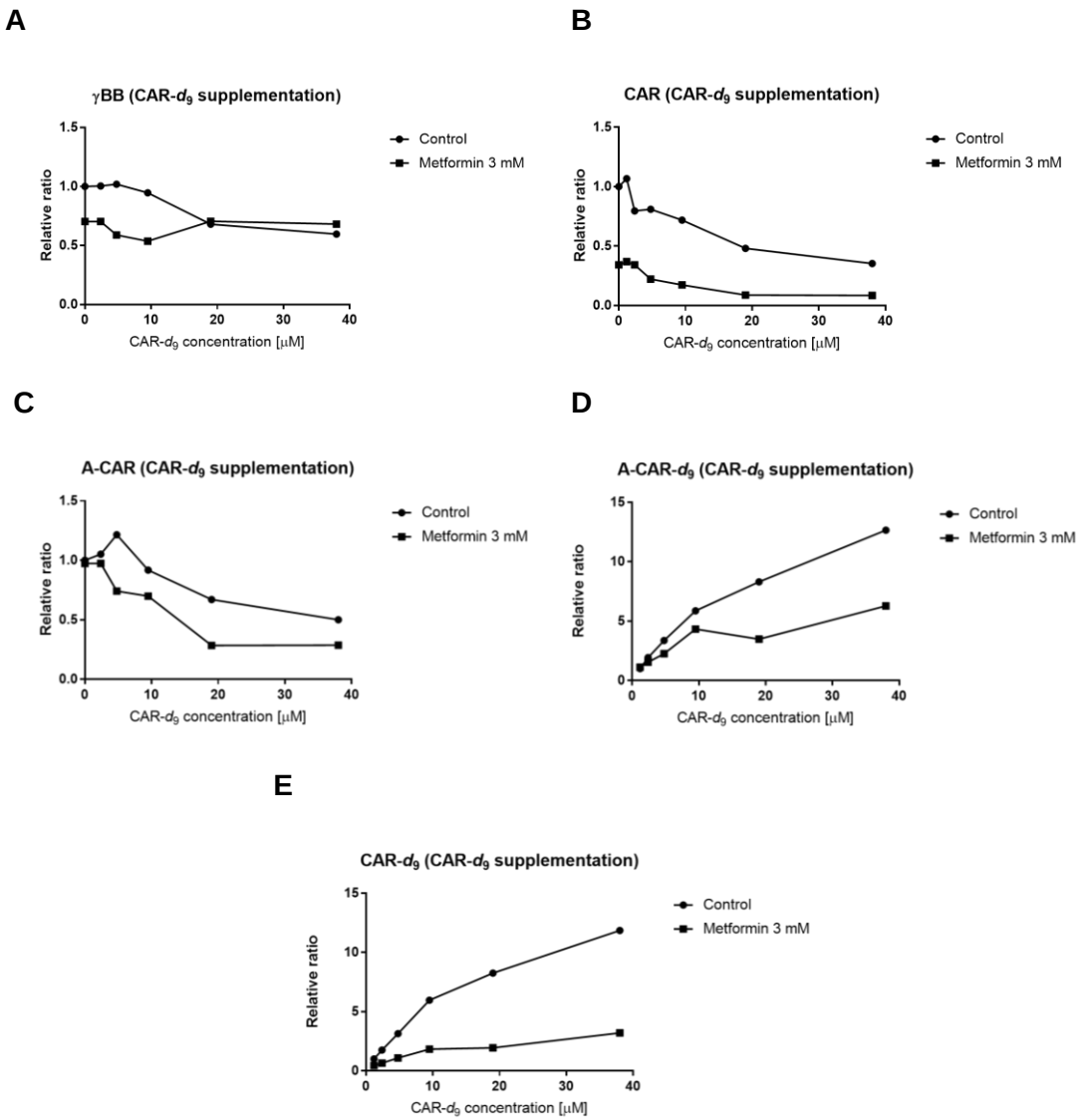


Figure 9-13: HPLC-MS/MS analysis of HepG2 cells treated with metformin (3 mM) and concentration range of CAR-d_9 (2.5 µM, 5 µM. 10 µM, 20 µM and 40 µM) for 24 h. Analysis for level of γBB (A), CAR (B), A-CAR (C), A-CAR-d_9 (D) and CAR-d_9 (E) (n=1; 1 x 10^6 cells/well); (A-CAR-d_9 identity was confirmed by MS/MS with the same method as γBB-d_9 identity in section 3.2.6).

Several conclusions can be drawn from the above data. Firstly, the data indicate that the presence of CAR-d_9 inhibits CAR biosynthesis (Figure 9-13 B: control). Secondly, CAT enzyme recognize CAR-d_9 as a substrate and forms A-CAR-d_9 as the product (Figure 9-13 D). Therefore, a high abundance of CAR-d_9 compared to CAR leads to CAT producing more A-CAR-d_9 than A-CAR. As an outcome, A-CAR formation is decreased upon CAR-d_9 supplementation (Figure 9-13 C: control vs Figure 9-13 D: control).

Particularly interesting is the fact that metformin lowers effects of CAR-d_9 supplementation for both A-CAR and A-CAR-d_9 (Figure 9-13 C and D). As previously metformin was demonstrated to increase A-CAR levels (see section 9.1.2), metformin was

considered as potential CAT enzyme enhancer. However, the above experiment with isotopic CAR-d_9 did not confirm such hypothesis, as metformin failed to enhance production of A-CAR-d_9.

These data together with the fact that metformin blocked incorporation of CAR-d_9 (Figure 9-13 E) may suggest that metformin acts as an antagonist of CAR transporting receptors. Subsequently, such antagonistic function may also regard receptors not only located on the cell surface but also on mitochondrial membrane causing A-CAR accumulation in the cytoplasmic extract.

The hypothesis of blocked CAR transporters may explain lowered levels of A-CAR and A-CAR-d_9 in the presence of metformin and CAR-d_9. Firstly, CAR-d_9 and metformin together significantly lower CAR biosynthesis which causes very low CAR utilisation for A-CAR synthesis (Figure 9-13 B and C). Low A-CAR levels, even if accumulated to some extent as a consequence of mitochondrial blockade by metformin cannot overcome the reduction of A-CAR caused by the presence of CAR-d_9. Secondly, the lowered A-CAR-d_9 levels (Figure 9-13 D) in a presence of metformin might be because metformin partially blocks CAR-d_9 incorporation (Figure 9-13 E); therefore, levels of created A-CAR-d_9 are not sufficient to be visibly accumulated by metformin.

The experiment above also shows that CAR-d_9 replaces CAR as an active substrate, while metformin is an inactive substrate towards CAR enzymes.

9.2.3 Study of competitive blockade of carnitine transporter receptors

Carnitine is involved in the multispecific transport system. Among receptors that recognize carnitine are Na^+ dependent OCTNs (OCTN1 and OCTN2; organic cation/carnitine transporter 1 and 2) [275], [276]. OCTNs together with other organic cation transporters (OCTs) belong to the family of solute carriers (SLC) that function mainly in the metabolite and drugs transport in tissues [277]. OCTNs are mostly localised in the external cell surface; however, there is also evidence for OCTN1 being expressed in the mitochondrial membrane, with examples of expression in HepG2 cell line [278]. Also, the SLC family contains mitochondrial carriers with central mitochondrial carnitine translocase (CACT) amongst them [279]. CACT shuttles carnitine acyl esters into mitochondrial matrix and allows for free carnitine to exit the mitochondria. Therefore, considering the critical role of carnitine in mitochondrial transport, it might be possible that both OCTN1 and CACT work in union to facilitate efficient carnitine shuttling.

Therefore, to further clarify the role for metformin/carnitine competition for transport by the OCTNs and CACT, I combined metformin treatment with a high concentration of the following compounds: CAR, γBB and A-CAR.

9.2.3.1 Effect of carnitine supplementation on carnitine transporters

Firstly, a concentration range of CAR was used as a supplement in HepG2 cell medium together with 3 mM metformin treatment.

HPLC-MS/MS analysis of samples revealed, similarly to CAR-d_9 supplementation, decreased level of γBB upon CAR and metformin treatment (Figure 9-14 A). CAR abundance naturally increased upon CAR supplementation (Figure 9-14 B: control). However, the presence of metformin reduced CAR incorporation (Figure 9-14 B: metformin). Importantly, the levels of A-CAR increased within the entire range of CAR supplementary concentrations, both with and without metformin (Figure 9-14 C).

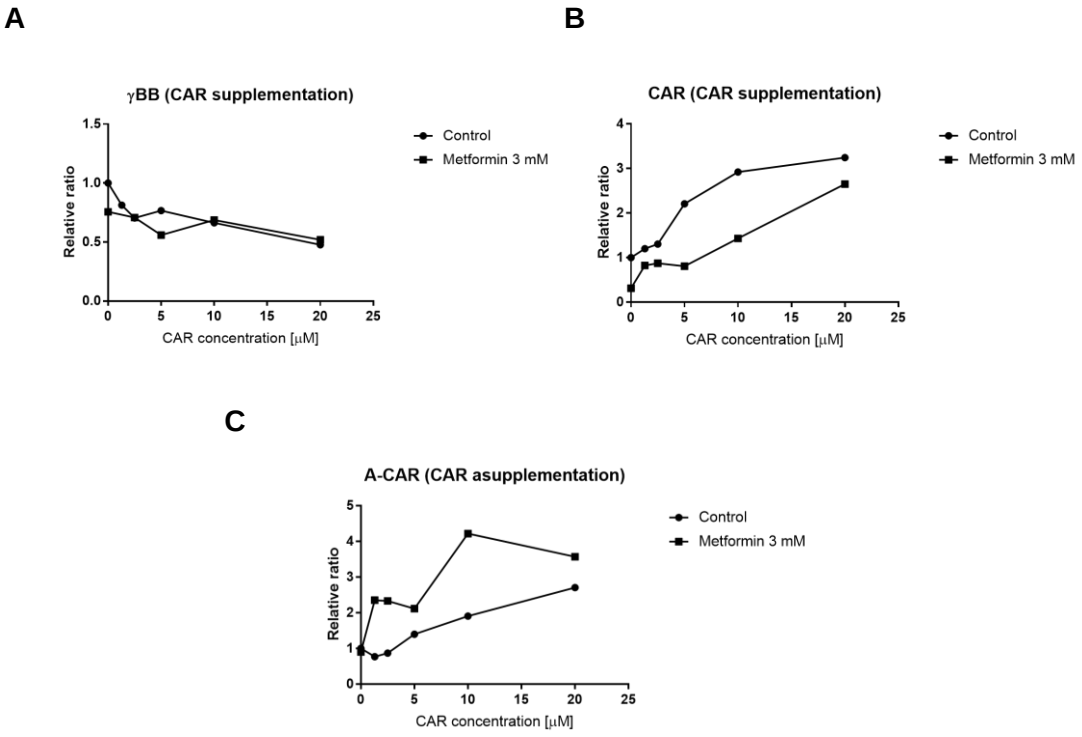


Figure 9-14: HPLC-MS/MS analysis of HepG2 cells treated with metformin (3 mM) and concentration range of CAR (1.25 μM, 2.5 μM, 5 μM, 10 μM and 20 μM) for 24 h. Analysis for γBB (A), CAR (B) and A-CAR (C) level (*n=1*; *1 x 10⁶ cells/well).*

In triplicate treatment with 100 μM CAR and 10 mM metformin, significant changes were observed (Figure 9-15). γBB decreased to 30%, 40% and 18%, respectively, showing that both CAR and metformin supplementation reduce γBB levels. CAR was increased 3-fold

upon CAR supplementation. However, metformin reduced CAR incorporation, leaving CAR levels at 97%, which was probably an average effect of CAR reduced uptake and inhibited biosynthesis. A-CAR was increased 6-fold upon CAR supplementation. With the addition of metformin, A-CAR accumulated up to 12-fold compared to its normal level in HepG2 cells.

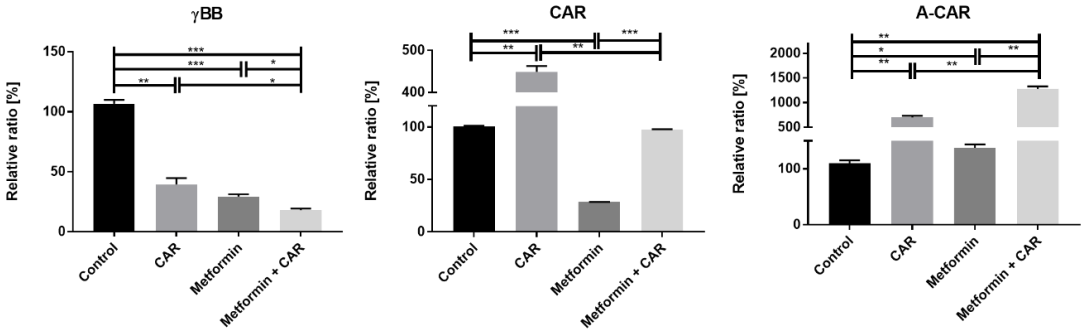


Figure 9-15: HPLC-MS/MS analysis of HepG2 cells treated with CAR 100 µM and 10 mM metformin to HepG2 for 24 h (1 x 10^6 cells/well; n=3; mean ± SEM); analysis for γBB, CAR and A-CAR; p-values for γBB: (p=0.0011), (p=0.0002), (p=0.0003), (p=0.0492), (p=0.0107), respectively; p-values for CAR: (p=0.0015), (p<0.00001), (p=0.0082), (p<0.0001), respectively; p-values for A-CAR: (p=0.0023), (p=0.0292), (p=0.0016), (p=0.0012), (p=0.0016).

To investigate whether metformin and phenformin share a similar mode of action as a family of biguanides, HepG2 cells were treated with 100 µM CAR supplementation and 100 µM phenformin. HPLC-MS/MS analysis revealed that similarly to metformin, phenformin and CAR reduce γBB abundance. Additionally, CAR incorporation was blocked by phenformin leaving it at 100% compared to control, and A-CAR increased by 11-fold in combined treatment (Figure 9-16).

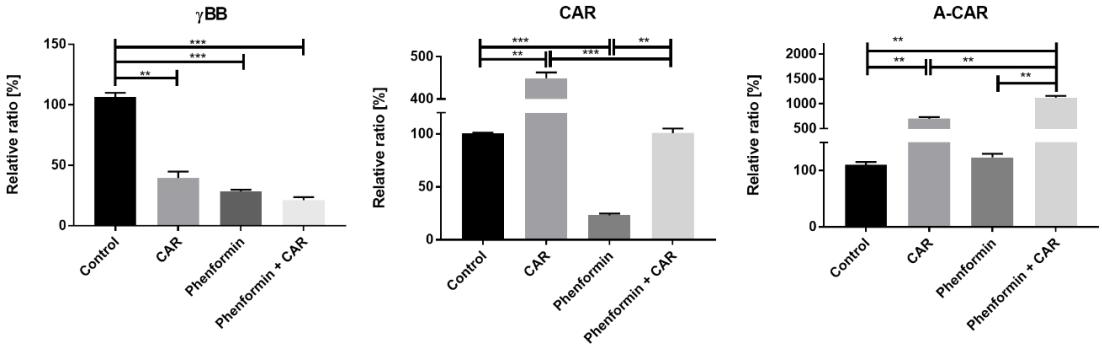


Figure 9-16: HPLC-MS/MS analysis of HepG2 cells treated with phenformin 100 µM and CAR 100 µM for 24 h (1 x 10^6 cells/well; n=3; mean ± SEM); analysis for γBB, CAR and A-CAR; p-values for γBB: (p=0.0011), (p=0.0005), (p=0.0001); p-values for CAR: (p=0.0015), (p=0.0001), (p=0.0012), (p=0.0001); p-values for A-CAR: (p=0.0023); (p=0.0013); (p=0.0015), (p=0.0012).

Therefore, this set of data suggests that likely biguanides share a similar mode of action by inhibiting CAR incorporation acting as an agonist of OCTN receptors. The increase of A-CAR accumulation during combined treatment also indicates inhibition of CACT mitochondrial transporters for A-CAR incorporation.

Very likely CAR supplementation impacts negatively on γBB level because CAR is also an active substrate for GBBH enzyme (and possibly previous carnitine biosynthesis enzymes i.e., TMLH) [210]. In contrast, biguanides do not act as an active substrate and only competitively block these enzymes.

9.2.3.2 Effect of γBB supplementation on carnitine transporters

Next, encouraged by interesting results of biguanides on CAR uptake, the role of biguanides on the absorption of γBB was investigated in greater details. It was of interest whether biguanides have a wider scope in their effects on the family of cation transporters.

Therefore, similarly, supplementation with a range of γBB concentrations was performed on HepG2 cells for 24 h. The HPLC-MS/MS analysis confirmed reduced γBB intake during metformin treatment (Figure 9-17 A). Surprisingly, γBB supplementation did not increase CAR biosynthesis, and metformin treatment additionally decreased γBB abundance (Figure 9-17 B). Subsequently, A-CAR levels were reduced for both treatments separately and in combination, without observation of A-CAR accumulation in either case (Figure 9-17 C).

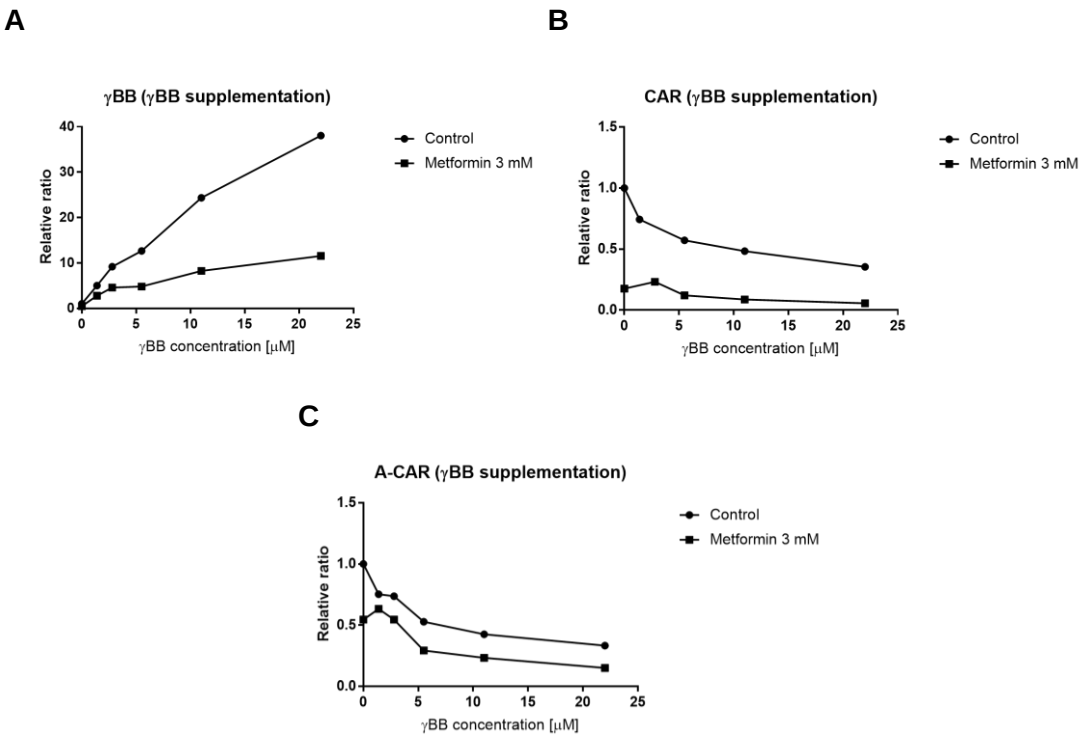


Figure 9-17: HPLC-MS/MS analysis of HepG2 cell treated with metformin 3 mM and concentration range of γBB (1.20 μM, 2.25 μM, 5.5 μM, 11 μM, 22 μM) for 24 h. Analysis for γBB (A), CAR (B) and A-CAR (C) level (n=1; 1 x 10^6 cells/well).

In triplicate treatment with 100 μM CAR and 10 mM metformin, significant changes in γBB incorporation were observed: a reduction by 2-fold. Again, γBB addition almost entirely inhibited CAR synthesis to 10% and reduced A-CAR levels to 10%. No A-CAR accumulation was observed (Figure 9-18).

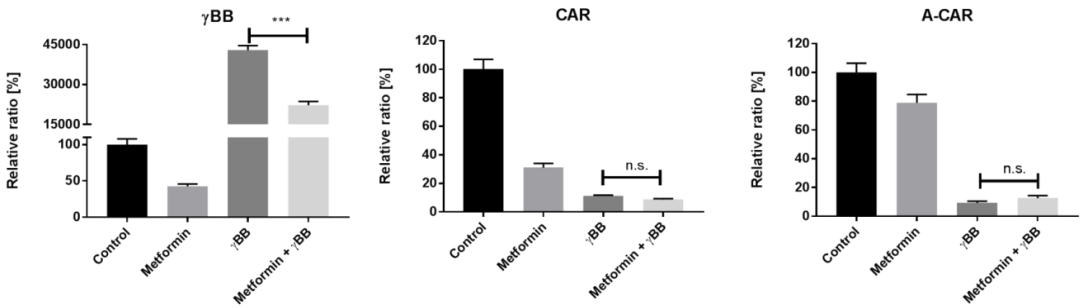


Figure 9-18: HPLC-MS/MS analysis of HepG2 cells treated with metformin (10 mM) and γBB (100 μM) for 24 h (1 x 10^6 cells/well; n=3; mean ± SEM); analysis for γBB, CAR and A-CAR level; p-values: for γBB (p= 0.0009), CAR (p=0.052), A-CAR (p=0.21).

To assess whether γBB uptake is impaired by the family of biguanides, 100 μM γBB supplementation with 100 μM phenformin was tested using the HepG2 cell line. HPLC-MS/MS analysis revealed that similarly to metformin, phenformin reduces γBB

incorporation by 60%. Additionally, the CAR abundance reduced to 19% and 11%, respectively. A-CAR was decreased to 15% upon γBB supplementation, while the addition of phenformin increased A-CAR to 32% (Figure 9-19).

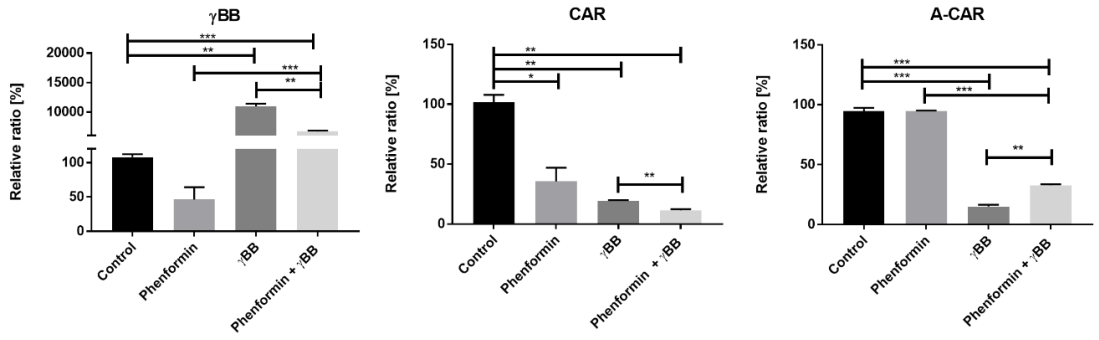


Figure 9-19: HPLC-MS/MS analysis of HepG2 cells treated with phenformin 100 µM and γBB 100 µM for 24 h (1 x 10^6 cells/well; n=3; mean ± SEM); analysis for γBB, CAR and A-CAR; p-values for γBB: (p=0.0016), (p=0.0008), (p=0.0007), (p=0.0043); for CAR: (p=0.0143), (p=0.0048), (p=0.0035), (p=0.0047); for A-CAR: (p=0.0001), (p=0.0007), (p<0.00001), (p=0.0019).

The data above suggest that likely the family of biguanides inhibits γBB incorporation, and as shown before reduce CAR uptake, most likely via targeting cationic ion transporters that shuttle both γBB and CAR into cells.

Interestingly, the data showing that extensive CAR supplementation lowers γBB levels, and the vast abundance of γBB inhibits CAR biosynthesis suggest that both molecules have cross-impact on the activity of CAR biosynthesis enzymes. Possibly due to the similar structure of γBB and CAR, both molecules are capable of inhibiting the enzymes involved in CAR biosynthesis. This observation supports recent literature reports that CAR can be a substrate for GBBH [210]. Therefore, metformin ability to inhibit CAR and γBB incorporation supports that the drug may also inhibit associated with CAR biosynthesis enzymes.

9.2.3.3 Effect of A-CAR supplementation on carnitine transporters

Finally, A-CAR was supplemented to assess the possible effect of metformin on mitochondrial receptors inhibition.

HepG2 cells were treated with a range of A-CAR for 24 h (Figure 9-20). Interestingly, supplementation with A-CAR caused a significant increase of CAR (Figure 9-20 B: control), what may be the subsequent effect of CAR recycling after shuttling the acetyl group into mitochondria. This hypothesis can be additionally supported by the fact that when A-CAR

was supplemented together with metformin, the increase in CAR was moderate (Figure 9-20 B: control vs mildronate), probably due to the blockage of A-CAR incorporation to mitochondria and lack of CAR recycling from mitochondria.

HPLC-MS/MS analysis revealed that γBB was slightly reduced with both treatments (Figure 9-20 B). For single A-CAR supplementation (Figure 9-20 B: control), such an effect is probably due to the subsequent increase of CAR that, as shown before in section 9.2.3.2, in excess leads to reduced γBB. However, when metformin was added, γBB formation is likely inhibited by the mode of action of metformin towards γBB producing enzymes (Figure 9-20 B: metformin).

Interestingly, metformin treatment did not show the change of A-CAR level in HepG2 cell extract (Figure 9-20 C: metformin). This result might be due to the observed average effect of dual metformin mode of action. Firstly, blocking OCTNs metformin inhibits A-CAR incorporation. However, at the same time, the A-CAR that was capable of getting into cell cytoplasm is getting accumulated as metformin blocks CACT and A-CAR entrance to mitochondria. In conclusion, the impaired A-CAR shuttle is masked, and the levels appear to not change.

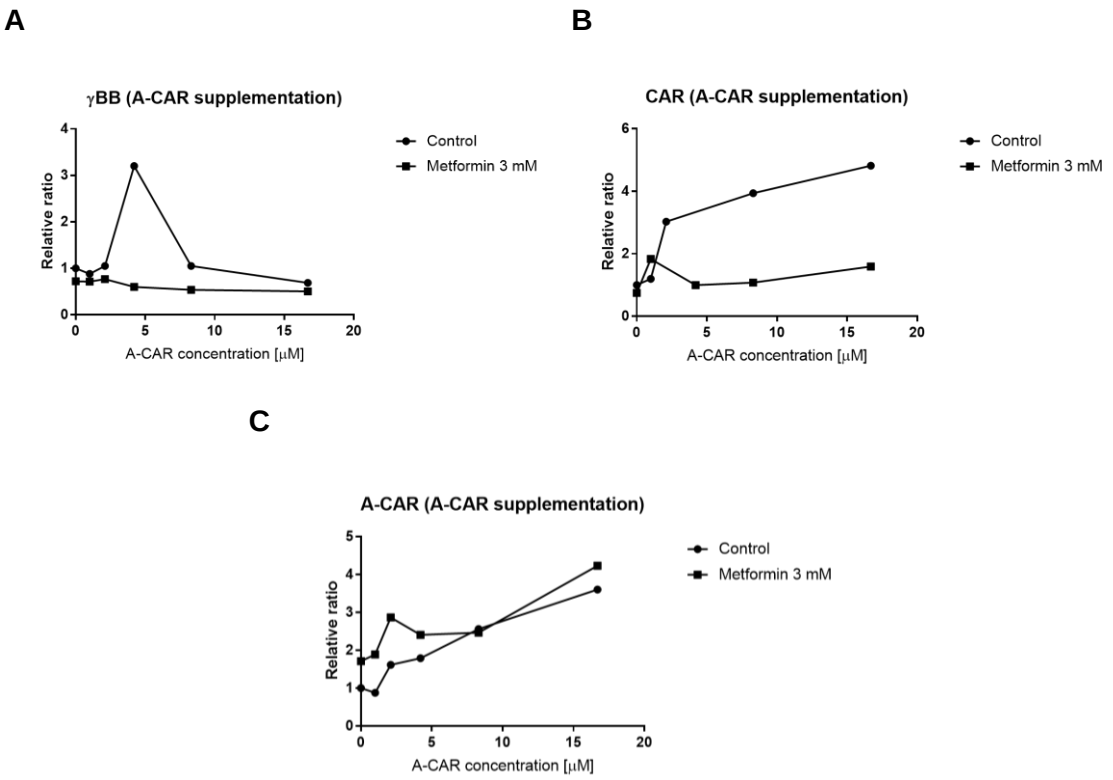


Figure 9-20: HPLC-MS/MS analysis of HepG2 cells treated with metformin (3 mM) and concentration range of A-CAR (1 µM, 2 µM, 4 µM, 8 µM and 16 µM) for 24 h. Analysis for γBB (A), CAR (B) and A-CAR (C) level (*n=1; 1 x 10⁶ cells/well).*

9.2.3.4 Extraction and analysis of purified mitochondria

To investigate whether metformin blocks mitochondrial CACT receptors, mitochondria were extracted from HepG2 cells exposed to a treatment with a range of metformin concentrations, according to a modified protocol from Frezza et al. [104]. HPLC-MS/MS analysis of the obtained mitochondrial extracts showed that metformin significantly reduces γBB, CAR and A-CAR (by 75%, 78% and 35%, respectively for 10 mM metformin treatment) (Figure 9-21). Therefore, the lack of A-CAR accumulation in mitochondria supports the hypothesis of metformin blockage of mitochondrial CACT receptors.

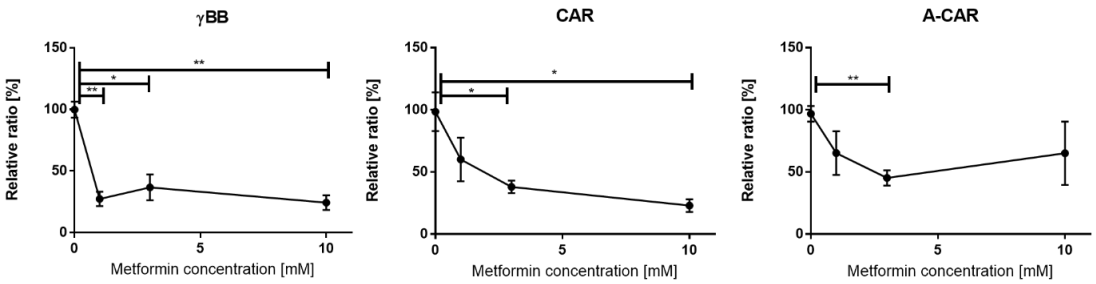


Figure 9-21: HPLC-MS/MS analysis of a mitochondrial extract of HepG2 cells treated with metformin concentration range (1 mM, 3 mM, 10 mM) for 24 h (1 x 10^6 cells/well; n=3; mean ± SEM); analysis for γBB, CAR and A-CAR; p-values for γBB: (p=0.001, 0.011. 0.001), p-values for CAR: (p=0.049, 0.030), p-values for A-CAR: (p=0.004).

9.2.3.5 Long acyl-CAR level examination

One of the other localisations of CAR in cells are peroxisomes, where CAR binds to longer acyl groups, products of long fatty acids β-oxidation [74]. Then, such carnitine esters are shuttled out from peroxisomes by yet unidentified enzymes in human cells (some reports show that it may be an orthologue of murine OCTN3 [280] and transported into mitochondria by CACT.

Therefore, it was investigated whether biguanides also affect peroxisomal shuttling. The additional *m/z* value was added to the developed HPLC-MS/MS method to track butyryl-CAR, which is representative medium chain acyl-CAR derivatives. Levels of this molecule were measured in HepG2 cell extract after individual and combined treatments with 50 µM mildronate, 10 mM metformin, 100 µM phenformin and 100 µM CAR.

HPLC-MS/MS analyses revealed that mildronate decreases the level of butyryl-CAR by 26% (Figure 9-22), while metformin and phenformin reduce it by nearly 90% (Figure 9-23). CAR supplementation increases butyryl-CAR by 6-fold, and in combination with metformin or phenformin brings butyryl-CAR levels back to nearly 100%.

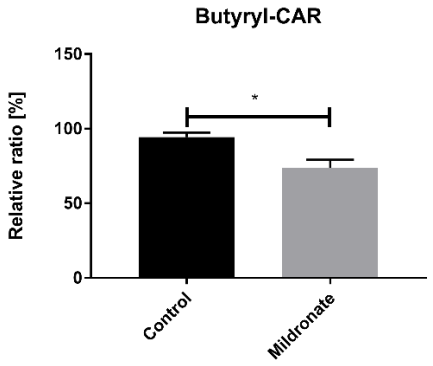


Figure 9-22: HPLC-MS/MS analysis of HepG2 cells treated with 50 µM mildronate for 24 h (1 x 10^6 cells/well; n=3; mean ± SEM); analysis for butyryl-CAR; p-value: (p=0.0376).

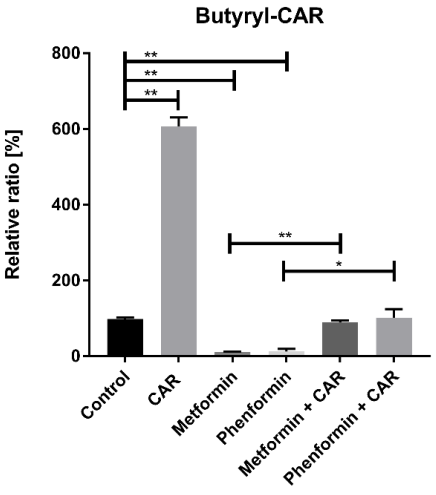


Figure 9-23: HPLC-MS/MS analysis of HepG2 cell treated with 100 µM CAR, 10 mM metformin, 100 µM phenformin and combination of treatments for 24 h (1 x 10^6 cells/well; n=3; mean ± SEM); analysis for butyryl-CAR p-values: (p=0.0017), (p=0.0023), (p=0.0012), (p=0.0022), (p=0.04480).

The results above have provided a better understanding towards the mode of action of biguanides. Biguanides, unlike mildronate, reduce medium-sized acyl-CAR abundance, meaning that formation of such molecules is inhibited by lack of sufficient CAR in peroxisomes and/or, these molecules accumulate in peroxisomes and are not able to be shuttled out into cytoplasm and then to mitochondria due to blocked OCTN3 receptors.

Interestingly, CAR addition increases butyryl-CAR levels significantly and can rescue the butyryl-CAR reduction caused by metformin and phenformin.

9.2.4 Examination of cell viability after metformin treatment

The data above shows that metformin lowers CAR levels, reduces fatty acid β-oxidation and leads to lower mitochondrial acetyl-CoA, thus lowering the Krebs cycle activity and reducing mitochondrial complex I activity. The mitochondrial complex I is responsible for electron transport and is associated with NAD(P)H-dependent enzymes [281]. The activity of NAD(P)H enzymes is used for cell viability measurement in MTT-dependent cytotoxicity assays.

Taking this into account, the NAD(P)H-dependent enzyme activity was explored as well as cytotoxicity after treatment with metformin and whether CAR supplementation affects such toxicity. Therefore, a range of concentrations of metformin and CAR was added to HepG2 cells, and then the cell viability was measured using the commercial Abcam cytotoxicity assay (Figure 9-24).

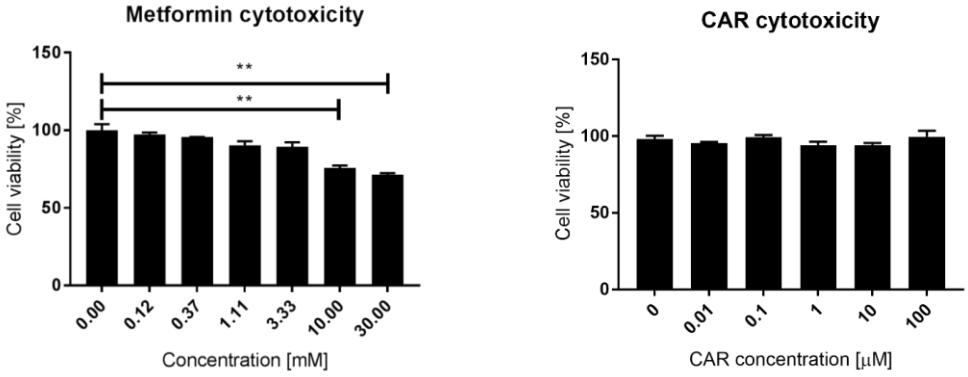


Figure 9-24: Cytotoxicity analysis of HepG2 cells treated with metformin (0-30 mM) or CAR (0-100 μM); (3 x 10^5 cells/well; n=4; mean ± SEM); p-values for metformin (p=0.005 and p=0.003, respectively).

At 10 mM and 30 mM, metformin resulted in 25-30% cell death, while CAR did not show cytotoxicity at any tested concentration. This result may indicate that cells after 24 h of culture require utilization of additional sources of carbon besides glucose supplemented in cell medium. However, since metformin most likely inhibits access of acetyl groups obtained from other sources i.e. β-oxidation in peroxisomes; cells enter apoptosis.

Next, HepG2 cells were exposed to combined treatment of 10 mM metformin with a range of CAR concentrations (Figure 9-25).

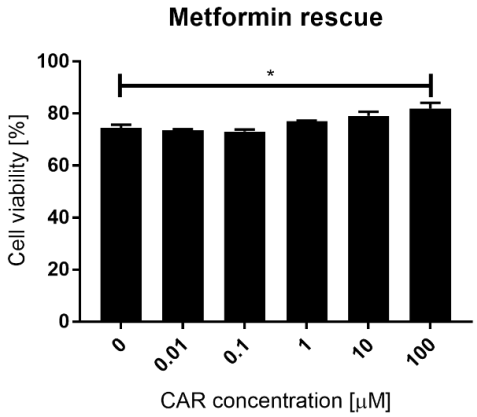


Figure 9-25: Cytotoxicity analysis of HepG2 cells treated with metformin (10 mM) and carnitine (0-100 μM) for 24 h (3 x 10^5 cells/well; n=4; mean ± SEM); p-value for metformin (p=0.0346).

100 μM CAR supplementation managed to rescue metformin cytotoxicity, improving cell viability from 74% to 82%. Above data shows that CAR appear to rescue cell survival, probably through improving the entry of acetyl groups to mitochondria, and thus regulating NAD(P)H-dependent enzymes, RedOx state and mitochondrial complex I activity. Therefore, that may also indicate an improvement of the Krebs cycle function and together with previous data indicates a beneficial role of CAR supplementation towards fatty acid β-oxidation.

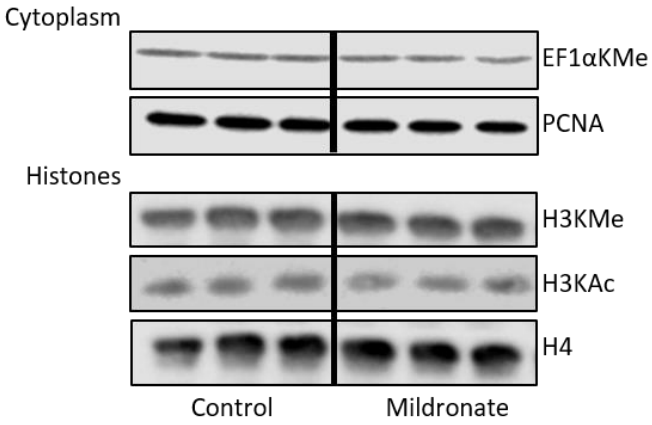
9.2.5 Impact of chosen modulators on epigenetic modifications

After the exploration of the biguanide mechanisms of action towards CAR biosynthesis and products of the β-oxidation shuttle into mitochondria, it was of interest whether these energy modulators impact protein PTMs, including epigenetic histone tail methylation and acetylation.

9.2.5.1 Mildronate impact on methylation and acetylation

Firstly, HepG2 cells were treated with 50 μM mildronate for 24 h. After western blotting analysis of cytoplasmic and histone extract, a 30% decrease in histone H3 lysine acetylation level was observed, but no change in histone H3 lysine methylation and 32% downregulation of elongation factor EF1α lysine methylation (Figure 9-26).

A



B

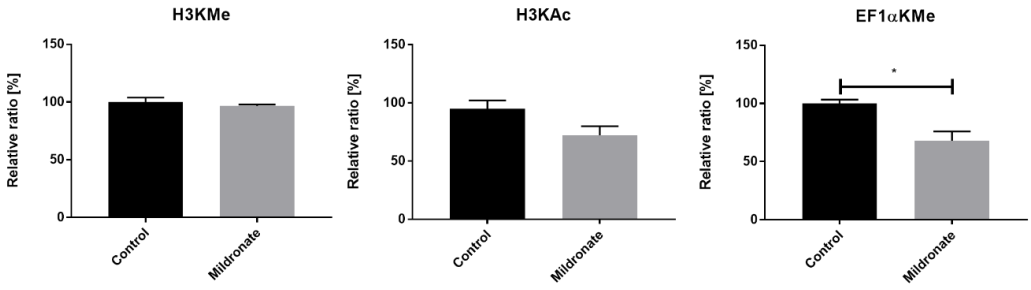


Figure 9-26: Western blot analysis (A: visual and B: quantitative) of histone and cytoplasmic fraction of HepG2 cells treated with 50 µM mildronate for 24 h (1 x 10^6 cells/well; n=3; mean ± SEM); p-value for EF1αKMe (p=0.04) and p-value for H3KAc (p=0.098).

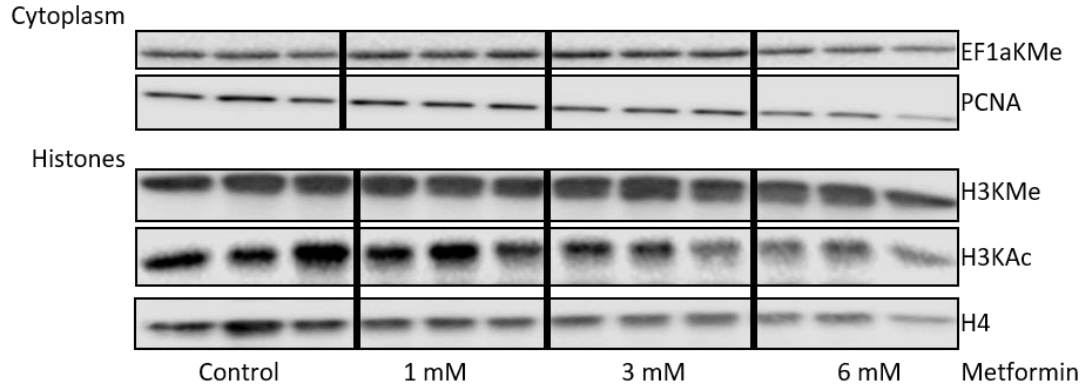
The results above suggest that mildronate may influence epigenetic changes through reduced lysine acetylation. It may be related to the fact that mildronate decreases the levels of free A-CAR. Therefore, mildronate may also impact the shuttling of acetyl groups into the nucleus.

Interestingly, mildronate also impacts the elongation factor EF1α lysine methylation. The exact reasons for this effect are unknown; however, it was found that energy metabolism, particularly insulin, can stimulate EF1α for protein synthesis [282].

9.2.5.2 Biguanides impact on methylation and acetylation

Next, a similar western blotting analysis was performed for HepG2 cells treated for 24 h with a range of metformin concentrations (Figure 9-27). Metformin appeared to increase the H3 lysine methylation up to 2-fold, however, also the decrease in loading control histone H4 levels were contributing to such increase in H3KMe ratio. At the cytoplasmic level, metformin increased EF1α methylation also up to 2-fold. Simultaneously, metformin decreased levels of global H3 lysine acetylation down to 75%.

A



B

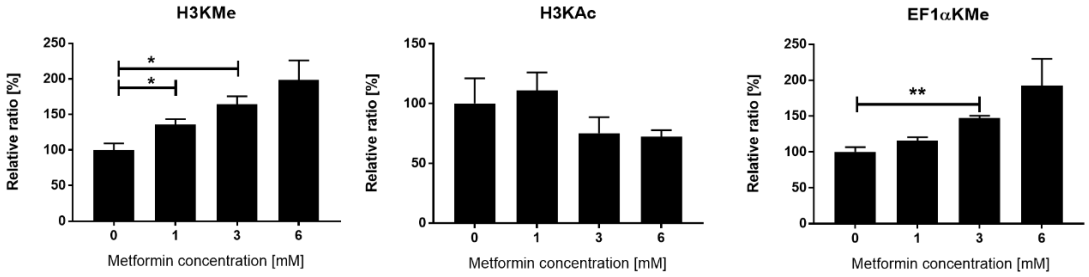
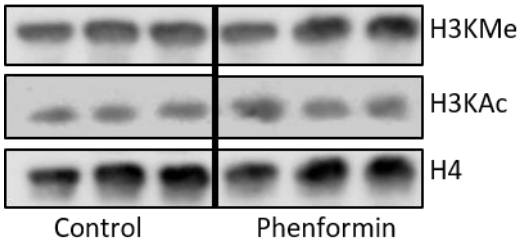


Figure 9-27: Western blot analysis (A: visual and B: quantitative) of histone and cytoplasmic fraction of HepG2 cells treated with metformin (1 mM, 3 mM, 6 mM) for 24 h (1 x 10^6 cells/well; n=3; mean ± SEM); H3 lysine methylation p-values for 3 mM (p=0.041), for 6 mM (p=0.013); EF1aMe (p=0.009).

Metformin, similarly to mildronate, decreased the level of acetylation of histone H3. Most probably metformin also blocks acetyl groups shuttle into the nucleus via inhibiting nuclear CAR receptors. The negative impact of metformin on cell viability, is the likely reason for the observed decrease in H4 levels at high metformin concentrations. Interestingly, metformin increases lysine methylation, which suggests that it may inhibit KDM activity by interfering with their mechanism of action.

Similarly, treatment with phenformin also increases methylation of histone H3, and increases levels of acetylation (by 12% and 40%, respectively) (Figure 9-28). However, the large error bar on the quantified levels of acetylation does not allow for further interpretation of this PTM. Nevertheless, the impact of phenformin on histone H3 lysine methylation levels supports a potential role of biguanides on KDM activity.

A



B

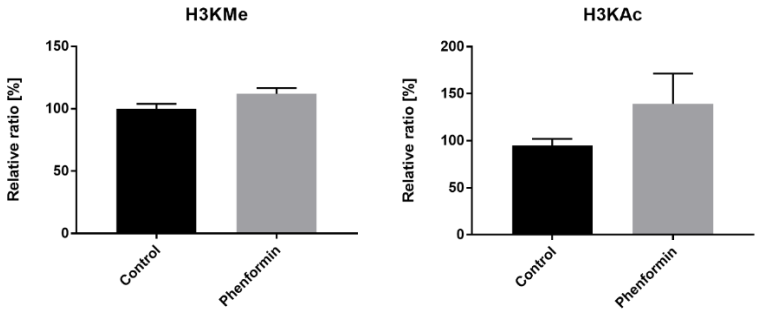


Figure 9-28: Western blot analysis (A: visual and B: quantitative) of histone extract of HepG2 cells treated with 100 µM phenformin for 24 h (1 x 10^6 cells/well; n=3; mean ± SEM); p-value for H3KMe (p=0.11); for H3KAc (p=0.30).

9.2.5.3 Metformin impact on methylation in S. cerevisiae

The western blot results showed the impact of metformin on total histone lysine trimethylation in human cells and, subsequently, suggested a new interface of metformin in the overall CAR biosynthesis pathway. Therefore, it was of interest to examine the molecular effect of metformin on free TML levels. However, since free TML levels were found to be too low in human cell line extract, the *S. cerevisiae* strains developed in section 6.2.1 were used. Two strains, wild-type (WT) and *shm1Δ* were exposed for 96 h to 6 mM metformin treatment. Next, the cell lysate was analysed via HPLC-MS/MS. The analysis revealed that metformin increases TML by 25% in WT and by almost 50% in the *shm1Δ* strain (Figure 9-29).

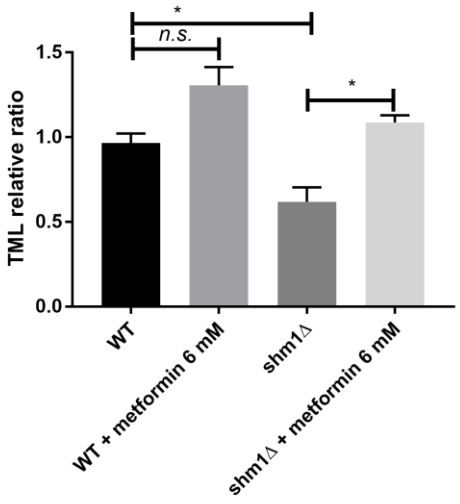


Figure 9-29: HPLC-MS/MS analysis of relative TML levels in S. cerevisiae WT cells and Δshm1 strains supplemented with 6 mM metformin after 96 h growth time; p-values: p=0.034 and p=0.016 (n=3, mean ± SD).

Therefore, the above results strengthen the previous data showing an increase of protein lysine methylation after exposure to metformin in HepG2 cells.

The observed increase in histone lysine methylation in both organisms, human HepG2 cells and *S. cerevisiae* and the previous finding of metformin inhibiting CAR biosynthesis enzymes suggest that metformin may act as potential inhibitor of 2OG-dependent enzymes. Therefore, it is possible that that mechanism may include KDMs and results in the observed increase in histone methylation.

Taking all data together, metformin has an impact on epigenetic changes, introducing an additional role of this anti-diabetic drug in regulating gene transcription.

9.3 Discussion

Carnitine is an essential metabolite for fatty acid usage as a source of energy. Currently available drugs that act as metabolic modulators interfere with glucose and insulin blood levels and subsequently with lipids consumption [261], [263]–[265]. This chapter has examined the role of clinically used energy metabolism modulators in CAR biosynthesis and linked these findings to epigenetic changes they induced.

The focus of this chapter was put on three clinically relevant molecules: mildronate, metformin and phenformin. The two latter substances belong to the same biguanides family of drugs, with phenformin being currently excluded from the market due to the frequent cases of lactic acidosis among patients [271]. The clinical relevance of these

drugs to the body metabolism is well explored; however, their exact mode of action is still a subject of investigations (Glueck et al., 2001; Edgars Liepinsh et al., 2011; Nie et al., 2017; Salpeter, Buckley, Kahn, & Salpeter, 2008, Shitara et al., 2013).

This chapter confirmed the literature reports that mildronate act as a substrate of the GBBH enzyme [240], [259]. However, metformin and phenformin appeared to be non-active inhibitors blocking CAR biosynthesis enzymes as well as inhibiting associated with CAR transporter receptors.

GBBH is an enzyme that accepts a broad group of inhibitors and, recently has been reported to also use CAR as a substrate [210]. Therefore, the similarity in structure of TMLH to GBBH enzymes may suggest that both γBB and CAR could play a role of substrates for that enzymes, yielding by-products that do not contribute to overall carnitine biosynthesis. Additionally, it was found that an excess of γBB and CAR is inhibitory, and non-specific, towards these enzymes.

Moreover, in the investigation using isotopic CAR-d_9, it was observed that biguanides do not block CAT enzyme that enables acetyl groups from acetyl-CoA binding to CAR.

However, it was found that biguanides as cationic molecules block CAR receptors OCTNs and CACT. Consequently, biguanides disable uptake of supplemented γBB, CAR and A-CAR, reduce A-CAR levels in mitochondria and lower medium-sized acyl group shuttle from peroxisomes to mitochondria. These findings support a recently published study performed on *octn1(-/-)* mice. Knockout mice were treated with phenformin and exhibited lower lactic acidosis in liver mitochondria suggesting a role of OCTN1 in phenformin uptake [272]. Additionally, phenformin, metformin and other biguanides have been shown to be accepted by other SLC family receptors, i.e. OCT1, OCT2 [283], [284] and multidrug and toxin extrusion receptors (MATE1 and MATE2-K) [285], [286]. Similarly, *oct1* knockout mice showed lower metformin uptake and protection from lactic acidosis [283].

Moreover, the known reduction of lactic acidosis might not only be connected with blockage of OCTNs but also CACTs. Their inhibition by biguanides may directly cause accumulation of the acetyl groups in the form of A-CAR in the cytoplasm and lead to negative impact on the cell Krebs cycle, RedOx states and viability. By inhibiting mitochondrial receptors, phenformin and metformin may negatively impact the regulation of oxidative damage. Evidence suggests role of biguanides in downregulation of mitochondrial respiratory complex I that helps ATP generation in mitochondria. Complex I is an NADH-dependent oxidoreductase that is the first and the most

complicated component in the mitochondrial respiratory chain [281]. Therefore, biguanides probably inhibit complex I through lowering acetyl group access into mitochondria, decreasing oxygen consumption in mitochondria and in turn cause lactic acidosis [287], [288].

This hypothesis would align with one of the research proposals that acetyl-CoA obtained from glucose compete with lipid substrates to enter into the Krebs cycle [289]. Some recent studies demonstrated that accumulation of acylcarnitine is linked with insulin resistance and possibly acylcarnitine may be a good diabetes biomarker [290], [291]. The observation in this chapter that metformin lowers butyryl-CAR levels would support the metformin role in prevention from diabetes.

Moreover, it has been reported that metformin increases the glucose uptake to the plasma membrane via glucose transporters i.e. GLUT1 and enhance insulin receptor activity [292]. Proposed in this chapter; metformin mode of action supports reported metformin glucose-lowering effect as glucose can be the only source of energy in case of an inhibited A-CAR shuttle. As an outcome, metformin shifts the fatty acid oxidation to glucose consumption by protection from the entrance of acyl products into mitochondria. Therefore, metformin redirects fatty acid β-oxidation route from mitochondria into peroxisomes.

Mutations in genes coding CAR receptors, i.e SLC22A5 gene coding OCTN2, cause systematic carnitine deficiency (SCD) in patients that leads to cardiomyopathy, weakness and altered carnitine reabsorption that could eventually be lethal [277]. However, currently this disorder is treatable with high doses of carnitine supplementation [293], [294]. In this chapter, it was observed that the oxidative stress and decreased cell viability upon metformin treatment had been rescued with CAR supplementation which suggests that carnitine plays a protective role in disturbed cell metabolism. Studies on carnitine supplementation in the human and mouse model demonstrated that carnitine stimulates glucose uptake and improves insulin tolerance. However, the benefits of carnitine supplementation remain a controversial subject [295]–[297], especially in the light of new findings that carnitine can be metabolised by gut microbiota resulting in the release of agents promoting atherosclerosis and cardiovascular diseases [298]–[300].

Finally, it was observed that biguanides impact epigenetic histone modifications. Biguanides reduce histone acetylation, which may be a consequence of blockage of transporting receptors and accumulation of acetyl- groups in the cytoplasm. Little is known regarding acetyl transport to the nucleus at the molecular level; however, there is

evidence for acetylcarnitine providing acetyl groups to the nucleus for histone acetylation [301]. Therefore, blockage of potential nuclear receptors with biguanides disables acetylcarnitine entrance to the nucleus and lowers histone lysine acetylation. Similarly, it may be possible that such inhibition relates to all acyl histones modifications.

Additionally, treatment with biguanide resulted in an increase in protein methylation in both human cells and *S. cerevisiae* providing more TML for CAR biosynthesis. However, simultaneously biguanides inhibit CAR biosynthesis enzymes. Together with evidence that metformin decreases Krebs cycle intermediates (2OG, citrate, malate, fumarate, succinate) [266], observations from this chapter lead to the conclusion that metformin (or biguanides in general) may be a 2OGXs inhibitors, including histone KDMs. This result can be confirmed with the recent observations that metformin can modify histone methylation, with an elevation of human H3K4Me2 and H3K27Me3 and mice H3K27me2 [263], [302], [303].

Metformin is a molecule that plays a wide range of functions in the human body. This chapter investigated metformin role in carnitine biosynthesis and carnitine shuttle system linking gained observations to epigenetic modifications. However, the benefits in energy metabolism that metformin brings are not fully understood at the molecular level.

10. Summary

In this study, a link between epigenetic modifications and the biosynthesis of carnitine which is a key molecule in fatty acid metabolism, has been clearly defined. Additionally, potential inhibitors of carnitine biosynthesis have been investigated (Figure 10-1). A number of methods were developed to gain insight in the relationship between cellular carnitine levels and protein lysine methylation status, including a principal HPLC-MS/MS method allowing for comparative quantification of carnitine biosynthesis intermediates in various biological samples and optimisation of the western blotting technique enabling for quantification of histone PTMs levels.

Firstly, I surveyed the range of epigenetic genes relevant to carnitine biosynthesis, utilizing *S. cerevisiae* as a model organism. Deletion of selected genes demonstrated that both KMTs and KDMs play important roles in carnitine biosynthesis by influencing the availability of the protein-derived TML that is a carnitine precursor. Interestingly, the investigated KMTs mostly increased TML abundance (i.e SET2 elongation factor family, CTM1), however, the role of KDMs appears to be more complex and requires a deeper understanding of their likely indirect impact on global TML levels. Also, further studies with SAHA show that inhibition of HDAC enzymes decreases CAR biosynthesis, suggesting that other PTMs may have an indirect impact on the level of lysine methylation. Ultimately, it is clear that the entire "epigenome" dynamics should be taken into consideration when assigning the role of epigenetics on carnitine metabolism and consequently fatty acids metabolism.

S. cerevisiae-derived strains have been additionally characterised in nutrition limited conditions (fermentable and non-fermentable growth), and together, this research suggests that the epigenetic link to carnitine biosynthesis is likely to be related to stress response mechanisms. This fact is particularly interesting as carnitine has been previously reported to act in cellular stress response and ageing [304], [305].

Secondly, it has been found that regulation of the cellular methylation pathway is also an important factor in carnitine biosynthesis as ultimately it provides the methyl group donor for KMT catalysis and TML synthesis. Supplementary manipulation of the methylation cycle equilibrium lead to various impacts on carnitine biosynthesis, both positive and negative: i.e. methionine and folic acid supplementation reduced carnitine levels, whereas betaine addition stimulated the carnitine biosynthesis. Due to the fact that these metabolites are popular dietary supplements (i.e folic acid during pregnancy to

provide methyl group for proper fetal development [201], [202] it is important to consider their possible side effects on fatty acid and energy metabolism.

Thirdly, it has been shown that the link of carnitine biosynthesis to epigenetics is also based on a common mechanism of action of JmjC domain-containing KDMs and two enzymes of CAR biosynthesis (TMLH and GBBH). All these enzymes are 2OG, Fe^{2+} and O_2 dependent oxygenases. Additionally, 2OG, their co-substrate, is a key intermediate in the Krebs cycle. Taken together, 2OG regulation may be one of the key factors in the association of epigenetics and energy metabolism. However, the development of specific 2OGXs inhibitors to act as potential therapeutic drugs is an extremely challenging task. In this study, I have examined various (general and specific) potential 2OGX inhibitors and I found that most of them were unspecifically targeting KDMs, TMLH and GBBH. These inhibitors did not allow clear assessment of their potency towards specific enzymes. Considering also the potential impact of tested inhibitors on the Krebs cycle, it was difficult to understand their particular role in energy metabolism.

Finally, I have investigated several metabolic modulators that already exist in the clinic for their potency towards carnitine. I demonstrated that mildronate and metformin, whose mechanism of action is still not well understood, indeed are acting through inhibition of carnitine biosynthesis. Additionally, metformin indicated a potency towards carnitine-related receptors such as OCTN and CACT and, consequently, reduced A-CAR shuttling into mitochondria. Interestingly, metformin also impaired the levels of histone acetylation, suggesting that carnitine may also shuttle acetyl groups into the nucleus. Consequently, besides managing energy metabolism, disturbing carnitine biosynthesis and transport, metformin additionally impacts on gene expression by altering histone PTMs.

To summarise, epigenetics still requires extensive work in order to understand its impact on cellular biochemistry at the molecular level. It is particularly challenging to study a link between epigenetics and energy metabolism due to a broad metabolites application, e.g. 2OG is involved in KDMs catalysis and in the Krebs cycle or acetyl groups are a substrate in the Krebs cycle and KATs catalysis. Nevertheless, this challenge is definitely worth accepting as progress in metaboloepigenetics may help in developing more specific and target therapies for such disorders as diabetes or cardiovascular diseases. Our study can bring new insight into the understanding of currently used metabolic drugs and present their new interactions with cellular metabolism through epigenetic changes.

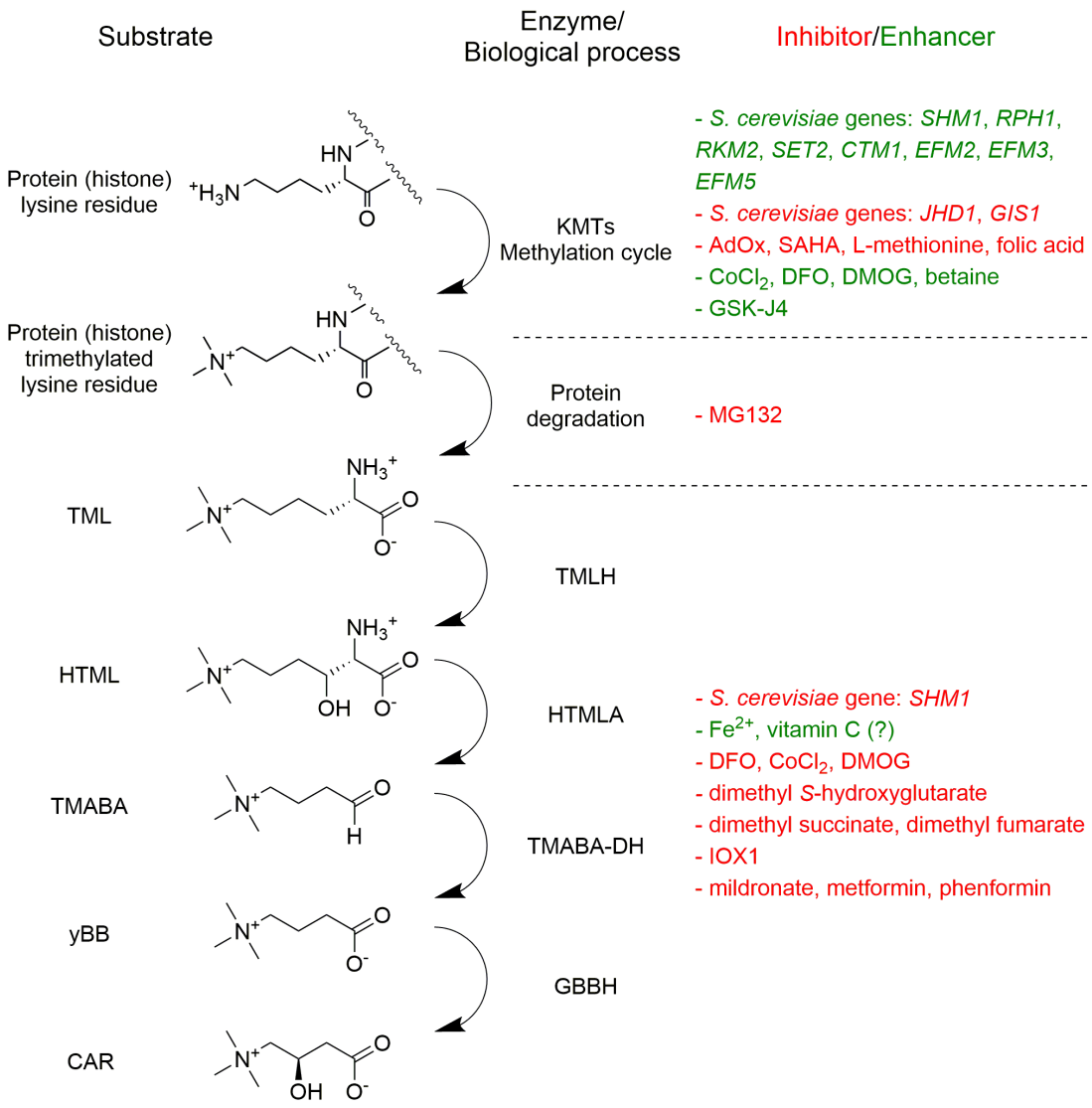


Figure 10-1: A model of carnitine biosynthesis link to epigenetics. Carnitine biosynthesis starts from histone lysine methylation, then trimethylated lysine is released from protein degradation, and next undergo four enzymatic reactions ultimately producing carnitine. Identified inhibitors (red) and enhancers (green) of each of carnitine biosynthesis stop are listed on the right side of the graph.

11. Appendix

11.1 Figures

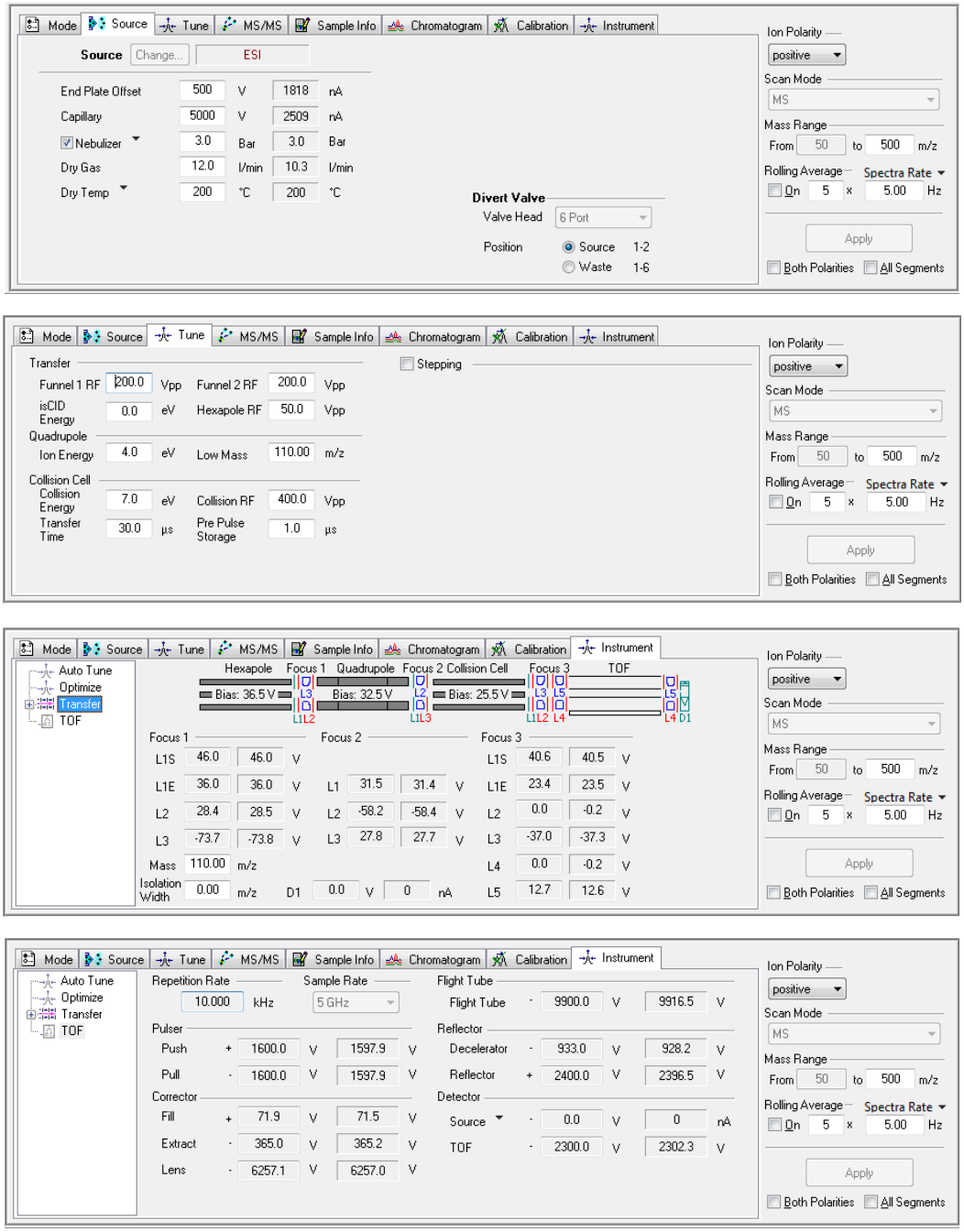


Figure 11-1: Mass spectrometry detection parameters after instrument tuning.

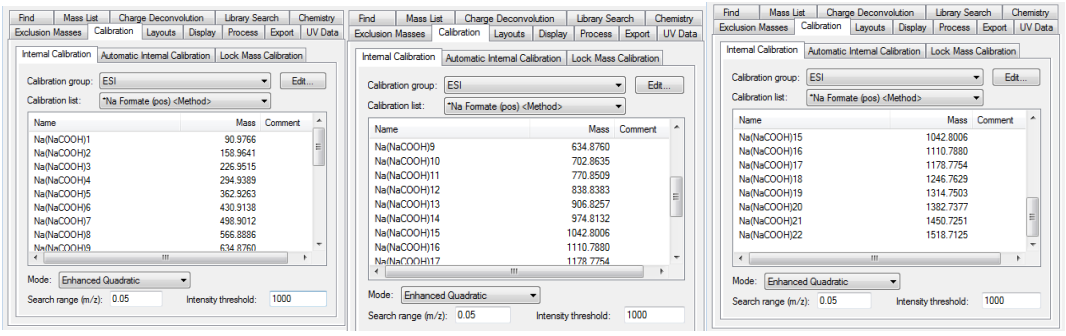


Figure 11-2: Calibration was performed using sodium formate in the range of m/z between 90.9766 and 1518.7125.

A: γBB



B: A-CAR

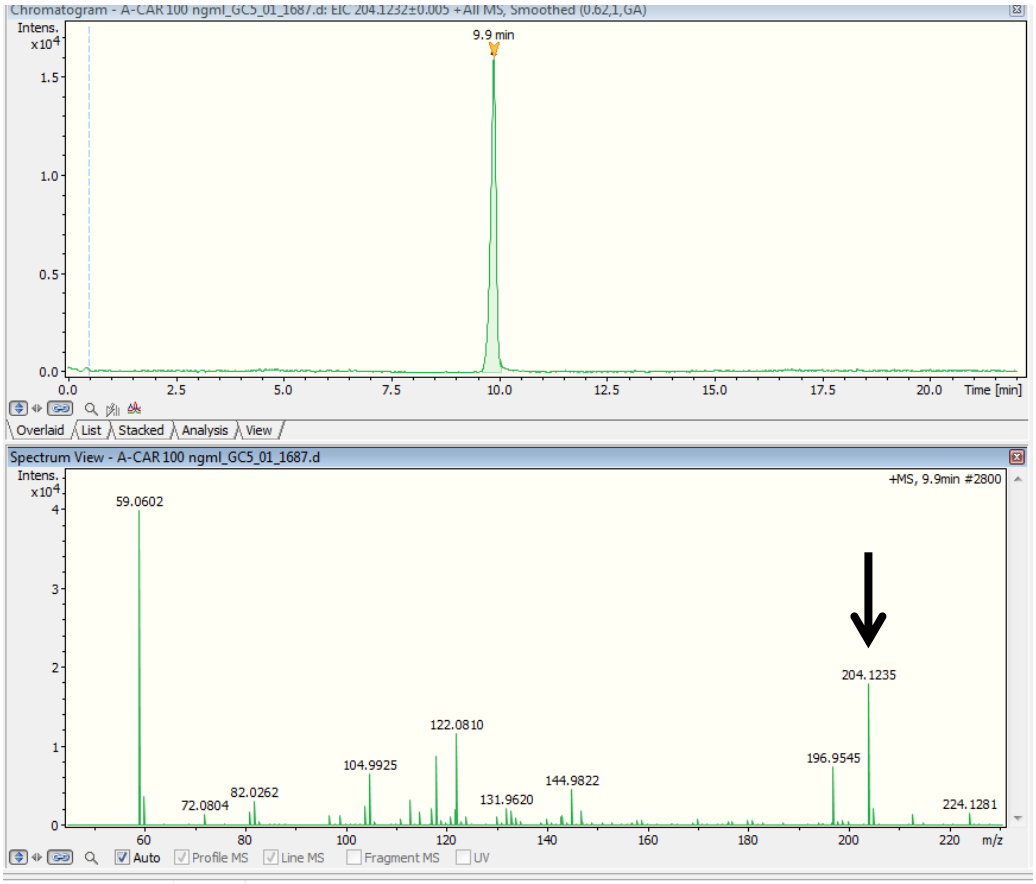
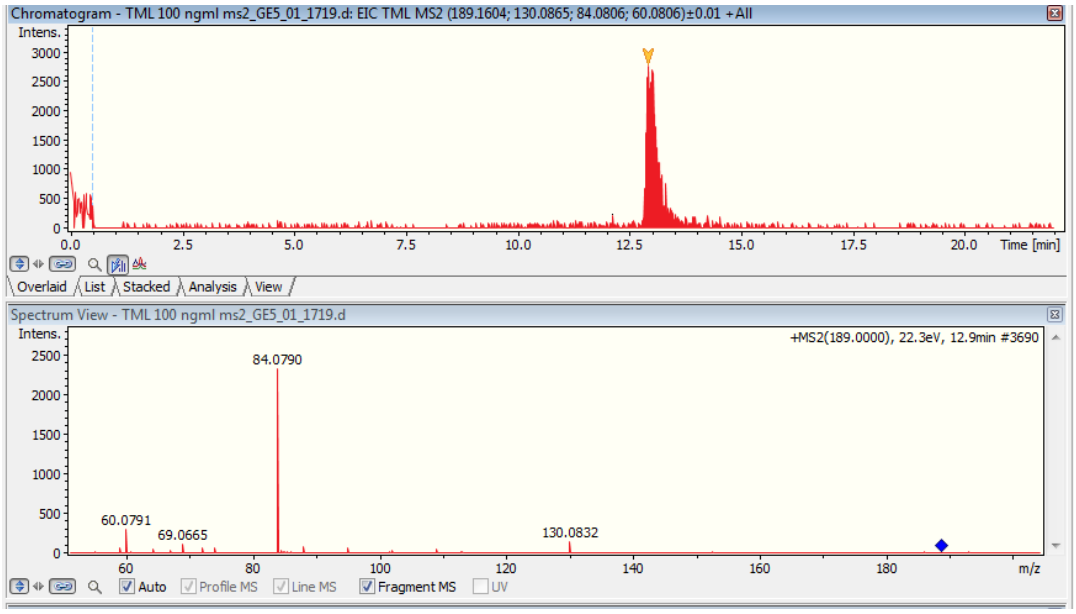
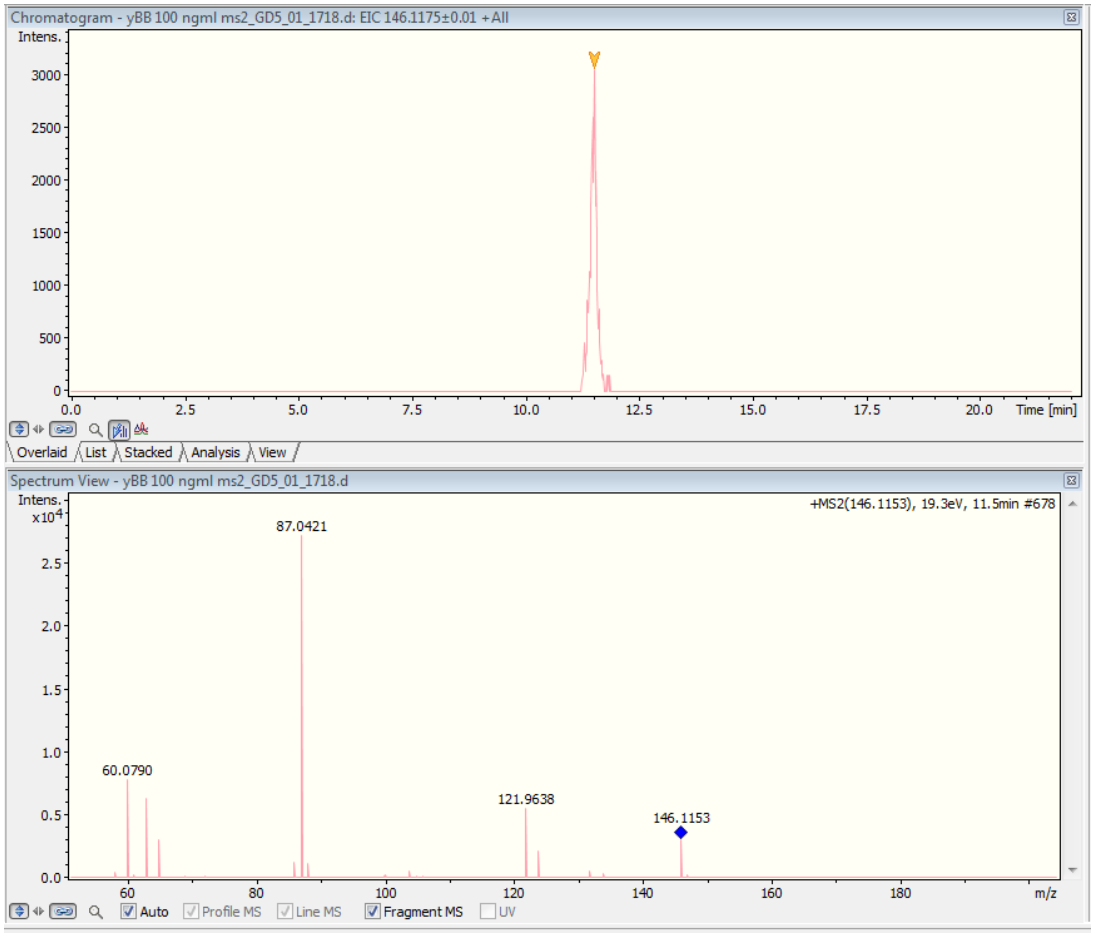


Figure 11-3: Elution time and MS analysis of each molecule at concentration 100 ng/mL. A: γBB retention time was 11.5 min, detected ion m/z was 146.1181, B: A-CAR retention time was 9.9 min, detected ion m/z was 204.1235.

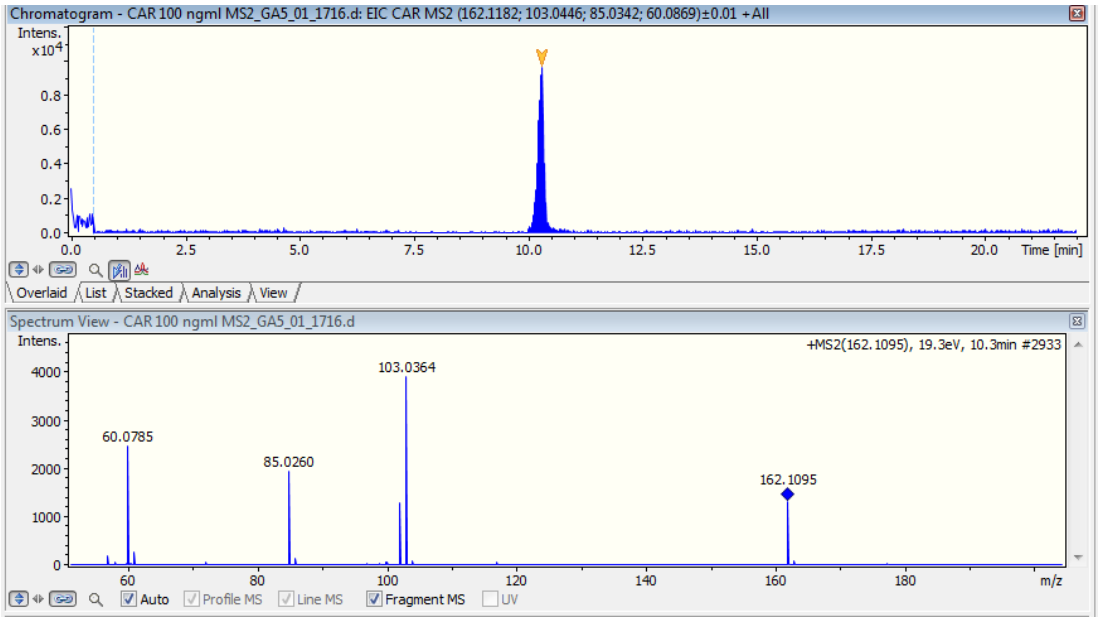
A: TML


Chromatogram - TML 100 ngml ms2_GE5_01_1719.d: EIC TML MS2 (189.1604; 130.0865; 84.0806; 60.0806)±0.01 +All
Intens.
Time [min]
Overlaid
List
Stacked
Analysis
View
Spectrum View - TML 100 ngml ms2_GE5_01_1719.d
+MS2(189.0000), 22.3eV, 12.9min #3690
84.0790
60.0791
69.0665
130.0832
m/z
Auto
Profile MS
Line MS
Fragment MS
UV

B: γBB


Chromatogram - yBB 100 ngml ms2_GD5_01_1718.d: EIC 146.1175±0.01 +All
Intens.
Time [min]
Overlaid
List
Stacked
Analysis
View
Spectrum View - yBB 100 ngml ms2_GD5_01_1718.d
+MS2(146.1153), 19.3eV, 11.5min #678
87.0421
60.0790
121.9638
146.1153
m/z
Auto
Profile MS
Line MS
Fragment MS
UV

C: CAR



D: A-CAR

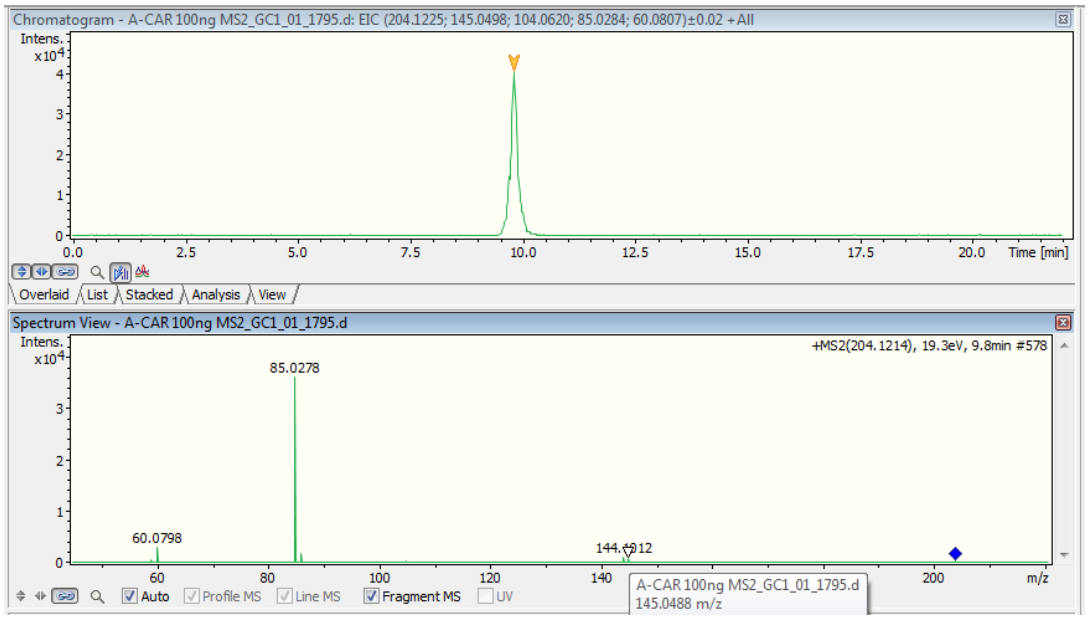
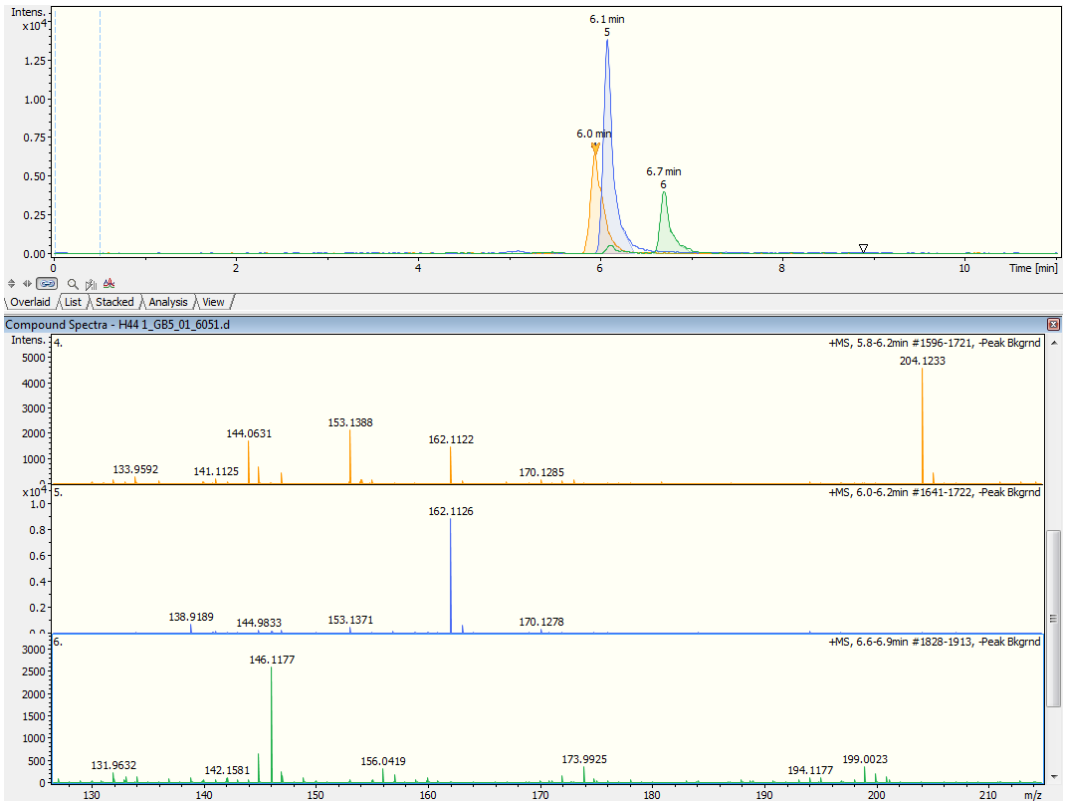


Figure 11-4: MS/MS spectrum for TML (red), γBB (pink), CAR (blue) and A-CAR (green) at 100 ng/mL. Analysis performed prior to HILIC 150 mm column separation method.

A



B

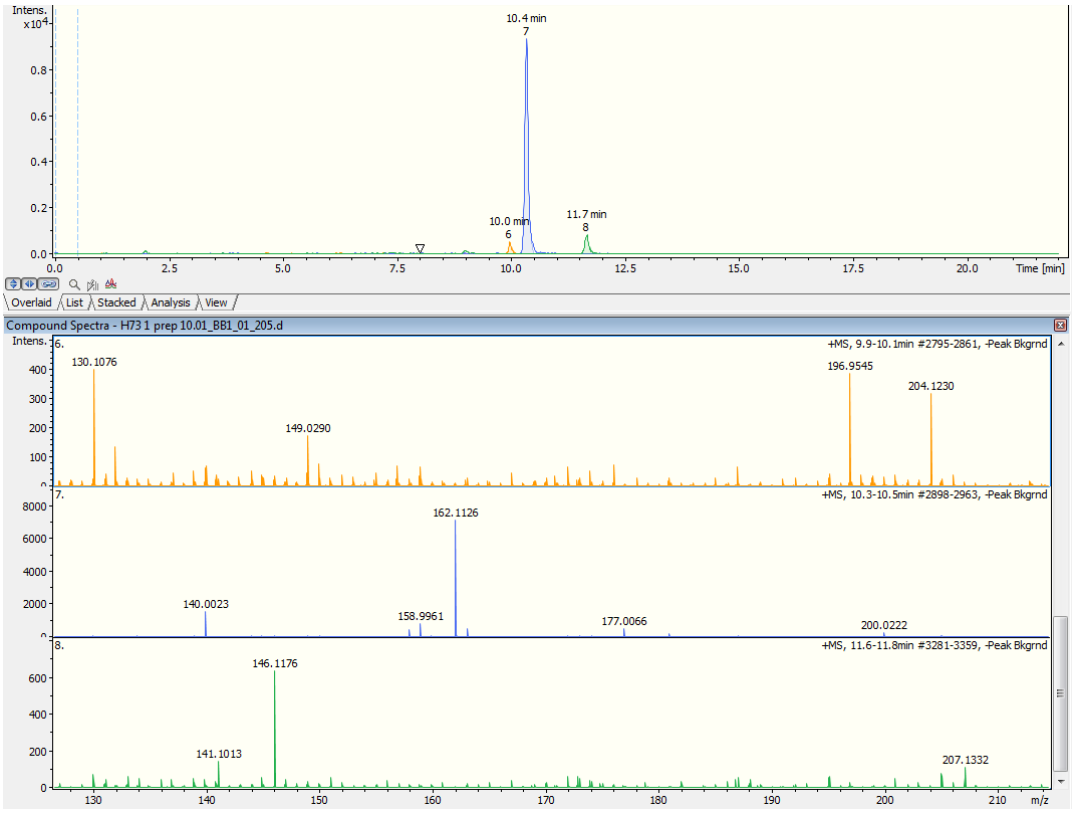
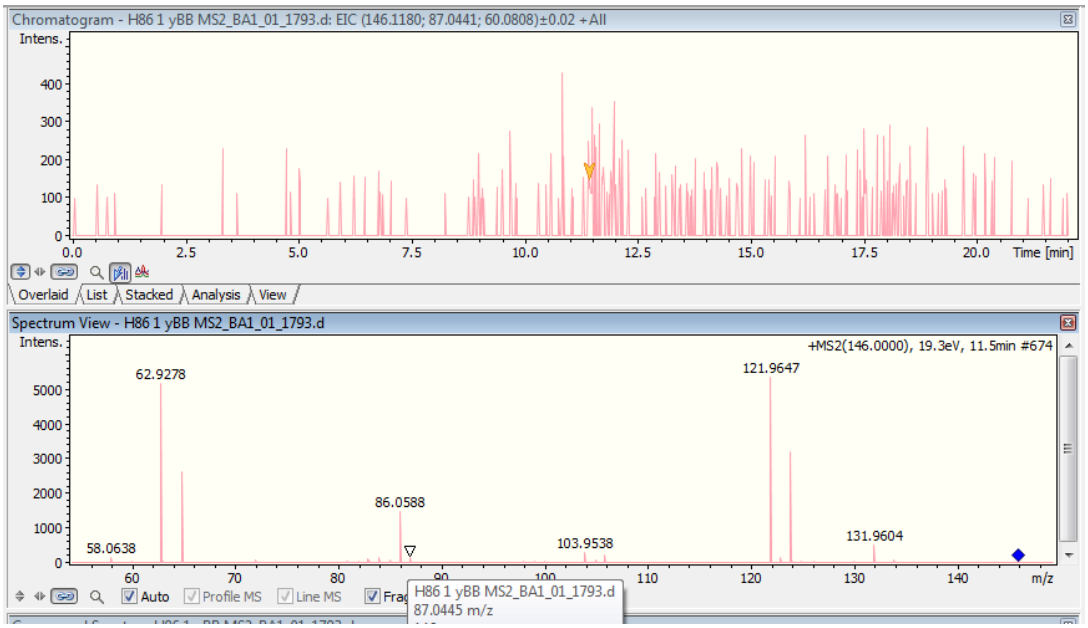
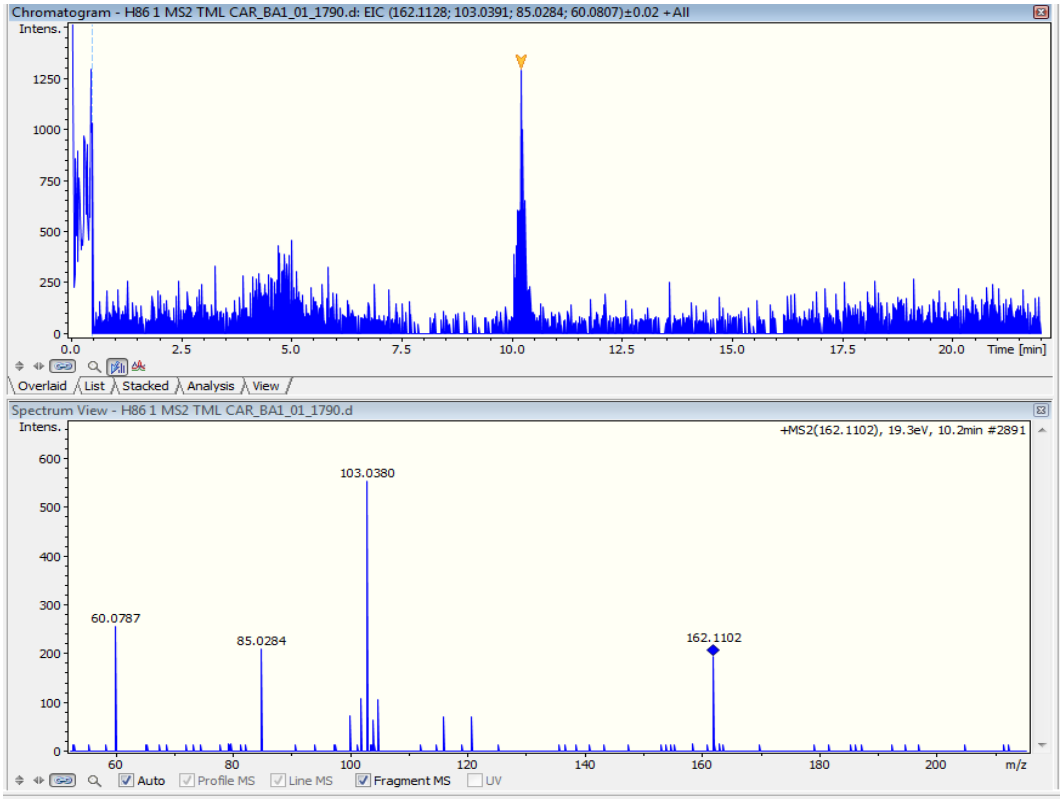


Figure 11-5: Elution times and MS analysis of human cells extract samples for CAR, A-CAR and γBB: A) HILIC 50 mm and B) HILIC 150 mm column.

A: yBB


Chromatogram - H86 1 yBB MS2_BA1_01_1793.d: EIC (146.1180; 87.0441; 60.0808)±0.02 + All
Intens.
Time [min]
Overlaid
List
Stacked
Analysis
View
Spectrum View - H86 1 yBB MS2_BA1_01_1793.d
+MS2(146.0000), 19.3eV, 11.5min #674
62.9278
121.9647
86.0588
58.0638
103.9538
131.9604
m/z
Auto
Profile MS
Line MS
H86 1 yBB MS2_BA1_01_1793.d
87.0445 m/z

B: CAR


Chromatogram - H86 1 MS2 TML CAR_BA1_01_1790.d: EIC (162.1128; 103.0391; 85.0284; 60.0807)±0.02 + All
Intens.
Time [min]
Overlaid
List
Stacked
Analysis
View
Spectrum View - H86 1 MS2 TML CAR_BA1_01_1790.d
+MS2(162.1102), 19.3eV, 10.2min #2891
103.0380
60.0787
85.0284
162.1102
m/z
Auto
Profile MS
Line MS
Fragment MS
UV

C: A-CAR

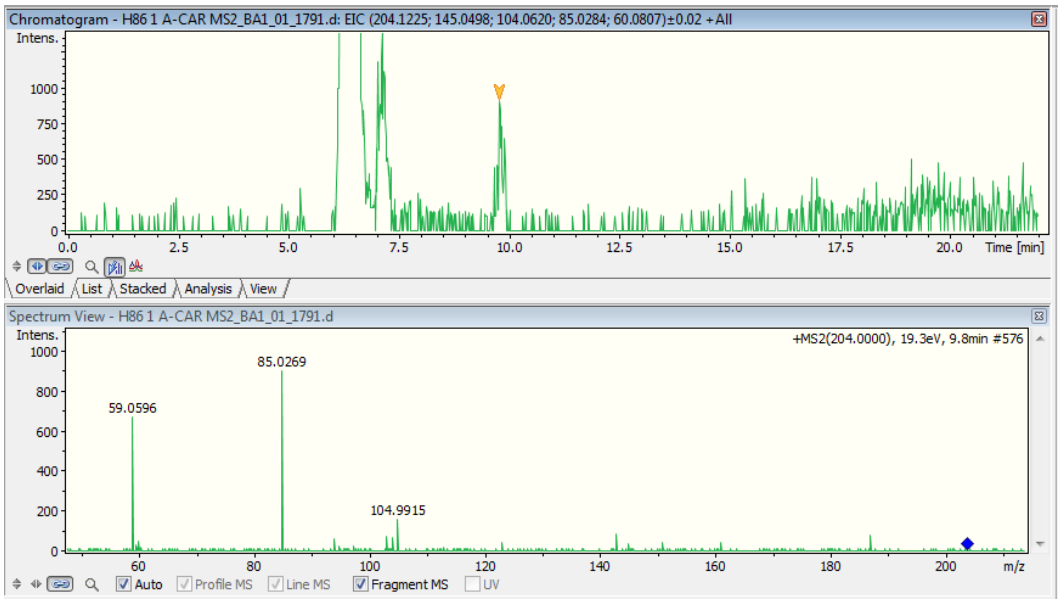


Figure 11-6: MS/MS analysis of γBB, CAR and A-CAR ions in human cells.

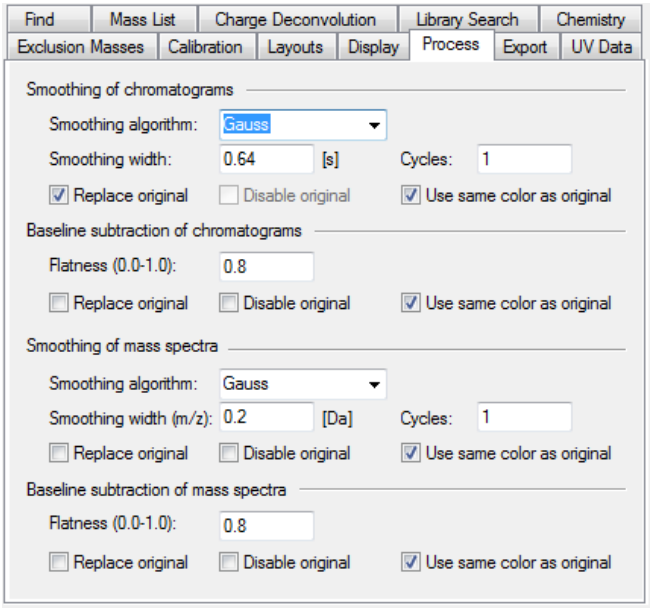
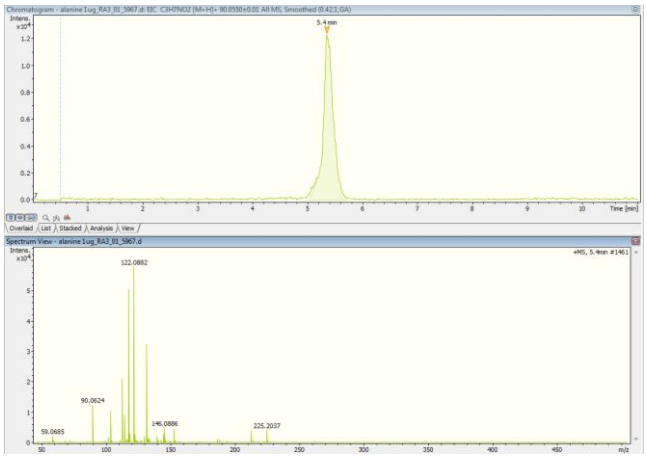
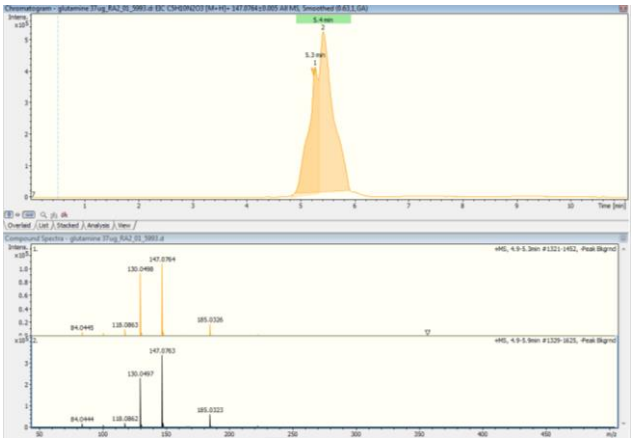


Figure 11-7: Process Properties: Chromatogram smoothing algorithm: Gauss, Smoothing width: 0.64 s, Cycles: 1; Mass Spectra smoothing algorithm: Gauss, Smoothing width: 0.2 Da, Cycles: 1

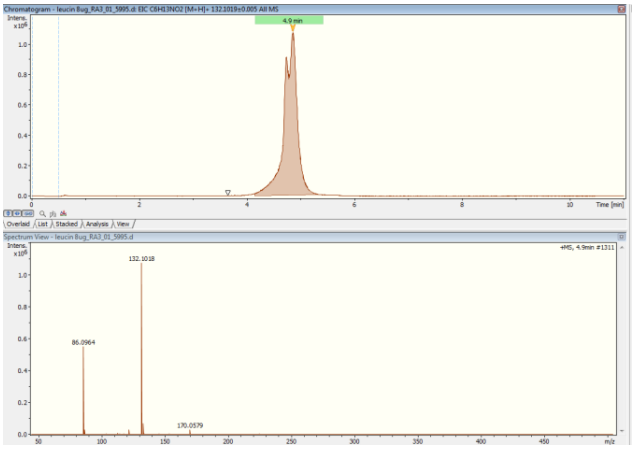
A: ALA



B: GLU



C: LEU



D: ISO

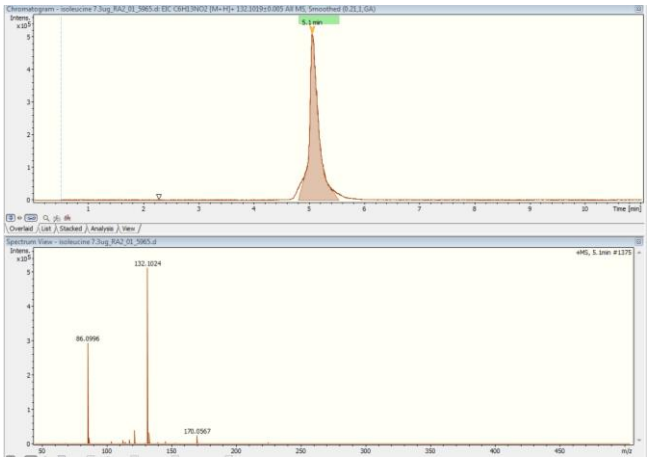


Figure 11-8: HPLC chromatograms and MS analysis of standards of amino acids that exposed good separation on the established method on HILIC 50 mm column: ALA, GLU, ISO and LEU.

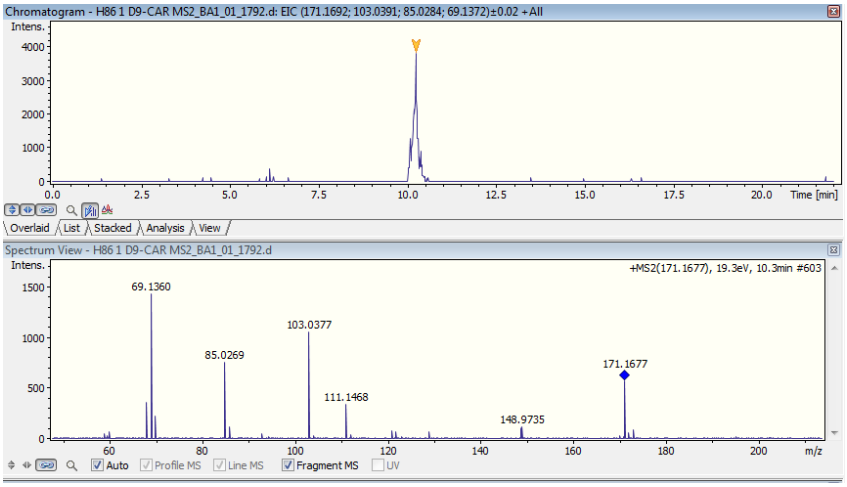


Figure 11-9: MS/MS analysis of CAR-d_9 peak in human cell lysate.

11.2 Tables

Table 11-1: Comparison of the elution time for each molecule in human lysate separated on HILIC 50 mm column to the standards separation.

HILIC 50 mm		
Molecule	**Retention time [min]**	**Expected retention time [min]**
TML	not found	8.1
γBB	6.7	6.8
CAR	6.1	6.2
A-CAR	6.0	6.1

Table 11-2: Comparison of the elution time for each molecule in human lysate separated on HILIC 150 mm column to the standards separation.

HILIC 150 mm		
Molecule	**Retention time [min]**	**Expected retention time [min]**
TML	not found	13.0
γBB	11.7	11.5
CAR	10.4	10.3
A-CAR	10.0	9.9

Table 11-3: Comparison of product ions after MS/MS analysis of the human sample to the fragmentation pattern of standards. On green: ions found in human extract after MS/MS fragmentation. In bold: the most abundant ion from standard fragmentation.

Ions	**γBB**	**CAR**	**A-CAR**
Product	121.9638		145.0488
		103.0364	144.1012
	87.0421	85.026	**85.0278**
	60.079	60.0785	60.0798

12. References

[1] J. Lee, E. Smith, and A. Shilatifard, "The language of histone crosstalk," *Cell*, vol. 142, no. 5, pp. 682–685, 2010.

[2] K. E. Gardner, C. D. Allis, and B. D. Strahl, "OPERating ON chromatin, a colorful language where context matters," *J Mol Biol*, vol. 409, no. 1, pp. 36–46, 2011.

[3] A. J. Bannister and T. Kouzarides, "Regulation of chromatin by histone modifications," *Cell Res*, vol. 21, no. 3, pp. 381–395, 2011.

[4] T. Jenuwein and C. D. Allis, "Translating the histone code," *Science (80-.).*, vol. 293, pp. 1074–1080, 2001.

[5] G. Egger, G. Liang, A. Aparicio, and P. A. Jones, "Epigenetics in human disease and prospects for epigenetic therapy," *Nature*, vol. 429, no. 6990, pp. 457–463, 2004.

[6] C. H. Waddington, "The epigenotype," *Endeavour*, pp. 18–20, 1942.

[7] A. Bird, "Perceptions of epigenetics," *Nature*, vol. 447, no. 7143, pp. 396–398, 2007.

[8] W. Reik, W. Dean, and J. Walter, "Epigenetic reprogramming in mammalian development," *Science (80-.).*, vol. 293, pp. 1089–1094, 2001.

[9] A. P. Feinberg and B. Tycko, "The history of cancer epigenetics," *Nat Rev Cancer*, vol. 4, pp. 143–153, 2004.

[10] M. Tan *et al.*, "Identification of 67 histone marks and histone lysine crotonylation as a new type of histone modification," *Cell*, vol. 146, no. 6, pp. 1016–1028, 2011.

[11] R. Y. Tweedie-Cullen *et al.*, "Identification of combinatorial patterns of post-translational modifications on individual histones in the mouse brain," *PLoS One*, vol. 7, no. 5, pp. 1–15, 2012.

[12] T. E. Spencer *et al.*, "Steroid receptor coactivator-1 is a histone acetyltransferase," *Nature*, vol. 389, no. 6647, pp. 194–198, 1997.

[13] E. Metzger *et al.*, "Phosphorylation of histone H3T6 by PKCB, controls demethylation at histone H3K4," *Nature*, vol. 464, no. 7289, pp. 792–796, 2010.

[14] P. Sassone-Corsi *et al.*, "Requirement of Rsk-2 for epidermal growth factor – activated phosphorylation of histone H3," *Science (80-.).*, vol. 285, pp. 886–892, 1999.

[15] Y. Chen *et al.*, "Lysine propionylation and butyrylation are novel post-translational modifications in histones," *Mol Cell Proteom*, vol. 6, no. 5, pp. 812–819, 2007.

[16] K. Zhang, Y. Chen, Z. Zhang, and Y. Zhao, "Identification and verification of lysine propionylation and butyrylation in yeast core histones using PTMap software identification and verification of lysine propionylation and butyrylation in yeast core histones using PTMap software," *J Proteome Res*, vol. 8, pp. 900–906, 2009.

[17] W. Kim *et al.*, "Systematic and quantitative assessment of the ubiquitin-modified proteome," *Mol Cell*, vol. 44, no. 2, pp. 325–340, 2011.

[18] C. Martin and Y. Zhang, "The diverse functions of histone lysine methylation," *Nat Rev Mol*, vol. 6, no. 11, pp. 838–849, 2005.

[19] A. Barski *et al.*, "High-resolution profiling of histone methylations in the human genome," *Cell*, vol. 129, pp. 823–837, 2007.

[20] T. G. Gillette and J. A. Hill, "Readers, writers and erasers: chromatin as the whiteboard of heart disease," *Circ Res*, vol. 116, no. 7, pp. 1245–1253, 2015.

[21] G. A. Khoury, R. C. Baliban, and C. A. Floudas, "Proteome-wide post-translational modification statistics: frequency analysis and curation of the swiss-prot database," *Sci Rep*, vol. 1, no. 90, pp. 1–5, 2011.

[22] Y. Y. Shi *et al.*, "Histone demethylation mediated by the nuclear amine oxidase homolog LSD1," *Cell*, vol. 119, no. 7, pp. 941–53, Dec. 2004.

[23] Y. I. Tsukada *et al.*, "Histone demethylation by a family of JmjC domain-containing proteins," *Nature*, vol. 439, no. 7078, pp. 811–816, 2006.

[24] R. J. Klose, E. M. Kallin, and Y. Zhang, "JmjC-domain-containing proteins and histone demethylation," *Nat Rev Genet*, vol. 7, no. 9, pp. 715–727, 2006.

[25] D. Balciunas Darius and H. Ronne, "Evidence of domain swapping within the jumonji family of transcription factors," *Trends Biochem Sci*, vol. 25, no. 6, pp. 274–276, 2000.

[26] I. J. Clifton, M. A. McDonough, D. Ehrismann, N. J. Kershaw, N. Granatino, and C. J. Schofield, "Structural studies on 2-oxoglutarate oxygenases and related double-stranded b-helix fold proteins," *J Inorg Biochem*, vol. 100, pp. 644–669, 2006.

[27] C. J. Schofield and P. J. Ratcliffe, "Oxygen sensing by HIF hydroxylases," *Nat Rev*

Mol, vol. 5, pp. 343–354, 2004.

[28] L. J. Walport, R. J. Hopkinson, and C. J. Schofield, "Mechanisms of human histone and nucleic acid demethylases," *Curr Opin Chem Biol*, vol. 16, no. 5–6, pp. 525–534, 2012.

[29] S. Markolovic, T. M. Leissing, R. Chowdhury, S. E. Wilkins, X. Lu, and C. J. Schofield, "Structure–function relationships of human JmjC oxygenases — demethylases versus hydroxylases," *Curr Opin Struct Biol*, vol. 41, pp. 62–72, 2016.

[30] M. A. McDonough, C. Loenarz, R. Chowdhury, I. J. Clifton, and C. J. Schofield, "Structural studies on human 2-oxoglutarate dependent oxygenases," *Curr Opin Struct Biol*, vol. 20, no. 6, pp. 659–672, 2010.

[31] M. T. Pedersen and K. Helin, "Histone demethylases in development and disease," *Trends Cell Biol*, vol. 20, no. 11, pp. 662–671, 2010.

[32] M. D. Shahbazian and M. Grunstein, "Functions of site-specific histone acetylation and deacetylation," *Annu Rev Biochem*, vol. 76, no. 1, pp. 75–100, 2007.

[33] P. A. Marks, "The clinical development of histone deacetylase inhibitors as targeted anticancer drugs," *Expert Opin Investig Drugs*, vol. 19, no. 9, pp. 1049–1066, 2010.

[34] H. Wapenaar and F. J. Dekker, "Histone acetyltransferases: challenges in targeting bi-substrate enzymes," *Clin Epigenetics*, vol. 8, no. 59, pp. 1–11, 2016.

[35] G. Blander and L. Guarente, "The Sir2 family of protein deacetylases," *Annu Rev Biochem*, vol. 73, pp. 417–435, 2004.

[36] C. D. Allis *et al.*, "New nomenclature for chromatin-modifying enzymes.," *Cell*, vol. 131, pp. 633–636, Nov. 2007.

[37] M. A. Glozak, N. Sengupta, X. Zhang, and E. Seto, "Acetylation and deacetylation of non-histone proteins," *Gene*, vol. 363, no. 1–2, pp. 15–23, 2005.

[38] J. Huang and S. L. Berger, "The emerging field of dynamic lysine methylation of non-histone proteins," *Curr Opin Genet. Dev*, vol. 18, no. 2, pp. 152–158, 2008.

[39] K. K. Biggar and S. S.-C. Li, "Non-histone protein methylation as a regulator of cellular signalling and function.," *Nat Rev Mol*, vol. 16, pp. 5–17, 2015.

[40] X. Zhang, H. Wen, and X. Shi, "Lysine methylation: beyond histones.," *Acta Biochim Biophys Sin*, vol. 44, no. 1, pp. 14–27, Jan. 2012.

[41] J. Huang *et al.*, "G9a and Glp methylate lysine 373 in the tumor suppressor p53," *J Biol Chem*, vol. 285, no. 13, pp. 9636–9641, 2009.

[42] J. S. Lee *et al.*, "Negative regulation of hypoxic responses via induced Reptin methylation.," *Mol Cell*, vol. 39, no. 1, pp. 71–85, Jul. 2010.

[43] S. Chuikov *et al.*, "Regulation of p53 activity through lysine methylation," *Nature*, vol. 432, no. 7015, pp. 353–360, 2004.

[44] D. Levy *et al.*, "Lysine methylation of the NF- kB subunit RelA by SETD6 couples activity of the histone methyltransferase GLP at chromatin to tonic repression of NF-kB signaling," *Nat. Immunol*, vol. 12, no. 1, pp. 29–36, 2010.

[45] C. Ea and D. Baltimore, "Regulation of NF-kB activity through lysine monomethylation of p65," *Proc Natl Acad Sci USA*, vol. 106, no. 45, pp. 18972–18977, 2009.

[46] M. Tahiliani *et al.*, "The histone H3K4 demethylase SMCX links REST target genes to X-linked mental retardation," *Nature*, vol. 447, no. 601–603, 2007.

[47] P. A. Jones and S. B. Baylin, "The fundamental role of epigenetic events in cancer," *Nat Rev Genet*, vol. 3, pp. 415–428, 2002.

[48] A. Merlo *et al.*, "5' CpG island methylation is associated with transcriptional silencing of the tumour suppressor p16/CDKN2/MTS1 in human cancers," *Nat Med*, vol. 1, no. 7, pp. 686–692, 1995.

[49] R. D. Morin *et al.*, "Somatic mutations altering EZH2 (Tyr641) in follicular and diffuse large B-cell lymphomas of germinal-center origin," *Nat. Genet*, vol. 42, no. 2, pp. 181–185, 2010.

[50] R. D. Morin *et al.*, "Frequent mutation of histone-modifying genes in non-Hodgkin lymphoma," *Nature*, vol. 476, no. 7360, pp. 298–303, 2011.

[51] G. van Haaften *et al.*, "Somatic mutations of the histone H3K27 demethylase gene UTX in human cancer," *Nat. Genet*, vol. 41, no. 5, pp. 521–523, 2009.

[52] S. Friso, S. Udali, D. De Santis, and S.-W. Choi, "One-carbon metabolism and epigenetics," *Mol Asp. Med*, 2016.

[53] M. A. Dawson and T. Kouzarides, "Cancer epigenetics: from mechanism to therapy," *Cell*, vol. 150, pp. 12–27, 2012.

[54] S. B. Baylin and P. A. Jones, "A decade of exploring the cancer epigenome —

biological and translational implications," *Nat Rev Cancer*, vol. 11, no. 10, pp. 726–734, 2011.

[55] P. Chi, C. D. Allis, and G. G. Wang, "Covalent histone modifications - miswritten, misinterpreted and mis-erased in human cancers," *Nat Rev Cancer*, vol. 10, no. 7, pp. 457–469, 2010.

[56] G. L. Gravina *et al.*, "Biological rationale for the use of DNA methyltransferase inhibitors as new strategy for modulation of tumor response to chemotherapy and radiation," *Mol. Cancer*, vol. 9, no. 305, pp. 1–16, 2010.

[57] J. E. Bolden, M. J. Peart, and R. W. Johnstone, "Anticancer activities of histone deacetylase inhibitors," *Nat Rev Drug Discov*, vol. 5, pp. 769–784, Sep. 2006.

[58] A. Chavez-Blanco *et al.*, "Histone acetylation and histone deacetylase activity of magnesium valproate in tumor and peripheral blood of patients with cervical cancer. A phase I study," *Mol Cancer*, vol. 4, no. 22, pp. 1–9, 2005.

[59] G. Bug *et al.*, "Clinical trial of valproic acid and all-trans retinoic acid in patients with poor-risk acute myeloid leukemia," *Cancer*, vol. 104, no. 12, pp. 2717–2725, 2005.

[60] W. K. Kelly and P. A. Marks, "Drug insight: histone deacetylase inhibitors—development of the new targeted anticancer agent suberoylanilide hydroxamic acid," *Nat Clin Pr. Oncol*, vol. 2, p. 150, Mar. 2005.

[61] M. Duvic and C. Zhang, "Clinical and laboratory experience of vorinostat (suberoylanilide hydroxamic acid) in the treatment of cutaneous T-cell lymphoma," *Br J Cancer*, vol. 95, pp. S13–S19, 2006.

[62] W. S. Xu, R. B. Parmigiani, and P. A. Marks, "Histone deacetylase inhibitors : molecular mechanisms of action," *Oncogene*, vol. 26, pp. 5541–5552, 2007.

[63] C. C. Thinnes, K. S. England, A. Kawamura, R. Chowdhury, C. J. Schofield, and R. J. Hopkinson, "Targeting histone lysine demethylases - Progress, challenges, and the future," *Biochim Biophys Acta*, vol. 1839, no. 12, pp. 1416–1432, 2014.

[64] T. A. McKinsey, "Therapeutic potential for HDAC inhibitors in the heart," *Annu Rev Pharmacol Toxicol*, vol. 52, no. 1, pp. 303–319, Jan. 2012.

[65] M. A. Reddy, E. Zhang, and R. Natarajan, "Epigenetic mechanisms in diabetic complications and metabolic memory," *Diabetologia*, vol. 58, pp. 443–455, 2015.

[66] C. N. Hales and D. J. P. Barker, “Type 2 (non-insulin-dependent) diabetes mellitus: the thrifty phenotype hypothesis,” *Diabetologia*, vol. 35, pp. 595–602, 1992.

[67] A. C. J. Ravelli *et al.*, “Glucose tolerance in adults after prenatal exposure to famine,” *Lancet*, vol. 351, no. 9097, pp. 173–177, Jan. 1998.

[68] C. Dina *et al.*, “Variation in FTO contributes to childhood obesity and severe adult obesity,” *Nat. Genet*, vol. 39, no. 6, pp. 724–726, 2007.

[69] T. Gerken *et al.*, “The obesity-associated FTO gene encodes a 2-oxoglutarate – dependent nucleic acid demethylase,” *Science (80-.).*, vol. 318, pp. 1469–1472, 2007.

[70] C. J. Rebouche, “Carnitine function and requirements during the life cycle.,” *FASEB J*, vol. 6, no. 15, pp. 3379–3386, Dec. 1992.

[71] K. Jaudzems *et al.*, “Inhibition of carnitine acetyltransferase by mildronate, a regulator of energy metabolism,” *J Enzym. Inhib Med Chem*, vol. 24, no. 6, pp. 1269–1275, 2009.

[72] G. Fraenkel and S. Friedman, “Carnitine,” *Vitam Horm*, vol. 15, pp. 73–118, 1957.

[73] G. Wolf, “The discovery of a vitamin role for carnitine: the first 50 years,” *J Nutr*, vol. 136, no. 8, pp. 2131–2134, Aug. 2006.

[74] J. Franken, S. Kroppenstedt, J. H. Swiegers, and F. F. Bauer, “Carnitine and carnitine acetyltransferases in the yeast Saccharomyces cerevisiae: a role for carnitine in stress protection,” *Curr Genet*, vol. 53, no. 6, pp. 347–360, 2008.

[75] K. Strijbis, F. M. Vaz, and B. Distel, “Enzymology of the carnitine biosynthesis pathway,” *IUBMB Life*, vol. 62, no. 5, pp. 357–362, 2010.

[76] J. H. Swiegers, N. Dippenaar, I. S. Pretorius, and F. F. Bauer, “Carnitine-dependent metabolic activities in Saccharomyces cerevisiae: three carnitine acetyltransferases are essential in a carnitine-dependent strain,” *Yeast*, vol. 18, no. 7, pp. 585–595, May 2001.

[77] F. M. Vaz, S. W. Fouchier, R. Ofman, M. Sommer, and R. J. A. Wanders, “Molecular and biochemical characterization of Rat -Trimethylaminobutyraldehyde dehydrogenase and evidence for the involvement of human aldehyde dehydrogenase 9 in carnitine biosynthesis,” *J Biol Chem*, vol. 275, no. 10, pp. 7390–7394, Mar. 2000.

[78] J. S. Volek, W. J. Kraemer, M. R. Rubin, A. L. Gómez, N. a Ratamess, and P. Gaynor, "L-carnitine L-tartrate supplementation favorably affects markers of recovery from exercise stress.," *Am J Physiol Endocrinol Metab*, vol. 282, no. 2, pp. E474–E482, Feb. 2002.

[79] J. Franken, A. Burger, J. H. Swiegers, and F. F. Bauer, "Reconstruction of the carnitine biosynthesis pathway from Neurospora crassa in the yeast Saccharomyces cerevisiae," *Appl Microbiol Biotechnol*, vol. 99, pp. 6377–6389, 2015.

[80] K. Strijbis *et al.*, "Identification and characterization of a complete carnitine biosynthesis pathway in Candida albicans," *FASEB J*, vol. 23, no. 8, pp. 2349–2359, Aug. 2009.

[81] R. A. Kaufman and H. P. Broquist, "Biosynthesis of carnitine in Neurospora crassa," *J Biol Chem*, vol. 252, no. 10, pp. 7437–7440, 1977.

[82] G. Wolf and C. R. A. Berger, "Studies on the biosynthesis and turnover of carnitine," *Arch Biochem Biophys*, vol. 92, no. 2, pp. 360–365, Feb. 1961.

[83] C. Loenarz and C. J. Schofield, "Physiological and biochemical aspects of hydroxylations and demethylations catalyzed by human 2-oxoglutarate oxygenases," *Trends Biochem Sci*, vol. 36, no. 1, pp. 7–18, 2011.

[84] Y. Wang *et al.*, "Phenotype and genotype variation in primary carnitine deficiency," *Genet Med*, vol. 3, no. 6, pp. 387–392, 2001.

[85] J. Nezu *et al.*, "Primary systemic carnitine deficiency is caused by mutations in a gene encoding sodium ion-dependent carnitine transporter," *Nat. Genet*, vol. 21, no. 1, pp. 91–94, 1999.

[86] E. C. Rose, C. A. di San Filippo, U. C. N. Erlingsson, O. Ardon, M. Pasquali, and N. Longo, "Genotype-phenotype correlation in primary carnitine deficiency," *Hum Mutat*, vol. 33, no. 1, pp. 118–123, 2012.

[87] Y. Wang, F. Taroni, B. Garavaglia, and N. Longo, "Functional analysis of mutations in the OCTN2 transporter causing primary carnitine deficiency: lack of genotype-phenotype correlation," *Hum Mutat*, vol. 16, no. 5, pp. 401–7, 2000.

[88] C. A. Stanley, "Carnitine deficiency disorders in children," *Ann NY Acad Sci*, vol. 1033, pp. 42–51, 2004.

[89] P. Rinaldo, C. A. Stanley, B. Y. L. Hsu, L. A. Sanchez, and H. J. Stern, "Sudden neonatal death in carnitine transporter deficiency," *J Pediatr*, vol. 131, no. 2, pp. 304–305, 1997.

[90] I. Rizos, "Three-year survival of patients with heart failure caused by dilated cardiomyopathy and L-carnitine administration," *Am Hear. J*, vol. 139, no. 2, pp. s120–s123, 2002.

[91] G. La Marca, S. Malvagia, S. Toni, B. Piccini, V. Di Ciommo, and G. F. Bottazzo, "Children who develop type 1 diabetes early in life show low levels of carnitine and amino acids at birth: Does this finding shed light on the etiopathogenesis of the disease?," *Nutr Diabetes*, vol. 3, pp. 1–8, 2013.

[92] P. A. Filipek, J. Juranek, M. T. Nguyen, C. Cummings, and J. J. Gargus, "Relative carnitine deficiency in autism," *J Autism Dev Disord*, vol. 34, no. 6, pp. 615–623, 2004.

[93] C. Nava *et al.*, "Analysis of the chromosome X exome in patients with autism spectrum disorders identified novel candidate genes, including TMLHE," *Transl Psychiatry*, vol. 2, no. e179, pp. 1–12, 2012.

[94] P. B. S. Celestino-Soper *et al.*, "A common X-linked inborn error of carnitine biosynthesis may be a risk factor for nondysmorphic autism," *Proc Natl Acad Sci USA*, vol. 109, no. 21, pp. 7974–7981, 2012.

[95] P. B. S. Celestino-Soper *et al.*, "Use of array CGH to detect exonic copy number variants throughout the genome in autism families detects a novel deletion in TMLHE," *Hum Mol Gen*, vol. 20, no. 22, pp. 4360–4370, 2011.

[96] M. H. Irwin, W. H. Moos, D. V. Faller, K. Steliou, and C. A. Pinkert, "Epigenetic treatment of neurodegenerative disorders: Alzheimer and Parkinson diseases," *Drug Dev Res*, vol. 77, no. 3, pp. 109–123, 2016.

[97] W. H. Moos *et al.*, "A new approach to treating neurodegenerative otologic disorders," *Biores Open Access*, vol. 7, no. 1, pp. 107–115, 2018.

[98] W. H. Moos *et al.*, "Epigenetic treatment of neuropsychiatric disorders: autism and schizophrenia," *Drug Dev Res*, vol. 77, no. 2, pp. 53–72, 2016.

[99] C. B. Brachmann *et al.*, "Designer deletion strains derived from Saccharomyces cerevisiae S288C : a useful set of strains and plasmids for PCR-mediated gene disruption and other applications," *Yeast*, vol. 14, pp. 115–132, 1998.

[100] R. D. Gietz and S. Akio, “New yeast-Escherichia coli shuttle vectors constructed with in vitro mutagenized yeast genes lacking six-base pair restriction sites,” *Gene*, vol. 74, no. 2, pp. 527–534, 1988.

[101] A. L. Goldstein and J. H. McCusker, “Three new dominant drug resistance cassettes for gene disruption in Saccharomyces cerevisiae,” *Yeast*, vol. 15, no. 14, pp. 1541–1553, 1999.

[102] Abcam, “Histone extraction protocol,” *Last accessed 01.10.2018*.

[103] G. Rumbaugh and C. A. Miller, “Epigenetic changes in the brain: measuring global histone modifications,” *Methods Mol Biol*, vol. 670, pp. 263–274, 2011.

[104] C. Frezza, S. Cipolat, and L. Scorrano, “Organelle isolation: functional mitochondria from mouse liver, muscle and cultured filroblasts,” *Nat Protoc*, vol. 2, no. 2, pp. 287–295, 2007.

[105] A. A. Duina, M. E. Miller, and J. B. Keeney, “Budding yeast for budding geneticists: a primer on the Saccharomyces cerevisiae model system,” *Genetics*, vol. 197, no. 1, pp. 33–48, 2014.

[106] J. M. Laurent, J. H. Young, A. H. Kachroo, and E. M. Marcotte, “Efforts to make and apply humanized yeast,” *Br. Funct Genomics*, vol. 15, no. 2, pp. 155–163, 2016.

[107] C. W. T. Van Roermund, Y. Elgersma, N. Singh, R. J. A. Wanders, and H. F. Tabak, “The membrane of peroxisomes in Saccharomyces cerevisiae is impermeable to NAD(H) and acetyl-CoA under in vivo conditions,” *EMBO J*, vol. 14, no. 14, pp. 3480–3486, 1995.

[108] W. J. Colucci and R. D. Gandour, “Carnitine acetyltransferase: a review of its biology, enzymology, and bioorganic chemistry,” *Bioorg Chem*, vol. 16, no. 3, pp. 307–334, 1988.

[109] J. M. Ellis, J. L. Frahm, L. O. Li, and R. A. Coleman, “Acyl-coenzyme A synthetases in metabolic control,” *Curr Opin Lipidol*, vol. 21, no. 3, pp. 212–217, 2010.

[110] T. Osumi, T. Hashimoto, and N. Ui, “Purification and properties of acyl-CoA oxidase from rat liver,” *J Biochem*, vol. 87, no. 6, pp. 1735–1746, 1980.

[111] N. C. Veitch, “Horseradish peroxidase: a modern view of a classic enzyme,” *Phytochemistry*, vol. 65, no. 3, pp. 249–259, 2004.

[112] Y. Oda, “Choline acetyltransferase: the structure, distribution and pathologic

changes in the central nervous system," *Pathol Int*, vol. 49, no. 11, pp. 921–37, 1999.

[113] R. D. Smith, J. A. Loo, C. G. Edmonds, C. J. Barinaga, and H. R. Udseth, "New developments in biochemical mass spectrometry: electrospray ionization," *Anal Chem*, vol. 62, no. 9, pp. 882–899, 1990.

[114] R. A. Yost and R. K. Boyd, "Tandem mass spectrometry: Quadrupole and hybrid instruments," *Methods Enzym.*, vol. 193, pp. 154–200, 1990.

[115] A. H. Payne and G. L. Glish, "Tandem mass spectrometry in quadrupole ion trap and ion cyclotron resonance mass spectrometers," *Methods Enzym.*, vol. 402, no. 05, pp. 109–148, 2005.

[116] Q. Hu, R. J. Noll, H. Li, A. Makarov, M. Hardman, and R. G. Cooks, "The Orbitrap: A new mass spectrometer," *J Mass Spectrom*, vol. 40, no. 4, pp. 430–443, 2005.

[117] A. G. Marshall, C. L. Hendrickson, and G. S. Jackson, "Fourier transform ion cyclotron resonance mass spectrometry: a primer," *Mass Spectrom Rev*, vol. 17, pp. 1–35, 1998.

[118] K. A. Neilson *et al.*, "Less label, more free: Approaches in label-free quantitative mass spectrometry," *Proteomics*, vol. 11, no. 4, pp. 535–553, 2011.

[119] S. A. McLuckey, "Principles of collision activation in analytical mass spectrometry.," *J Am Soc Mass Spectrom*, vol. 3, pp. 599–614, 1992.

[120] A. James and C. Jorgensen, "Basic design of MRM assays for peptide quantification," in *LC-MS/MS in Proteomics. Methods in Molecular Biology (Methods and Protocols)*, P. Cutillas and J. Timms, Eds. Totowa, NJ: Humana Press, 2010, p. 658:167-185.

[121] R. G. Cooks, "Collision-induced dissociation: Readings and commentary," *J Mass Spectrom*, vol. 30, no. 9, pp. 1215–1221, 1995.

[122] B. Buszewski and S. Noga, "Hydrophilic interaction liquid chromatography (HILIC)-a powerful separation technique," *Anal Bioanal Chem*, vol. 402, pp. 231–247, 2012.

[123] H. Huang, S. Lin, B. a Garcia, and Y. Zhao, "Quantitative proteomic analysis of histone modifications," *Chem Rev*, vol. 115, no. 6, pp. 2376–2418, 2015.

[124] A. H. K. Al Temimi, B. J. G. E. Pieters, Y. V. Reddy, P. B. White, and J. Mecinović,

"Substrate scope for trimethyllysine hydroxylase catalysis," *Chem Commun*, vol. 52, pp. 12849–12852, 2016.

[125] K. Plath *et al.*, "Role of histone H3 lysine 27 methylation in X inactivation," *Science (80-.).*, vol. 300, no. 5616, pp. 131–135, 2003.

[126] S. Kernstock *et al.*, "Lysine methylation of VCP by a member of a novel human protein methyltransferase family," *Nat Commun*, vol. 3, no. 1, pp. 1–11, 2012.

[127] D. R. Ahlf, P. M. Thomas, and N. L. Kelleher, "Developing top down proteomics to maximize proteome and sequence coverage from cells and tissues," *Curr Opin Chem Biol*, vol. 17, pp. 787–794, 2013.

[128] M. Gstaiger and R. Aebersold, "Applying mass spectrometry-based proteomics to genetics, genomics and network biology," *Nat Rev Genet*, vol. 10, no. 9, pp. 617–627, 2009.

[129] R. Aebersold and M. Mann, "Mass spectrometry-based proteomics," *Nature*, vol. 422, pp. 198–207, 2003.

[130] A. D. Catherman, O. S. Skinner, and N. L. Kelleher, "Top down proteomics: facts and perspectives," *Biochem Biophys Res Commun*, vol. 445, no. 4, pp. 683–693, 2014.

[131] R. A. Zubarev, N. L. Kelleher, and F. W. McLafferty, "Electron capture dissociation of multiply charged protein cations. A nonergodic process," *J Am Chem Soc*, vol. 120, no. 13, pp. 3265–3266, 1998.

[132] J. E. P. Syka, J. J. Coon, M. J. Schroeder, J. Shabanowitz, and D. F. Hunt, "Peptide and protein sequence analysis by electron transfer dissociation mass spectrometry," *Proc Natl Acad Sci USA*, vol. 101, no. 26, pp. 9528–9533, 2004.

[133] D. M. Good, M. Wirtala, G. C. McAlister, and J. J. Coon, "Performance characteristics of electron transfer dissociation mass spectrometry," *Mol Cell Proteom*, vol. 6, no. 11, pp. 1942–1951, 2007.

[134] R. A. Zubarev, "Electron-capture dissociation tandem mass spectrometry," *Curr Opin Biotechnol*, vol. 15, no. 1, pp. 12–16, 2004.

[135] Y. Zhang, B. R. Fonslow, B. Shan, M. C. Baek, and J. R. Yates, "Protein analysis by shotgun/bottom-up proteomics," *Chem Rev*, vol. 113, no. 4, pp. 2343–2394, 2013.

[136] J. Mitchell Wells and S. A. McLuckey, "Collision-induced dissociation (CID) of

peptides and proteins," *Methods Enzym.*, vol. 402, no. 2005, pp. 148–185, 2005.

[137] B. Domon and R. Aebersold, "Mass spectrometry and protein analysis," *Science (80-.).*, vol. 312, no. 5771, pp. 212–217, 2006.

[138] J. K. Eng, A. L. McCormack, and J. R. Yates, "An approach to correlate tandem mass spectral data of peptides with amino acid sequences in a protein database," *J Am Soc Mass Spectrom*, vol. 5, pp. 976–989, 1994.

[139] D. Bonenfant, M. Coulot, H. Towbin, P. Schindler, and J. van Oostrum, "Characterization of histone H2A and H2B variants and their post-translational modifications by mass spectrometry," *Mol Cell Proteom*, vol. 5, no. 3, pp. 541–552, 2006.

[140] E. M. Duncan *et al.*, "Cathepsin L proteolytically processes histone H3 during mouse embryonic stem cell differentiation," *Cell*, vol. 135, no. 2, pp. 284–294, 2008.

[141] S. Takechi and T. Nakayama, "Sas3 is a histone acetyltransferase and requires a zinc finger motif," *Biochem Biophys Res Commun*, vol. 266, no. 2, pp. 405–410, 1999.

[142] Y. Chen, W. Chen, M. H. Cobb, and Y. Zhao, "PTMap - A sequence alignment software for unrestricted, accurate, and full-spectrum identification of post-translational modification sites," *Proc Natl Acad Sci USA*, vol. 106, no. 3, pp. 761–766, 2009.

[143] F. M. Vaz and R. J. A. Wanders, "Carnitine biosynthesis in mammals.," *Biochem J*, vol. 361, pp. 417–429, 2002.

[144] S. Girgis *et al.*, "Molecular cloning, characterization and alternative splicing of the human cytoplasmic serine hydroxymethyltransferase gene," *Gene*, vol. 210, pp. 315–324, 1998.

[145] A. J. MacFarlane *et al.*, "Cytoplasmic serine hydroxymethyltransferase regulates the metabolic partitioning of methylenetetrahydrofolate but is not essential in mice," *J Biol Chem*, vol. 283, no. 38, pp. 25846–25853, 2008.

[146] H. M. van Rossum *et al.*, "Requirements for carnitine shuttle-mediated translocation of mitochondrial acetyl moieties to the yeast cytosol," *MBio*, vol. 7, no. 3, pp. 1–14, 2016.

[147] S. Ghaemmaghami *et al.*, "Global analysis of protein expression in yeast," *Nature*, vol. 425, no. 203, pp. 737–741, 2003.

[148] T. Kim and S. Buratowski, "Two Saccharomyces cerevisiae JmjC domain proteins demethylate histone H3 Lys36 in transcribed regions to promote elongation," *J Biol Chem*, vol. 282, no. 29, pp. 20827–20835, 2007.

[149] D. Schaft *et al.*, "The histone 3 lysine 36 methyltransferase, SET2, is involved in transcriptional elongation," *Nucleic Acids Res*, vol. 31, no. 10, pp. 2475–2482, 2003.

[150] S. L. McDaniel *et al.*, "H3K36 methylation regulates nutrient stress response in Saccharomyces cerevisiae by enforcing transcriptional fidelity," *Cell Rep*, vol. 19, no. 11, pp. 2371–2382, 2017.

[151] N. Terzi, L. S. Churchman, L. Vasiljeva, J. Weissman, and S. Buratowski, "H3K4 trimethylation by Set1 promotes efficient termination by the Nrd1-Nab3-Sen1 pathway," *Mol Cell Biol*, vol. 31, no. 17, pp. 3569–3583, 2011.

[152] M. Soloveychik *et al.*, "Mitochondrial control through nutritionally regulated global histone H3 lysine-4 demethylation," *Sci Rep*, vol. 6, pp. 1–12, 2016.

[153] B. D. Strahl *et al.*, "Set2 is a nucleosomal histone H3-selective methyltransferase that mediates transcriptional repression," *Mol Cell Biol*, vol. 22, no. 5, pp. 1298–1306, 2002.

[154] P. A. San-Segundo and G. S. Roeder, "Role for the silencing protein Dot1 in meiotic checkpoint control.," *Mol Biol Cell*, vol. 11, no. 10, pp. 3601–3615, 2000.

[155] B. Polevoda, M. R. Martzen, B. Das, E. M. Phizicky, and F. Sherman, "Cytochrome c methyltransferase, Ctm1p, of yeast," *J Biol Chem*, vol. 275, no. 27, pp. 20508–20513, 2000.

[156] L. Zhang, J. J. Hamey, G. Hart-smith, M. A. Erce, and M. R. Wilkins, "Elongation factor methyltransferase 3 – A novel eukaryotic lysine methyltransferase," *Biochem Biophys Res Commun*, vol. 451, no. 2, pp. 229–234, 2014.

[157] M. C. Dzialo *et al.*, "Translational roles of elongation factor 2 protein lysine methylation," *J Biol Chem*, vol. 289, no. 44, pp. 30511–30524, 2014.

[158] M. C. Dzialo, K. J. Travaglini, S. Shen, J. A. Loo, and S. G. Clarke, "A new type of protein lysine methyltransferase trimethylates Lys-79 of elongation factor 1A,"

Biochem Biophys Res Commun, vol. 455, pp. 382–389, 2014.

[159] E. Davydova *et al.*, "Identification and characterization of a novel evolutionarily conserved lysine-specific methyltransferase targeting eukaryotic translation elongation factor 2 (eEF2)," *J Biol Chem*, vol. 289, no. 44, pp. 30499–30510, 2014.

[160] D. B. Kushner, B. D. Lindenbach, V. Z. Grdzelishvili, A. O. Noueiry, S. M. Paul, and P. Ahlquist, "Systematic, genome-wide identification of host genes affecting replication of a positive-strand RNA virus.," *Proc Natl Acad Sci USA*, vol. 100, no. 26, pp. 15764–15769, 2003.

[161] J. J. Hamey and M. R. Wilkins, "Methylation of elongation factor 1A: where, who, and why?," *Trends Biochem Sci*, vol. 43, no. 3, pp. 211–223, 2018.

[162] M. E. Jakobsson, E. Davydova, J. Malecki, A. Moen, and P. Falnes, "Saccharomyces cerevisiae eukaryotic elongation factor 1A (eEF1A) is methylated at Lys-390 by a METTL21-like methyltransferase," *PLoS One*, vol. 10, no. 6, pp. 1–18, 2015.

[163] T. R. Porras-Yakushi, J. P. Whitelegge, and S. Clarke, "A novel SET domain methyltransferase in yeast: Rkm2-dependent trimethylation of ribosomal protein L12ab at lysine 10," *J Biol Chem*, vol. 281, no. 47, pp. 35835–35845, 2006.

[164] S. Tu *et al.*, "Identification of histone demethylases in Saccharomyces cerevisiae," *J Biol Chem*, vol. 282, no. 11, pp. 14262–14271, 2007.

[165] R. J. Klose, K. E. Gardner, G. Liang, H. Erdjument-Bromage, P. Tempst, and Y. Zhang, "Demethylation of histone H3K36 and H3K9 by Rph1: a vestige of an H3K9 methylation system in Saccharomyces cerevisiae?," *Mol Cell Biol*, vol. 27, no. 11, pp. 3951–3961, 2007.

[166] I. Pedruzzi, N. Bürckert, P. Egger, and C. De Virgilio, "Saccharomyces cerevisiae Ras/cAMP pathway controls post-diauxic shift element-dependent transcription through the zinc finger protein Gis1," *EMBO J*, vol. 19, no. 11, pp. 2569–2579, 2000.

[167] G. Liang, R. J. Klose, K. E. Gardner, and Y. Zhang, "Yeast Jhd2p is a histone H3 Lys4 trimethyl demethylase," *Nat Struct Mol Biol*, vol. 14, no. 3, pp. 243–245, 2007.

[168] D. J. Seward *et al.*, "Demethylation of trimethylated histone H3 Lys4 in vivo by JARID1 JmjC proteins," *Nat Struct Mol Biol*, vol. 14, no. 3, pp. 240–242, 2007.

[169] A. Shirai, M. Sadaie, K. Shinmyozu, and J. I. Nakayama, "Methylation of ribosomal

protein L42 regulates ribosomal function and stress-adapted cell growth," *J Biol Chem*, vol. 285, no. 29, pp. 22448–22460, 2010.

[170] M. K. Mateyak and T. G. Kinzy, "eEF1A: Thinking outside the ribosome," *J Biol Chem*, vol. 285, no. 28, pp. 21209–21213, 2010.

[171] C. M. Spahn *et al.*, "Domain movements of elongation factor eEF2 and the eukaryotic 80S ribosome facilitate tRNA translocation," *EMBO J*, vol. 23, no. 5, pp. 1008–1019, 2004.

[172] P. A. Ortiz, R. Ulloque, G. K. Kihara, H. Zheng, and T. G. Kinzy, "Translation elongation factor 2 anticodon mimicry domain mutants affect fidelity and diphtheria toxin resistance," *J Biol Chem*, vol. 281, no. 43, pp. 32639–32648, 2006.

[173] E. T. Polastro *et al.*, "Evidence that trimethylation of iso-I-cytochrome c from Saccharomyces cerevisiae affects interaction with the mitochondrion," *FEBS Lett*, vol. 86, no. 1, pp. 17–20, 1978.

[174] S. K. Syed, S. Kim, and W. K. Paik, "Comparative studies on S-adenosyl-L-methionine binding sites of protein N-methyltransferases, using 8-azido-S-adenosyl-L- methionine as photoattinity probe," *Protein J*, vol. 12, no. 5, pp. 603–611, 1993.

[175] K. S. Egorova, O. M. Olenkina, and L. V. Olenina, "Lysine methylation of nonhistone proteins is a way to regulate their stability and function," *Biochem*, vol. 75, no. 5, pp. 535–548, 2010.

[176] C.-Y. Liang, L.-C. Wang, and W.-S. Lo, "Dissociation of the H3K36 demethylase Rph1 from chromatin mediates derepression of environmental stress-response genes under genotoxic stress in Saccharomyces cerevisiae," *Mol Biol Cell*, vol. 24, no. 20, pp. 3251–3262, 2013.

[177] J. Orzechowski Westholm, S. Tronnersjö, N. Nordberg, I. Olsson, J. Komorowski, and H. Ronne, "Gis1 and Rph1 regulate glycerol and acetate metabolism in glucose depleted yeast cells," *PLoS One*, vol. 7, no. 2, pp. 1–19, 2012.

[178] D. H. Chen, K. T. Wu, C. J. Hung, M. Hsieh, and C. Li, "Effects of adenosine dialdehyde treatment on in vitro and in vivo stable protein methylation in HeLa cells," *J Biochem*, vol. 136, no. 3, pp. 371–376, 2004.

[179] H. Xiao, Z. Gu, G. Wang, and T. Zhao, "The possible mechanisms underlying the impairment of HIF-1a pathway signaling in hyperglycemia and the beneficial

effects of certain therapies," *Int J Med Sci*, vol. 10, no. 10, pp. 1412–1421, 2013.

[180] J. P. van Dijken, R. A. Weusthuis, and J. T. Pronk, "Kinetics of growth and sugar consumption in yeasts," *Antonie Van Leeuwenhoek*, vol. 63, no. 3–4, pp. 343–352, 1993.

[181] S. Honigberg, "Similar environments but diverse fates: responses of budding yeast to nutrient deprivation," *Microb. Cell*, vol. 3, no. 8, pp. 302–328, 2016.

[182] J.-Q. Engle, K. M.; Mei, T-S.; Wasa, M.; Yu, J.-H. Kim, A. Roy, D. Jouandot II, and K. H. Chob, "The glucose signaling network in yeast," *Biochim Biophys Acta*, vol. 11, no. 6, pp. 5204–5210, 2013.

[183] L. Galdieri, S. Mehrotra, S. Yu, and A. Vancura, "Transcriptional regulation in yeast during diauxic shift and stationary phase," *OMICS*, vol. 14, no. 6, pp. 629–638, 2010.

[184] N. A. Oey, N. van Vlies, F. A. Wijburg, R. J. Wanders, T. Attie-Bitach, and F. M. Vaz, "L-carnitine is synthesized in the human fetal-placental unit: potential roles in placental and fetal metabolism," *Placenta*, vol. 27, no. 8, pp. 841–846, 2006.

[185] D. López-Terrada, S. W. Cheung, M. J. Finegold, and B. B. Knowles, "Hep G2 is a hepatoblastoma-derived cell line," *Hum Pathol*, vol. 40, no. 10, pp. 1512–1515, 2009.

[186] W. C. Russell, F. L. Graham, J. Smiley, and R. Nairn, "Characteristics of a human cell line transformed by DNA from human adenovirus type 5," *J Gen Virol*, vol. 36, no. 1, pp. 59–72, 1977.

[187] W. F. Scherer, "Studies on the propagation in vitro of poliomyelitis viruses: IV. Viral multiplication in a stable strain of human malignant epithelial cells (strain HeLa) derived from an epidermoid carcinoma of the cervix," *J Exp Med*, vol. 97, no. 5, pp. 695–710, 1953.

[188] J. D. Finkelstein, "The metabolism of homocysteine: pathways and regulation," *Eur J Pediatr*, vol. 157, pp. S40–S44, 1988.

[189] R. A. Waterland and R. L. Jirtle, "Transposable elements: targets for early nutritional effects on epigenetic gene regulation," *Mol Cell Biol*, vol. 23, no. 15, pp. 5293–5300, Aug. 2003.

[190] H. Zhu, S. Pan, S. Gu, E. Morton Bradbury, and X. Chen, "Amino acid residue

specific stable isotope labeling for quantitative proteomics," *Rapid Commun Mass Spectrom*, vol. 16, no. 22, pp. 2115–2123, 2002.

[191] S.-E. Ong *et al.*, "Stable isotope labeling by amino acids in cell culture, SILAC, as a simple and accurate approach to expression proteomics," *Mol Cell Proteom*, vol. 1, no. 5, pp. 376–386, 2002.

[192] M. K. Doherty, C. Whitehead, H. McCormack, S. J. Gaskell, and R. J. Beynon, "Proteome dynamics in complex organisms: using stable isotopes to monitor individual protein turnover rates," *Proteomics*, vol. 5, no. 2, pp. 522–533, 2005.

[193] R. J. Tomko and M. Hochstrasser, "Molecular architecture and assembly of the eukaryotic proteasome," *Annu Rev Biochem*, vol. 82, no. 1, pp. 415–445, 2013.

[194] Y. Ohsumi, "Historical landmarks of autophagy research," *Cell Res*, vol. 24, no. 1, pp. 9–23, 2014.

[195] L. Huang and C. Chen, "Proteasome regulators: activators and inhibitors," *Curr Med Chem*, vol. 16, no. 8, pp. 931–939, 2009.

[196] G. T. James, "Inactivation of the protease inhibitor phenylmethylsulfonyl fluoride in buffers," *Anal Biochem*, vol. 86, no. 2, pp. 574–579, Jun. 1977.

[197] W. Zhou, W. Zhu, L. Ma, F. Xiao, and W. Qian, "Proteasome inhibitor MG-132 enhances histone deacetylase inhibitor SAHA-induced cell death of chronic myeloid leukemia cells by an ROS-mediated mechanism and downregulation of the Bcr-Abl fusion protein," *Oncol Lett*, vol. 10, no. 5, pp. 2899–2904, 2015.

[198] T. Suganuma and J. L. Workman, "Crosstalk among histone modifications," *Cell*, vol. 135, pp. 604–607, 2008.

[199] V. M. Richon, "Cancer biology: mechanism of antitumour action of vorinostat (suberoylanilide hydroxamic acid), a novel histone deacetylase inhibitor," *Br J Cancer*, vol. 95, pp. S2–S6, 2006.

[200] M. Hermes, H. Osswald, and D. Kloor, "Role of S-adenosylhomocysteine hydrolase in adenosine-induced apoptosis in HepG2 cells," *Exp Cell Res*, vol. 313, pp. 264–283, 2007.

[201] T. O. Scholl and W. G. Johnson, "Folic acid: influence on the outcome of pregnancy," *Am J Clin Nutr*, vol. 71, p. 129S–303S, 2000.

[202] R. J. Berry *et al.*, "Prevention of neural-tube defects with folic acid in China," *N*

Engl J Med, vol. 341, no. 20, pp. 1485–1490, 1999.

[203] U. Keller, C. van der Wal, G. Seliger, C. Scheler, F. Röpke, and K. Eder, "Carnitine status of pregnant women: effect of carnitine supplementation and correlation between iron status and plasma carnitine concentration.," *Eur J Clin Nutr*, vol. 63, no. 9, pp. 1098–1105, 2009.

[204] E. P. Plaisance *et al.*, "Dietary methionine restriction increases fat oxidation in obese adults with metabolic syndrome," *J Clin Endocrinol Metab*, vol. 96, no. 5, pp. 836–840, 2011.

[205] V. L. Malloy, R. A. Krajcik, S. J. Bailey, G. Hristopoulos, and J. D. Plummer, "Methionine restriction decreases visceral fat mass and preserves insulin action in aging male Fischer 344 rats independent of energy restriction," *Aging Cell*, vol. 5, pp. 305–314, 2006.

[206] R. A. Miller, G. Buehner, Y. Chang, J. M. Harper, R. Sigler, and M. Smith-Wheelock, "Methionine-deficient diet extends mouse lifespan, slows immune and lens aging, alters glucose, T4, IGF-I and insulin levels, and increases hepatocyte MIF levels and stress resistance," *Aging Cell*, vol. 4, pp. 119–125, 2005.

[207] J. Du *et al.*, "Betaine supplementation enhances lipid metabolism and improves insulin resistance in mice fed a high-fat diet," *Nutrients*, vol. 10, no. 131, pp. 1–17, 2018.

[208] S. Li, H. Wang, X. Wang, Y. Wang, and J. Feng, "Betaine affects muscle lipid metabolism via regulating the fatty acid uptake and oxidation in finishing pig," *J Anim Sci Biotechno*, vol. 8, pp. 1–9, 2017.

[209] C. Loenarz and C. J. Schofield, "Expanding chemical biology of 2-oxoglutarate oxygenases," *Nat Chem Biol*, vol. 4, no. 3, pp. 152–156, Mar. 2008.

[210] I. K. H. Leung *et al.*, "Structural and mechanistic studies on g-butyrobetaine hydroxylase," *Chem Biol*, vol. 17, no. 12, pp. 1316–1324, 2010.

[211] K. Sajnani, F. Islam, R. A. Smith, V. Gopalan, and A. K. Y. Lam, "Genetic alterations in Krebs cycle and its impact on cancer pathogenesis," *Biochimie*, vol. 135, pp. 164–172, 2017.

[212] R. Myllyla, K. Majamaa, V. Giinzler, H. M. Hanauske-Abel, and K. I. Kivirikko, "Ascorbate is consumed stoichiometrically in the uncoupled reactions catalyzed by prolyl 4-hydroxylase and lysyl hydroxylase," *J Biol Chem*, vol. 259, no. 9, pp.

5403–5406, 1984.

[213] E. Flashman, S. L. Davies, K. K. Yeoh, and C. J. Schofield, “Investigating the dependence of the hypoxia-inducible factor hydroxylases (factor inhibiting HIF and prolyl hydroxylase domain 2) on ascorbate and other reducing agents,” *Biochem J*, vol. 427, no. 1, pp. 135–142, Apr. 2010.

[214] A. A. Salahudeen *et al.*, “An E3 ligase possessing an iron-responsive hemerythrin domain is a regulator of iron homeostasis,” *Science (80-.).*, vol. 326, pp. 722–727, 2009.

[215] H. J. Knowles, R. R. Raval, A. L. Harris, and P. J. Ratcliffe, “Advances in brief effect of ascorbate on the activity of hypoxia-inducible factor in cancer cells,” *Cancer Res*, vol. 63, pp. 1764–1768, 2003.

[216] C. N. Kontoghiorghe and G. J. Kontoghiorghes, “Efficacy and safety of iron-chelation therapy with deferoxamine, deferiprone, and deferasirox for the treatment of iron-loaded patients with non-transfusion-dependent thalassemia syndromes,” *Drug Des Devel Ther*, vol. 10, pp. 465–481, 2016.

[217] L. Wang *et al.*, “A small molecule modulates Jumonji histone demethylase activity and selectively inhibits cancer growth,” *Nat Commun*, vol. 4, pp. 1–11, 2013.

[218] M. Nangaku and K. U. Eckardt, “Hypoxia and the HIF system in kidney disease,” *J Mol Med*, vol. 85, no. 12, pp. 1325–1330, 2007.

[219] J. R. Hickok, D. Vasudevan, W. E. Antholine, and D. D. Thomas, “Nitric oxide modifies global histone methylation by inhibiting Jumonji C domain containing demethylases,” *J Biol Chem*, vol. 288, no. 22, pp. 16004–16014, 2013.

[220] L.-L. Cao *et al.*, “Iron chelation inhibits cancer cell growth and modulates global histone methylation status in colorectal cancer,” *BioMetals*, vol. 31, no. 5, pp. 797–805, 2018.

[221] J. Stivelman, G. Schulman, M. Fosburg, J. M. Lazarus, and R. M. Hakim, “Kinetics and efficacy of deferoxamine in iron-overloaded hemodialysis patients,” *Kidney Int*, vol. 36, pp. 1125–1132, 1989.

[222] T. Maruyama *et al.*, “Efficacy of L-carnitine supplementation for improving lean body mass and physical function in patients on hemodialysis: a randomized controlled trial,” *Eur J Clin Nutr*, vol. 73, pp. 293–301, 2019.

[223] L. F. Huergo and R. Dixon, “The Emergence of 2-oxoglutarate as a master regulator metabolite,” *Microbiol Mol Biol Rev*, vol. 79, no. 4, pp. 419–435, 2015.

[224] B. S. Nelson, D. M. Kremer, and C. A. Lyssiotis, “New tricks for an old drug,” *Nat Chem Biol*, vol. 14, pp. 990–994, 2018.

[225] A. V. Zhdanov, I. A. Okkelman, F. W. J. Collins, S. Melgar, and D. B. Papkovsky, “A novel effect of DMOG on cell metabolism: direct inhibition of mitochondrial function precedes HIF target gene expression,” *Biochim Biophys Acta*, vol. 1847, no. 10, pp. 1254–1266, 2015.

[226] W. Xu *et al.*, “Oncometabolite 2-hydroxyglutarate is a competitive inhibitor of α-ketoglutarate-dependent dioxygenases,” *Cancer Cell*, vol. 19, no. 1, pp. 17–30, 2011.

[227] L. Dang *et al.*, “Cancer-associated IDH1 mutations produce 2-hydroxyglutarate,” *Nature*, vol. 462, no. 7274, pp. 739–744, 2009.

[228] J. Losman *et al.*, “(R)-2-Hydroxyglutarate is sufficient to promote leukemogenesis and its effects are reversible,” *Science (80-.).*, vol. 339, no. 6127, pp. 1–9, 2013.

[229] M. Xiao *et al.*, “Inhibition of α-KG-dependent histone and DNA demethylases by fumarate and succinate that are accumulated in mutations of FH and SDH tumor suppressors,” *Genes Dev*, vol. 26, no. 12, pp. 1326–1338, 2012.

[230] A. M. Cervera, J. P. Bayley, P. Devilee, and K. J. McCreath, “Inhibition of succinate dehydrogenase dysregulates histone modification in mammalian cells,” *Mol Cancer*, vol. 8, p. 89, 2009.

[231] E. Letouzé *et al.*, “SDH mutations establish a hypermethylator phenotype in paraganglioma,” *Cancer Cell*, vol. 23, no. 6, pp. 739–752, 2013.

[232] B. E. Baysal *et al.*, “Mutations in SDHD, a mitochondrial complex II gene, in hereditary paraganglioma,” *Science (80-.).*, vol. 287, no. 5454, pp. 848–851, 2000.

[233] D. Astuti *et al.*, “Gene mutations in the succinate dehydrogenase subunit SDHB cause susceptibility to familial pheochromocytoma and to familial paraganglioma,” *Am J Hum Genet*, vol. 69, pp. 49–54, 2001.

[234] E. K. Oermann, J. Wu, K. L. Guan, and Y. Xiong, “Alterations of metabolic genes and metabolites in cancer,” *Semin Cell Dev Biol*, vol. 23, no. 4, pp. 370–380, 2012.

[235] R. Myllyla, L. Tuderman, and K. I. Kivirikko, “Mechanism of the prolyl

hydroxylaser reaction 2. Kinetic analysis of the reaction sequence," *Eur J Biochem*, vol. 80, pp. 349–357, 1977.

[236] R. Chowdhury *et al.*, "The oncometabolite 2-hydroxyglutarate inhibits histone lysine demethylases," *EMBO Rep*, vol. 12, no. 5, pp. 463–469, 2011.

[237] R. W. D. Welford, I. Schlemminger, L. A. McNeill, K. S. Hewitson, and C. J. Schofield, "The selectivity and inhibition of AlkB," *J Biol Chem*, vol. 278, no. 12, pp. 10157–10161, 2003.

[238] E. D. MacKenzie *et al.*, "Cell-permeating a-ketoglutarate derivatives alleviate pseudohypoxia in succinate dehydrogenase-deficient cells," *Mol Cell Biol*, vol. 27, no. 9, pp. 3282–3289, 2007.

[239] K. S. Hewitson *et al.*, "Hypoxia-inducible factor (HIF) asparagine hydroxylase is identical to factor inhibiting HIF (FIH) and is related to the cupin structural family," *J Biol Chem*, vol. 277, no. 29, pp. 26351–26355, 2002.

[240] S. Islam, T. M. Leissing, R. Chowdhury, R. J. Hopkinson, and C. J. Schofield, "2-oxoglutarate-dependent oxygenases," *Annu Rev Biochem*, vol. 87, pp. 585–620, 2018.

[241] J. Bonnici, A. Tumber, A. Kawamura, C. J. Schofield, and C. J. Schofield, "Inhibitors of both the N -methyl lysyl- and arginyl-demethylase activities of the JmjC oxygenases," pp. 1–8, 2018.

[242] P. A. C. Cloos *et al.*, "The putative oncogene GASC1 demethylates tri- and dimethylated lysine 9 on histone H3," *Nature*, vol. 442, pp. 307–311, May 2006.

[243] I. Hoffmann *et al.*, "The role of histone demethylases in cancer therapy," *Mol Oncol*, vol. 6, pp. 683–703, 2012.

[244] M. Vinogradova *et al.*, "An inhibitor of KDM5 demethylases reduces survival of drug-tolerant cancer cells," *Nat Chem Biol*, vol. 12, no. 7, pp. 531–538, 2016.

[245] A. Kawamura *et al.*, "Highly selective inhibition of histone demethylases by de novo macrocyclic peptides," *Nat Commun*, vol. 8, pp. 1–10, 2017.

[246] S. S. Ng *et al.*, "Crystal structures of histone demethylase JMJD2A reveal basis for substrate specificity," *Nature*, vol. 448, pp. 87–92, 2007.

[247] R. Schiller *et al.*, "A cell-permeable ester derivative of the JmjC histone demethylase inhibitor IOX1," *ChemMedChem*, vol. 9, no. 3, pp. 566–751, 2014.

[248] H. Watarai *et al.*, "Impact of H3K27 demethylase inhibitor GSKJ4 on NSCLC cells alone and in combination with metformin," *Anticancer Res*, vol. 36, no. 11, pp. 6083–6092, 2016.

[249] R. Hamamoto, V. Saloura, and Y. Nakamura, "Critical roles of non-histone protein lysine methylation in human tumorigenesis," *Nat Rev Cancer*, vol. 15, no. 2, pp. 110–124, 2015.

[250] W. Rizwani, C. Schaal, S. Kunigal, D. Coppola, and S. Chellappan, "Mammalian lysine histone demethylase KDM2A regulates E2F1-mediated gene transcription in breast cancer cells," *PLoS One*, vol. 9, no. 7, pp. 1–13, 2014.

[251] C.-E. Hu, Y.-C. Liu, H.-D. Zhang, and G.-J. Huang, "JMJD2A predicts prognosis and regulates cell growth in human gastric cancer," *Biochem Biophys Res Commun*, vol. 449, no. 1, pp. 1–7, 2014.

[252] E. Liepinsh *et al.*, "Inhibition of L-carnitine biosynthesis and transport by methyl-γ-butyrobetaine decreases fatty acid oxidation and protects against myocardial infarction," *Br J Pharmacol*, vol. 172, no. 5, pp. 1319–1332, 2015.

[253] T. Aoyagi *et al.*, "Inhibition of carnitine synthesis protects against left ventricular dysfunction in rats with myocardial ischemia," *J Cardiovasc Pharmacol*, vol. 30, no. 4, pp. 468–476, 1997.

[254] P. J. Pollard *et al.*, "Accumulation of Krebs cycle intermediates and over-expression of HIF1a in tumours which result from germline FH and SDH mutations," *Hum Mol Gen*, vol. 14, no. 15, pp. 2231–2239, Aug. 2005.

[255] S. E. Wilkins, S. Karttunen, R. J. Hampton-Smith, I. Murchland, A. Chapman-Smith, and D. J. Peet, "Factor inhibiting HIF (FIH) recognizes distinct molecular features within hypoxia-inducible fFactor-a (HIF-a) versus ankyrin repeat substrates," *J Biol Chem*, vol. 287, no. 12, pp. 8769–8781, 2012.

[256] W. Du *et al.*, "HIF drives lipid deposition and cancer in ccRCC via repression of fatty acid metabolism," *Nat Commun*, vol. 8, no. 1769, pp. 1–12, 2017.

[257] R. Turner, "Effect of intensive blood-glucose control with metformin on complications in overweight patients with type 2 diabetes (UKPDS 34)," *Lancet*, vol. 352, no. 9131, pp. 854–865, 1998.

[258] W. C. Knowler *et al.*, "Reduction in the incidence of type 2 diabetes with lifestyle intervention or metformin.," *N Engl J Med*, vol. 346, no. 6, pp. 393–403, 2002.

[259] K. Tars *et al.*, “Targeting carnitine biosynthesis: discovery of new inhibitors against γ-butyrobetaine hydroxylase,” *J Med Chem*, vol. 57, no. 6, pp. 2213–2236, Mar. 2014.

[260] M. Dambrova, E. Liepinsh, and I. Kalvinsh, “Mildronate: cardioprotective action through carnitine-lowering effect,” *Trends Cardiovasc Med*, vol. 12, no. 6, pp. 275–279, 2002.

[261] E. Liepinsh, E. Skapare, B. Svalbe, M. Makrecka, H. Cirule, and M. Dambrova, “Anti-diabetic effects of mildronate alone or in combination with metformin in obese Zucker rats,” *Eur J Pharmacol*, vol. 658, no. 2–3, pp. 277–283, 2011.

[262] World Anti-Doping Agency, “The world anti-doping code. International Standard. Prohibited List. Januray 2018,” *Last accessed 30.03.2019*, 2018.

[263] L. Nie *et al.*, “The landscape of histone modifications in a high-fat-diet-induced obese (DIO) mouse model,” *Mol Cell Proteom*, vol. 16, no. 7, pp. 1324–1334, 2017.

[264] S. R. Salpeter, N. S. Buckley, J. A. Kahn, and E. E. Salpeter, “Meta-analysis: metformin treatment in persons at risk for diabetes mellitus,” *Am J Med*, vol. 121, no. 2, pp. 149–157, 2008.

[265] C. J. Glueck *et al.*, “Metformin reduces weight, centripetal obesity, insulin, leptin, and low-density lipoprotein cholesterol in nondiabetic, morbidly obese subjects with body mass index greater than 30,” *Metabolism*, vol. 50, no. 7, pp. 856–861, 2001.

[266] X. Yu *et al.*, “Anti-tumor activity of metformin: from metabolic and epigenetic perspectives,” *Oncotarget*, vol. 8, no. 3, pp. 5619–5628, 2017.

[267] S. M. Haffner, S. Lehto, T. Ronnemaa, K. Pyorala, and M. Laakso, “Mortality from coronary heart disease in subjects with type 2 diabetes and in nondiabetic subjects with and without prior myocardial infarction,” *N Engl J Med*, vol. 339, no. 4, pp. 229–234, 1998.

[268] T. Almdal, H. Scharling, J. S. Jensen, and H. Vestergaard, “The independent effect of type 2 diabetes mellitus on ischemic heart disease, stroke, and death,” *JAMA Intern Med*, vol. 164, pp. 1422–1426, 2004.

[269] D. Kirpichnikov, S. I. McFarlane, and J. R. Sowers, “Metformin: an update,” *Ann Intern Med*, no. 137, pp. 25–33, 2002.

[270] H. Wu *et al.*, "Metformin alters the gut microbiome of individuals with treatment-naive type 2 diabetes, contributing to the therapeutic effects of the drug," *Nat Med*, vol. 23, no. 7, pp. 850–858, 2017.

[271] C. J. Bailey, "Biguanides and NIDDM," *Diabetes Care*, vol. 15, no. 6, pp. 755–772, 1992.

[272] Y. Shitara, N. Nakamichi, M. Norioka, H. Shima, Y. Kato, and T. Horie, "Role of organic cation/carnitine transporter 1 in uptake of phenformin and inhibitory effect on complex I respiration in mitochondria," *Toxicol Sci*, vol. 132, no. 1, pp. 32–42, 2013.

[273] R. L. Puntel, C. W. Nogueira, and J. B. T. Rocha, "Krebs cycle intermediates modulate thiobarbituric acid reactive species (TBARS) production in rat brain in vitro," *Neurochem Res*, vol. 30, no. 2, pp. 225–235, 2005.

[274] J. Butler and B. Halliwell, "Reaction of iron-EDTA chelates with the superoxide radical," *Arch Biochem Biophys*, vol. 218, no. 1, pp. 174–178, 1982.

[275] I. Tamai *et al.*, "Cloning and characterization of a novel human pH-dependent organic cation transporter, OCTN1," *FEBS Lett*, vol. 419, no. 1, pp. 107–111, 1997.

[276] X. Wu, P. D. Prasad, F. H. Leibach, and V. Ganapathy, "cDNA sequence, transport function, and genomic organization of human OCTN2, a new member of the organic cation transporter family," *Biochem Biophys Res Commun*, vol. 246, no. 3, pp. 589–595, 1998.

[277] S. K. Nigam, "What do drug transporters really do?," *Nat Rev Drug Discov*, vol. 14, no. 1, pp. 29–44, 2015.

[278] A. M. Lamhonwah and I. Tein, "Novel localization of OCTN1, an organic cation/carnitine transporter, to mammalian mitochondria," *Biochem Biophys Res Commun*, vol. 345, no. 4, pp. 1315–1325, 2006.

[279] F. Palmieri, "Molecular aspects of medicine the mitochondrial transporter family SLC25: identification, properties and physiopathology," *Mol Asp. Med*, vol. 34, no. 2–3, pp. 465–484, 2013.

[280] A.-M. Lamhonwah, C. A. Ackerley, A. Tilups, V. D. Edwards, R. J. Wanders, and I. Tein, "OCTN3 is a mammalian peroxisomal membrane carnitine transporter," *Biochem Biophys Res Commun*, vol. 338, pp. 1966–1972, 2005.

[281] L. K. Sharma, J. Lu, and Y. Bai, “Mitochondrial respiratory complex I: structure, function and implication in human diseases,” *Curr Med Chem*, vol. 16, no. 10, pp. 1266–1277, 2009.

[282] R. E. Rhoads, “Signal transduction pathways that regulate eukaryotic protein synthesis,” *J Biol Chem*, vol. 274, no. 43, pp. 30337–30340, 1999.

[283] D.-S. Wang, J. W. Jonker, Y. Kato, H. Kusuhara, A. H. Schinkel, and Yuichi Sugiyama, “Involvement of organic cation transporter 1 in hepatic and intestinal distribution of metformin,” *J Pharmacol Exp Ther*, vol. 302, no. 2, pp. 510–515, 2002.

[284] N. Kimura *et al.*, “Metformin is a superior substrate for renal organic cation transporter OCT2 rather than hepatic OCT1.,” *Drug Metab Pharmacokinet*, vol. 20, no. 5, pp. 379–386, 2005.

[285] S. Masuda *et al.*, “Identification and functional characterization of a new human kidney–specific H+/organic cation antiporter, kidney-specific multidrug and toxin extrusion 2,” *J Am Soc Nephrol*, vol. 17, pp. 2127–2135, 2006.

[286] Y. Tanihara, S. Masuda, T. Sato, T. Katsura, O. Ogawa, and K. Inui, “Substrate specificity of MATE1 and MATE2-K, human multidrug and toxin extrusions / H+-organic cation antiporters,” *Biochem Pharmacol*, vol. 74, pp. 359–371, 2007.

[287] M. R. Owen, E. Doran, and A. P. Halestrap, “Evidence that metformin exerts its anti-diabetic effects through inhibition of complex 1 of the mitochondrial respiratory chain,” *Biochem J*, vol. 348, no. 3, pp. 607–614, Jun. 2000.

[288] M.-Y. El-Mir, V. Nogueira, E. Fontaine, N. Avéret, M. Rigoulet, and X. Leverve, “Dimethylbiguanide inhibits cell respiration via an indirect effect targeted on the respiratory chain complex I dimethylbiguanide inhibits cell respiration via an indirect effect targeted on the respiratory chain complex I,” *J Biol Chem*, vol. 275, no. 1, pp. 223–228, 2000.

[289] P. J. Randle, P. B. Garland, C. N. Hales, and E. A. Newsholme, “The glucose fatty-acid cycle its role in insulin sensitivity and the metablic disturbances of diabetes mellitus,” *Lancet*, vol. 281, no. 7285, pp. 785–789, Apr. 1963.

[290] S. J. Mihalik *et al.*, “Increased levels of plasma acylcarnitines in obesity and type 2 diabetes and identification of a marker of glucolipotoxicity,” *Obesity*, vol. 18, no. 9, pp. 1695–1700, 2010.

[291] M. R. Soeters *et al.*, “Muscle acylcarnitines during short-term fasting in lean healthy men,” *Clin Sci*, vol. 116, pp. 585–592, 2009.

[292] J. E. Gunton, P. J. D. Delhanty, S. Takahashi, and R. C. Baxter, “Metformin rapidly increases insulin receptor activation in human liver and signals preferentially through insulin-receptor substrate-2,” *J Clin Endocrinol Metab*, vol. 88, no. 3, pp. 1323–1332, 2003.

[293] I. Tein *et al.*, “Impaired skin fibroblast carnitine uptake in primary systemic carnitine deficiency manifested by childhood carnitine-responsive cardiomyopathy,” *Pediatr Res*, vol. 28, no. 3, pp. 247–255, 1990.

[294] C. A. Stanley *et al.*, “Chronic cardiomyopathy and weakness or acute coma in children with a defect in carnitine uptake,” *Ann Neurol*, vol. 30, no. 5, pp. 709–716, 1991.

[295] G. Mingrone, “Carnitine in type 2 diabetes,” *Ann NY Acad Sci*, vol. 1033, pp. 99–107, 2004.

[296] M. González-Ortiz, S. O. Hernández-González, E. Hernández-Salazar, and E. Martínez-Abundis, “Effect of oral L-carnitine administration on insulin sensitivity and lipid profile in type 2 diabetes mellitus patients,” *Ann Nutr Metab*, vol. 52, no. 4, pp. 335–338, 2008.

[297] B. Capaldo, R. Napoli, P. Di Bonito, G. Albano, and L. Sacca, “Carnitine improves peripheral glucose disposal in non-insulin-dependent diabetic patients,” *Diabetes Res Clin Pr.*, vol. 14, pp. 191–195, 1991.

[298] R. A. Koeth *et al.*, “Intestinal microbiota metabolism of l-carnitine, a nutrient in red meat, promotes atherosclerosis,” *Nat Med*, vol. 19, no. 5, pp. 576–585, 2013.

[299] J. R. Ussher, G. D. Lopaschuk, and A. Arduini, “Gut microbiota metabolism of L-carnitine and cardiovascular risk,” *Atherosclerosis*, vol. 231, no. 2, pp. 456–461, 2013.

[300] Z. Wang *et al.*, “Gut flora metabolism of phosphatidylcholine promotes cardiovascular disease,” *Nature*, vol. 472, no. 7341, pp. 57–63, 2011.

[301] P. Madiraju, S. V Pande, M. Prentki, and S. R. M. Madiraju, “Mitochondrial acetylcarnitine provides acetyl groups for nuclear histone acetylation,” *Epigenetics*, vol. 4, no. 6, pp. 399–403, 2009.

[302] P. Banerjee, H. Surendran, D. R. Chowdhury, K. Prabhakar, and R. Pal, “Metformin mediated reversal of epithelial to mesenchymal transition is triggered by epigenetic changes in E-cadherin promoter,” *J Mol Med*, vol. 94, pp. 1397–1409, 2016.

[303] E. Cuyas *et al.*, “Metformin directly targets the H3K27me3 demethylase KDM6A/UTX,” *Aging Cell*, vol. 17, pp. 1–15, 2018.

[304] V. Calabrese, A. M. Giuffrida Stella, M. Calvani, and D. A. Butterfield, “Acetylcarnitine and cellular stress response: roles in nutritional redox homeostasis and regulation of longevity genes,” *J Nutr Biochem*, vol. 17, no. 17, pp. 73–88, 2006.

[305] V. Palermo, C. Falcone, M. Calvani, and C. Mazzoni, “Acetyl-L-carnitine protects yeast cells from apoptosis and aging and inhibits mitochondrial fissio,” *Aging Cell*, vol. 9, pp. 570–579, 2010.